Permanent Magnet Linear Generators for Marine Wave Energy Converters

Submitted by Nikola Gargov, to the University of Exeter as a thesis for the degree of Doctor of Philosophy in Renewable Energy, April 2013

I certify that all material in this thesis which is not my own work has been identified and that no material has previously been submitted and approved for the award of a degree by this or any other University.

Signature: ……

“Our greatest glory is not in never falling, but in getting up every time we fall”

Confucius

Abstract

Direct drive Permanent Magnet Linear Generators (PMLGs) are used in energy converters for energy harvesting from marine waves. Greater reliability and simplicity can be achieved for Wave Energy Converters (WECs), by using direct drive machines linked to the power take-off device, in comparison with WECs using rotational generators combined with hydraulic or mechanical interfaces to convert linear to rotational torque. However, owing to the relatively low velocities of marine waves and the desire for significant energy harvesting by each individual unit, direct drive PMLGs share large permanent magnet volumes and hence, high magnetic forces. Such forces can generate vibrations and reduce the lifetime of the bearings significantly, which is leading to an increase in maintenance costs of WECs. Additionally, a power electronics converter is required to integrate the generator's electrical output to meet the requirements for connection to the national grid.

This thesis is concerned mainly with the fundamental investigation into the use PMLGs for direct drive WECs. Attention is focused on developing several new designs based on tubular long stator windings topologies and optimisation for flat PMLGs. The designs are simulated as air- and iron-cored machines by means of Finite Element Analysis (FEA). Furthermore, a new power electronics control system is proposed to convert the electrical output of the long stator generators.

Various wave energy-harvesting technologies have been reviewed and it has been found that permanent magnet linear machines demonstrate great potential for integration in WECs. The main reason is the strong exaltation flux provided

by the high number of permanent magnets. Such flux, combined with design simplicity, can deliver high induced voltage as well as structural integrity.

In the thesis, a flat single and double structured iron-cored PMLG is studied and optimised. Several magnetic force mitigation techniques are investigated and an optimisation is conducted. The optimisation is concerned mainly with increasing electrical output power and reducing the magnetic forces in the generators. As a result, an optimal design introducing the idea of separated magnetic cores has been proposed. The FEA simulations reveal that magnetic separation in the yoke can increase significantly the energy-harvesting capability of PMLGs.

Furthermore, the concept of the design of long stator windings for tubular PMLGs is studied. Two long stator generators having different magnetisation topologies and similar sizes to existing machine are modelled and compared to the existing machine. The similar-sized existing and proposed PMLGs are simulated by FEA. In this way, settings such as different boundary conditions, symmetry boundaries and material properties are used to gain confidence in the simulated results of the proposed machines. Moreover, the simulated results for the existing PMLG are verified against previously performed numerical simulations and practical tests delivered and published as part of other research. The outcome for the proposed PMLGs reveals several advantages for the long stator design, such as lower cogging forces and higher energy harvesting and a lower price of the raw structural materials.

Additionally, the thesis proposes and simulates a new design for an air-cored PMLG. To boost the output power, the proposed design is based on a long stator topology adopting two sets of permanent magnet rings sandwiching copper windings in a tubular structure. The design is compared with a current

machine in FEA and the results show significant reduction in radial forces and an increase in energy harvesting.

Finally, a novel power electronics control system, bypassing inactive coils is suggested and simulated as part of the grid integration system for the long stator PMLGs. The new system achieves a reduction in the thermal losses in the power electronics switches in comparison with existing systems. The power electronics system and the generator have been simulated in Matlab coupled externally with FEA (JMAG Designer).

Acknowledgements

I would like to express my deep gratitude to my principal supervisor Dr. Ahmed Zobaa for his great support throughout my entire research. I sincerely appreciate his continuous encouragement.

I would like to express my gratitude to Dr. Mohammad Abusara and Dr. Lars Johanning who helped me with the preparation of my thesis.

I want also to take the opportunity to thank Prof. George Smith for his help in organising my off-campus work at Brunel University.

My thanks go to my ever-supportive and loving parents for their encouragement and help and to my beloved wife Soyoung, for her constant support and encouragement.

Contents

List of Figures

List of Tables

List of Abbreviations

2D:	Two Dimensional
3D:	Three Dimensional
AC:	Alternating Current
AWS:	Archimedes Wave Swing
SVC	Static VAr Compensator
STATCOM	Static Compensator
DC:	Direct Current
EMF:	Electromotive Force
FE:	Finite Element
FEA:	Finite Element Analysis
FEM:	Finite Element Method
FWSM:	Field Wound Synchronous Machines
LGPM:	Longitudinal Flux Permanent Magnet Machine
LS-PMLG:	Long Stator Tubular Permanent Magnet Linear Generator
MMF, mmf:	Magneto Motive Force
NdFeB:	Neodymium Iron Boron
NFM:	Nodal Force Method
PMLG:	Permanent Magnet Linear Generator
PV:	Photo Voltaic
RMS:	Root Mean Square
RoI:	Return of Investment
SS-PMLG:	Short Stator Tubular Permanent Magnet Linear Generator

TFM:	Transverse Flux Machine
VHM:	Vernier Hybrid Machine
VRPM:	Variable Reluctance Permanent Magnet Machine
WEC:	Wave Energy Converter

List of Symbols

A_r	Area [m^2]
B	Magnetic flux density [Wb/m2 or T]
$\mathrm{B_u}$	Buoyancy force [N]
$\mathrm{C_d}$	Damping coefficient [$\mathrm{Ns^{-1}}$]
$\mathrm{D_r}$	Drag coefficient [Ns/m]
$\mathrm{F_E}$	Existing force on the body in [N]
$\mathrm{F_L}$	Lorentz force [N]
$\mathrm{f_i^{\Omega}}$	Surface forces [N]
$\mathrm{f_i^{\Gamma}}$	Magnetic volume [A/m]
$\mathrm{f_0}$	Natural (resonant) frequency of WEC [Hz]
$\mathrm{f_{ni}}$	Force acting on the $\mathrm{n^{th}}$ node [N]
$\mathrm{F_R}$	Radiation force required to create the wave [N]
$\mathrm{g_a}$	Air gap length [m]
$\mathrm{H_c}$	Coercivity [A/m]
$\mathrm{I_c}$	Coil current [A]
$\mathrm{i_q}$,$\mathrm{i_d}$	Current in the q and the d axis [A]
$\mathrm{I_n}$	Inertia [Ns2/m]
$\mathrm{I_w}$	Winding current [A]
$\mathrm{K_e}$	Electric loading [A/m]
$\mathrm{k_s}$	Spring constant [$\mathrm{Nm^{-1}}$]
$\mathrm{L_e}$	Length of the coil [m]
$\mathrm{l_{gap}}$	Length of the air gap [m]
$\mathrm{L_{mut}}$	Mutual inductance [H]

L_{self}	Self-inductance [H]
l_{tooth}	length of the coil`s slots [m]
M_A, m_a	Mass [kg]
M_p	Magnetic pole [m]
N, N_{ii}	Number of winding turns
N_n	Nodal shape function of the n^{th} node
P	Active power [W]
p	Number of winding sections connected in series
P_s	Phase slot [m]
q	Number of slots per pole and phase
$R_{winding}$	Resistance of windings [Ω]
$S_1 - S_{19}$	Magnetic reluctance [H^{-1}]
S1 - S30	Power electronics switch
T_f	Period of the motion [m]
t_h	Magnet thickness [m]
V1-V16	Voltmeters
V_A	Velocity [m/s]
V_e	Electromagnetic force [V]
v_s	Displacement [m]
w_w	Magnet width [m]
w_m	Magnetic co-energy density [J/m^3]
X_A	Displacement [m]
x_t	Position of the translator [m]
x_t	Velocity [m/s]
z	Linear displacement [m]

λ_w	Wave length [m]
λ_{im}	Flux linked with the i -phase winding [Wb-turns]
ω_f	Angular velocity of the translator [rad/s]
ω_p	Pole pitch [m]
φ_d	Phase angle [rad]
Φ_{ii}	Maximum flux [Wb]
Φ_{PM}	Flux flow due to a single magnet [Wb]
ϕ	Flux density [Wb]
ψ_m	Total magnetic flux [Wb]
μ_0	Permeability of the air [H/m]

1. Introduction into the Research

1.1. The Aim of the Research

This thesis aims to discover new designs of PMLGs to deliver:

- A reduction in unwanted magnetic forces, such as cogging forces and the magnetic attraction between two iron surfaces.
- An increase in electrical energy harvesting in comparison with existing generators.

1.2. The Objectives of the Research

In this thesis, the aim is to be delivered by:

- Investigating the effects of different Permanent Magnet (PM) magnetisation topologies and force reduction techniques on the magnetic forces and electrical output power of longitudinal PMLGs for marine wave energy harvesting.
- Proposing innovative PMLGs and drawing a comparison with existing machines.
- Analytical and numerical simulations of PMLGs, using FEA (JMAG-Designer) and Matlab/Simulink.

1.3. Research Methodology

This thesis is conducted by multi-dimensional approaches in order to achieve its aims and objectives. The research methods are based on analytical and FEA numerical modelling, though which simulations of existing and new linear generators are performed.

Analytical models of PMLGs based on their magnetic circuits are created and static calculations of the magnetic flux are conducted.

Moreover, in the thesis, FEA (JMAG-Designer) is used to perform dynamic simulation of PMLGs. This method is chosen owing to the high accuracy of the 3D FEA numerical simulation results. The greatest benefit of FEA is that it solves the magnetic and the electrical circuits simultaneously, evaluating electrical variables such as currents, voltages and powers, as well as magnetic forces and flux distribution. Therefore, the effect of small design changes on the overall performance can be observed with high accuracy.

Because of the limited components of JMAG's internal library, complicated power electronics control problems cannot be solved. Thus, to solve such problems, JMAG is connected externally with Matlab/Simulink. This configuration allows a wide observation of the above spectrum of parameters as well as an implementation of real-time control systems using power electronics.

Owing to the high number of boundary conditions involved in the numerical analysis, a small mistake, especially in the symmetrical settings of the 3D models, could cause a significant difference in the outcomes. Therefore, verifying the boundary conditions and the settings for FEA by experimental results enhances the confidence in the selected FEA settings. To validate the

simulations for the existing iron-cored generator the following steps are performed.

- A dynamic simulation and test results for a permanent magnet generator are obtained from published research, where the PMLG description, including physical dimensions and material properties and the mechanical/electrical output results, are sufficient to model and verify the same generator in FEA. The verification includes the electrical power outputs such as electromotive force (EMF), phase voltages and currents, the cogging forces and the magnetic flux distribution in the machine. By verifying these FEA results, the correct boundary conditions and symmetry settings can be obtained for accurate 3D dynamic simulations.
- The proposed tubular long stator generator has been modelled by FEA using the same boundary conditions, symmetry settings, material properties and dimensions (wherever possible).
- The modelled machines are simulated analytically and numerically and the evaluated results compared with the existing generator.
- Another comparison involving the calculation of approximate prices for the raw assembly materials is also performed. Such comparability involves certain errors because it does not take into account potential difficulties in the manufacturing and the assembly process. It can be used as an approximate high-level indication for benchmarking the cost of the existing and proposed machines.

Electrical machines with three phase windings can connect directly to a three-phase AC/DC/AC (back-to-back) converter. Owing to the wide use of such converters, they can be classified as standard. On the other hand, because of

the complicated winding arrangement, the long stator generator requires non-standard grid integration systems to convert the output to DC via either a passive or an active rectifier. The rectifier system used in Chapter 4 is a passive long stator rectifier in which all coils are treated as different phases and are rectified with diodes.

On the other hand, the active control proposed for long stator generators in Chapter 5, is more efficient in terms of thermal loss but it is more complicated. It adds the EMFs of the energised coils, grouping them in three phases. As a result, a standard three-phase rectifier can be used as part of the back-to-back converter in the grid integration system. The system is simulated in Matlab/Simulink externally coupled with JMAG by an S-function link. Therefore, an advantage of this system over separated simulation is the real-time two-way communication channel between the control system in Matlab/Simulink and the generator switches in JMAG during dynamic simulations.

1.4. Structure of the Thesis

This thesis is structured from the revision and investigation of current research to the proposals for PMLGs and it is divided into six chapters as follows:

Chapter 1 is an introduction to the topic of the research. This chapter contains the aims, objectives and the research methodology of the thesis.

Chapter 2 comprises a literature review in which the main technologies for marine wave energy harvesting and direct drive linear generators are analysed.

In **Chapter 3,** an investigation of flat iron-cored PMLGs for wave energy is conducted. It aims to achieve a reduction in the cogging forces and to increase the electrical output of flat PMLGs:

- In the first type of generator, the excitation flux is provided by permanent magnets located on one side of the windings. The investigation aims to show how the different number of slots per pole and phase and the different number of winding sections affect the generator's cogging force and electrical output power.
- In the second type, two sets of windings sandwich the PMs from both sides. In this chapter, the influence of the number of slots per pole and phase and the number of winding sections are analysed with regard to the generator's cogging force and output power. Furthermore, an optimal design proposing the use of a magnetically separated translator yoke is suggested.

In **Chapter 4**, an investigation of tubular iron-cored long stator PMLGs is carried out. A novel design for a long stator generator is proposed and compared with an existing similar-sized three-phase generator. The simulations made in this chapter suggest that using a long stator tubular design could be more beneficial owing to the reduction of the cogging force and the price of the structural materials.

Three kinds of generators are modelled and simulated. The first kind is an existing three-phase linear generator, for which the results are verified with the source. The second and the third types are long stator tubular linear generators with axial and radial magnetised magnets. A comparison of the dynamic performance of the three machines is drawn.

Chapter 5 proposes a novel long stator tubular air-cored permanent linear generator for wave energy harvesting. The generator has an air-cored translator sandwiched between two sets of permanent magnets. The design suggests higher power output and the elimination of cogging forces compared with existing similar-sized iron-cored generator. However, the price of the structural materials for the air-cored machine is likely to be higher.

Moreover, a new inactive coil bypassing system is proposed. The bypassing system achieves a lower level of thermal losses in comparison with previously proposed systems.

Chapter 6 presents a conclusion of the thesis and suggests recommendations for future work based on the results of this research.

2. Literature Review

2.1. Brief History of Wave Energy

An interest in sustainable sources for energy started initially following the oil crisis in the 1970s as an alternative to nuclear energy. However, at that time, nuclear energy was regarded as more economical and efficient in terms of the cost of energy generation. As a result, after several years of research and development, the UK's "deep-sea" research programme was closed in 1984 due to financial reasons. However, around 10 years later, both interest and funding were renewed. Despite the research having started twenty years ago, many problems have still not been solved. Most of the unsolved problems are technical but there are political issues as well (Ross 1995). Consequently, these problems are preventing commercial success. Therefore, solving those problems is vital for the future of the generation of wave energy.

2.2. Environmental Impact

A comparison among the various electricity generation types in terms of CO_2 released to the atmosphere over the entire lifetime, has been analysed by the Kyoto protocol and the so-called carbon credit scheme (Domingues, Silva et al. 2008).

As seen in Figure 1, Photo-Voltaic (PV) systems have one of the highest carbon footprints among renewable sources. However, Figure 2 indicates that

carbon release is likely to decrease in the future. During the process of manufacturing the silicon, around 60% of the total CO_2 is released, because the PV silicon panels are made from quartz sand exposed to high temperatures.

Marine generation is still not a fully developed branch of renewable energy and most of the CO_2 emissions are produced during the manufacture of the structural materials. Most of the carbon is released due to the high volumes of steel used in the foundations and the supporting structures of the WECs. In general, marine energy does not output any pollution during normal operation. However, the operational conditions (seabed and seawater environment) require further investigation. The impact of the onsite installation on the flora and fauna has to be analysed. A detailed seabed study could provide critical information regarding the best locations for wave generation plants. Such an investigation is likely to reduce the maintenance, installation and mooring costs and increase the safety of the cables. Furthermore, a study of the flora and fauna (such as migration) can avoid foreseen problems related to interaction with the sea life or birds. A recent carbon footprint evaluation is illustrated in Figure 2, which shows that the footprint of low-carbon sources is generally lower than the footprint of fossil fuel source.

In hydro generation, most of the carbon emissions are released during the construction of the facilities. The massive water dams and the walls involve digging operations and use of high volumes of steel for the concrete structures.

At present, wind generation is one of the most developed and recognised renewable sources and it has one of the lowest carbon footprints. The majority of the carbon is released during the production of the epoxy/fibreglass blades.

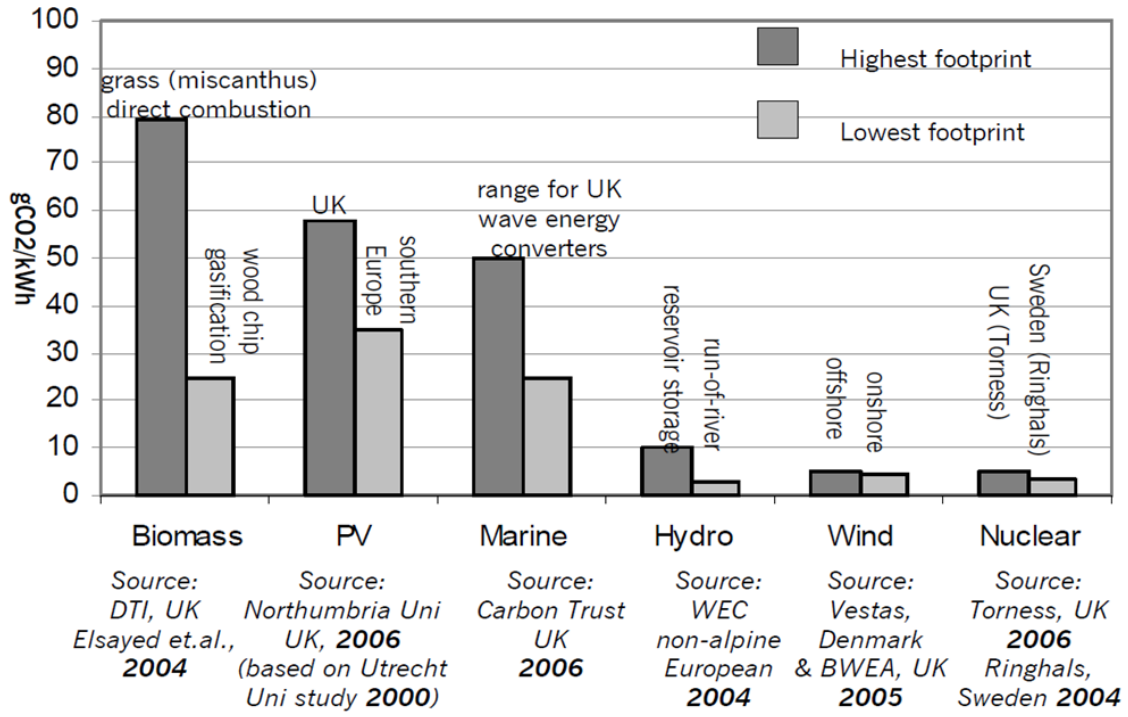

Figure 1 Carbon footprints for UK & European 'low carbon' technologies

(Parliamentary Office of Science and Technology 2006)

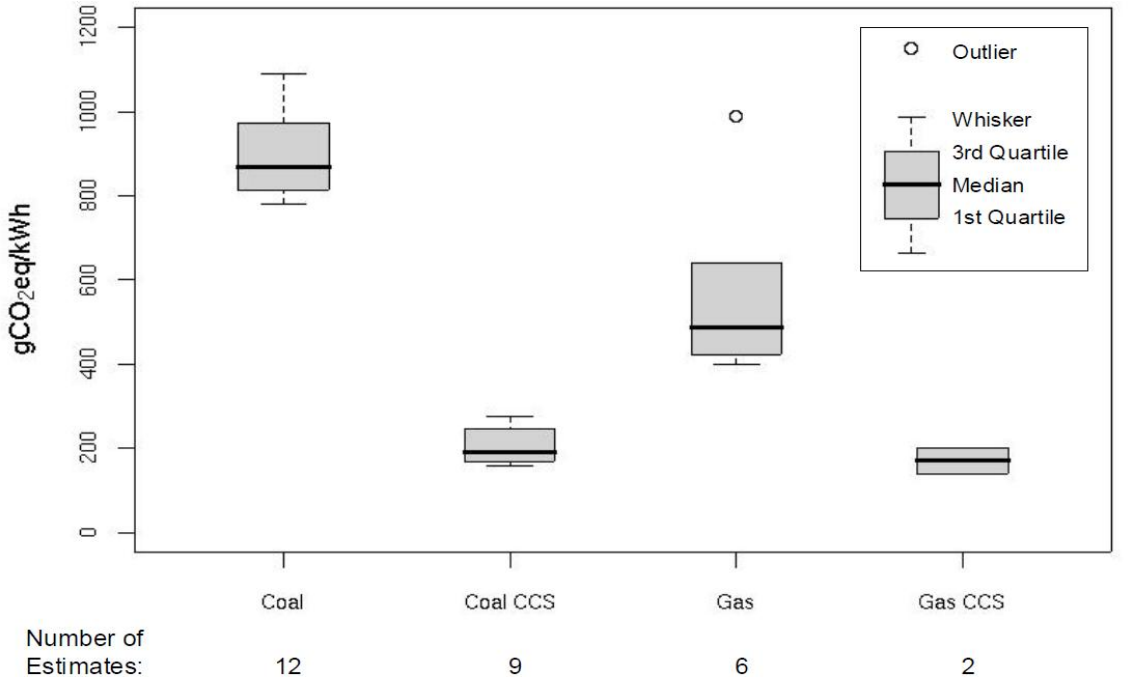

(a) International carbon footprints of fossil-fuel electricity

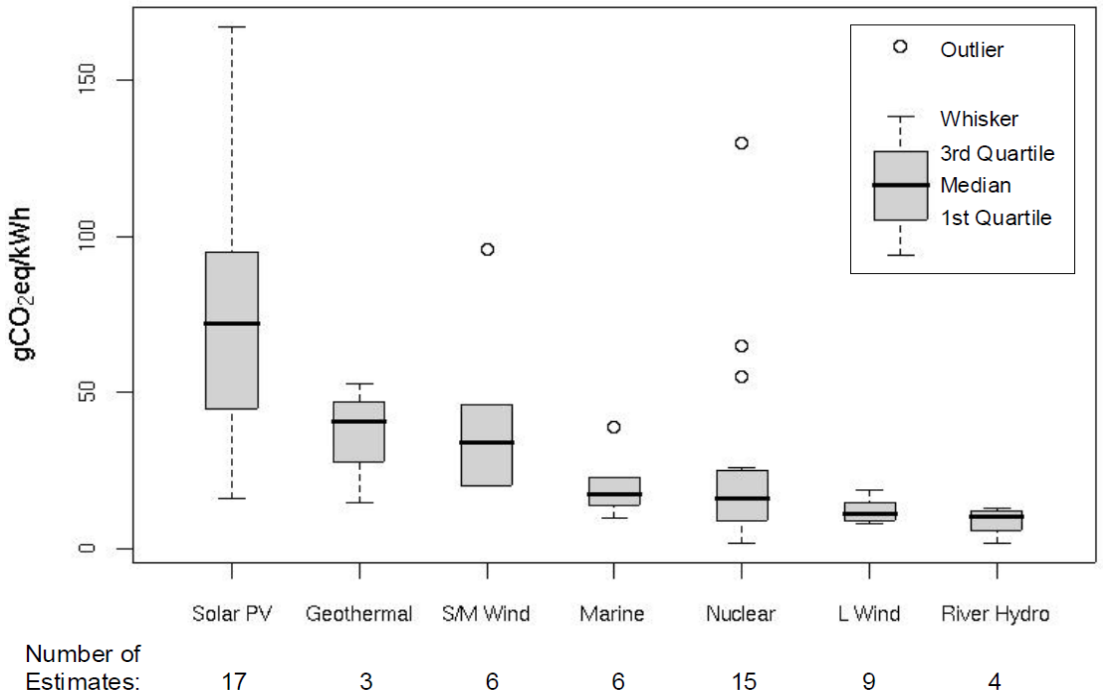

(b) International carbon footprints for low-carbon electricity

Figure 2 Current carbon footprints of generation technologies

(Parliamentary Office of Science and Technology June 2011)

Nuclear energy also has one of the lowest carbon footprints due to the absence of carbon emissions during normal operation. The most significant carbon emissions over the lifetime of the technology are released during the decommissioning of the plant and the maintenance/storage of the nuclear waste. Furthermore, another significant cause of carbon emissions comes from the mining of the uranium. The long-term footprint of nuclear plants is likely to increase due to limited high-grade uranium deposits, because the use of low-grade uranium will lead to more carbon emissions in order to produce the same amount of energy.

The carbon footprints of coal and gas plants are traditionally high. However, they are expected to decrease due to the highly efficient turbines boosting

efficiency from 35% to 50% (Entec UK Limited 2010). Additionally, technologies such as Carbon Capture and Storage (Christensen 2005) have the potential to mitigate a significant part of the atmospheric carbon release.

2.3. Marine Waves

Marine waves are generated by the wind in combination with Earth's gravity. The passing wind causes tension on the water surface. On a small scale, waves are generated by this tension. Larger scale waves are amplified by the wind and the Earth's gravity.

Generally, the ocean climate is a superposition of waves generated locally (by local winds) and passing waves generated by distant sources. The locally generated waves and the travelling waves are referred to as seas and swells, respectively. Typically, seas contain steeper waves with shorter periods and swells consist of low-steepness waves with longer periods. Seas include a large number of individual waves featuring a wide range of wave patterns with varying periods, directions and heights.

In realistic wave conditions, the total wave pattern includes different kinds of waves and therefore, it varies in wide ranges. This pattern highlights one of the main difficulties for WECs because they have to be designed to operate in conditions much rougher than the average for the region. As a result, the safety factors have to be increased and hence so too do the costs of the WECs.

2.4. Wave Energy Generation

Potentially, marine wave energy is a huge source of renewable energy. In the last two decades, several technologies have been proposed. Some of the

technologies are already in the commercial stage of development and use fast-velocity generators in combination with hydraulic systems. Other technologies, such as direct drive linear generators are at less advanced stages of development due to mechanical and electrical issues. In general, marine wave energy is more challenging in comparison with other renewable sources such as wind and solar energy. The main reason for this is that WECs have to function in harsh operating conditions.

2.4.1. Ocean Energy Recourses

A study presented in (Thorpe 1999) reports that the wave power has global potential of more than 1 TW. However, this potential cannot be considered as fully achievable. The locations with the highest wave power levels considered as attractive options for power generation are shown in Figure 3.

Owing to its geographic location, the UK has one of the highest potentials for wave energy generation. Studies suggest that marine wave power around the UK has enormous potential of up to 120 GW (Clément, McCullen et al. 2002, Thorpe 1999). Considering the capacity of the UK's peak electricity demand of around 60 GW, marine wave energy harvesting has significant potential in contributing to the energy requirements.

Figure 3 Wave power levels expressed in kW/m crest length (Polinder, Scuotto 2005)

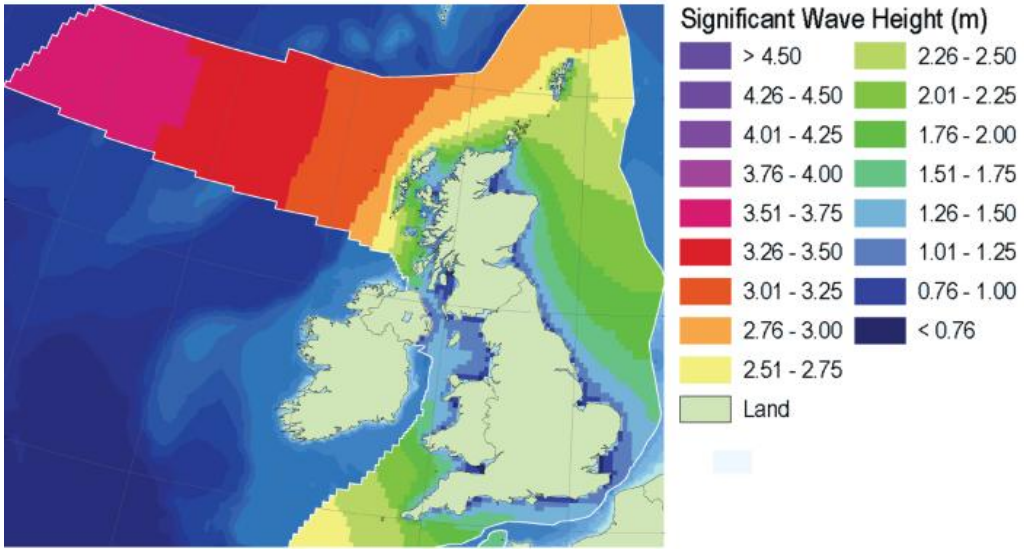

Figure 4 Wave resource in the UK (ABPmer The Mt Office 2008)

However, challenges are foreseen in relation to the collection and transportation of the electrical power to the shore. The main reason for such challenges is the environment in which the submerged cables and substations operate. Different issues emerge relating to the onshore transportation of the power, where reinforcements of the transmission and distribution systems have

to be made for reliable and economic transportation of the electrical power. Furthermore, the intermittency in power delivery of the wave energy converters needs to be addressed, as it requires other sources of rapid power response on stand-by, such as synchronous generators, interconnectors and demand side response.

2.4.2. Challenges in Wave Power Generation

The main challenges facing marine wave energy are summarised in Figure 5. Even though some of the technologies (such as hydraulics and fluid turbines) are well developed, the operating conditions continue to cause problems during installation and maintenance. The installation and operational costs of WECs are expected to be relatively higher in comparison with wind and PV energy converters.

Another issue for direct drive generators is the manufacturing cost. In comparison with fast-velocity rotational machines, the manufacturing cost of direct drive permanent magnet linear machines, rated at the same power, is considerably higher. The main reason for this is the slow translational velocities of the marine waves.

Figure 5 Main challenges for Wave Energy Converters (Markus Mueller and Robin Wallace 2008)

Furthermore, the high volume of permanent magnet material used in the slow moving direct drive linear generators causes high attraction forces between the stator and the translator of the machines. Such forces can reduce significantly the life of the bearings and hence, reduce the reliability and the lifetime of the WECs (Thorburn, Leijon 2007).

2.4.3. Wave Power Generation Technologies

During the last couple of decades, several WECs have been proposed. The technologies vary depending on the location of the WECs with regard to the shore. WECs also differ in their construction and the generator connectivity to the power take-off device, the type of generator and the fluid used for useful motion generation.

Generally, direct drive generators can increase the reliability and efficiency of the WEC by reducing the components of the system and excluding interconnections between systems (such as hydraulics or gearboxes). However, owing to the low linear vertical velocities of the waves, direct drive generators have much larger sizes in comparison with fast-velocity rotational generators with the same rated power.

2.4.3.1. Attenuator

Pelamis is a device floating on the water surface, which attenuates the passing waves. The concept has been developed by Pelamis Wave Power Ltd. The structure consists of semi-submerged cylindrical bodies connected by hinged joints (Figure 6). The entire structure is oriented in a position perpendicular to the wave front. In such a way, the energy is extracted by the relative motion of the cylindrical bodies during the passing wave.

Figure 6 Pelamis (Bulatov, Perry et al. 2009)

The relative motion between the cylindrical bodies is absorbed by hydraulic rams pressurising oil. In order to smooth the output of the WEC, the pressurised oil is contained in smoothing accumulators that act as energy storage. The

energy from the pressurised oil is converted to electricity by means of hydraulic motors driving electrical generators.

Pelamis is currently in a relatively advanced stage of commercial development. It combines conventional high-velocity induction generators with hydraulic systems (Ahmed, Nishida et al. 2010). An advantage of such a system is the implementation of two already proven technologies. Despite its complexity, Pelamis has been deployed successfully and it is operating in a number of sites around Europe (Ahmed, Nishida et al. 2010).

2.4.3.2. Wave Point Absorber

Wave point absorbers are near-shore or deep water deployed WECs, which consist of a floating buoy, typically having a cylindrical or spherical shape. The buoy can be connected to a capsule containing a direct drive linear generator. The capsule can be deployed on the seabed (Figure 7b) or fixed over the surface by a supporting structure (Figure 7a).

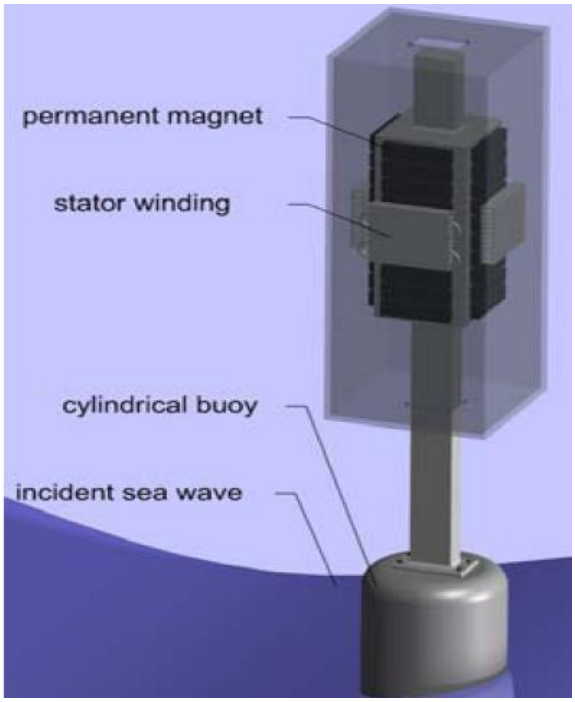

(a) Wave Point Absorber with non-flexible shaft (Kimoulakis, Kakosimos et al. 2010)

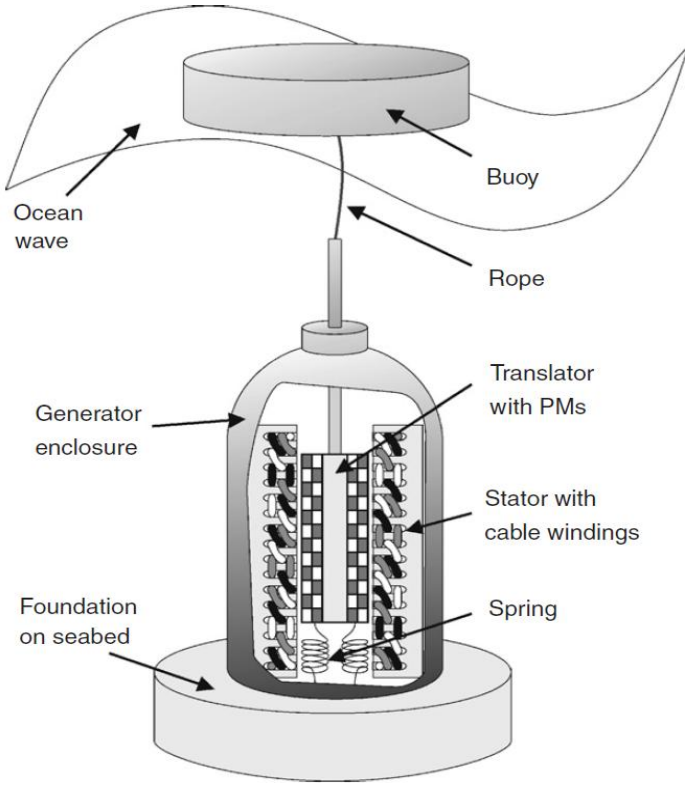

(b) Wave Point Absorber with rope (Thorburn, Leijon 2007)

Figure 7 Wave point absorbers with direct drive electrical generator

Generally, two types of construction employing either a non-flexible shaft (Figure 7a) (Kimoulakis, Kakosimos et al. 2010) or a rope (Figure 7b) (Falnes 1997, Thorburn, Leijon 2007) have been proposed for WECs having direct drive electrical generators. The design using a non-flexible shaft is simpler, but it has only one degree of freedom and the energy absorption is limited up to 50% (Evans D. 1976). Furthermore, the forces normal to the motion axis are likely to be higher when using the non-flexible shaft design due to the restriction of the motion of the translator.

Conversely, an advantage of the design using a rope is that the flexibility of the rope provides additional degrees of freedom and hence, the energy absorption can be increased. Another difference in design is given by the springs, which have to be installed in order to pull the translator back to its lowest point (Figure 7b).

Hydraulic systems have also been adopted for WECs. In Figure 8a, a system using a hose pump made of semi-elastic material is used as a power take-off system (Abigail Wacher 2010). The difference in the volume of water inside the hose between the crest and the trough of the passing wave is used to generate water flow through the hose. The water is pushed to a Pelton turbine through a hydraulic system and the turbine generates electricity directly.

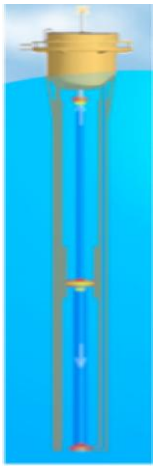

(a) AquaBuOY Wave Energy Converter (Abigail Wacher 2010)

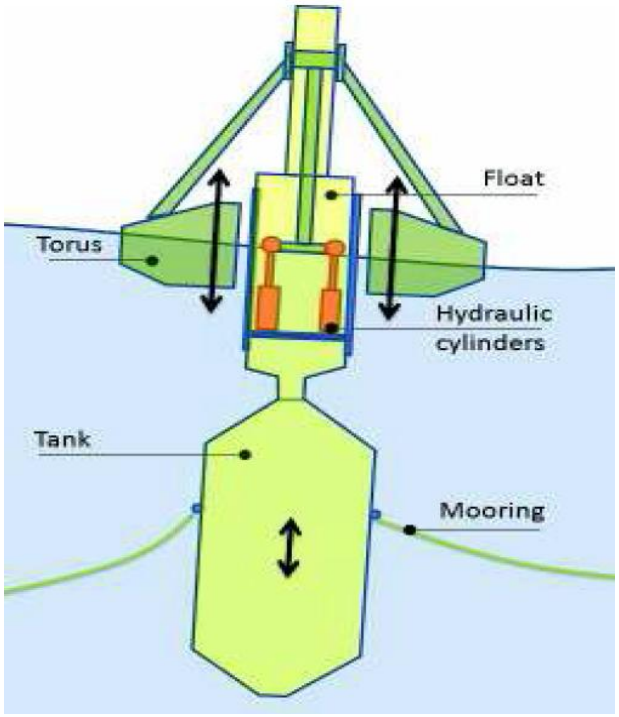

(b) Hydraulic WEC (Wavebob) (Kristof Schlemmer, Franz Fuchshumer, Norbert Böhmer, Ronan Costello, Carlos Villegas 2011)

Figure 8 Wave Point Absorbers

In Figure 8b, the Wavebob (Kristof Schlemmer, Franz Fuchshumer, Norbert Böhmer, Ronan Costello, Carlos Villegas 2011) is presented. The torque in this point absorber is extracted by hydraulic cylinders pressurising oil. This WEC

benefits from its structure, whereby the entire device is floating and there is no permanent connection to the seabed. Such a design increases the survivability of the WEC and contributes to continuous power production under extreme weather conditions.

Generally, the wave point absorbers have much simpler structure in comparison with the WECs using the conversion from a low-velocity linear motion to a high- velocity rotational one. However, owing to the low-velocity and high-torque motion of the floater, direct drive PMLGs are large.

2.4.3.3. Oscillating Wave Energy Converter

The oscillating wave energy converter (Figure 9) is a semi-submerged WEC. The device extracts energy caused by wave surges. The torque from the oscillating arm can be captured by a direct drive electrical generator (Keysan, McDonald et al. 2010) or by a fluid pump.

Figure 9 Oyster hydraulic pumps (Keysan, McDonald et al. 2010)

The fluid is transported to an onshore generator station to drive turbines. The Oyster device shown in Figure 9 has been developed by QUB and Aquamarine Power (Keysan, McDonald et al. 2010).

2.4.3.4. Oscillating Water Column

The Oscillating Water Column is a device installed on the shoreline. The basic operating principle of extracting energy is based on the difference in the water level of marine waves (Hodgins, Mueller et al. 2010, O'Sullivan, Lewis 2011, Alberdi, Amundarain et al. 2011). The waves create flow of an air in an air chamber with two ends (Figure 10). The first end is submerged and the other is open to the atmosphere. The difference in sea level during every wave creates bi-directional movement of air through the air chamber, passing the turbine blades.

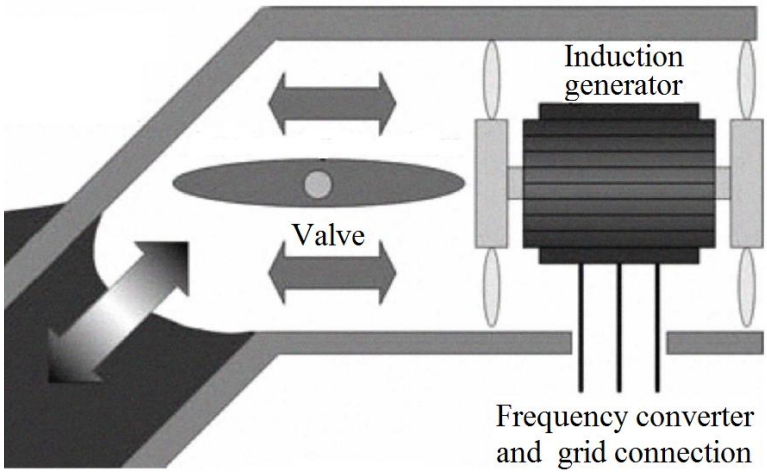

Figure 10 Oscillating Water Column (Hodgins, Mueller et al. 2010)

In order to capture the energy of the bi-directional air movement, an apparatus such as a Wells Turbine can be installed (Ormaza, Goitia et al. 2009). The Wells Turbines convert the bi-directional airflow into a unidirectional

rotational motion of the turbine shaft. Hence, an electrical generator can be connected directly to the turbine shaft. The rotational velocity of the generator depends on the wave pattern and the size of the air chamber. The airflow and the velocity of the turbine can be controlled by using the valve shown in Figure 10. Another way of controlling the electrical output and of protecting the turbine from over-spinning can be a valve that releases part of the pressure to the atmosphere.

2.4.3.5. Overtopping Device

The basic principle of the overtopping device is to collect water from the overtopping waves by means of a reflector and ramps (Figure 11). The water is collected in a reservoir above sea level and due to the gravity force, it is returned back to the sea passing through a turbine.

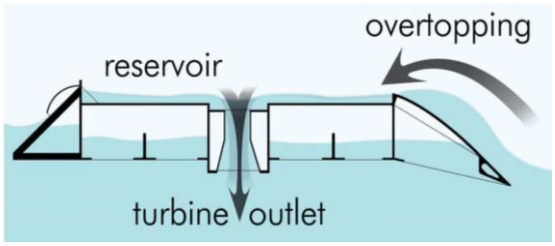

Figure 11 Overview of overtopping device (Polinder, Scuotto 2005)

The water flow through the reflector can be regulated easily and hence, the output can be stabilised. Additionally, the height and the angle of the ramps can be regulated, such that the overtopping device can work in a wide range of sea states.

The Wave Dragon is an example of an operating overtopping device. It was deployed in 2003 at Nissum Bredning (Denmark). The device has total rated

power of 20 kW, combining seven PM generator turbines and a 55 m^3 water reservoir (Polinder, Scuotto 2005).

2.4.3.6. Archimedes Wave Swing

The Archimedes Wave Swing (AWS) is an offshore WEC. Typically, the AWS is deployed around 5 – 10 km from the shore and water depth of up to 50 m (Czech, Bauer et al. 2009), due to the dependency of the output on the amplitude of the passing waves.

The AWS is a capsule anchored to on the seabed, which consists of an expandable air-filled chamber and a direct drive linear generator. The basic operating principle is based on the difference in the water pressure over the length of every wave (Figure 12).

When the crest of the wave passes the AWS, the air in the air-chamber is pressurised. After the crest passes the AWS, the pressure inside the chamber is reduced in conjunction with the lower water pressure and thus, the air in the chamber expands. As a result, only one degree of freedom can be achieved with the AWS.

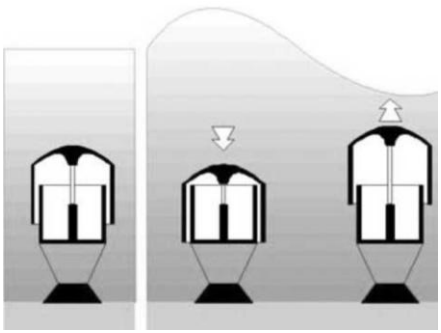

Figure 12 Archimedes Wave Swing (Polinder, Damen et al. 2004)

The design of the AWS can lead to great high robustness and security owing to the fully submerged body and the absence of rope connections.

2.4.3.7. Interproject Sweden Buoy

A schematic diagram of the Interproject Sweden Buoy (IPS) is shown in Figure 13. The device comprises a float and a submerged cylinder.

A rod is connected to a piston inside the cylinder. The water column in the cylinder fixes the piston, forcing it to move with it. The relative motion of the float and the rod can be used to generate electric power.

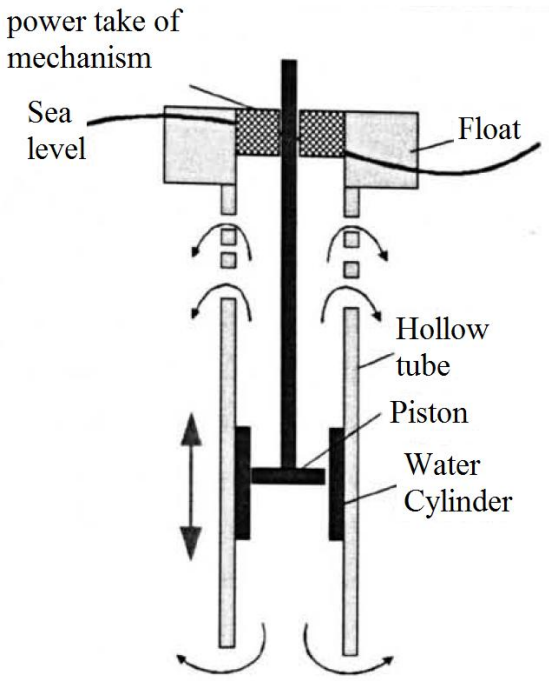

Figure 13 Operational principle of IPS (Taylor, Mackay 2001)

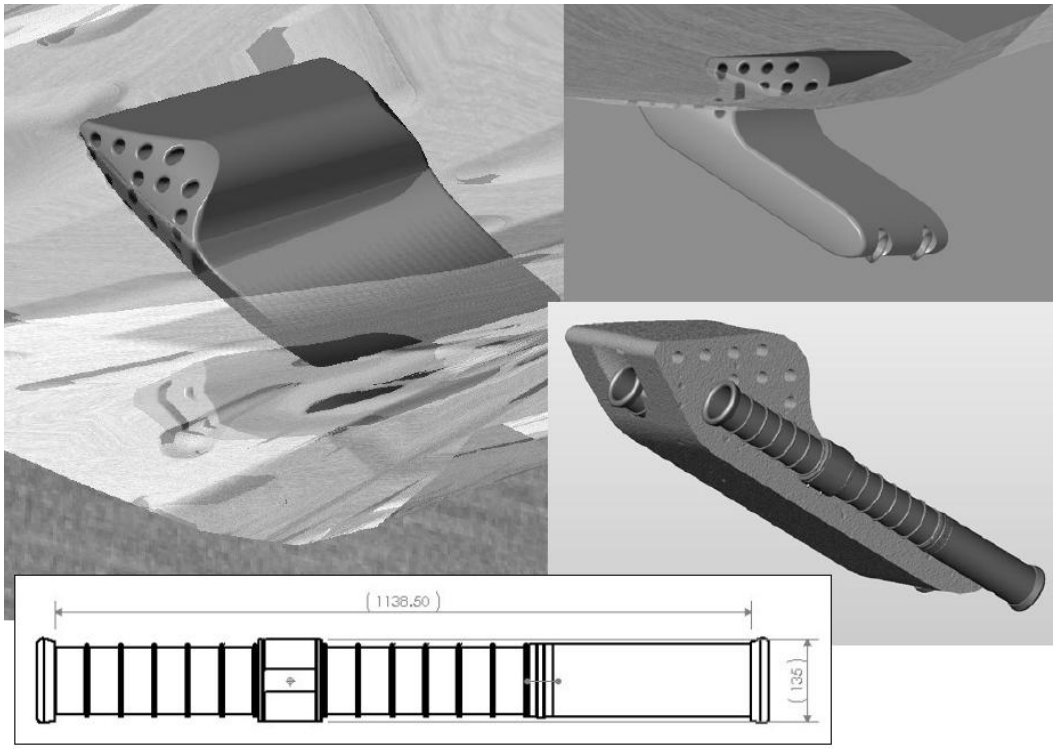

Figure 14 Overview of IPS (Taylor, Mackay)

This motion can be converted to electricity by a direct drive linear generator or a fluid pump-turbine system connected to a shore-based rotational generator (Taylor, Mackay 2001). A view of the entire body of the IPS is shown in Figure 14.

2.5. Direct Drive Wave Energy Converter

Wave energy converter is a general title for devices that convert the kinetic energy of marine waves to electricity. The investigated linear generators in this thesis are designed with the presumption that they will be driven by a floating buoy on the water surface (Figure 15), or installed in an Archimedes Wave Swing (Prado, Polinder 2011).

The buoy can be connected to the linear generator via either a non-flexible shaft or a flexible rope. The design of a WEC using a non-flexible shaft is

described in (Yang G., Chun-yang et al. 2003) and (Li, Bai et al. 2010). In this design the buoy and the generator are installed on the same shaft, and therefore they will have the same motion pattern.

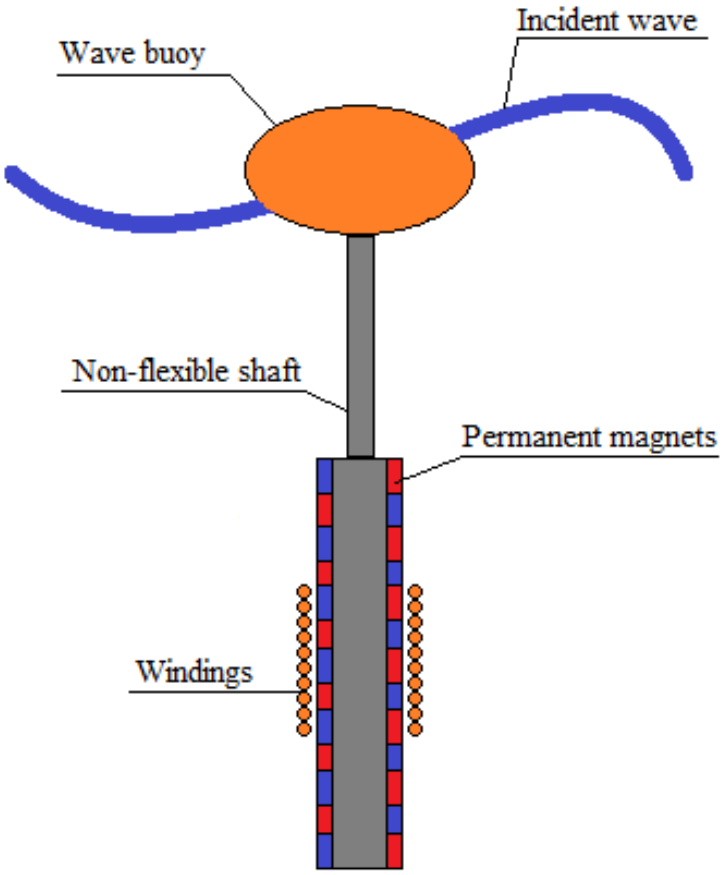

Figure 15 Overall structure of direct drive WEC using non-flexible shaft

In both of the above cases, due to the direct coupling of the power take-off device and the generator, the generated voltage and the electrical frequency are in direct ratio with the translator's velocity (Polinder, Slootweg et al. 2003). As a result, large fluctuations in the output voltage and in the electrical frequency are observed during normal operation of the WEC. In order to stabilise the fluctuations, a power electronics converter and energy storage can be installed between the generator and the electrical grid (Yang G., Chun-yang et al. 2003).

Generally, continuous operation of electro-magnetic machines depends on the forces acting on the bearings. A calculation of the forces is interesting from many perspectives and is an important parameter for studying several operational aspects, such as the generator bearing system, the buoy line forces and the mechanical stress and fatigue in the supporting structure. Additionally, the magnetic forces can produce sound emissions (i.e., underwater noise).

The direct drive WECs has several advantages over hydraulic systems such as the simple design, which has the potential to lead to high robustness of the WEC and therefore, a reduction in maintenance costs. However, at present, there are several challenges associated with direct drive linear machines that restrict the development of the technology. This thesis is concerned with several important parameters (cogging forces and output electrical power) that need to be addressed to increase the commercial success of direct drive WECs.

2.6. Generator Technologies for Direct Drive Systems

Marine wave energy is currently seen as a renewable energy source of huge potential (Tavana 2009). Some of the main requirements for offshore WECs are reliability and robustness. A WEC using a linear generator coupled directly by a prime mover is a promising solution for marine energy harvesting owing to its design simplicity. Furthermore, the simplification implied by the use of direct drive technology has the potential to exclude interface systems, transforming the linear motion of the floater to a fast-velocity rotational motion. In this chapter, the current technologies for linear direct drive generator designs for WECs are reviewed and their advantages and disadvantages outlined.

2.6.1. Linear Induction Machine

The absence of slip-rings and collectors in the assembly of an induction machine reduces the production and maintenance costs in comparison with other machines (Wells, Chapman et al. 2001). The operation of linear induction machines involves an external source of winding excitation. This excitation can be provided by the electrical grid or by a reactive power source (SVC, STATCOM). The armature currents (three-phase with ±120 degree phase shift) create a translational magnetic field in the air gap between the stator and the translator. This field generates currents in the translator's cage. Hence, the combination of the translating magnetic field generated by the stator and the translator's induced currents generates torque in the translator. The translator starts to translate with a lower velocity than the velocity of the magnetic field of the stator. This kind of operation is also known as motor mode. The machine starts to operate in generator mode when the translating velocity of the translator exceeds the velocity of the induced magnetic field (an external torque is applied). A disadvantage of this machine is that the windings require an external source of excitation.

2.6.2. Linear Field Wound Synchronous Machine

The Field Wound Synchronous Machine (FWSM) is an electrical machine with an externally excited field winding. The magnetic fields generated by the stator currents and the translator do not go out of phase under normal operation of the machine. The linear FWSM has been proposed for WECs (Vining, Lipo et al. 2009, Vining, Lipo et al. 2010). The presented design has a translator

located between two magnetic cores in a double-fed linear machine (Figure 16a).

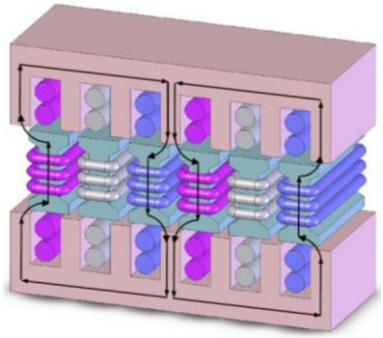

(a) Linear Field Wound Synchronous Machine (Vining, Lipo et al. 2009)

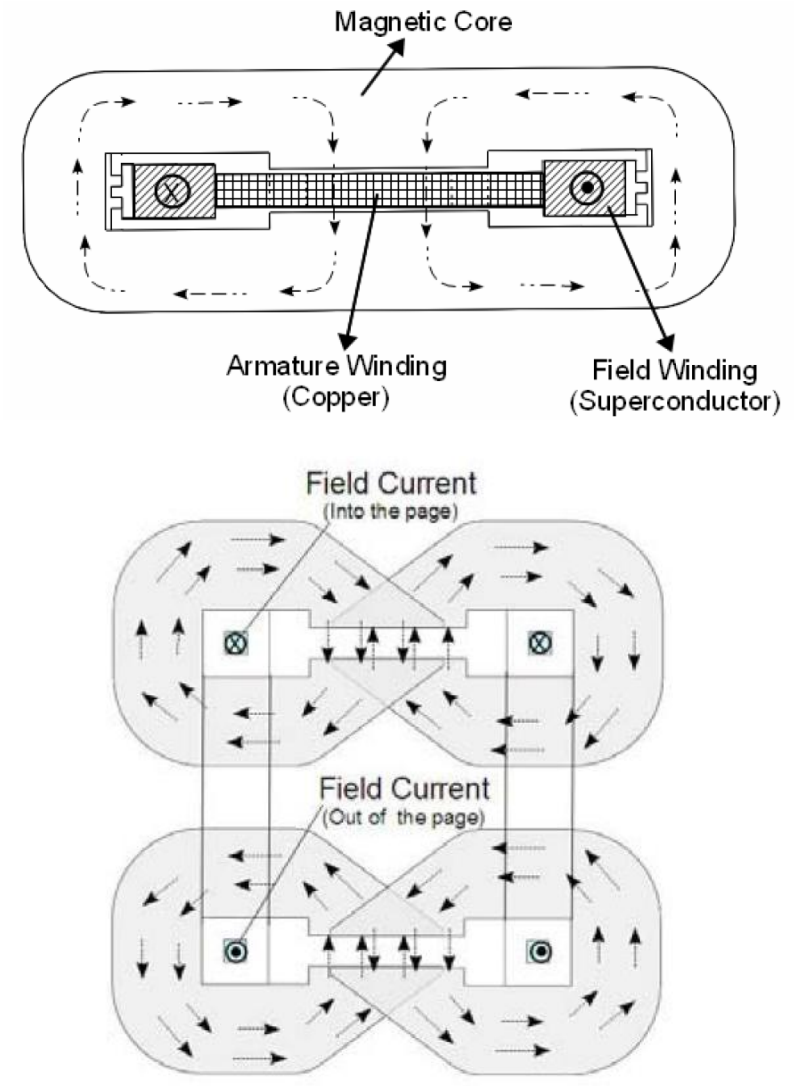

(b) Linear Superconducting Homopolar Machine (Keysan, Mueller 2012)

Figure 16 Linear Field Wound Synchronous Machines

FWSMs do not have permanent magnets in their assembly. Therefore, the cogging forces will appear only when the excitation winding is energised. An advantage of the machine, suggested in (Vining, Lipo et al. 2009), is the switching between different operating modes: synchronous (DC-supplied translator), asynchronous (AC-supplied translator) and short-circuited squirrel cage.

A control technique for the double-fed linear machine is proposed in (Vining, Lipo et al. 2010). The control is based on tracking the velocity and maintaining the orthogonality between the stator and the translator's magnetic flux. Similarly, the study (Vining, Lipo et al. 2010) reports the reduction of the number of three-phase inverters used in the grid integration system to only one. A comparison is made with the double fed induction machine, which requires two inverters. On the other hand, there exist potential problems associated with the electrical connections, the air gap tolerance and the linear bearings of the wound field translator (Guinevere, Lipo et al. 2010).

Another field winding air-cored homopolar machine is presented in (Keysan, Mueller 2012). The generator has a stationary superconducting coil, which simplifies the cooling system and eliminates transient forces on the superconducting coil (Figure 16b).

2.6.3. Transverse Flux Machine

The Transverse Flux Machine (TFM) is shown in Figure 17 and Figure 18. The design of the machine can vary but the main operational principle remains the same (Mueller 2002, Hasanien, Abd-Rabou et al. 2010, Schutte, Strauss 2010, Zou, Wang et al. 2011). In a TFM, the flux is provided by PMs. The

magnets are translating between sets of magnetic cores providing different paths of magnetic flux. During translation, the flux changes its direction with frequency proportional to the translational velocity.

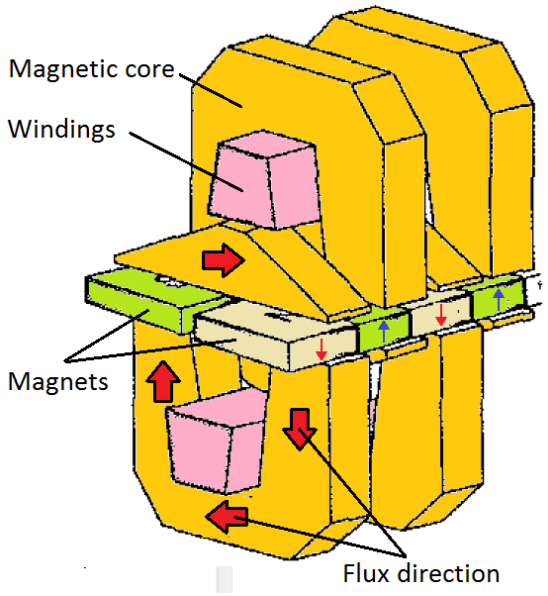

Figure 17 TFM with surface mounted magnets (Mueller 2002)

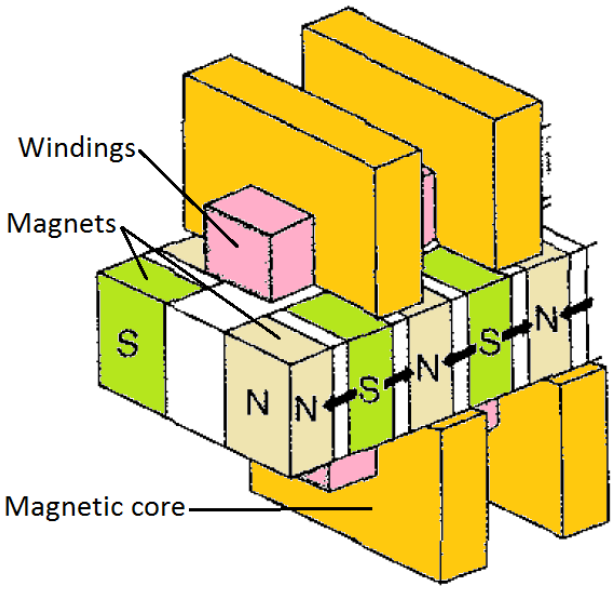

Figure 18 TFM with buried magnets (Mueller 2002)

The complicated assembly of the machine requires a high number of individual elements to support the flux flowing though the separated magnetic

C-cores surrounding the windings. Therefore, problems related to the reliability of the supporting structure maintaining high cogging forces (generating vibrations) can be expected. Another problem related to the supporting structure maintaining the constant pulling magnetic forces generated between the magnets and the magnetic cores also occurs. Furthermore, complications during the fitting of the high number of individual elements are expected during the manufacture of the machine.

The electric loading of the machine can be approximated as:

$$K_e = \frac{H_c t_h}{w_w} \tag{2.1}$$

where H_c is the coercivity, t_h is the magnet thickness and w_w is the magnet width in the direction of the displacement (Mueller 2002). The flux density in the air gap can be given as:

$$B = \frac{N I_w}{2} \frac{\mu_0}{\left(2g_a + \frac{t_h}{\mu_r}\right)} \tag{2.2}$$

where N is the number of winding turns, I_w is the winding current, μ_0 is air permeability and g_a is the air gap length. Formula (2.2) does not take into account the saturation in the iron cores. Similarly, the fringing effect has been ignored with the assumption that the magnets' magneto-motive force is directly proportional to their thickness.

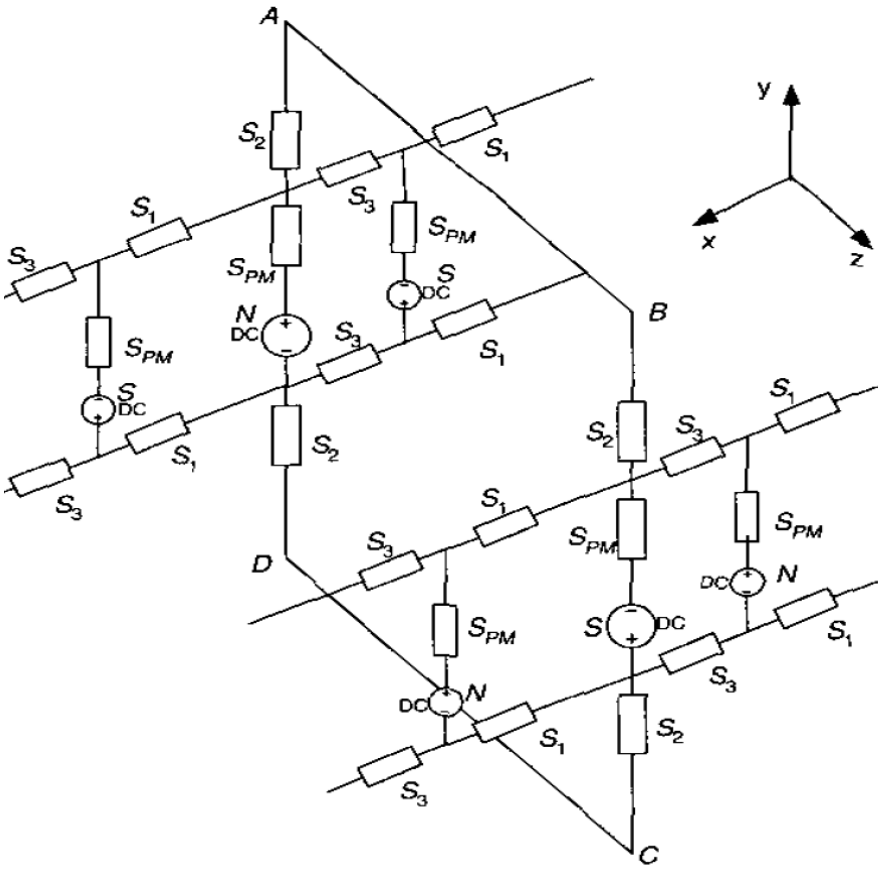

Figure 19 Section of TFM magnetic equivalent circuit (Mueller 2002)

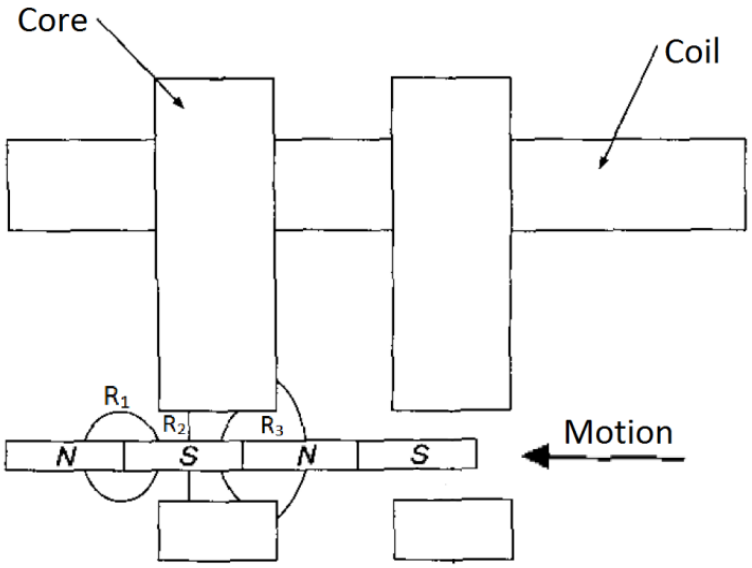

Figure 20 Magnetic reluctances in TFM (Mueller 2002)

A three dimensional equivalent circuit is shown in Figure 19. The figure shows a common section of a single-sided linear TFM, in which the main flux

path follows within the *A-B-C-D* contour. S_{PM} is the reluctance of the permanent magnets, S_1 is the reluctance occurring between neighbouring magnets, S_2 represents the reluctance in the air gap and S_3 is the reluctance occurring between the neighbouring magnets passing the magnetic core. Similarly, in this model, it is assumed that the iron has zero magnetic reluctance.

The EMF can be calculated by applying Faraday's law:

$$V_e = N \frac{d\Phi}{dx_t} \frac{dx_t}{dt} \tag{2.3}$$

where x_t is the position of the translator and Φ is the flux density.

2.6.4. Vernier Hybrid Machine

The Vernier Hybrid Machine (VHM) is a concept described in (Mueller, Baker 2003, Spooner, Haydock 2003). Both the windings and the PMs are mounted on the stator of the machine. The translator is made from silicon steel sheets and it provides the path for the magnetic flux.

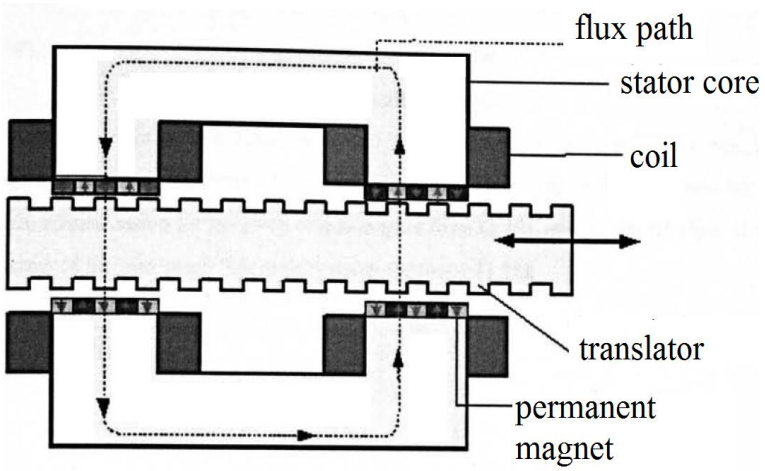

Figure 21 Vernier Hybrid Machine (Baker 2003)

The translator teeth are aligned with the magnets in a way that provides low reluctance paths for the magnets with the same magnetisation direction.

As a result, the total flux is provided by the magnets having anti-clockwise magnetising direction at the position shown in Figure 21 and clockwise direction when the translator is displaced by a distance equal to one tooth. This arrangement allows a rapid flux reversal over a short distance and therefore, higher electrical frequency compared with the displacement frequency.

2.6.5. Longitudinal Flux Permanent Magnet Machine

The Longitudinal Flux Permanent Magnet machine is a linear generator in which the windings' excitation is provided by the PMs that are usually mounted on the translator and the windings mounted in the stator (Ghita, Chirila et al. 2008). The purpose of this arrangement is to avoid the use of hardware such as cables or slip lines to transfer the electrical power from the windings.

Several designs adopting different magnetisation directions and flux paths have been proposed in (Wang, Jewell et al. 1999, Faiz, Ebrahimi-salary et al. 2009, Shibaike, Sanada et al. 2007). The magnetisation of the permanent magnets, affects the magnetic losses, the induced voltage and the output power of the PMLG. An analytical description for tubular generators for load and no-load performance has been done and verified by FEM in (Wang, Jewell et al. 1999). A cylindrical coordinate system has been used to describe the magnetisation topologies named as radial, axial and Halbach. The schematic two-dimensional views of the three topologies are shown in Figure 22.

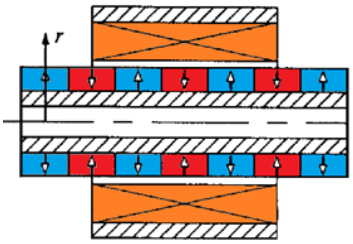

(a) Radial Magnetisation

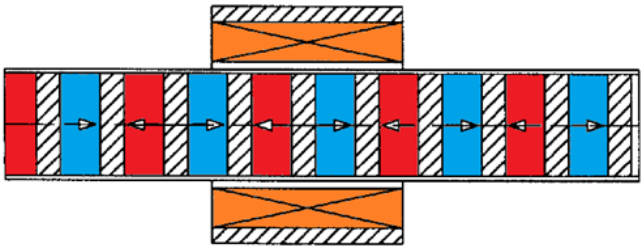

(b) Axial Magnetisation

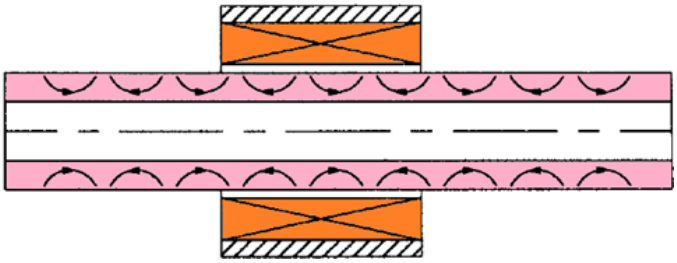

(c) Halbach Magnetisation

Figure 22 Tubular linear generator topologies (Wang, Jewell et al. 1999)

In (Shibaike, Sanada et al. 2007), comparisons among surface magnet, inset magnet and buried magnet structures have also been made, examining the influence of different magnetisation types upon the efficiency, output power, iron losses and copper losses.

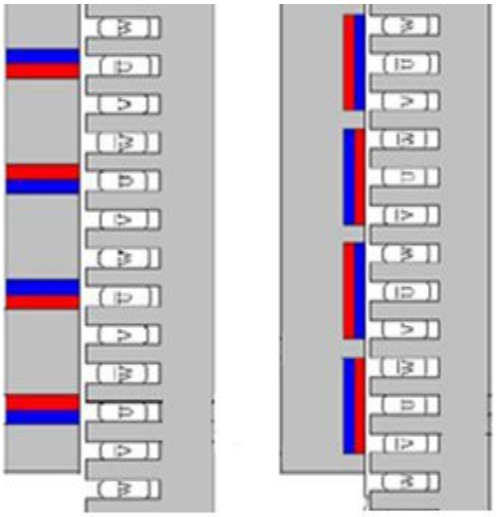

(a) (b)

Figure 23 Magnet topologies, (a) inset structure, (b) buried structure (Shibaike, Sanada et al. 2007)

The results presented in (Shibaike, Sanada et al. 2007) reveal that the buried magnet structure has higher output power and efficiency. However, higher iron and copper losses are reported for the buried structure.

2.6.6. Discussion

A synthesis of the characteristics and results reported in the literature for different types of linear generators have been done. It is difficult to outline the best design owing to the different sizes of the machines in the table. However, based on the power output and the material cost, the PMLG with stator iron can be selected as a good solution. On the other hand, the maintenance cost has not been taken into account in the comparison.

The biggest disadvantage of the FWSM is the requirement of external excitation. Some of the options to solve this issue are capacitors or grid supplied reactive power.

The design complexity is the main issue confronting the variable reluctance generators. Owing to complicated design that involves a high number of elements, the assembly cost is expected to be high. Furthermore, such a complex structure is likely to be affected by vibrations, which could cause structural damage.

The VHM is an attractive solution due to the small volume of PM materials used in the assembly. However, relatively high cogging forces have been reported (Mueller, Baker 2003).

2.7. Structures for Direct Drive Linear Permanent Magnet Generators

Owing to the nature of marine waves and the high power output requirements, direct drive linear generators are large. Such structures involve high volumes of steel and PM material causing high magnetic forces. Consequently, these forces affect the bearings and generate noise, vibrations and unwanted cogging forces.

In this section, the basic characteristics of the different structures proposed for direct drive generators are reviewed. Furthermore, cogging forces are explained and the current force reduction techniques presented.

2.7.1. Flat Structure

Generators with a flat structure are presented and analysed in (Ahn, Lee et al. 2008, Hodgins, Keysan et al. 2012, Shibaike, Sanada et al. 2007). The generator's windings can be energised from two sets of PMs (Thorburn, Leijon

2007) sandwiching the windings (Figure 24), or from a single side of PMs. By using the flat structure, the sides of the generator remain free; therefore, installing and maintaining the bearings might be easier in comparison with other kinds of PMLGs. In (Hodgins, Keysan et al. 2012), a design using multiple flat sections assembled in one body has been proposed. This assembly allows a range of power levels to be produced from the same generator by using a different number of flat sections stacked together. Similarly, the structure can reduce the manufacturing cost and increase robustness.

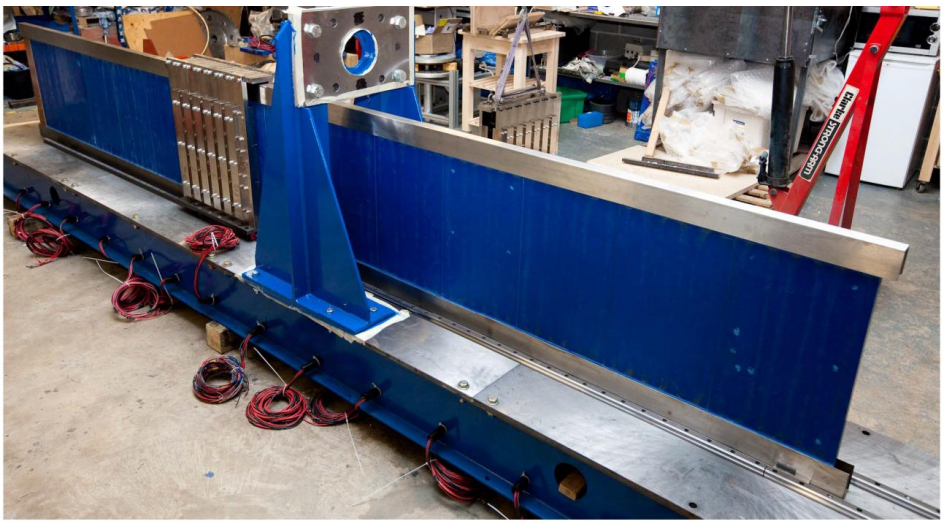

Figure 24 Flat PMLG (Hodgins, Keysan et al. 2010)

Another benefit of the PMLG proposed in (Hodgins, Keysan et al. 2012) is the possibility of the isolation of faulty sections during normal operation. This feature reduces the maintenance cost and it will contribute to higher maintenance flexibility.

An investigation of double-sided PMLGs for wave energy harvesting has been conducted in (Garcia-Alzorriz, Grau et al. 2011) and (Joseph, Cronje 2007).

2.7.2. Multiple Side Structure

The main idea of multiple-sided PMLG structures is to reduce the attraction forces acting on the bearings by opposing them. As a result, a cancellation effect of the attraction forces can be achieved. Another benefit is that the length of copper wire in the windings and hence, the power output of the PMLG can be increased.

The PMLGs' windings are assembled by coils. These coils could be physically separated in the generator structure and connected externally, such as in the model shown in Figure 25a. Another distribution technique involves the coils passing all sides of the multi-sided machine, such as in the model shown in Figure 25b. In this case the coils are connecting the sides of the generator.

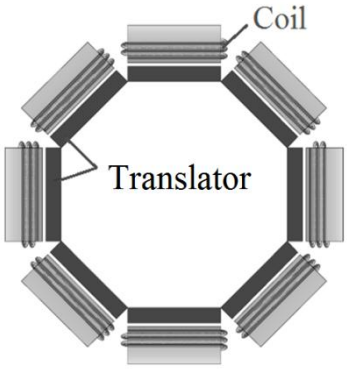

(a) Windings passing a single side

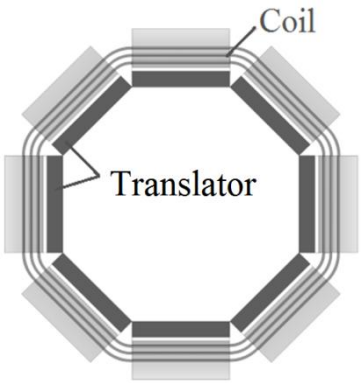

(b) Windings passing all sides

Figure 25 Multiple sides PMLG (Ivanova, Agren et al. 2005)

A drawback of the PMLG design shown in Figure 25b is the potential difficulty in disassembling the sides of the generator during maintenance. Keeping the sides of the generator separated makes disassembly easier. However, higher extra ohmic losses are caused by the extra cable length used. In general, the manufacturing cost of multi-sided generators is likely to be higher than that of double-sided generators due to the complexity of the construction (Ivanova, Agren et al. 2005).

2.7.3. Tubular Structure

The tubular structure of a PMLG can be seen in Figure 26. An advantage of the tubular design is the reduction of the magnetic forces experienced at the edges between the magnetic core and the PMs.

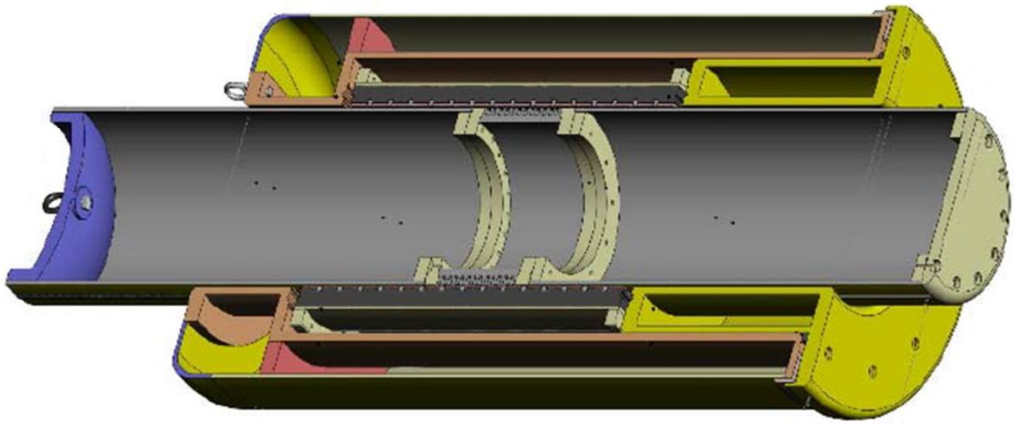

Figure 26 Tubular PMLG (Prudell, Stoddard et al. 2010)

It has been indicated that the tubular structure is most applicable for PMLGs because of the use of the simplest linear bearings among all the linear machines shown in (Szabo, Oprea et al. 2007). Tubular PMLGs have been investigated in (Prudell, Stoddard et al. 2010, Minciunescu, Scortescu et al. 2010, Pirisi, Mussetta et al. 2010). One of the main benefits of the tubular design is the theoretical elimination of radial forces in an ideal tubular PMLG. However, due to eccentricities in construction and radial movements across the air gap, total cancellation cannot be achieved (Prudell, Stoddard et al. 2010). Moreover, (Bracco, Giorcelli et al. 2011, van Zyl, Jeans et al. 1999) indicated that tubular machines achieve the highest power among linear machines. However, problems associated with the assembly and the dynamics of tubular PMLGs have been reported in (Minciunescu, Scortescu et al. 2010).

2.7.4. Type of Magnetic Core

2.7.4.1. Iron–cored Linear Generators

Iron-cored machines are used because of the low magnetic reluctance of the silicon steel. Furthermore, in order to decrease the losses and to increase the permeability of the magnetic core, laminated silicon steel sheets are used widely in the assembly of the iron-cored machines. The highest magnetic reluctance in the iron-cored magnetic circuit is caused by the air gap between the stator and the translator.

As the air gap is the region with the highest magnetic reluctance in the iron-cored machines, it has significant influence on the generator`s output. Minimising the air gap tolerance reduces the total magnetic reluctance. However, high magnetic forces have been reported between the PMs and the silicon steel. Therefore, maintaining a low air gap tolerance in combination with desirable high output power is a challenge (Faiz, Ebrahimi-salary et al. 2009).

2.7.4.2. Air-cored Linear Generators

Air-cored generators have been proposed and investigated in (Vermaak, Kamper 2010, Hodgins, Keysan et al. 2012, Liu, Lin et al. 2010, Baker, Mueller et al. 2004). Eliminating the high static magnetic forces between the stator and the translator can be achieved by removing the iron from one of them. However, the elimination of the iron increases the total reluctance of the magnetic circuit significantly. As a result, the induced voltage is much lower in comparison with PMLGs using iron in their magnetic cores (Figure 27).

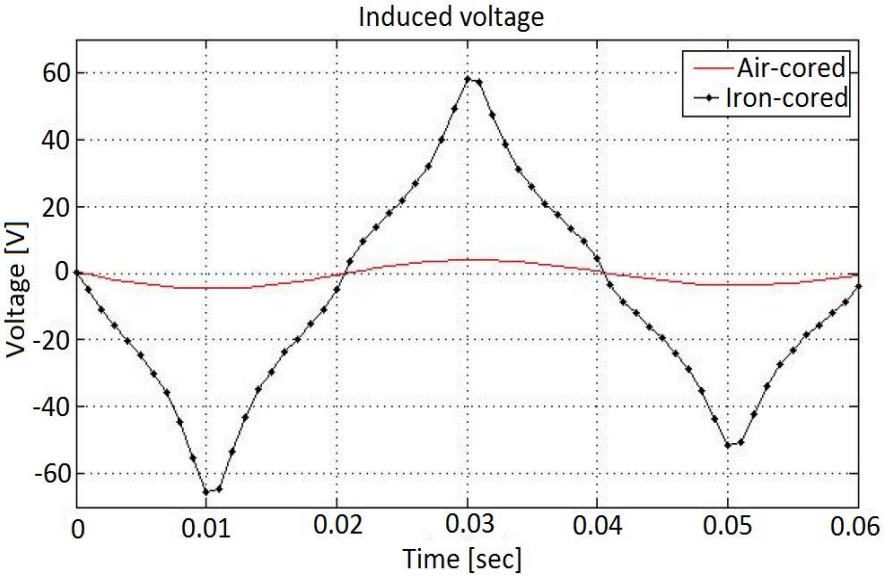

Figure 27 Induced voltage for iron-cored and air-cored generator (Oprea, Martis et al. 2010)

In order to achieve similar electrical output as the iron-cored PMLGs, the volume of the PMs has to be increased. Such an increase would also raise the price of the machine. However, due to the force reduction in air-cored generators, the cost of maintenance and the price of the bearing system are likely to be reduced substantially (McDonald, Crozier et al. 2009).

2.7.5. Number of Phases of Linear Generators

The number of phases in the PMLGs depends on the design and the connection among the coils (sections) in the windings. If the total length of the generator coils is shorter than the length of the PMs (Prudell, Stoddard et al. 2010), the generator is referred to as “short stator”. The short stator configuration benefits because all the coils are energised and therefore, they generate voltage during the displacement of the PMs.

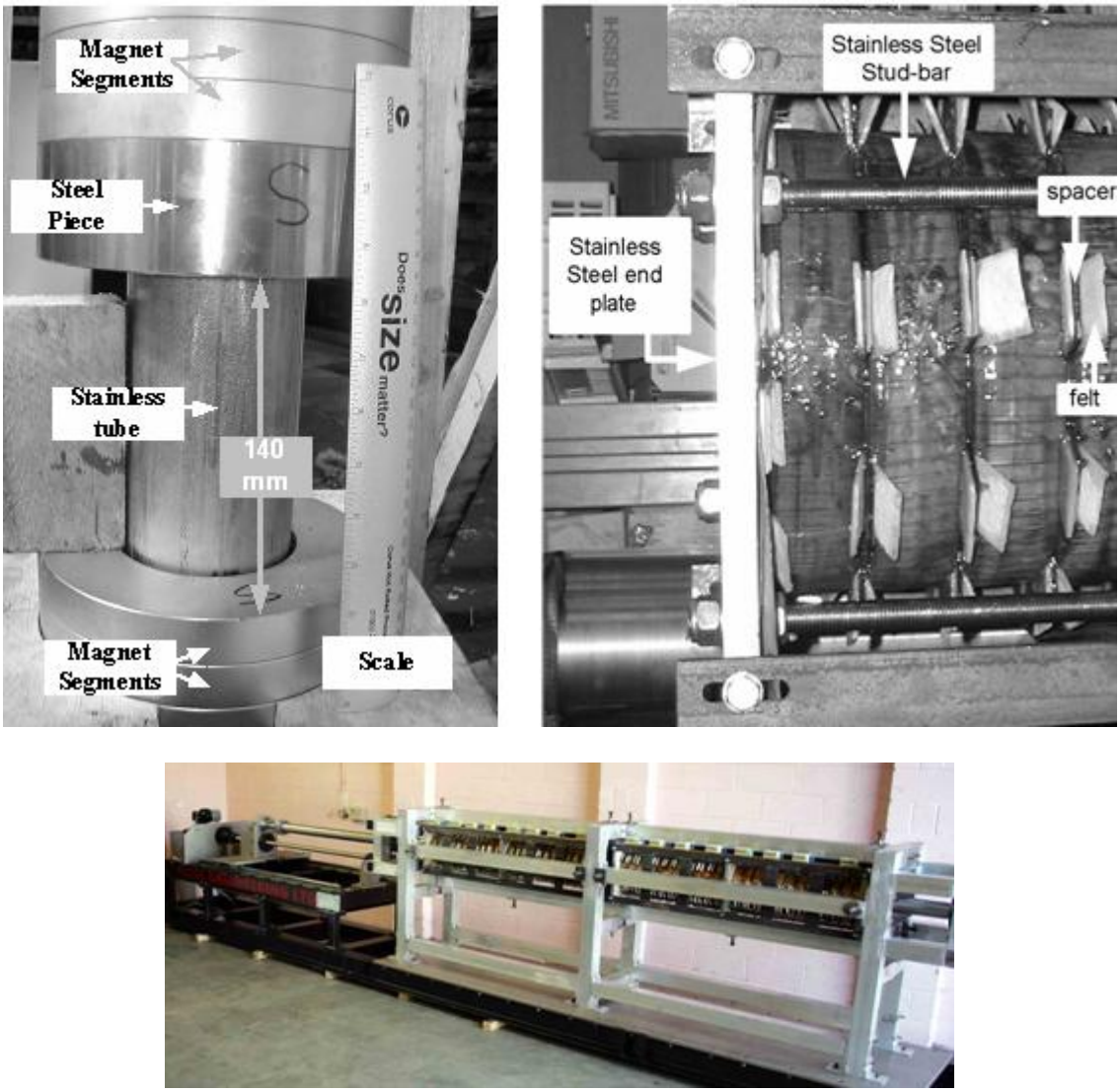

Figure 28 Long Stator design proposed in (Baker, Mueller et al. 2007)

Another PMLG design has been proposed in (Baker, Mueller et al. 2007) with is tubular PMLG using 48 coils installed in the stator (Figure 28). The total length of the coils (stator) is longer than the total length of the PMs. In the thesis, this topology and coil arrangement is referred to as “long stator”. In the long stator configuration, not all the coils are covered by the PMs and hence, not all coils generate voltage during the translation of the PMs.

To increase the generated voltage, the coils can be connected in series (Figure 29) but to avoid the impedance of the inactive coils’, they have to be insulated from the electrical circuit. An inactive coil bypassing system has been

proposed in (Ran, Tavner et al. 2006). The system uses a bypassing pair of thyristors connected in parallel with every coil. Because of the current passing each thyristor switch, high thermal losses are registered in the thyristors (Ran, Mueller et al. 2011). As a result, a new system that reduces the thermal losses has been proposed in (Ran, Mueller et al. 2011). The new system adopts individual rectification on every coil, where all the coils are connected to a low-voltage DC bus after rectification. A drawback of this system is the high number of components.

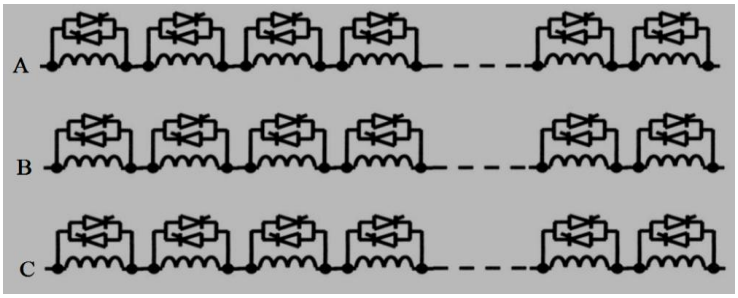

Figure 29 Inactive coil bypass system proposed in (Ran, Tavner et al. 2006)

In general, the long stator generator concept reduces the amount of PM material used in the assembly, because the entire flux established by the PMs crosses part of the coils at any time of operation. Therefore, it can be concluded that the magnets are used more efficiently in comparison with the short stator PMLG design proposed in (Prudell, Stoddard et al. 2010).

Another flat long stator design, proposed in (Hodgins, Keysan et al. 2012), is simulated and tested for a flat air-cored PMLG called C-GEN. The structure has several advantages over existing generators:

- air-cored design leads to magnetic force reduction and elimination of cogging forces
- reduction of the PM material used in the generator

- improved bearing access
- due to high number of copper coils, potential problems with coils overheating are reduced
- coil failure does not result in significant reduction of energy harvesting.

On the other hand, the long stator generator also has several drawbacks:

- a complicated winding arrangement that requires the design of a special grid integration system.

Despite the drawbacks, the author believes that such a design has the potential to decrease the overall price of a WEC system owing to the lower volume of PMs and the reduction of the magnetic forces, which leads to longer lifetime of the bearing in comparison with iron-cored PMLGs.

2.7.6. Forces in Linear Machines

With vertical velocities of marine waves varying between 0 and 2 m/s and the desire for high energy harvesting, the size of PMLG can be large (Figure 30).

Figure 30 Direct drive PMLG in AWS compared with human size (Polinder, Mueller et al. 2007)

Furthermore, in order to minimise the total reluctance of the magnetic circuit, the air gap has to be as small as possible. On the other hand, reduction of the air gap increases the magnetic attraction between the magnets and the steel core.

2.7.6.1. Cogging forces

Cogging forces are caused by the interaction between the magnetic field of the PMs and the iron core of the PMLG. Such interaction has a latching effect on the translator. Moreover, the cogging forces are independent from the magnetic fields generated by the armature currents (Bascetta, Magnani et al. 2007). A visualisation of the cogging forces is shown in Figure 31.

The cogging forces try to align the magnets with the steel core in a position that minimises the total reluctance of the magnetic circuit. When a minimum

reluctance path is established at a certain position, the magnetic forces oppose any external force trying change this position (position on the Y-axis). The cogging forces generate both vibrations that have to be maintained by the bearings and the supporting structure and unwanted noise and latching of the generator's translator (Prudell, Stoddard et al. 2010, Ashabani, Milimonfared et al. 2008, Shabani, Milimonfared et al. 2007).

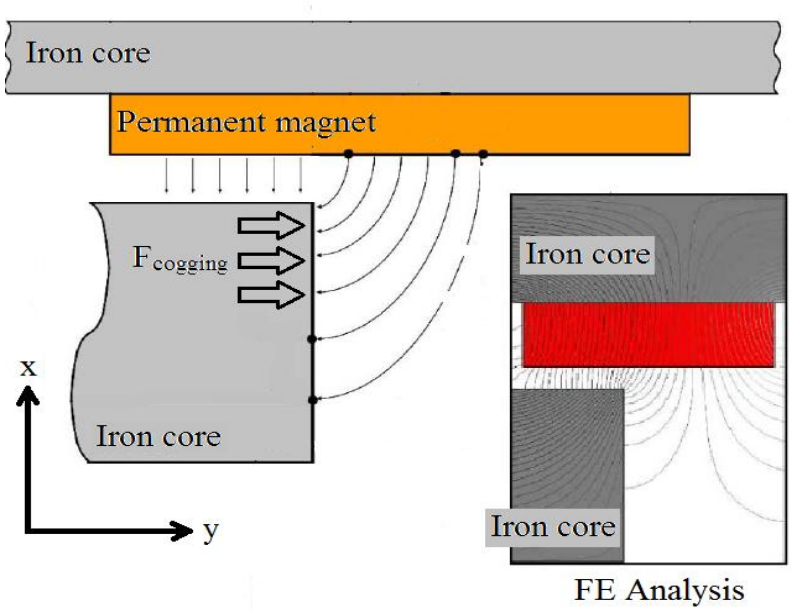

Figure 31 Cogging forces (Choi, Baek 2009)

Another source of magnetic force is at the longitudinal ends of the linear machine. The large difference in the magnetic reluctance, between the steel and the air at the end areas of the generator accumulates magnetic forces. These forces try to maintain the position with the lowest magnetic reluctance (Choi, Baek 2009).

2.7.6.2. Reduction of the Cogging forces

The reduction of the cogging forces has been investigated in recent years and several reduction techniques have been proposed (Faiz, Ebrahimi-salary et

al. 2009, Kimoulakis, Kakosimos et al. 2011, Faiz, Ebrahimi-Salari et al. 2010, Li, Bai et al. 2009, Kimoulakis, Kladas et al. 2009, Ahn, Lee et al. 2008).

One technique for reducing the cogging forces is skewing of the PMs. The skewing angle of the magnets can be seen in Figure 32a. The skewing angle versus the axis of the shaft has a large effect on the cogging force. By reducing the angle (Figure 32a) the cogging force curves are being displaced in such a way that the peak force is reduced. Skewing the magnets can reduce the cogging forces by up to 88% (Faiz, Ebrahimi-salary et al. 2009); however, the study does not take into account the effect of this optimisation on the output power of the machine. The cogging force resulting from the dynamic simulation of different skewing angles can be seen in Appendix A.

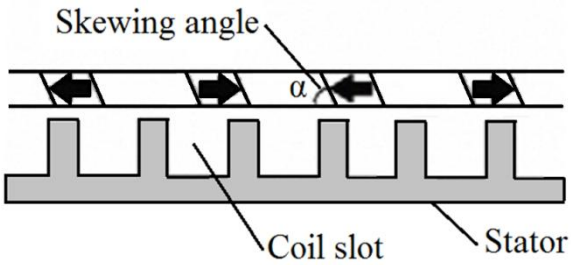

(a) Skewing angle of the magnets

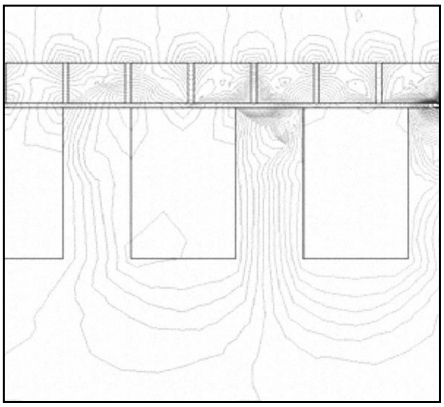

(b) Open coil slots

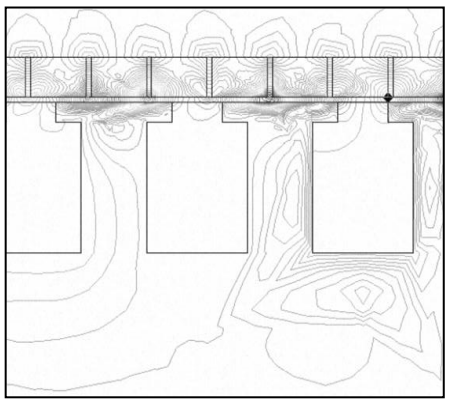

(c) Semi closed coils slots

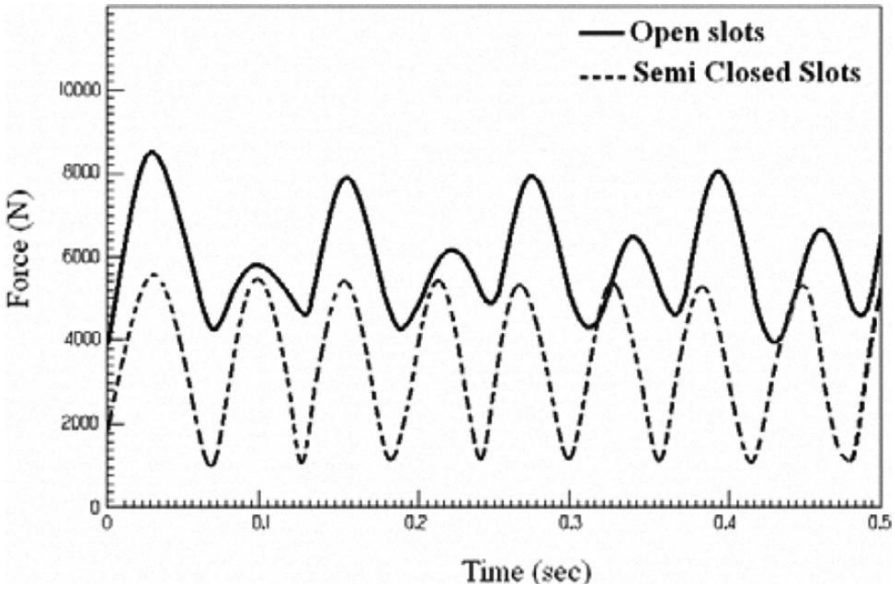

(d) Cogging torque difference for open and semi closed slots

Figure 32 Cogging force mitigation (Faiz, Ebrahimi-salary et al. 2009)

Similarly, another very effective way to decrease the cogging forces is by reducing the air regions among the teeth (Figure 32b and Figure 32c). The use of semi-closed coil slots rather than open slots can decrease the cogging force by 34% (Faiz, Ebrahimi-salary et al. 2009). The main advantage of the semi-closed slots is the reduction of the magnetic reluctance in the air gap allowing the translator to move more easily from one position with an established low magnetic reluctance to another Figure 32d.

Additionally, a comparison of PMLGs using different directions of magnetisation (axial versus radial) with regard to the cogging forces is made in (Faiz, Ebrahimi-salary et al. 2009). The study reveals a 70% reduction of the cogging forces when radial magnetised PMs are used.

An alternative reduction technique is shown in (Li, Bai et al. 2009), where the ratio between the width of the stator slots (a) and the width of the stator teeth (b) is altered (Figure 33b). Two-dimensional FEM simulations suggest a 50% reduction (Figure 33d) when a ratio of $a/b = 0.875$ is applied. This technique is achieves partial cancellation of the cogging force. However, the study does not investigate the effects on the power output caused by flux bypassing the windings over the shoes of the stator slots (red arrow in Figure 33b).

In the same article, another simulation with a four-sided PMLG was carried out. The experiment investigates the misalignment between the sides of the PMLG in Figure 33a. The results reveal no reduction in the cogging forces at constant velocity of the translator. In fact, the cogging forces peak doubled as the misalignment was applied.

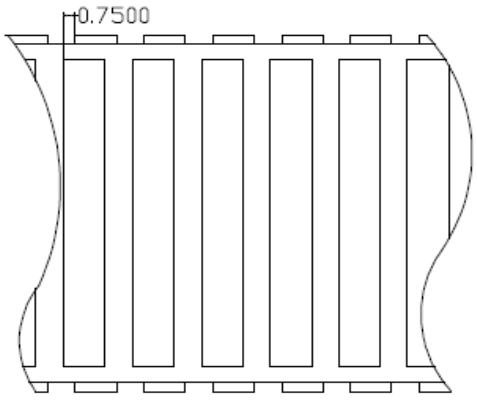

(a) Adjacent sides permanent magnets “allotopia”

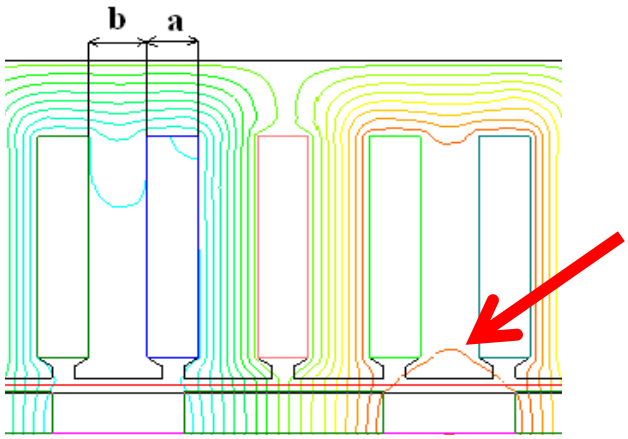

(b) Width of the stator slot (a) and the width of the stator teeth (b)

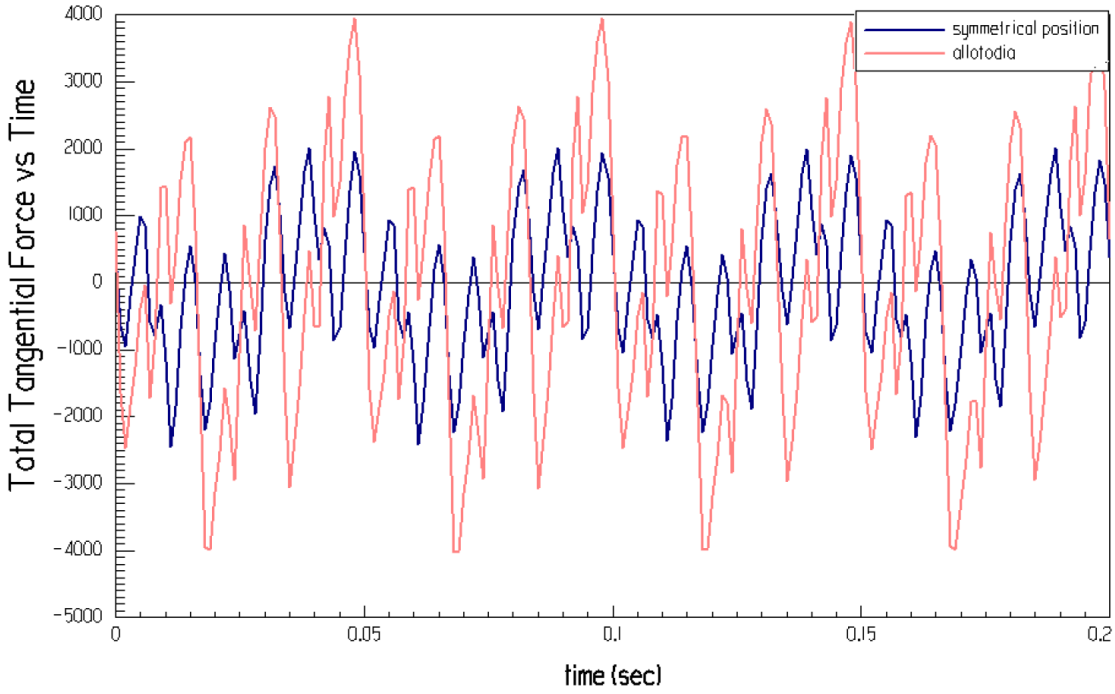

(c) Forces comparison between symmetrical pattern and allotopia

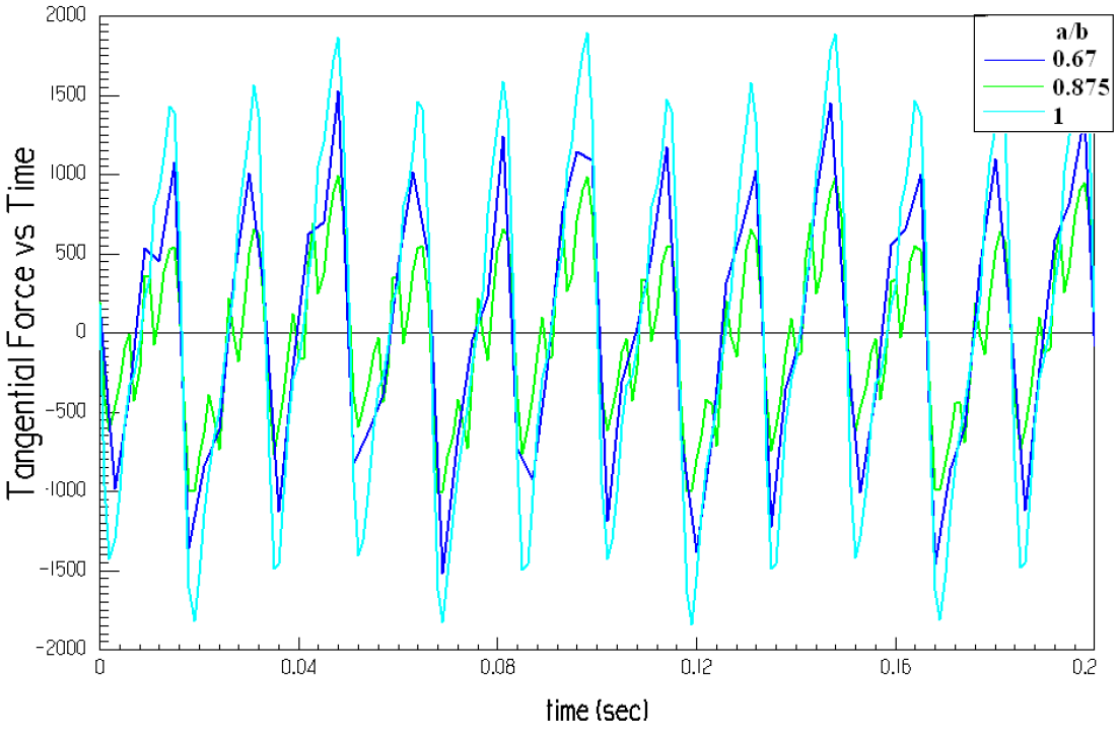

(d) Comparison between difference $\mathbf{a}/\mathbf{b}$ ratios

Figure 33 Effect of "allotopia" on the cogging forces (Li, Bai et al. 2009)

A different approach for cogging force reduction, shown in (Kimoulakis, Kladas et al. 2009), involves manipulating the profile shape of the PMs. The shapes investigated in the article are shown in Figure 34. The results are obtained by means of FEM and reveal that a bevelled bottom profile reduces the cogging forces the most.

In (Kimoulakis, Kladas et al. 2009), the optimal ratio between the pole width (W_{pole}) and the magnet width (W_{magnet}) is investigated. The simulations suggest that a ratio of $W_{magnet}/W_{magnet} = 0.7$ can reduce the cogging forces significantly.

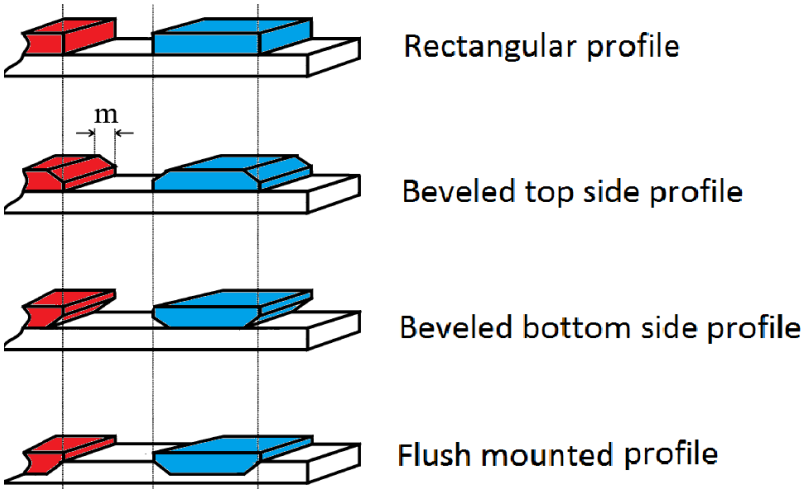

(a) Permanent magnet profile shapes

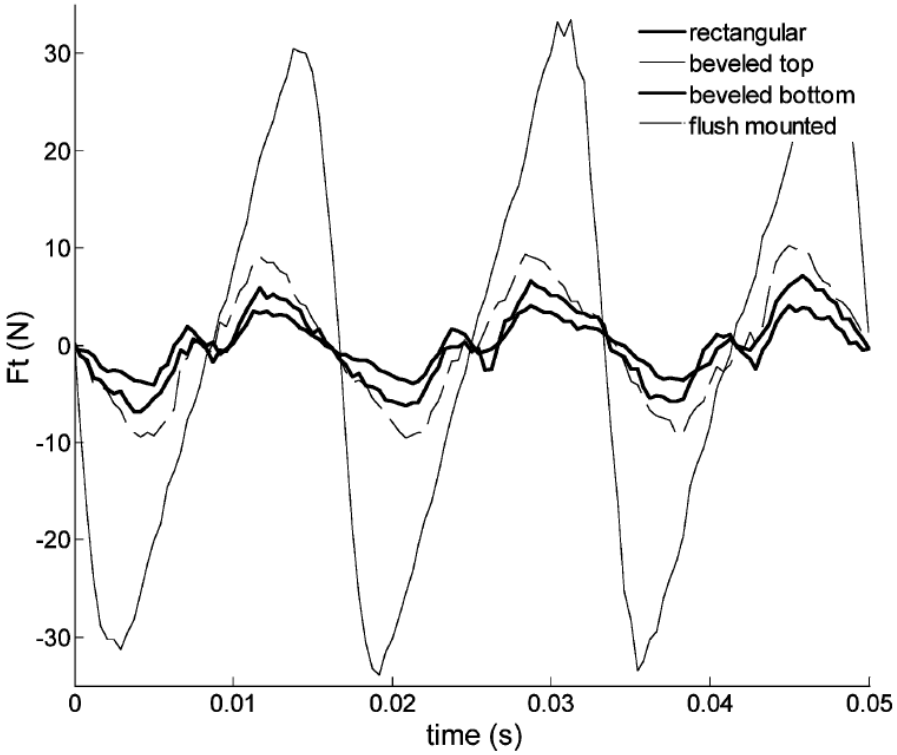

(b) Variation of cogging force among difference profile shapes

Figure 34 Permanent magnet profile shapes investigated in (Kimoulakis, Kladas et al. 2009)

Another kind of skewing of the PMs that has been proposed (Ahn, Lee et al. 2008) is shown in Figure 35. The results report a reduction of around 50% in the detent force for the skewed pattern PMLG.

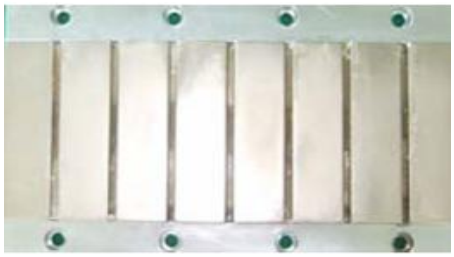

(a) Basic pattern

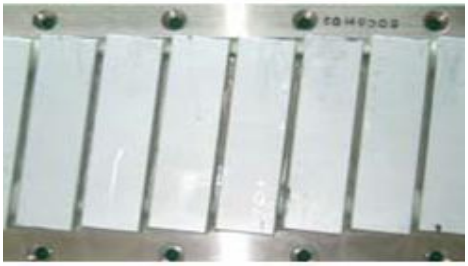

(b) Skewed pattern

(c) V-skewed pattern

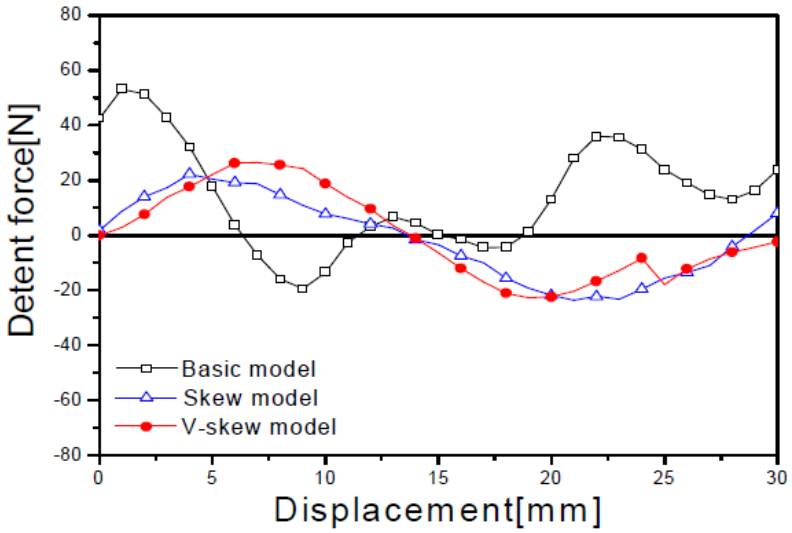

(d) Experimental results for cogging force at different skew patterns

Figure 35 Different skew patterns (Ahn, Lee et al. 2008)

This technique archives a reduction of the cogging forces by deliberate misalignment of the PMs with reference to the winding slots. For the skewed pattern, different flux is transferred alongside the length of every winding slot (Appendix A) and therefore, the magnetic attraction between the PMs and the winding slots is dispersed. As a result, the total cogging force is reduced. Furthermore, investigations carried out in (Ahn, Lee et al. 2008) show how the force optimisation techniques affect the power output and the efficiency of the PMLG. Such an investigation is very important because it shows the wider impact of the proposed force reduction techniques.

Also, a different technique for cogging force reduction, shown in (Shabani, Milimonfared et al. 2007, Ashabani, Milimonfared et al. 2008), consists of the slotting of the pole-pieces. The basic idea behind this technique is reducing the magnetic attraction between the poles and the winding yoke by the introduction of high-reluctance slots with larger air-gaps (Figure 36). By using the technique, a reduction of around 30% to 40% can be achieved. However, the study does not show the additional magnetic reluctance added to the magnetic circuit due to the increased air gap length in the slots. Likewise, the effects on the output power or induced voltage have not been mentioned.

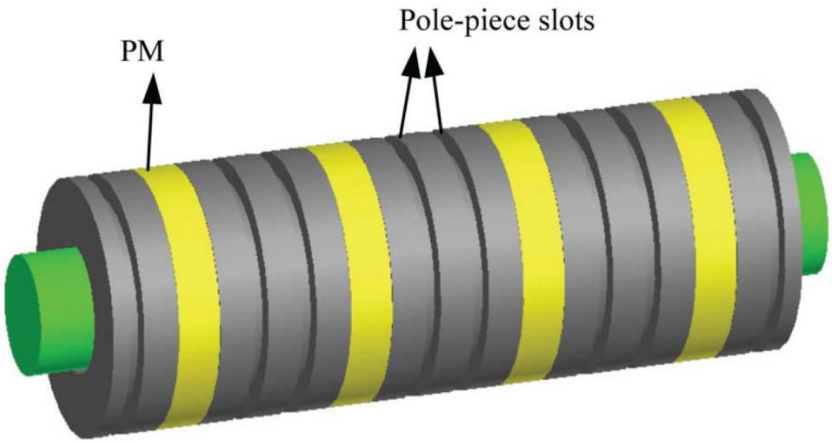

(a) Slotting of the poles

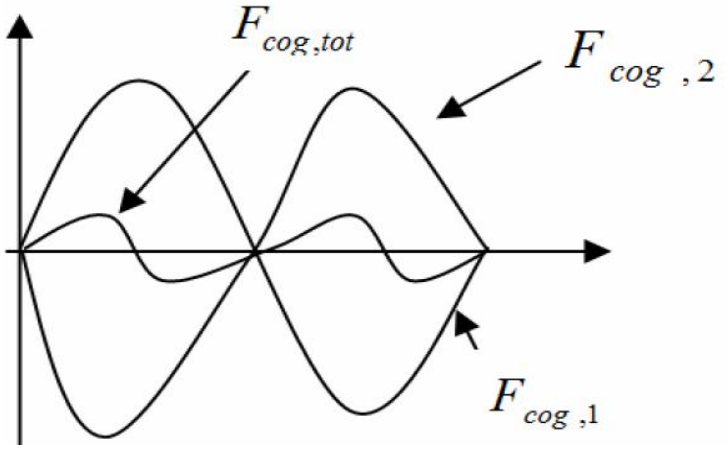

(b) Total cogging force after slotting the magnetic poles

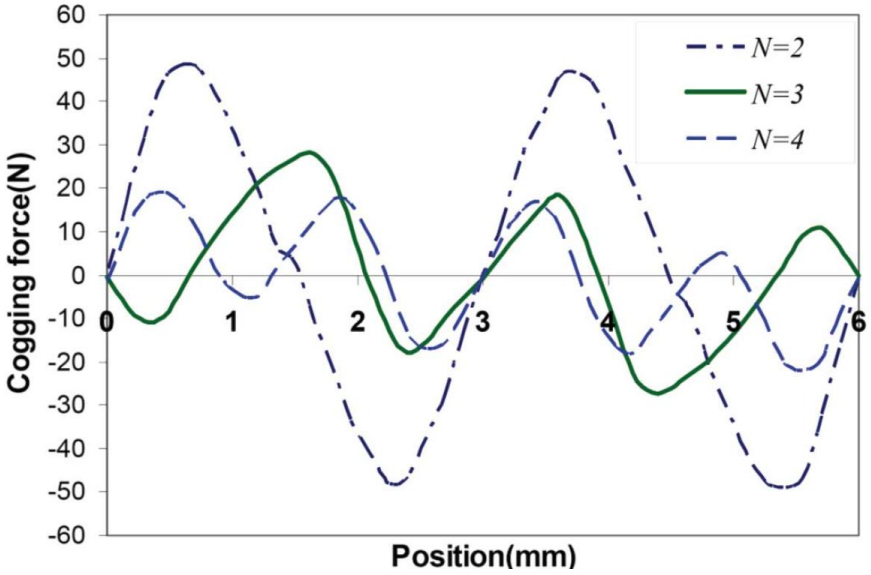

(c) Cogging force for difference number of slot pieces

Figure 36 Basic idea of the pole-piece slotting (Shabani, Milimonfared et al. 2007)

One of the most common techniques for cogging force reduction is the deliberate misalignment of the magnets with respect to the stator shoes. This can be achieved by changing the number of slots per pole and phase (q). The number of slots per pole and phase for a PMLG is the ratio between the integer number of phase slots, distributed in an integer number of poles (Ivanova, Agren et al. 2005) (Figure 37). A geometrical description of the number of slots per pole and phase can be given as:

$$q = \frac{M_p}{3P_s} \tag{2.4}$$

where M_p is the length of the magnetic pole and P_s is the length of the phase slot.

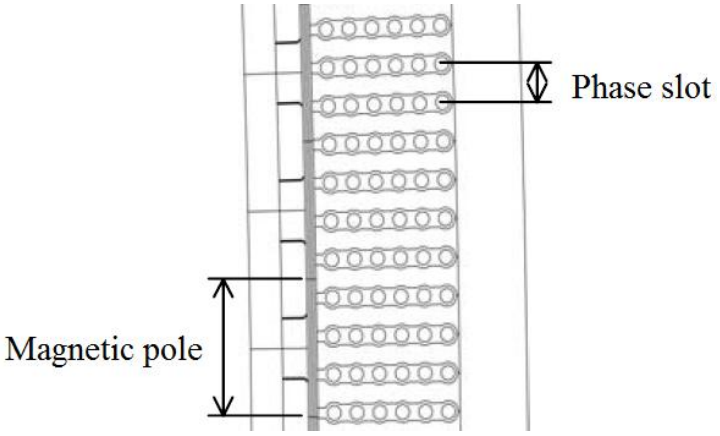

Figure 37 Number of slots per pole and phase *q* (Ivanova, Agren et al. 2005)

Practically, by varying the number of slots per pole *q* and phase from one (with regard to 2.29), the misalignment between the coils and the poles in a single phase becomes higher but the cogging force is reduced.

Overall, the above techniques achieve significant levels of cogging force reduction. However, as the optimisation is mainly multidirectional, the effects of the techniques on other factors such as output power have to be investigated further. Slotting of the poles/magnets can be used as an effective method for force reduction which does not affect the power output significantly.

Furthermore, the introduction of winding yoke shoes contributes to cogging torque reduction as well as a reduction of the total magnetic reluctance of the machine. Such a reduction of the magnetic reluctance will increase the generated voltage and hence, the output power.

Similarly, shaping the PM profile and altering *q* can be used for force reduction, where optimal values have to be selected with regard to the desired electrical output, the ability of the bearing to cope with the level of vibrations caused by the cogging forces and the volume of PMs.

2.7.6.3. Lorentz forces

The Lorentz force is generated by the magnetic field established by the PMs (McDonald, Crozier et al. 2009) and current flowing in the coils. It can be written as:

$$F_L = \int_v JxB_d \, dv \tag{2.5}$$

where B_d is the flux density and J is the current density. This specialises to:

$$F_L = -\int_v J_z B_{d_y} \, dv \tag{2.6}$$

if the current is in the *Z*-direction and the motion is in the *X*-direction. For single N - turn coils, the forces can be written as:

$$F_L = -NI_c L_e B_{avg} \tag{2.7}$$

where L_e is the length of the coil, I_c is the current and

$$B_{avg} = \frac{1}{A_c}\left(\int_{a^+} B_y \, da - \int_{a^-} B_y \, da\right) \tag{2.8}$$

where areas a^+ and a^- on which the integration is performed coincide with the cross-sectional area A_c of the two coil sides. The total forces can be calculated using (2.7) and (2.8).

2.7.7. Iron Losses in Electrical Machines

Generally, three kinds of iron losses occur in electrical machines. The first kind is due to hysteresis. These losses appear when a ferromagnetic material, such as the silicon stainless steel, is exposed to an alternating magnetic field. Owing to the variation of the field, the orientation of the magnetic dipoles varies over time. This causes a continuous hysteresis cycle in which, energy is lost during each cycle. The energy loss is in the form of heat generated in the magnetic cores. The amount of heat is proportional to the operational frequency of the field, which is determined by the translational velocity of the PMLG's translator. Generally, direct drive PMLGs have low levels of hysteresis losses because of the generally low frequency of the PMs' field.

The second type of losses are eddy current losses. The ferromagnetic cores in most electrical machines are good conductors of current. When the magnetic flux varies during translation, currents (also called eddy currents) are generated in the magnetic core via Faraday induction. Owing to the ohmic resistance of the core, the eddy currents generate heat. This problem can be solved by laminating the magnetic cores, whereby the lamination is parallel to the direction of the flux and the single segments are insulated electrically from each other. Thus, the eddy currents are reduced significantly because of the reduced cross-sectional area available for induction.

The third kind of loss is that associated with the copper. These losses are caused by the electrical resistance of the copper conductor in the windings. The effect of these losses is the heating up of the machine's windings.

2.8. Control and Integration of Direct Drive Wave Energy Converters

Several control techniques proposing adjustments to alter the normal frequency of a WEC's floating buoy have been proposed in (Babarit, Clément 2006, Nolan, Ringwood et al. 2005, Schoen, Hals et al. 2008, Babarit, Cuclos et al. 2003), for which the choice of control system is highly dependent on the type of the WEC.

A technique shown in Figure 38, involves a deliberate holding of the floating buoy, releasing it at a moment when sufficient buoyancy force has been accumulated.

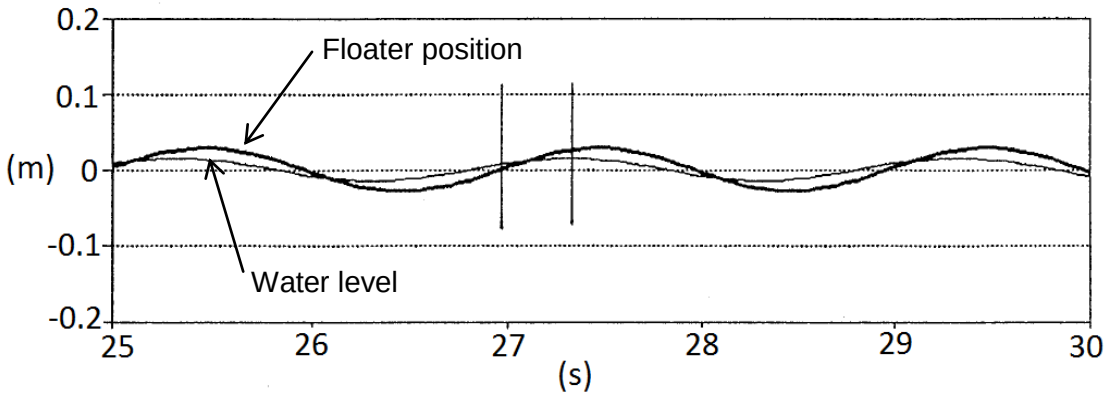

(a) Vertical oscillation of WEC without holding of the floater (Falnes 1997)

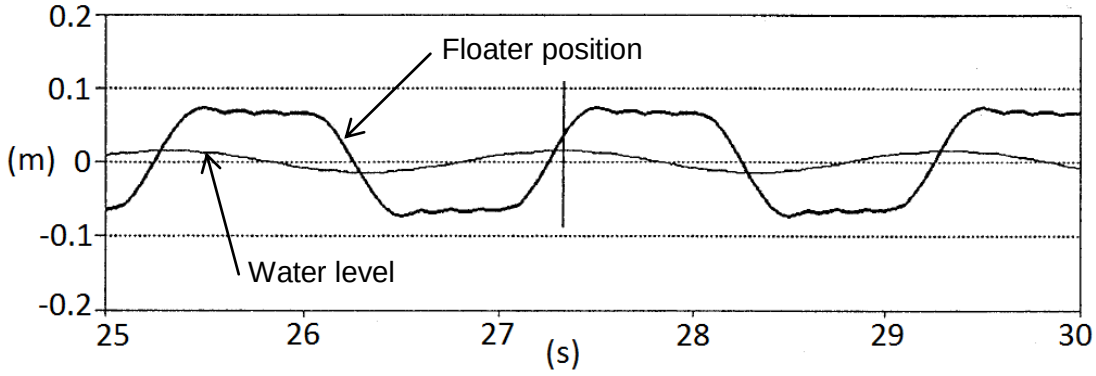

(b) Vertical oscillation of WEC with holding of the floater (Falnes 1997)

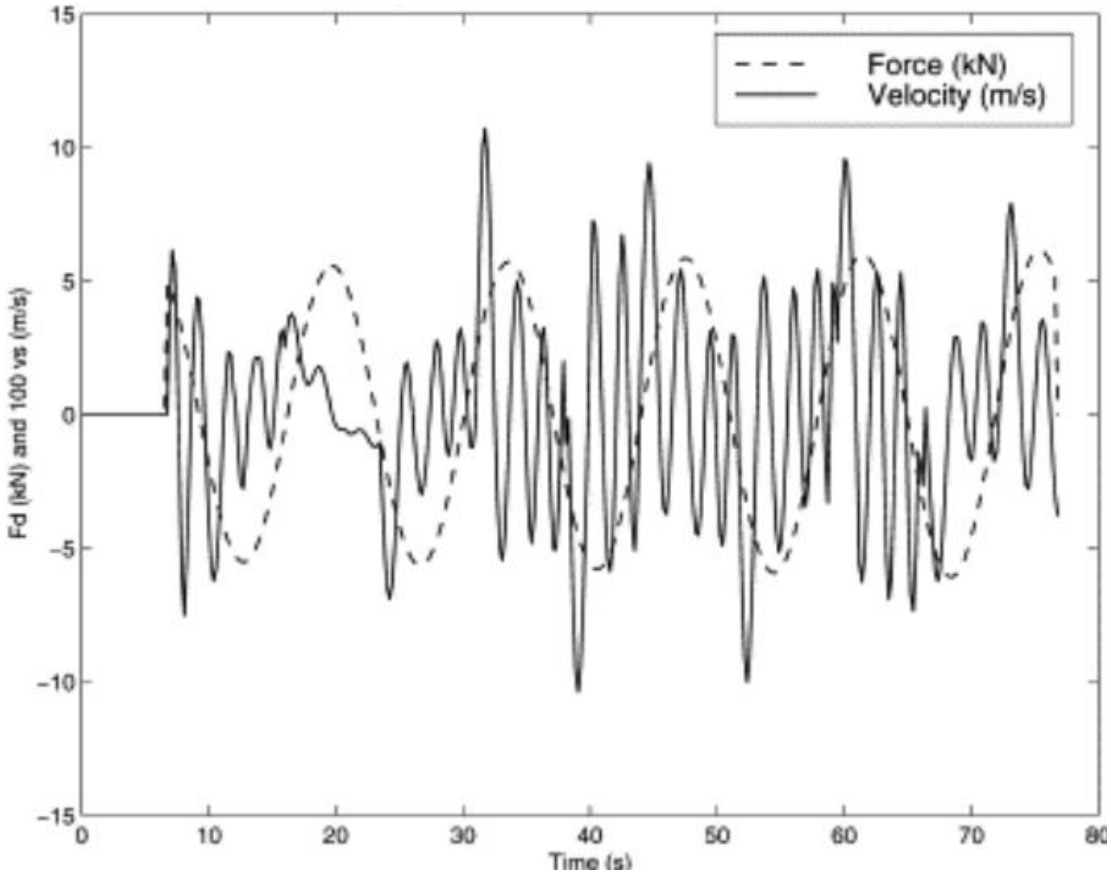

(c) Excitation force and velocity using holding technique (latching) on sinusoidal force (Korde 2002)

Figure 38 Effect from latching

The advantage of holding can be seen in Figure 38b, where the thinner curve represents the incident wave (water level) and the thicker curve shows the

oscillating floater position. The main purpose of holding the stator in place and then releasing it is to maximise the trust force and the buoy velocity of the floater, as well as keeping them in phase. By this technique, maximum power can be extracted from the wave (Salter, Taylor, Caldwell 2002). The effect of the latching on a sinusoidal force can be seen in Figure 38c.

Every WEC has to transfer its power to the national electricity grid. To achieve this, a grid integration system needs to be installed. This system has to maintain a constant voltage and frequency on its output. Such a requirement can be achieved by using a power electronics system shown in Figure 39.

In the diagram, it is assumed that the PMLG has three-phase output with ±120 degree phase shift. The voltage amplitude and the electrical frequency can vary significantly depending on sea conditions.

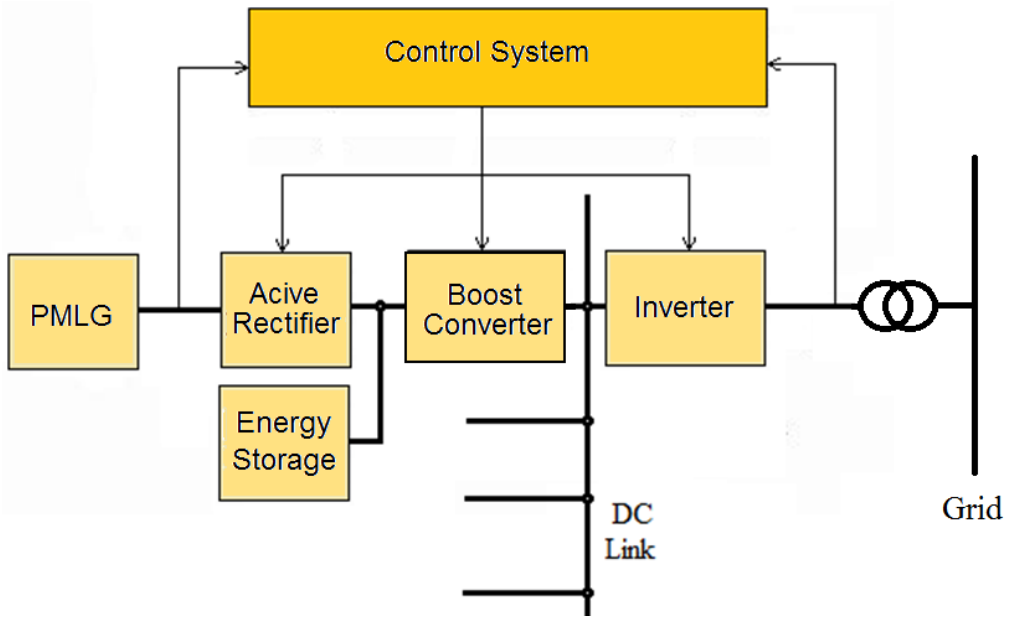

Figure 39 Control of the grid integration system

The PMLG is connected to the active rectifier, which transforms the PMLG's AC output to DC. The challenge at this stage is that the active rectifier should

maintain certain voltage margins at its output in order to satisfy the input requirements of the boost converter. This can be achieved by active control from the control system and energy storage (capacitor banks) maintaining the DC voltage level.

The voltage at the stage between the active rectifier and the boost converter is still low, because of the low power transfer from a single machine. The main two functions of the boost converter are to increase and maintain the voltage. A feedback loop provided by the control system can maintain these requirements in real time. After the voltage is raised at the output terminals of the boost converter, it is fed in a DC Link. The DC Link is a common collective bus for the entire WEC array and hence, at this level the voltage is maintained high to reduce thermal losses caused by large currents flowing into switches and cables. After the collective power is fed into the DC Link, it can be exported to the grid over an inverter and transformer. Similar control systems have been described in (Annuar, Macpherson et al. 2012, Thorburn, Leijon 2007, Wu, Zhang et al. 2009, Mueller 2002, Zanxiang Nie, Xi Xiao et al. 2013).

2.8.1. Energy Storage

Sea conditions are predictable but not controllable; therefore, it is a challenge to stabilise the output of the WECs. Such an issue is common for all renewable technologies. For this reason, energy storage can be used to stabilise the output of the WEC. The size of the storage can vary with the waves' intensity at a particular location. Therefore, this has to be selected based on the wave climate.

The type of energy storage mechanism differs for every kind of technology. In Pelamis, energy storage is achieved by high-pressure tanks with hydraulic fluid. In this case, the capacity of the storage is dependent mainly on the volume of the tanks. In the overtopping device, storage is achieved by collecting the seawater in a reservoir. Similarly, the storage capacity can be increased by enlarging the size of the reservoir.

For WECs using direct drive linear generators, such as the AWS and the Wave Point Absorber, the most common technique is a capacitor bank connected to the DC link (Figure 39). In such a case, additional capacitors (batteries) have to be installed to increase the storage capacity. Storing energy in batteries is a mature and diverse technology. Batteries have high surge-to-weight-ratios and are recyclable. However, they have rather short operational life and contain toxic materials.

Another form of storage is Compressed Air Energy Storage. Compressed air can be considered as good alternative because it is an environmentally clean way of storing energy, it does not include any chemical reactions in its cycle and overall efficiencies from 50% to 70% have been reported (Joseph Simmons, Ardeth Barnhart, Stanley Reynolds, Young-Jun Son, Alex Cronin AUGUST 2010, Brian Elmegaard , Perry Y. Li, Eric Loth, Terrence W. Simon, James D. Van de Ven, Stephen E. Crane). Storing energy in compressed air can deliver potentially huge amounts of energy, fast response times and it is generally considered as an inexpensive way of storing energy. However, the technology requires sealed storage containers.

Kinetic energy can be stored in rotating masses (Flywheel energy storage). The mass is rotated by an electric motor, which can also be used as a generator. Flywheels benefit from low maintenance and long lifespan. To

reduce maintenance, magnetic bearings can be used. Similarly, the mass rotating in a vacuum can reduce the friction of the air and therefore increase the efficiency. Furthermore, flywheels do not release any carbon emissions and do not have toxic components. As the mass is spinning at all times, high response time can be achieved. On the other hand, flywheels suffer from high acquisition cost as well as low storage capacity (Andreas Oberhofer July 2012).

Another form of energy storage is a Superconducting Magnetic Energy Storage. The concept of this system is to store energy in the form of an electromagnetic field in a superconducting coil. The coil consists of a conductor operating at very low temperatures and having zero electrical resistance. This can potentially deliver overall efficiency of 90% to 95%. The cycle does not contain an environmental hazard; however, it does require a cooling system to maintain the temperature low and it is expensive in production and maintenance. This system can be used for frequency balancing in real time owing to its fast response times but it is not efficient for long-term use because of energy losses of approximately 12% per day (Andreas Oberhofer July 2012).

2.9. Discussion

In this chapter, the currently proposed designs for direct drive linear generators for WECs are presented and a discussion outlining some of their advantages and disadvantages has been conducted.

The author's observation is that there is a lack of investigation how the proposed force reduction techniques affects the electrical power output of the machines in many of the publications. As the electrical output is an essential factor in the time for the Return of Investment (RoI) of the WEC, this is a highly important point that needs to be addressed.

From the publications reviewed in the chapter, it can be concluded that the iron- and the air-cored PM linear machines offer significant potential for direct drive WECs. The main reasons for this are the strong excitation flux provided by the high number of PMs delivering high induced voltage and also the simplicity the in design, which contributes to the structural integrity.

3. Investigation into Flat Iron-cored Permanent Magnet Linear Generator

3.1. Introduction

In this chapter, a design for a flat longitudinal flux PMLG for a marine wave energy converter is analysed. The influence of parameters, such as the number of slots per pole, phase q and the number of translator's winding sections (coils) are analysed with respect to the cogging forces and to the output power of the PMLG. By taking into account the above parameters, an optimisation of the PMLG is performed. The optimisation aims to reduce the forces of magnetic attraction between the stator and the translator, in addition to increasing the electrical output of the generator. By reducing the magnetic attraction forces, the maintenance cost of the WEC can be reduced. Additionally, increasing the energy harvesting of the generator will reduce the RoI time of the WEC.

Three-dimensional FEA is used for solving the combined field and circuit equations of the generator. FEA is used as a simulation tool because of its high accuracy when applying small design changes. Moreover, the simulations are performed using 3D FEA with a time-varying electromagnetic field, taking into consideration the nonlinearity of the silicon steel in the magnetic cores of the generator. Furthermore, full-size generator models are simulated, taking into account the magnetic flux distribution in the air gap and in the regions at the longitudinal ends. An experimentally recorded vertical marine wave displacement is applied to the generator's translator in the simulations.

3.2. Investigation into Single Sided Iron-Cored Linear Generator

3.2.1. Generator Description

In this chapter, it is assumed that the PMLG's stator is assembled from the permanent magnets, the separators, and the upper magnetic core. The separators are made from non-magnetic and non-electrical conducting material and they are required in order to maintain the position of the permanent magnets against axial displacement. In addition, the PMLG's translator is assembled from the lower magnetic core and the windings (Figure 40b).

The magnetic cores of the machine are formed by laminated silicon steel with a 95% stacking factor and they are treated as magnetically nonlinear material with single value magnetisation characteristics.

The translator teeth are finished with shoes to optimise the flux distribution. Generally, the implementation of shoes decreases both the power ripple and the magnetic reluctance of the air gap. In addition, reduction of the cogging forces in linear machines can be also achieved (Ivanova, Agren et al. 2005). The windings' excitation flux is provided by Neodymium-Iron-Boron magnets with magnetisation direction parallel to the Y-axis (Figure 40b). Furthermore, in order to increase the accuracy of the simulation results, the PMLG has full translator models and therefore, the influence of the longitudinal ends can be taken into account. Moreover, a repetitive boundary condition is applied to the translator, which is a common approach for linear generator simulations (Danielsson, Eriksson et al. 2006).

Generally, the single-sided PMLG can be used in WEC but high attraction forces will be generated in the Y-axis. Another configuration can be achieved by stacking a number of single-sided PMLGs in a single structure in such a way that the forces in the Y-axis are reduced (by opposing them). Similar single-sided design and multiple-sided structures are shown in (Danielsson, Leijon et al. 2005, Ivanova, Agren et al. 2005, Leijon, Bernhoff et al. 2005).

In this chapter, the investigation is focused mainly on the cogging forces and the power delivery of a single-sided unit. However, the forces in the Y-axis are also presented because they are important for the design of the welding, the connections and the supporting structure.

In the simulations, the translating velocity applied to the PMLG is a vertical time-velocity sequence of waves that has been recorded by a wave probe for a period of 150 seconds near the southeast coast of the UK (Figure 40c).

The number of slots per pole and phase q for the generator shown in Figure 40 is 1.2 (6/5). This means that five poles have the same length as six three-phase translator slots (or eighteen single-phase slots). For convenience, the value of q = 6/5 can be also presented as 1.2. Thus, one pole covers 1.2 translator slots. By using such a presentation for q, it is possible to analyse values that differ from the standard ones shown in (Ivanova, Agren et al. 2005).

3.2.2. Load and No-load Operational Characteristics

The EMF of the permanent magnet linear generator can be shown as:

$$\mathrm{V_e} = \frac{d\lambda_{im}}{dt} = \frac{d\lambda_{im}}{dz} * \frac{dz}{dt} \tag{3.1}$$

where λ_{im} is the flux linked with the i - phase winding, which can be calculated by:

$$\lambda_{im} = N_{ii} * \varphi_{ii} = N_{ii} * \Phi_{ii} * \cos(\omega * t) \quad (3.2)$$

$$= N_{ii} * \Phi_{ii} * \cos\left(\frac{\pi}{\omega_p} * z\right)$$

where ω_p is the pole pitch, z is the linear displacement, N_{ii} is the number of turns in the i - phase and Φ_{ii} is the maximum flux calculated via the FEA. The EMF in phase A is:

$$V_{\mathrm{a}} = \frac{d\lambda_{Am}}{dz} * \frac{dz}{dt} = -N_A * \Phi_A * \sin\left(\frac{\pi}{\omega_p} * z\right) * \frac{dz}{dt} \quad (3.3)$$

The EMF from phases B and C can be calculated by applying phase shifts of ±120 degrees.

The voltage and the current under load in phase A can be calculated as:

$$V_A = -r_A * i_A + L_{self} * \frac{di_A}{dt} + L_{mut}\left(\frac{di_B}{dt} + \frac{di_C}{dt}\right) + E_A \quad (3.4)$$

$$\frac{di_A}{dt} = \frac{1}{L_{self}}\left(V_A + r_A * i_A - L_{mut}\left(\frac{di_B}{dt} + \frac{di_C}{dt}\right) - E_A\right) \quad (3.5)$$

where L_{self} and L_{mut} are the self and mutual inductances, respectively. The equivalent circuit of the PMLG is shown in Figure 40a.

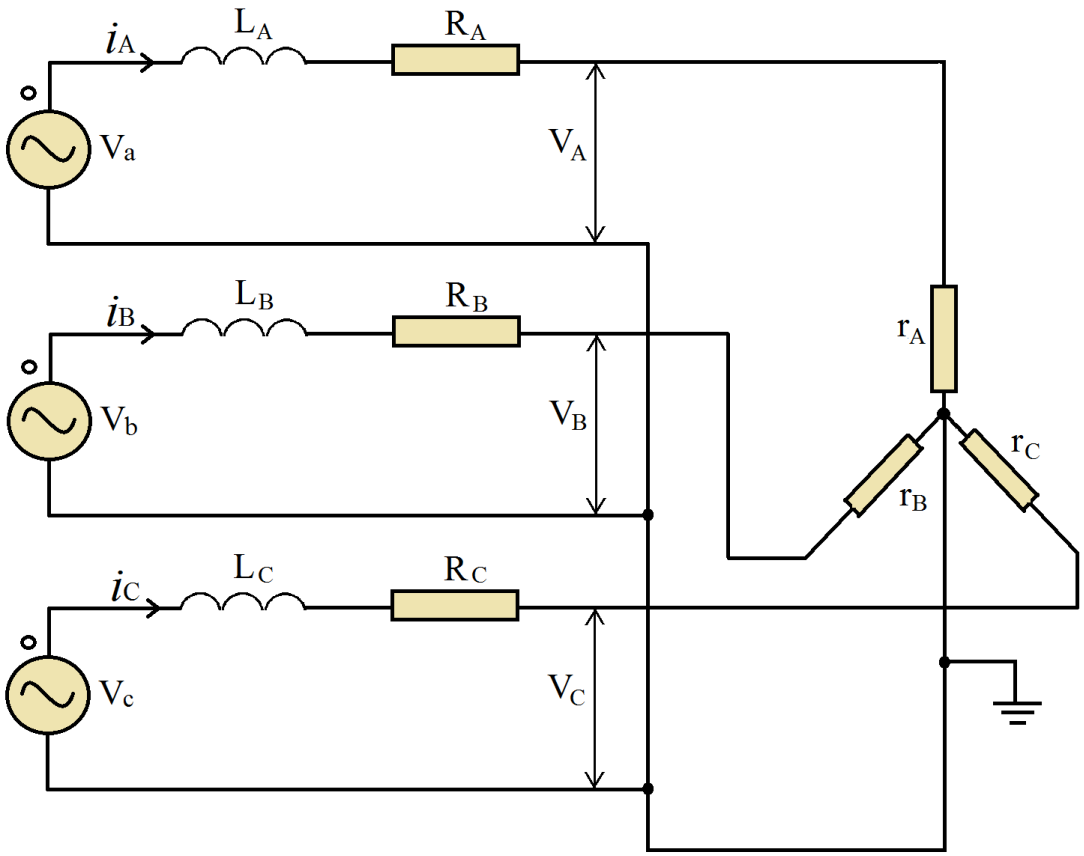

(a) Equivalent circuit of the PMLG

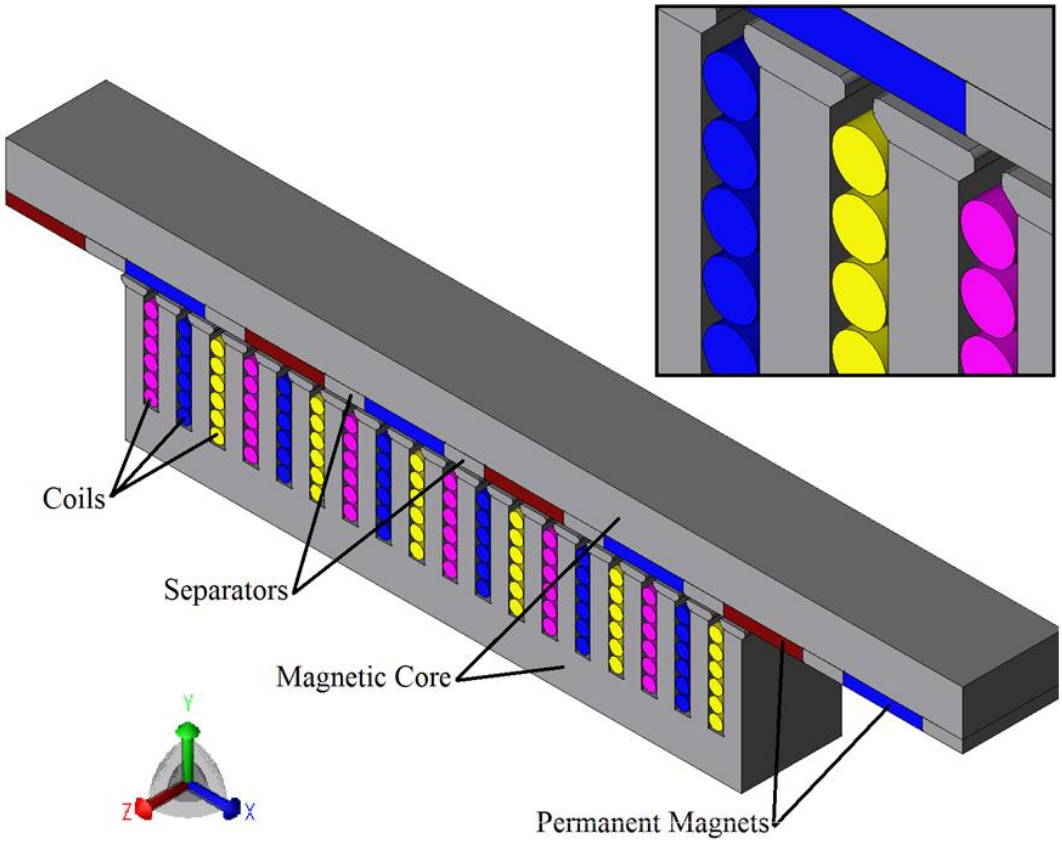

(b) 3D view of single sided base model of the PMLG

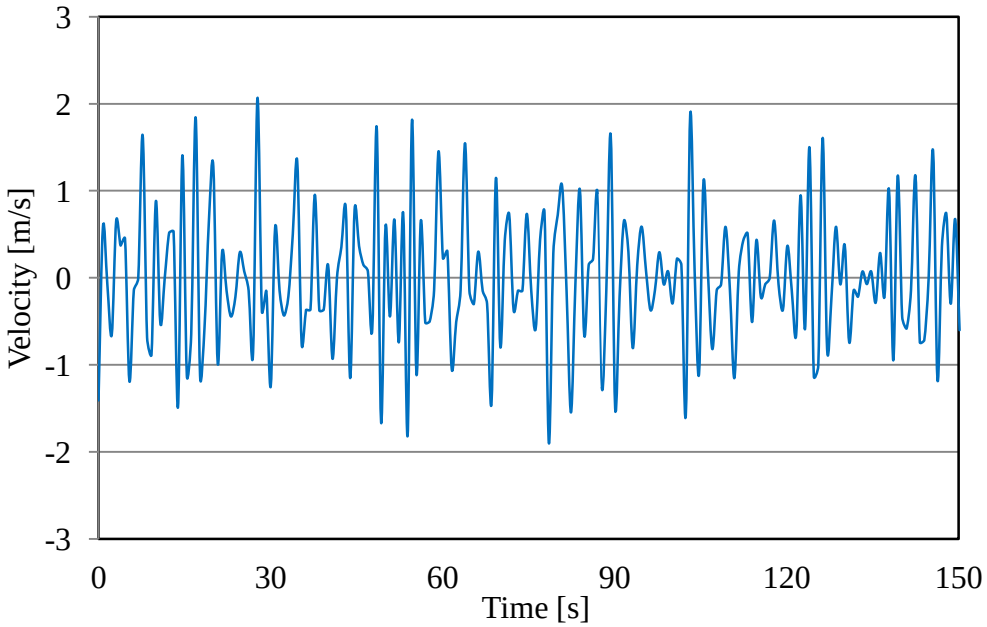

(c) Experimentally recorded vertical time- velocity sequence of marine waves

Figure 40 Single sided PMLG and recorded time-velocity sequence

Table 1 Main Dimensions of the single sided PMLG

DIMENSIONS		
Parameter	Axis	
Translator length [mm]	X	612
Translator width [mm]	Z	600
Winding length [mm]	Y	88
Translator height [mm]	Y	151
Permanent magnet length [mm]	X	85
Pole pitch length [mm]	X	118.8
Coil slot length [mm]	X	15
Translator teeth length [mm]	Y	18
Air gap length [mm]	Y	3
ELECTRICAL CHARACTERISTICS		
Number of turns per winding section		24
Number of turns per coil		4
Number of slot per pole and phase, q		1.2 (6/5)
Winding resistance [ohm]		0.9
Resistive three-phase star connected load [ohm]		5

The main dimensions of the generator are shown in Table 1. The generator has three-phase windings, where each winding consists of six winding sections connected in series. Furthermore, each winding section consists of six coils connected in parallel, as shown in Appendix C. Each winding is shifted by ±120 degrees from the other two. Additionally, every winding has a total resistance of 0.9 ohm (base model). Additional explanation about the circuit arrangement is given in Appendix C. The single- and the double-sided generator designs are inspired by (O. Danielsson, K. Thorburn, M. Eriksson, M. Leijon 2003), although

the parameters have been scaled down (where appropriate) to the sizes shown in Table 1.

3.2.3. Magnetic circuit of the machine

The magnetic circuit of the single-side PMLG is shown in Figure 41, in which Φ_{PM} is the Magneto Motive Force (MMF) source of the permanent magnets and S_C and S_{C1m} are the reluctances in the magnetic core. Similarly, S_1 to S_{19} are the magnetic reluctances of the teeth of the translator, S_{a1} to S_{a19} are the magnetic reluctances in the air gap between the permanent magnet and every single tooth. They are identified by colour codes on the right-hand side of the figure. In this magnetic circuit, it is assumed that every magnetic pole (covered by the length of the translator teeth) is connected with the closest four translator teeth. At certain positions of the translator where the teeth (end shoes) are located between two magnetic poles, they are linked with both poles and linkage is given as two reluctances: S_{ai} and S_{ai*} (i - tooth number). Furthermore, the values of S_{PM} are the magnetic reluctances of the permanent magnets and S_{air} represents the reluctance of the air between the magnets outside the translator. These reluctances (S_{air}) are constant and they do not affect the main magnetic circuit. The purpose of showing them is to present the magnetic circuit outside the length of the translator.

The magnetic poles located outside of the translator are connected with the final one or two translator teeth. If the permanent magnet (at the longitudinal end) is outside of the translator length, it is considered that the magnet is connected to the final tooth (S_{a1}). Alternatively, if the magnet covers the last

tooth it is considered that the magnet is connected to the final two translator teeth (S_{18*} and S_{19}).

The analytical modelling technique does not take into account the effects of the saturation of iron in the magnetic cores of the generator.

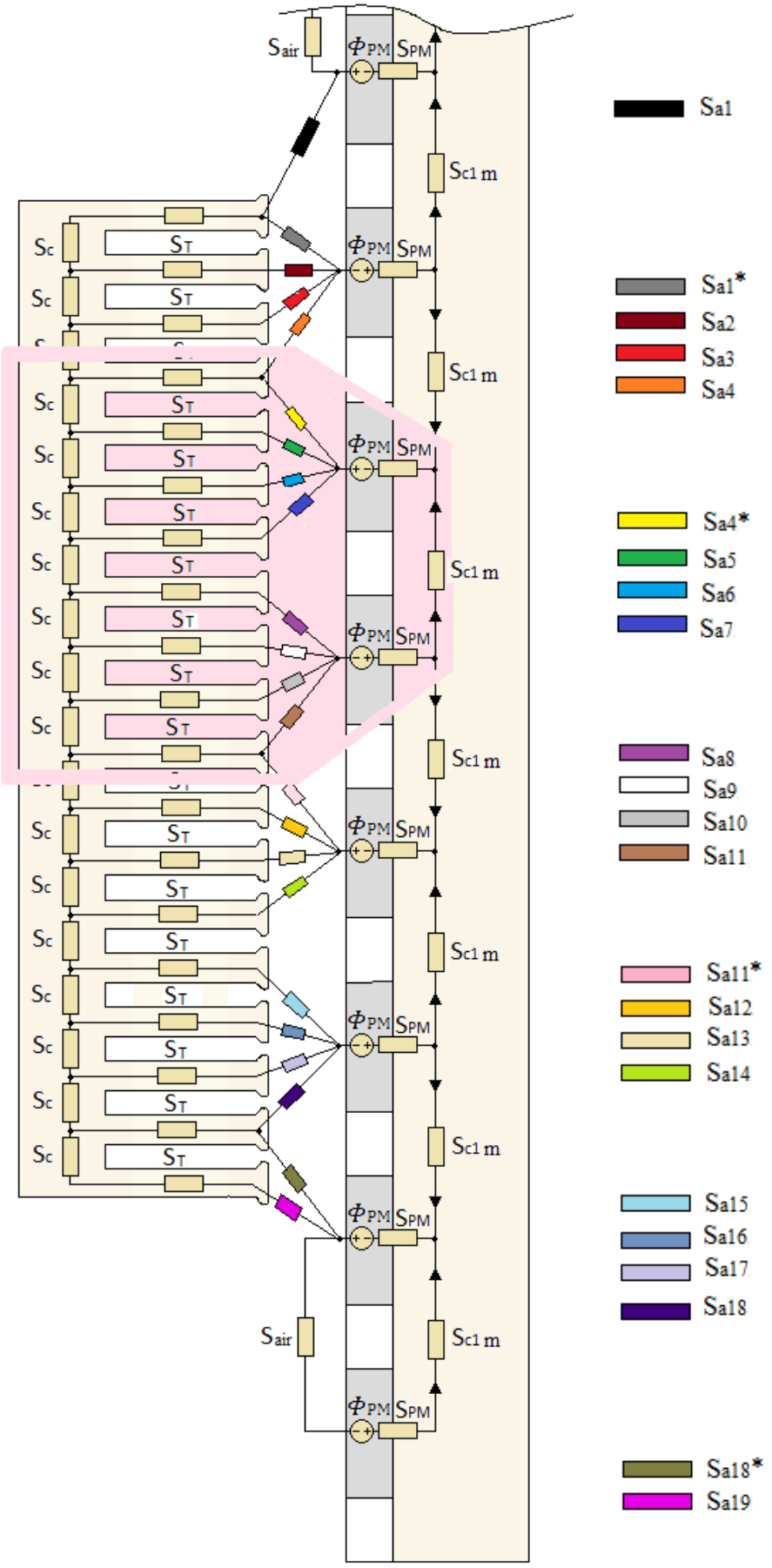

Figure 41 Magnetic circuit of the single sided PMLG

The voltages generated in the coils are dependent on the magnetic flux passing the teeth surrounding them (flux over S_T). The flux path in the translator, contributing to voltage generation (therefore, to energy harvesting) is through reluctances $S_C - S_T - S_{a(1-19)} - \Phi_{PM} - S_{PM} - S_{C1} - S_{PM} - \Phi_{PM} - S_{a(1-19)} - S_T - S_C$.

However, when a tooth is located between two poles such as the 4th, 11th and 18th teeth in Figure 41, part of the flux goes through the tooth shoe, bypassing the tooth. For instance, in the case of the 4th tooth, part of the magnetic flux will follow the contour of $S_{a4} - S_{a4*} - \Phi_{PM} - S_{PM} - S_{C1} - S_{PM} - \Phi_{PM} - S_{a4}$. Such leakage of flux is not beneficial to energy harvesting and can be considered a loss. A reduction of the flux can be achieved by altering the width of the shoes along the X-axis.

The total magnetic reluctance of a single-sided PMLG's section with a length of 8 teeth can be presented as:

$$S_{Total} = 2 * S_E + 2 * S_{PM} + S_{C1m} + S_C \tag{3.6}$$

where S_{Total} is the total magnetic reluctance of the area indicated by pink shading in Figure 41. Furthermore, where S_E is one-half of the reluctance of the translator, it can be calculated as follows (Appendix C):

$$S_E = \frac{{S_{Tt}}^4 + {S_C}^3 * S_T + 6 * {S_{Tt}}^3 * S_C + 5 * {S_C}^2 * {S_{Tt}}^2}{4 * {S_{Tt}}^3 + {S_C}^3 + 10 * {S_{Tt}}^2 * S_C + 6 * {S_C}^2 * S_{Tt}} \tag{3.7}$$

$$S_{Tt} = S_T + S_{a\,nn} \tag{3.8}$$

where nn is the number of the reluctances shown on the right-hand side (with colour code) in Figure 41 and can be presented as:

$$S_{a\,nn} = \frac{l_{gap}}{\mu_0 * A_r} \tag{3.9}$$

$$S_T = \frac{l_{tooth}}{\mu_c * A_r} \tag{3.10}$$

$$S_c = \frac{l_{core}}{\mu_c * A_r} \tag{3.11}$$

where l_{gap} is the length of the air gap between the centre of the permanent magnet and the centre of the shoes and l_{tooth} is the length of the coil`s slots in the magnetic core. The permeability of the air and the magnetic core are given by μ_0 and μ_c [H/m] respectively and A_r is the area of the pole face.

Using the equivalent reluctance the magnetic circuit can be presented as simple circuit with an MMF source connected to a single magnetic reluctance. Hopkinson's law is a counterpart to Ohm's law and can be used in magnetic circuits:

$$\Phi_{PM} = \psi_m * S_E \tag{3.12}$$

$$\psi_m = \frac{\Phi_{PM}}{S_E} \tag{3.13}$$

where ψ_m is the total magnetic flux of the magnetic circuit (i.e., the flux passing S_{c1m}). Similarly, the magnetic flux density in the air gap can be presented as:

$$B = \frac{\psi_m}{A_r}. \tag{3.14}$$

The analytical calculations are performed using Matlab and the results for the flux density in the air gap show a difference of 5.5% in comparison with the FEA results for a static simulation.

3.2.3.1. Finite Element Analysis flux distribution

The magnetic circuit of the machine, simulated by FEA, leads to the two main flux distribution modes shown in Figure 42. If translation with constant velocity occurs, the magnetic patterns will oscillate between the two modes shown in Figure 42. In the pole-concentrated magnetic distribution mode, the flux is distributed mainly under the magnetic poles.

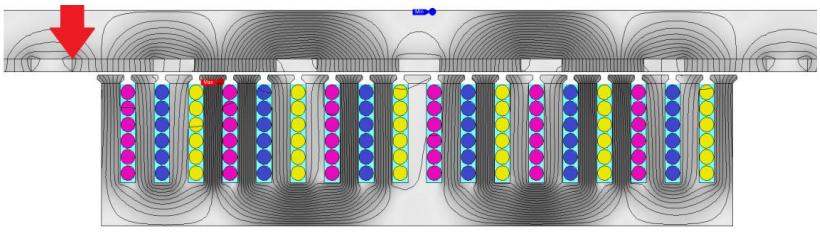

(a) Pole concentrated flux distribution mode

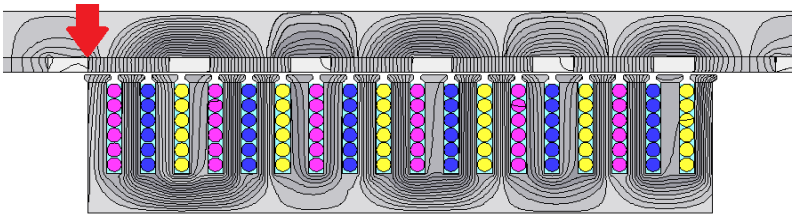

(b) Even flux distribution mode

Figure 42 Different flux distributions in the PMLG

Such distribution leads to high concentration of flux and therefore the operating point of the teeth is close to saturation. The saturation level in the translator for the even flux distribution mode (Figure 42b) is lower due to the grater distributed flux in the magnetic core.

3.2.4. Force Calculations in Finite Element Analysis

The continuous operation of every electro-magnetic machine depends on the forces acting on the bearings. The forces of attraction are caused by the interaction between the permanent magnets and the iron core of the PMLG. The longitudinal ends of the generator become additional sources of force because of the big step-change in the magnetic reluctance (Choi, Baek 2009).

The calculation of the forces is interesting from many perspectives, and is an important parameter in studying: the generator bearing system, the buoy line forces, the mechanical stress, and fatigue in the supporting structure.

The force calculation analyses are done on the 2D models and verified by the 3D models of the machines. The 2D models have a mesh of around 25 000 to 50 000 elements (depending on the size of the machine) and the 3D models have a mesh with 300 000 to 600 000 elements (also depending on size of the machine).

The number of elements for the 3D models is based on the period of the waveform of the cogging force at the maximum velocity of the translator (Appendix D). Furthermore, the element choice for the 2D model is selected based on the deviation from the 3D results. For example, if the element number for the 2D models is low, the deviation from the 3D results (voltage, current and forces) will be high. The deviation decreases with an increasing number of elements for the 2D models. However, at a certain point there is saturation, whereby increasing further the number of elements for the 2D models does not contribute to a lesser deviation. As a result, the number of elements for the 2D models is based on the above saturation point.

In the 2D and the 3D models, a repetitive boundary has been applied for the translator on the X-axis in order to reduce the mesh size. Moreover, full windings are used without applying symmetrical/asymmetrical FEM coils (winding circuit is the same as seen in Figure 43) and therefore, no repetitive boundary is applied on the winding yoke. Furthermore, in the 2D simulations, the reparative boundary has been applied in the Z-axis, where the length of the boundary is the same as the actual width of the machine in 3D.

3.2.5. Simulated Results

The simulations in this chapter are performed by means of 2D and 3D FEM, where the 2D results are verified with the corresponding full 3D model. In Figure 43, the magnetic flux density and the magnetic orientation (as vectors) are shown. In addition, a comparison between the 2D and 3D FEM simulations is shown in Figure 44.

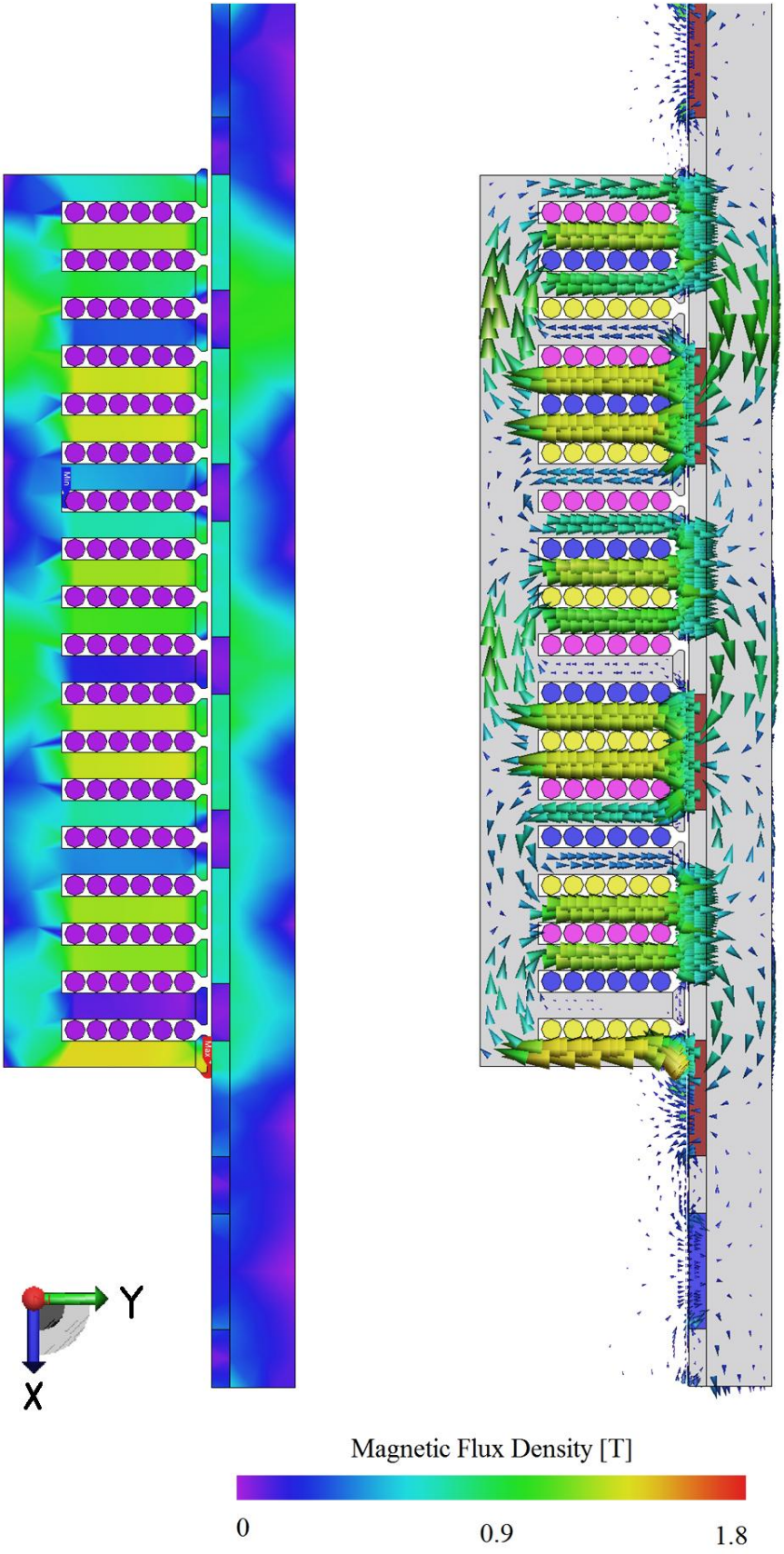

Figure 43 Magnetic flux distribution in the single sided PMLG

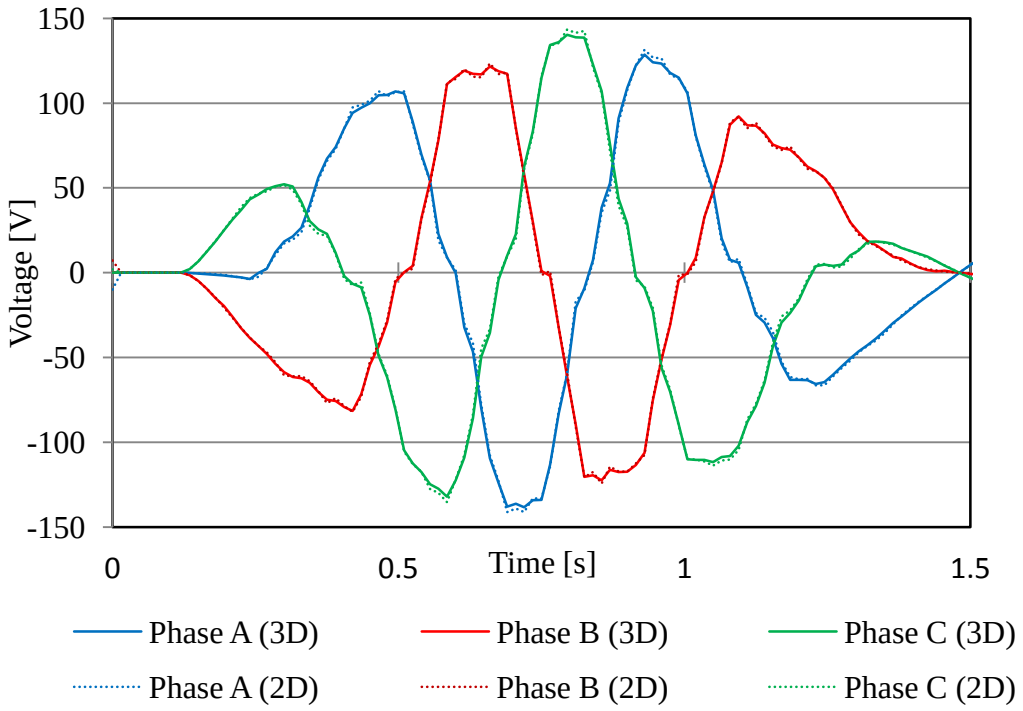

(a) No-load voltage comparison

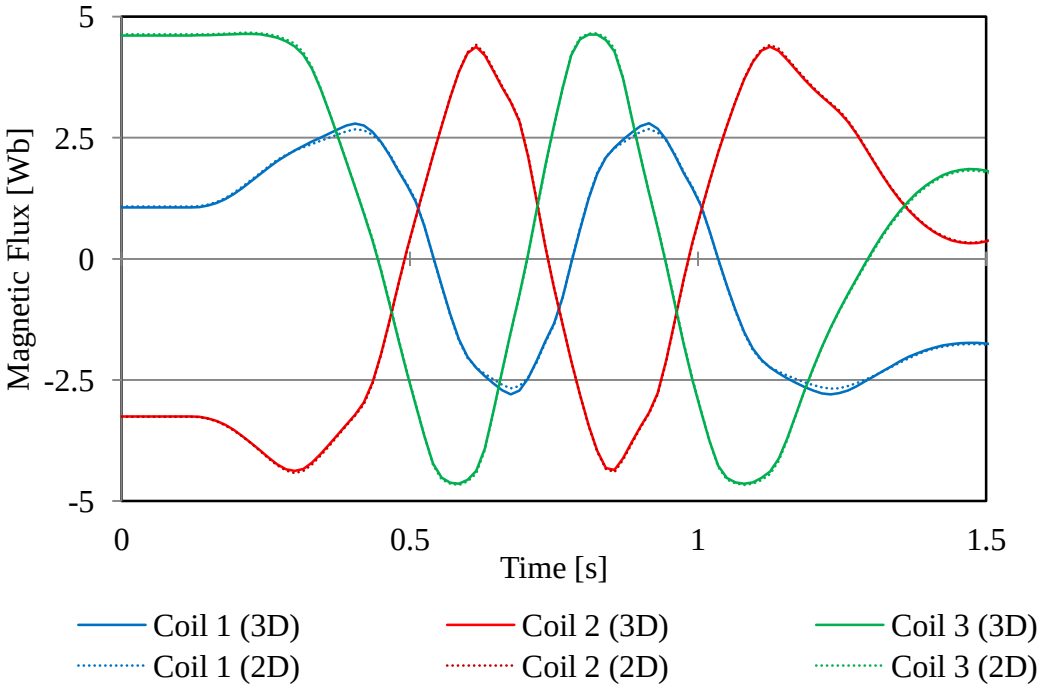

(b) Magnetic flux comparison

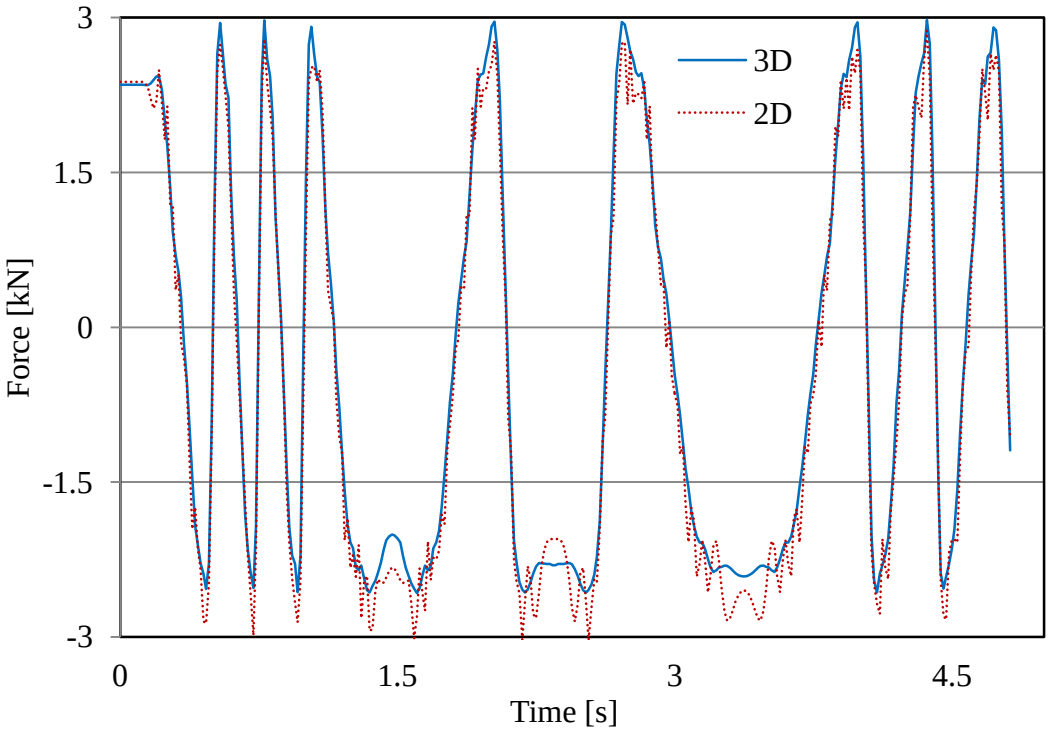

(c) Cogging force comparison

Figure 44 Comparisons between 2D and 3D FEM simulation results

For the simulations in Figure 44a and Figure 44b, a sine wave has been applied as the velocity for the translator. The sine wave has period of 1.5s and amplitude of 0.76m/s. For the simulation in Figure 44c, part of the graph shown in Figure 45c is used to present the difference in cogging force. The current density of the copper coil wires is 0.43 A/mm^2 at peak power (a consideration is made that 75% of the cross-sectional area of the coils is copper and 25% is insulation).

The comparison confirms that the magnetic flux and the voltage are very similar. However, a difference can be observed in the cogging forces (Figure 44c).

3.2.5.1. Magnetic Forces

A comparison is presented in Figure 45c between the magnetic force at no-load, (cogging force) and the magnetic force under load. The total force is the sum of the cogging force and the magnetic force caused by the armature reaction in the machine.

In Figure 45c it can be observed that the total force can be several times higher than the cogging forces. However, the cogging force has much higher frequency which can cause vibrations, underwater noise and electrical power oscillations (Kimoulakis, Kladas et al. 2009, Faiz, Ebrahimi-Salari et al. 2010, Shabani, Milimonfared et al. 2007, Ashabani, Milimonfared et al. 2008). Another unwanted effect that can be caused by the cogging force is mechanical resonance, which occurs when the frequency of the cogging forces is similar to the resonant frequency of the supporting structure or the generator itself.

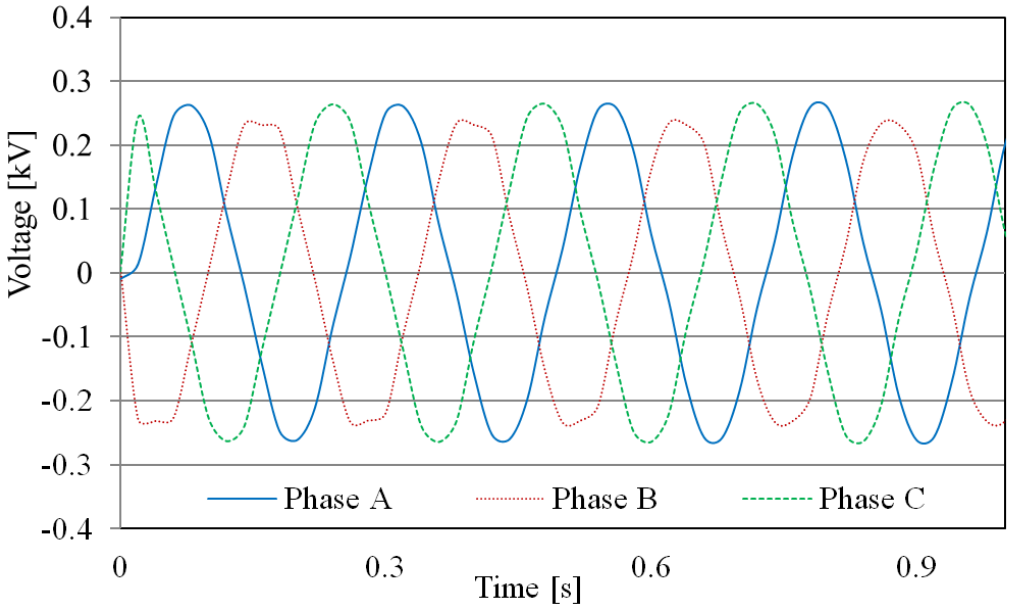

(a) No-load phase voltage

(b) Three-phase power and current under load

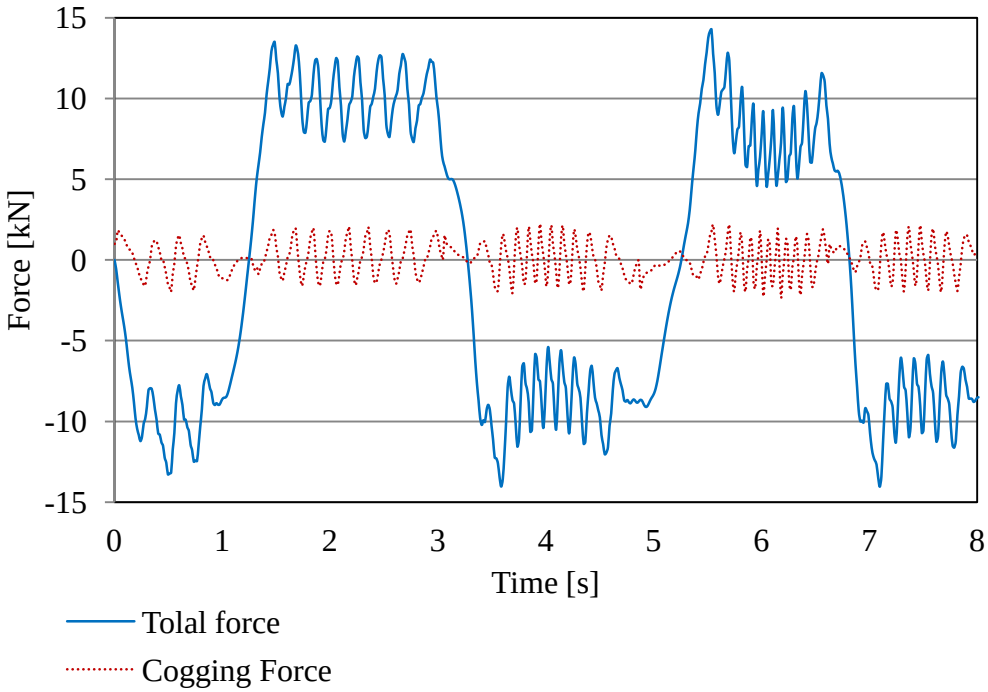

(c) X-axis forces at load and no-load (cogging force)

Figure 45 Results for the base model at constant velocity of 1m/s

In the simulations under load, a three-phase (star connected) 5-ohm active load is connected to the generator windings. Furthermore, a constant velocity of 1 m/s is applied to the machine translator.

3.2.5.2. Different Numbers of Slots per Pole and Phase q

In this chapter, the magnetic force levels for different values of q are presented as single numbers, where the number is evaluated from the simulated force in the time domain. The intention is to present an optimal number for q. The method for calculating the single numbers by using the sample graph in Figure 46a is explained below:

1. The data shown in Figure 46a is converted to absolute values in Figure 46b.

2. In Figure 46b, the values of the peak force (in red circle) and 60% of the peak are established.
3. The upper part of the graph (from 60% to 100%) shown as the pink area in Figure 46b is analysed.
4. The values within the pink area where the tangent to the graph is parallel to the time axis are obtained. The values are shown as blue dots in Figure 46b.
5. Finally, an average of the values obtained from the blue dots in Figure 46b, is calculated and this average number is taken as representative of the force level in the sample graph.

The main objective of the above technique is to calculate two factors. The first is to show the average amplitude of the peak forces (60% to 100%) and the other is to take into account how often the generator reach forces higher than 60%. For example, if the majority of the peaks lie between 60% and 70%, a lower average will be established in comparison with the case where the majority of forces lie between 70% and 80%. Therefore, by using this method, not only can the peak force can be taken into account but also, it can be assessed how often that peak force is reached.

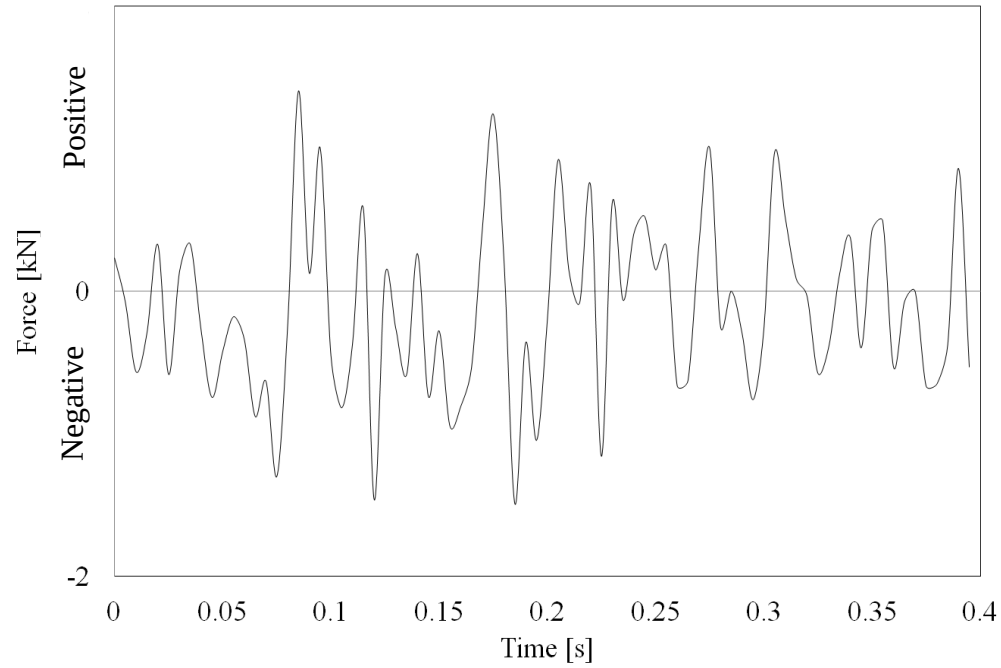

(a) Sample graph in time domain

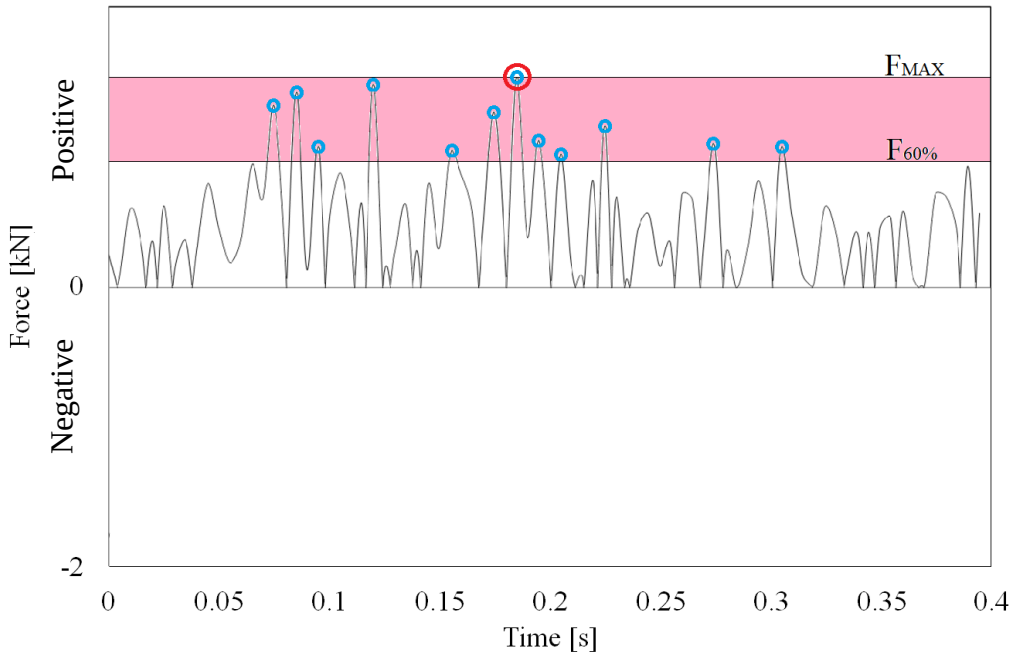

(b) Evaluation of single number representing the sample graph

Figure 46 Calculating single number representing the cogging forces

The purpose of this approach is to evaluate a single number, which is representative of the peak forces of the entire simulation period in the time

domain. The minimum level (in this case 60%) can be altered. The decision that only forces higher than 60% are to be included is made in order to include a greater number of peaks. The high number of peaks is important in reducing the error in the peak forces from the FEA simulations.

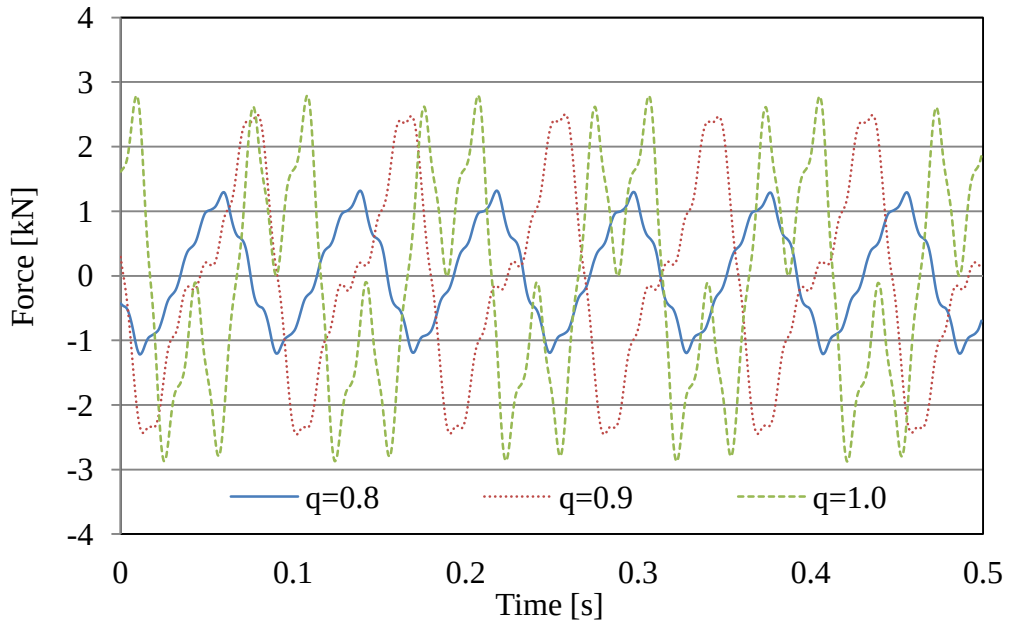

(a) Cogging forces (X-axis) for q = 0.8, 0.9, 1.0

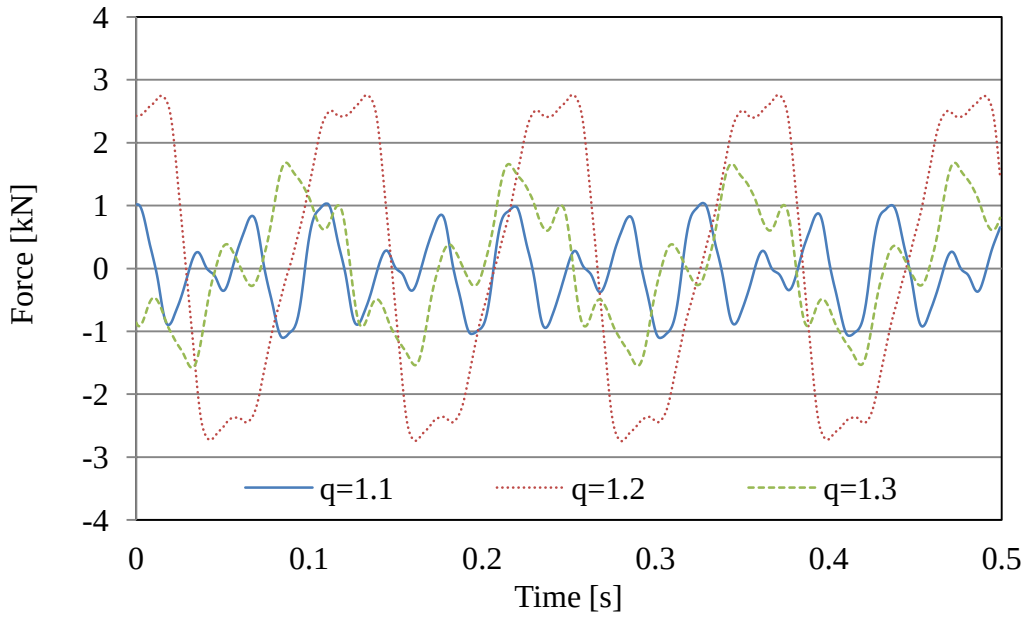

(b) X-axis (cogging forces) for q = 1.1, 1.2, 1.3

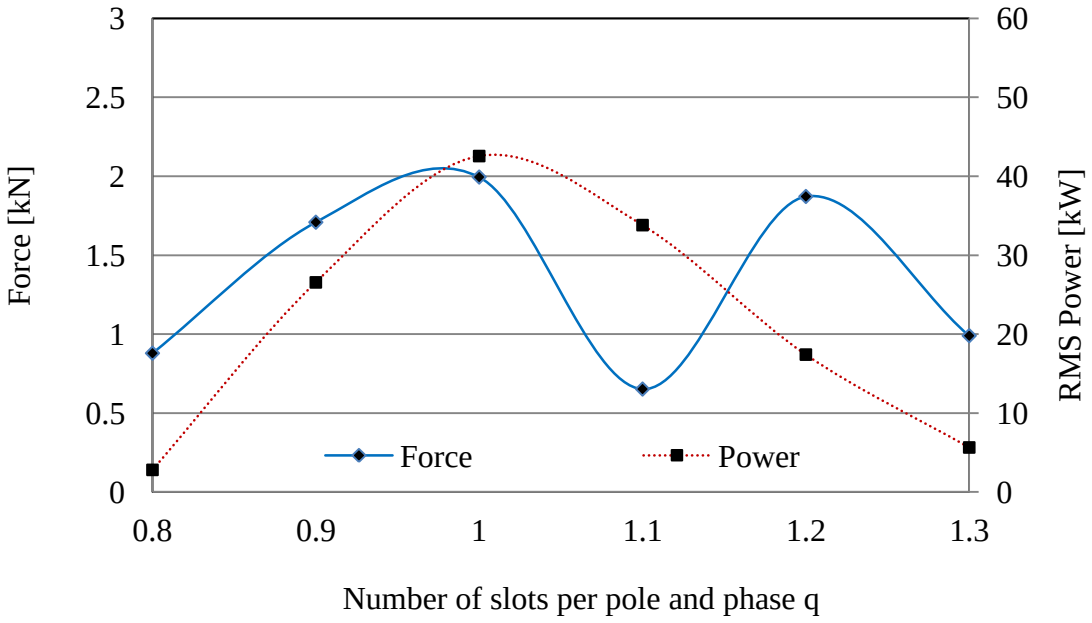

(c) X-axis cogging force as single values and RMS power output for different number of q

Figure 47 X-axis forces for single sided PMLG

It is shown in Figure 47c that the highest RMS power can be established at q = 1, where the flux seen by each winding section has the highest amplitude. However, at the value of q = 1, there is high force disturbance. Such forces parallel to the X axis can also affect the latching/unlatching control systems of the WEC.

In Figure 47c the cogging forces for every value of q are presented as single values using the approach shown above. It can be observed that the generator model with q = 1.1 has the lowest number of cogging forces and relatively high output power and therefore, this can be considered as an optimal choice for q.

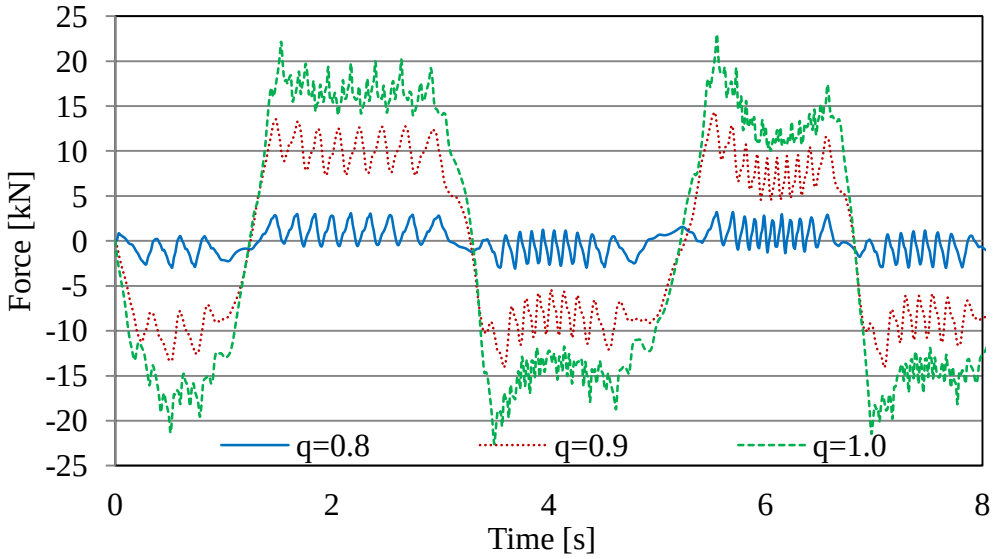

(a) X-axis forces under-load for q = 0.8, 0.9, 1.0

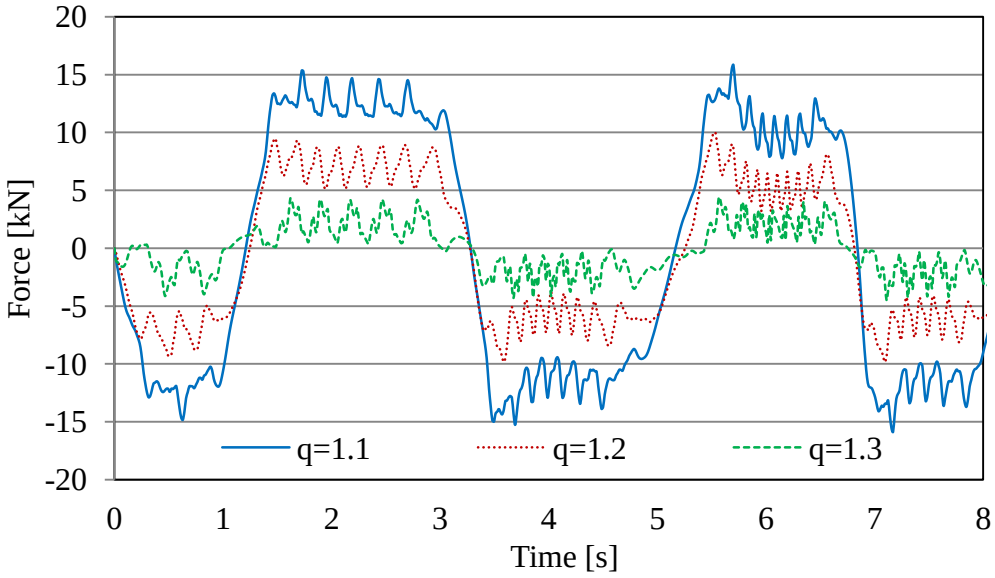

(b) X-axis forces under-load for q = 1.1, 1.2, 1.3

Figure 48 X-axis total forces under-load for different values of $\boldsymbol{q}$

The simulated magnetic total forces when the generator is connected to an active electrical load are shown in Figure 48. It can be seen that the cogging force can be several times lower that the total force, where the total force is the sum of the armature reaction in the PMLG and the cogging force. However, the frequency of the cogging forces could be up to twenty times higher. In addition,

the amplitude of the total force is dependent on the power output of the machine, i.e., the magnitude of the armature currents.

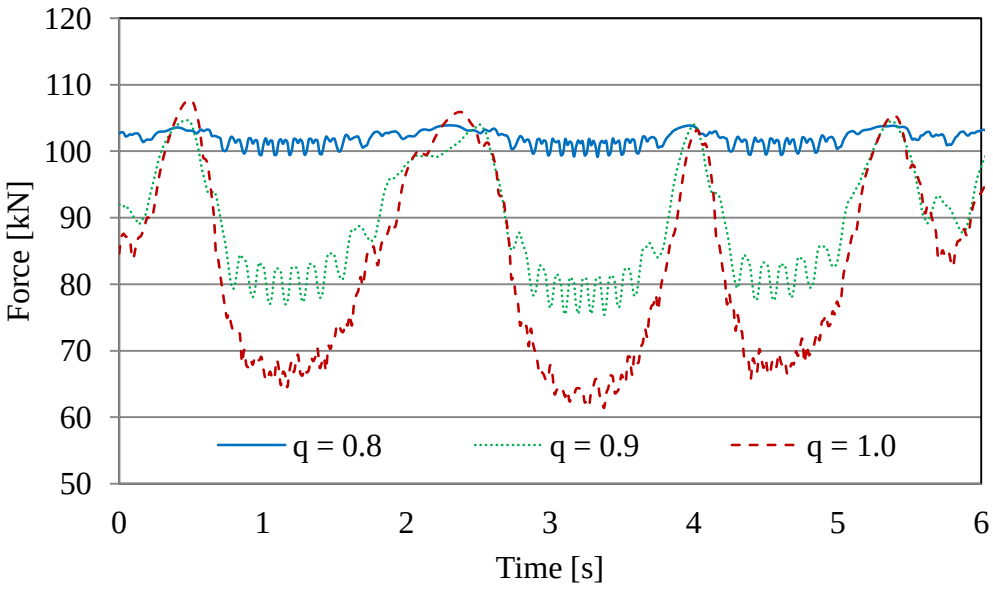

(a) Forces under load in Y-axis for $\boldsymbol{q}$ = 0.8, 0.9, 1.0

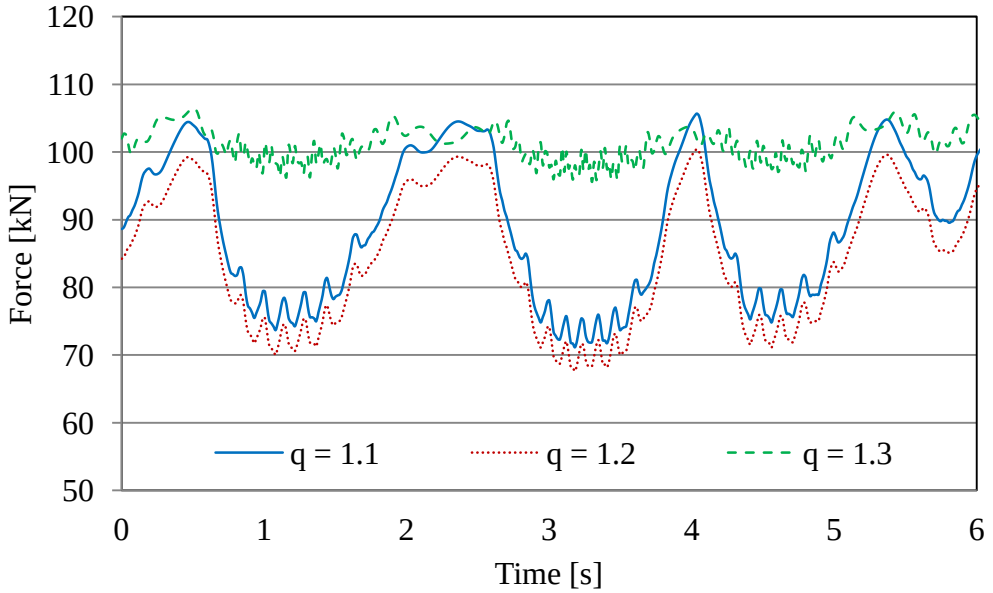

(b) Forces under load in Y-axis for q = 1.1, 1.2, 1.3

Figure 49 Y-axis forces under-load for different values of $\boldsymbol{q}$

The magnetic forces in the Y-axis are shown in Figure 49, which illustrates that the attraction force in the Y-axis is very high and that the force is only

positive, due to the single-sided magnet arrangement. The machine's bearing might find such high forces difficult to handle. The forces can be eliminated by stacking several single-sided structures in a multiple-sided PMLG (such as two or four sides). In theory, all the forces in the Y-axis are opposing and eliminating. However, because of imperfections in construction, this cannot be fully achieved fully and some of the force (in the Y-axis) remains.

3.2.5.3. The Effect of Different Number of Winding Sections

This chapter presents results from simulations of the single-sided PMLG with windings distributed from two to nine sections (coils), where all parameters remain the same as the base model, except for the number of sections and consequently, the translator yoke length. The winding sections are connected in series (Appendix C) and each of them has 0.15-ohm resistance. Therefore, the resistances of the windings vary with the number of sections connected, which can be calculated by:

$$R_{winding} = p \times 0.15 \tag{3.15}$$

where p is the number of winding sections connected in series. The simulation results are presented in Figure 50, where a significant difference in the electrical output can be observed when varying the numbers of sections.

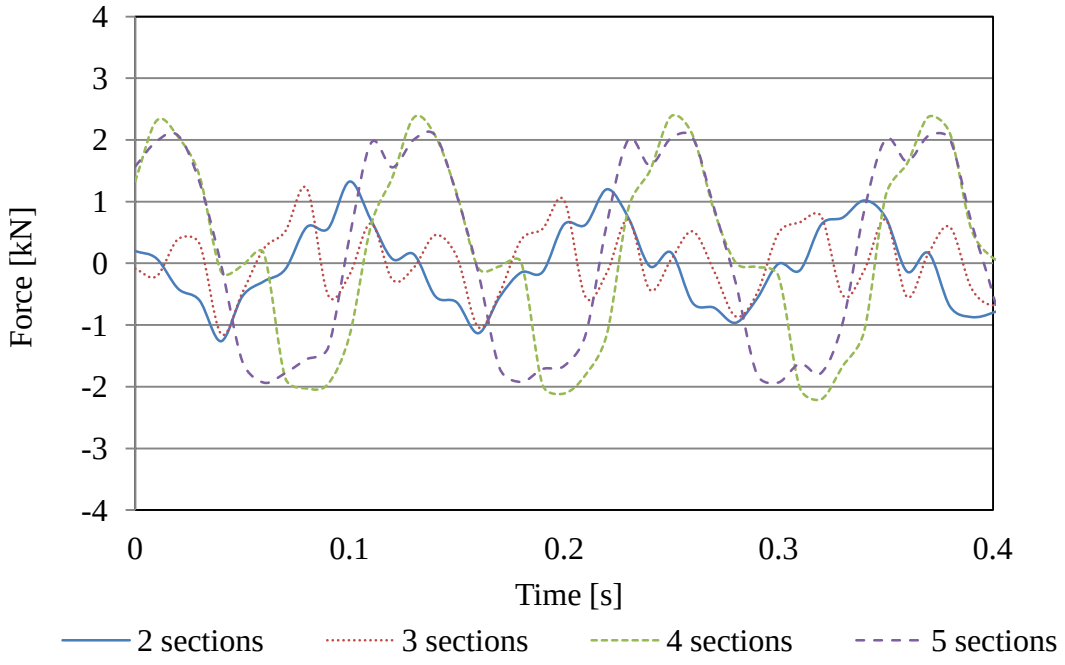

(a) X-axis cogging force for generator with 2, 3, 4 and 5 winding sections

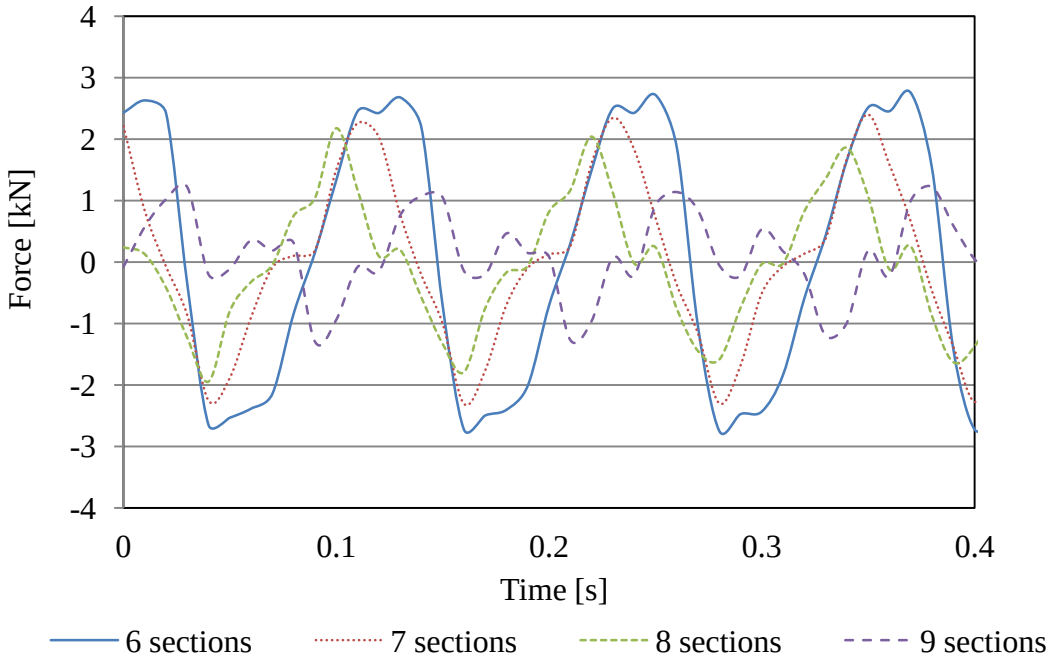

(b) X-axis cogging force for generator with 6, 7, 8 and 9 winding sections

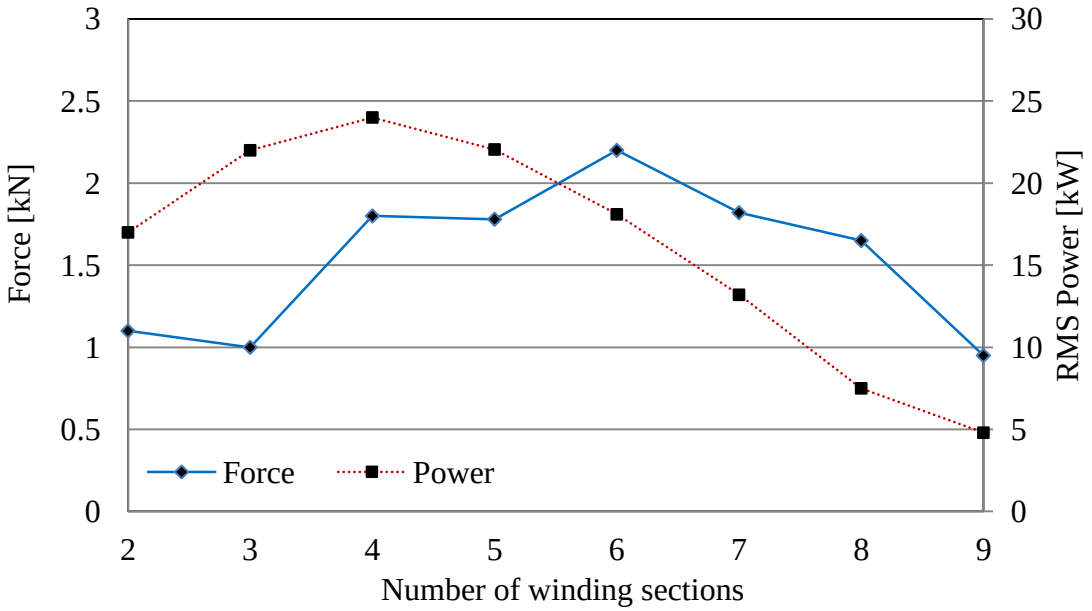

(c) X-axis (cogging force) as single values and RMS power output for different number of winding sections

Figure 50 X-axis forces and RMS power output

It can be considered that the high power output is delivered in the range from two to six sections. However, the highest forces also appear in this area. Therefore, a consideration could be made (Figure 50c) where the optimal number of winding sections is three, based on the lowest ratio between the output power and the level of cogging forces. However, it is important to note that this optimal number, presented in this set of results, is valid only for generators where q = 1.2. For generators with different values of q, the optimum number can be different.

3.2.5.4. Different Number of Magnets Mounted on the Translator

The simulations in this section are made by applying a fixed base model's stator and a number of magnets mounted on the translator, depending on the length of the translator yoke. The generators with six and seven magnets covering the

translator's length are shown in Figure 51.

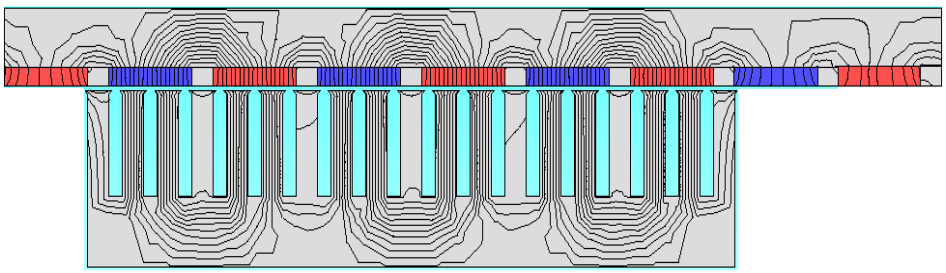

(a) PMLG with 6 magnets covering the length of the translator yoke

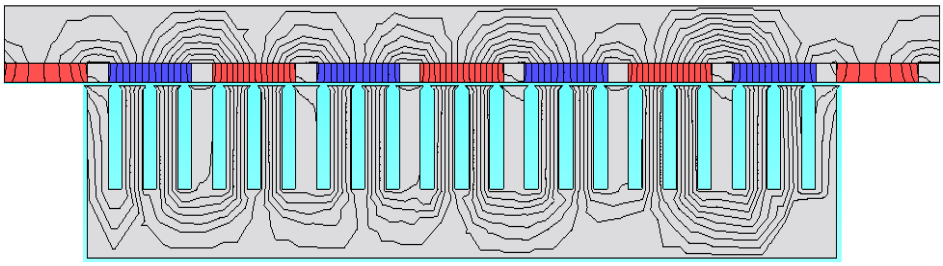

(b) PMLG with 7 magnets covering the length of the translator yoke

Figure 51 Flux distribution in PMLG with even and odd number of magnets

It has been established previously that odd and even poles cause different flux distributions within the magnetic core (Danielsson, Leijon 2007). The obtained results for the static flux distribution show high similarity to the results from (Danielsson, Leijon 2007) (Figure 51).

The effect of the different flux distribution on the PMLG's cogging forces is investigated in this section. The investigation involves three sets of generators with even and odd numbers of magnets.

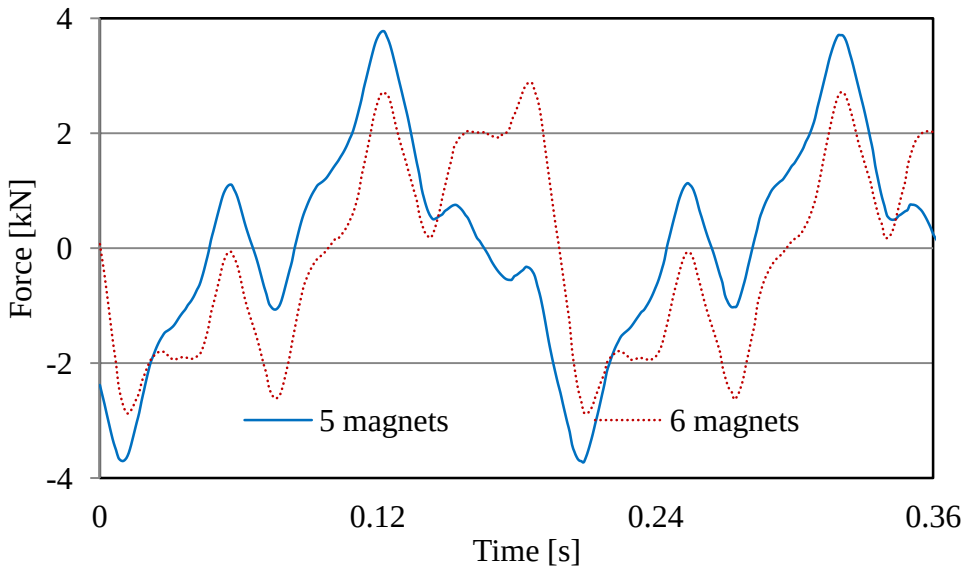

(a) Cogging force for models with 5 and 6 magnets

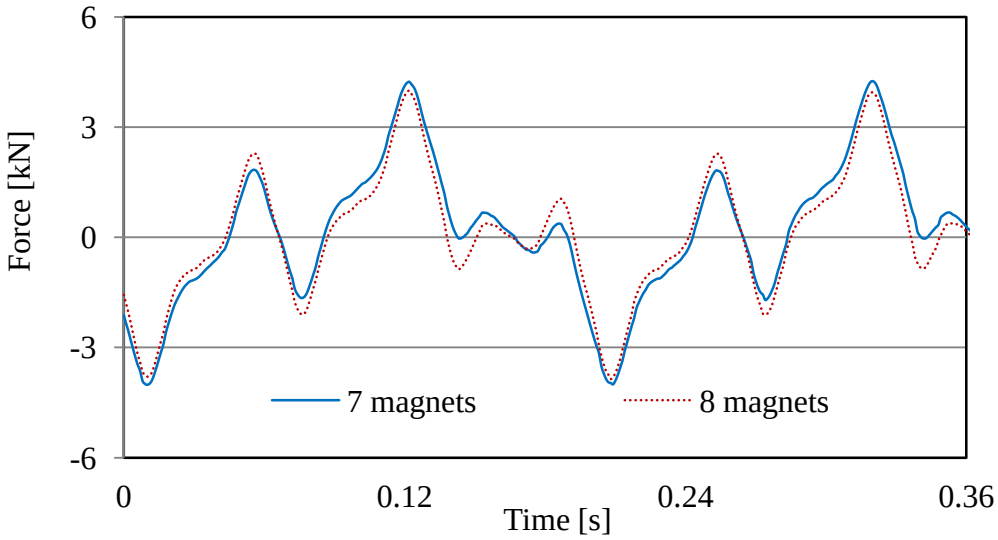

(b) Cogging force for models with 7 and 8 magnets

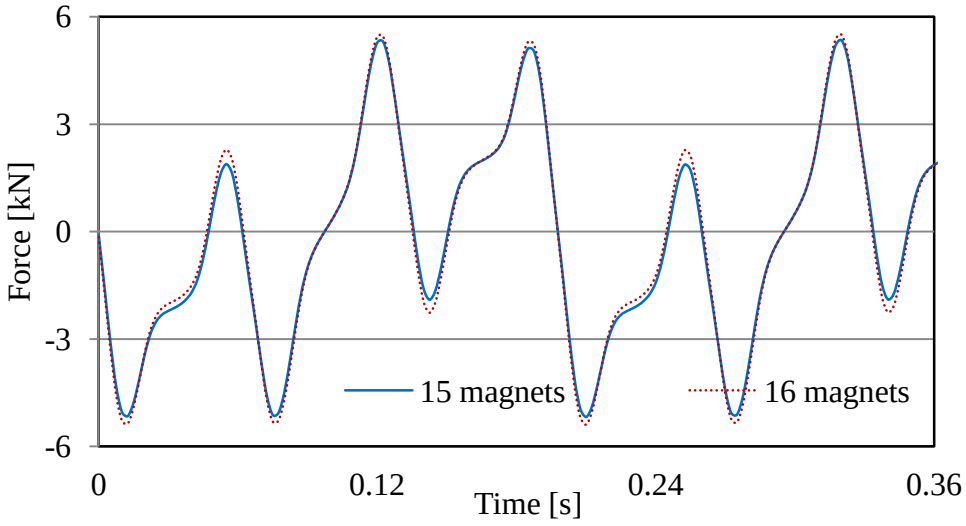

(c) Cogging force for models with 15 and 16 magnets

Figure 52 Different number of magnets mounted on the translator

The cogging forces for the first set: five and six magnets are shown in Figure 52a, the other two sets with 7 and 8 magnets and 15 and 16 magnets are shown in Figure 52b and Figure 52c, respectively. It can be observed that short translators with an odd number magnets cause a reduction of cogging forces compared with translators with an even number of magnets. The difference in the cogging forces between the odd and even numbers of magnets is up to 32%. As the length of the translator is increased, the difference in the cogging forces between the even and odd numbers of magnets is decreased (Figure 52b and Figure 52c).

The single-sided PMLG has the disadvantage of having very high magnetic attraction forces in the Y-axis. The forces remain at any operation mode and velocity. Furthermore, the forces can be destructive for the system's bearings. As a result, a double-sided generator is considered as an alternative approach, which can deliver a reduction of the forces. This reduction is achieved by adding a mirror copy of the winding yoke, placed symmetrically opposite the existing one. In this way, the attraction forces between the magnets and the steel are in opposing directions, resulting a significant reduction of the total magnetic force on the

permanent magnets (in the Y-axis).

3.3. Investigation into Double-Sided Iron-Cored Linear Generator

3.3.1. Generator Description

In this section it is assumed that the PMLG`s stator is assembled from the permanent magnets and the separators. Similarly, the translator is collected from two aligned magnetic cores on both sides of the stator with copper coils placed in slots.

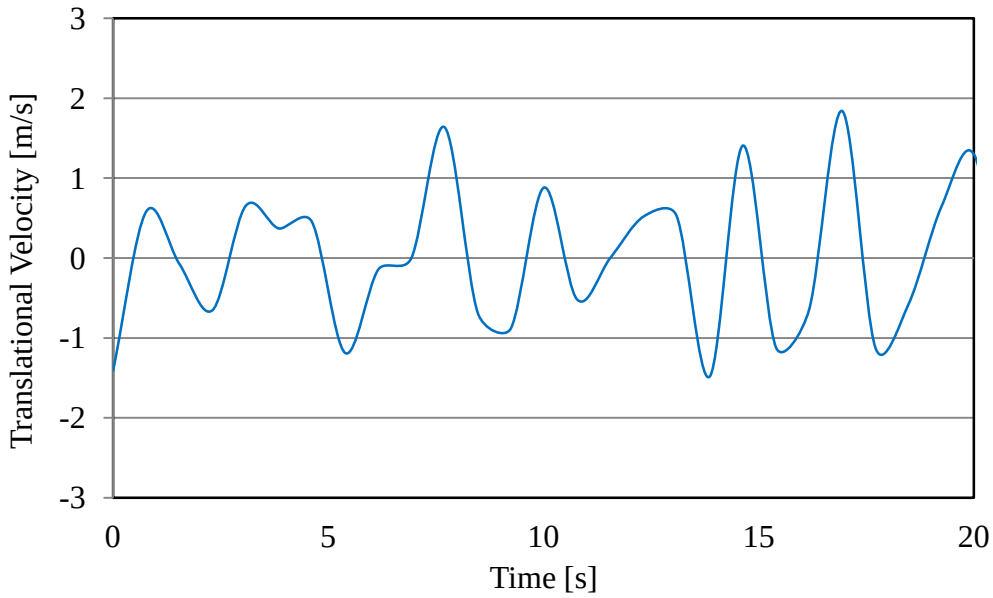

Figure 53 Linear velocity of the translator

The magnetic cores are formed from laminated silicon steel with a stacking factor of 95%. In the FEA simulations, the magnetic cores are treated as magnetically nonlinear materials with single value magnetisation characteristics. Furthermore, the translator teeth are finished with edge-shaped shoes forming semi-closed slot openings. The use of semi-closed slot openings decreases the

power ripple and reduces the magnetic reluctance of the air gap (Ivanova, Agren et al. 2005). Similarly, the generator's excitation is provided by NdFeB-35 magnets with a magnetisation direction parallel to the Y-axis.

The motion applied on the translator is an experimentally recorded vertical velocity/time sequence of stochastic sea conditions. The sequence was recorded by a wave probe over a period of 20 seconds near the South East coast of the UK (

Figure **53**). The focus of this chapter is to achieve an optimisation of the PMLG. Therefore, it is considered that the translator follows strictly the motion of the water surface and the effect of control techniques (such as the latching) on the translator is not taken into account.

The generator shown in Figure 54 has three windings assembled by six winding sections connected in series. Each winding section consists of six coils connected in parallel. The voltages generated from each winding are shifted by ±120 degrees. Therefore, a standard three-phase rectifier can be connected directly to the generator terminals.

The magnetic circuit of the machine is shown in Figure 55, where the magnetic reluctances in the air gap vary in the same way as the single sided PMLG shown the previous section. Also, the number of slots per pole and phase q is 1.2 (Figure 54). Furthermore, the winding configuration and electrical characteristics used for the double-sided machine are the same as those used for the single-sided machine, which can be seen in Table 2. In the double-sided machine, the windings are doubled; therefore, so is the total electrical resistance of the windings. The winding sections of the double-sided PMLG are connected in series forming three-phases (Appendix D).

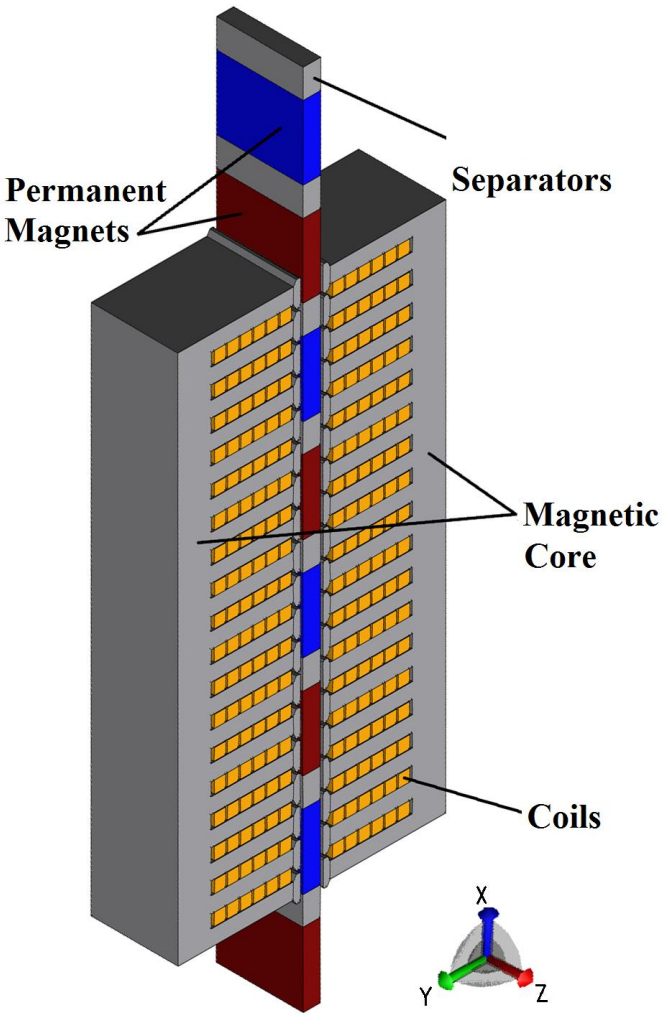

Figure 54 PMLG with six winding sections

The flux distribution modes shown in section 3.3.3.1. are also present in the double-sided structure. Generally, the total magnetic reluctance of the double-sided generator is higher in comparison with the single-sided one because is double the air gap. However, the double-sided structore allows the installation of twice as many coils, contributing to higher generated voltages and therefore, better use of the PM flux can be achieved.

Table 2 Main Dimensions of the double sided PMLG

DIMENSIONS		
Parameter	Axis	
Translator length [mm]	X	612
Translator width [mm]	Z	600
Winding length [mm]	Y	88
Translator height [mm]	Y	318
Permanent magnet length [mm]	X	85
Pole pitch length [mm]	X	118.8
Coil slot length [mm]	X	15
Translator teeth length [mm]	Y	18
Air gap length [mm]	Y	2x3
ELECTRICAL CHARACTERISTICS		
Number of turns per winding section		24
Number of turns per coil		4
Number of slot per pole and phase, q		1.2 (6/5)
Total Winding resistance [ohm]		1.8
Resistive three-phase star connected load [ohm]		5

The main dimensions and the electrical characterictics are given in Table 2. The two winding yokes are connected in series, whereby coils 16, 26, 36, 46, 56 and 66 from the first magnetic yoke are connected with coils 11, 21, 31, 41 and 51, respectively, from the second yoke (Appendix C).

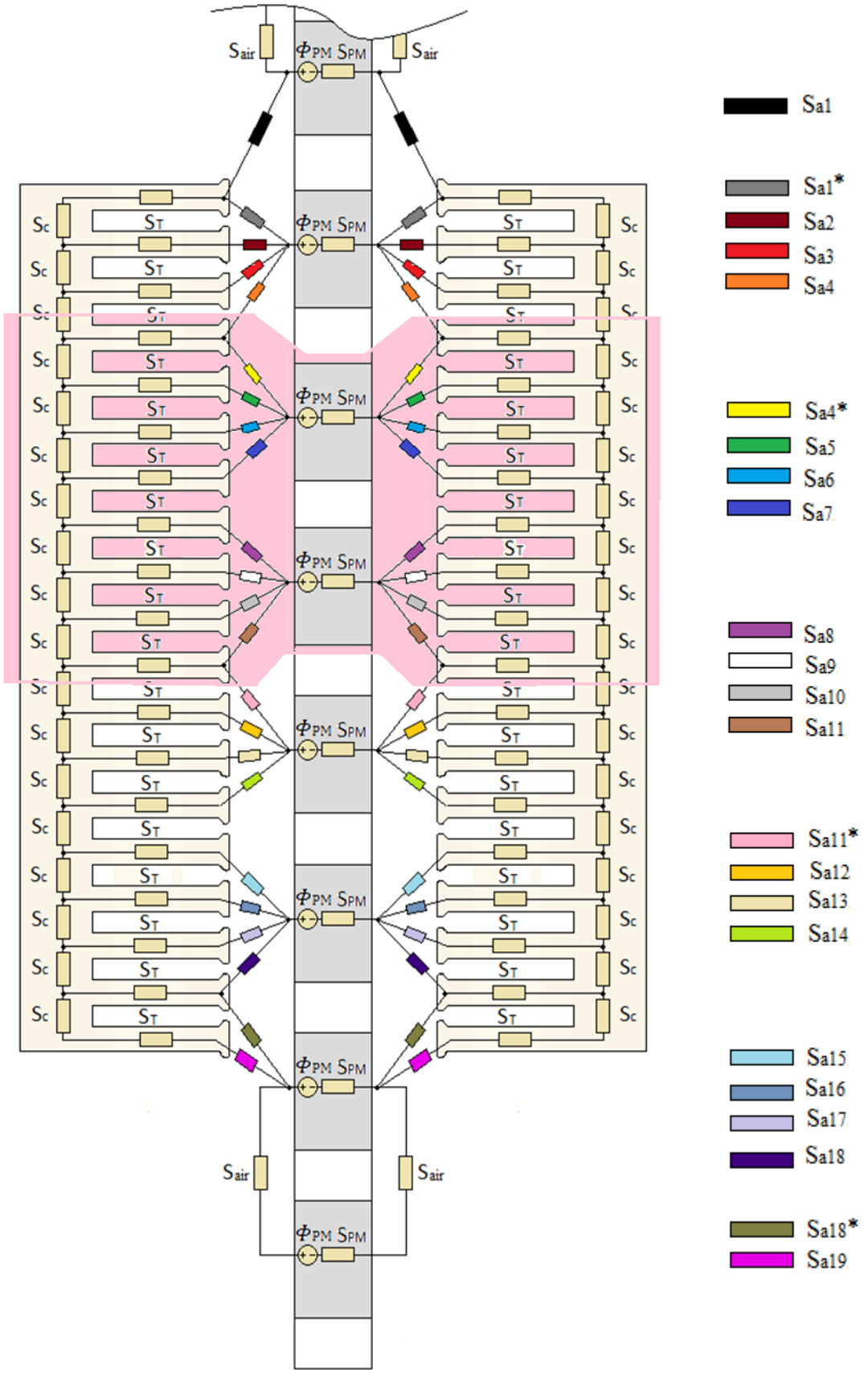

Figure 55 Magnetic circuit of double sided PMLG

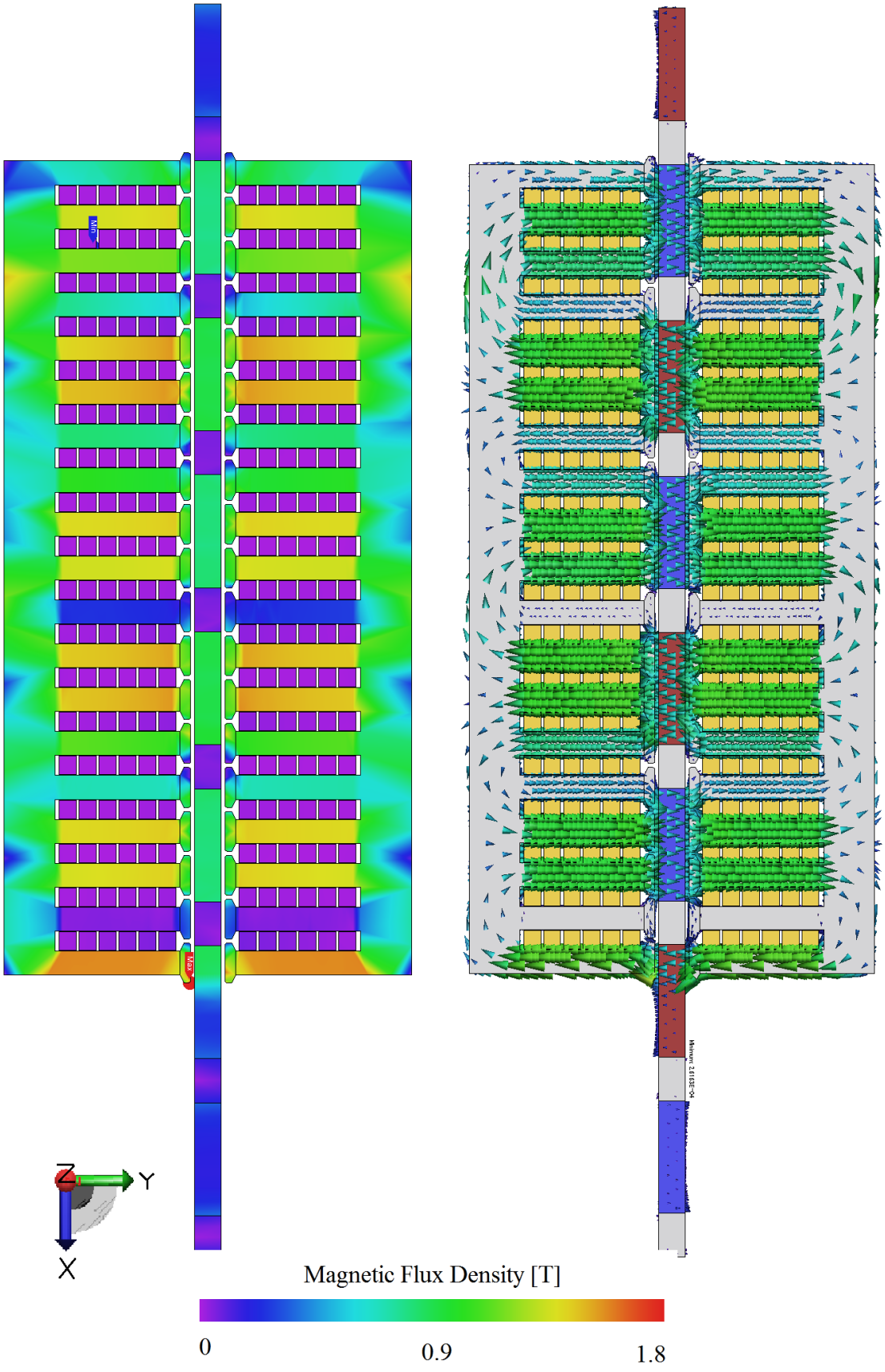

Figure 56 Magnetic flux density in the linear generator

The total magnetic reluctance of a section with a length of two poles is given in (3.16) (pink area in Figure 55). The total magnetic reluctance is calculated in the same way as the reluctance for the single-sided PMLG and represents the reluctance of an equivalent circuit that has a single flux source and a single reluctance (pink area in Figure 55):

$$S_{Total} = 4 * S_E + 2 * S_{PM} + 2 * S_C. \quad (3.16)$$

The magnetic circuit of the double-sided structure is a mirror copy of the single-sided one with the same dimensions of the poles and teeth, etc. The analytical calculations of the flux density in the air gap of the double-sided model reveal a difference of 7% in comparison with the static FEA simulation results for the flux density.

3.3.2. Finite Element Simulation Results

3.3.2.1. Effect of Number of Slots per Pole and Phase q

In this section, the magnetic forces between the stator and translator are shown in the X- and Y-axes. The forces parallel to the X-axis do not affect the bearings directly due to the free bearing motion on the X-axis but they do cause latching of the translator, unwanted noise and vibrations (Prudell, Stoddard et al. 2010). The forces parallel to the Y-axis are directly destructive to the bearings and the supporting structure due to the translator's locked freedom on the Y-axis.

The forces affect the bearings and the supporting structure in different ways and therefore, minimising them is important with regard to maintenance costs and the structural integrity of the WEC.

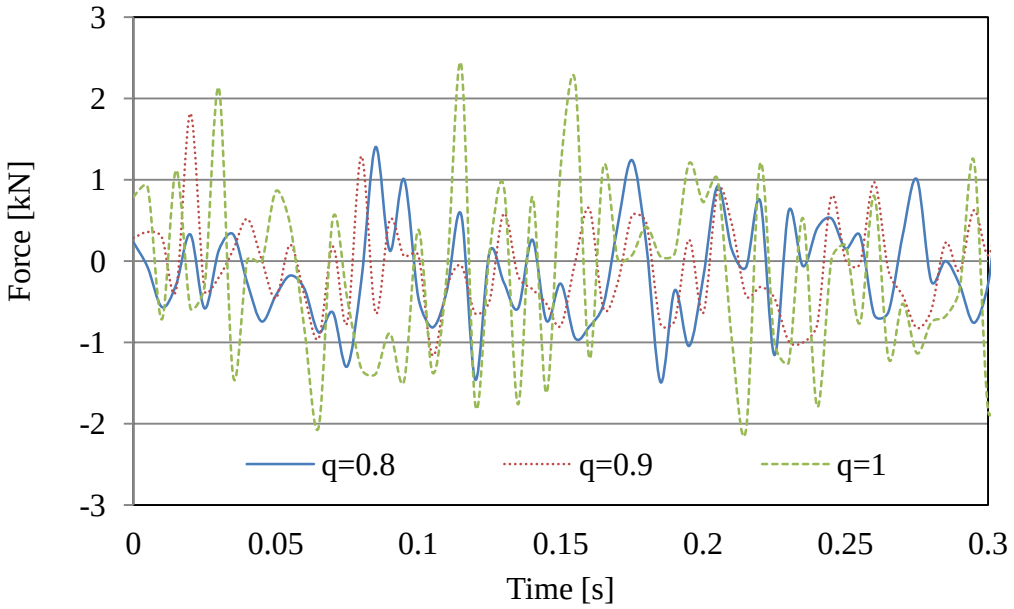

(a) Y-axis magnetic forces for q = 0.8, 0.9 and 1.0

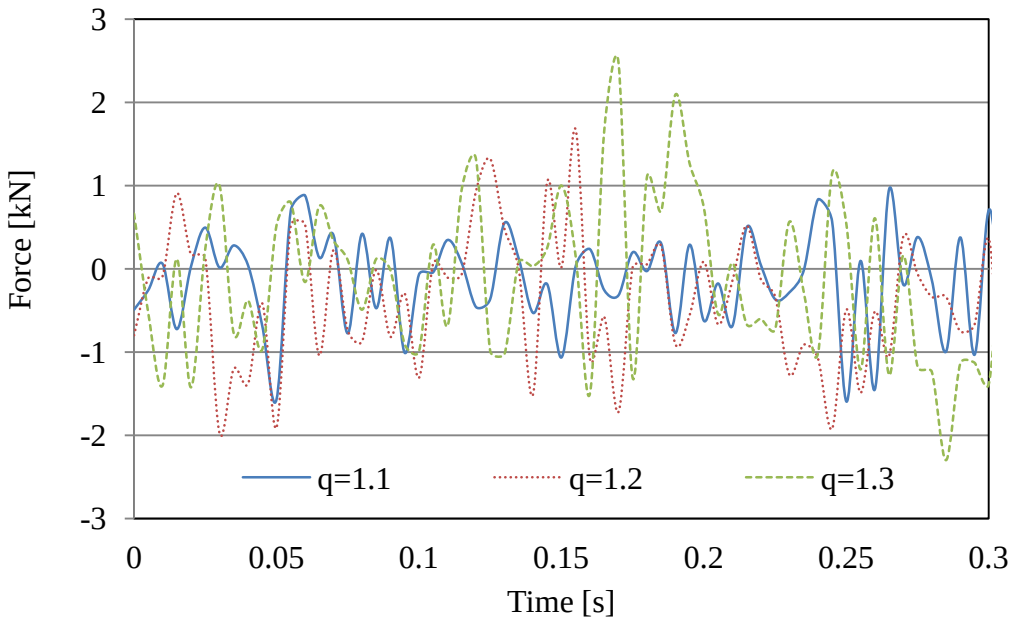

(b) Y-axis magnetic forces for q = 1.1, 1.2 and 1.3

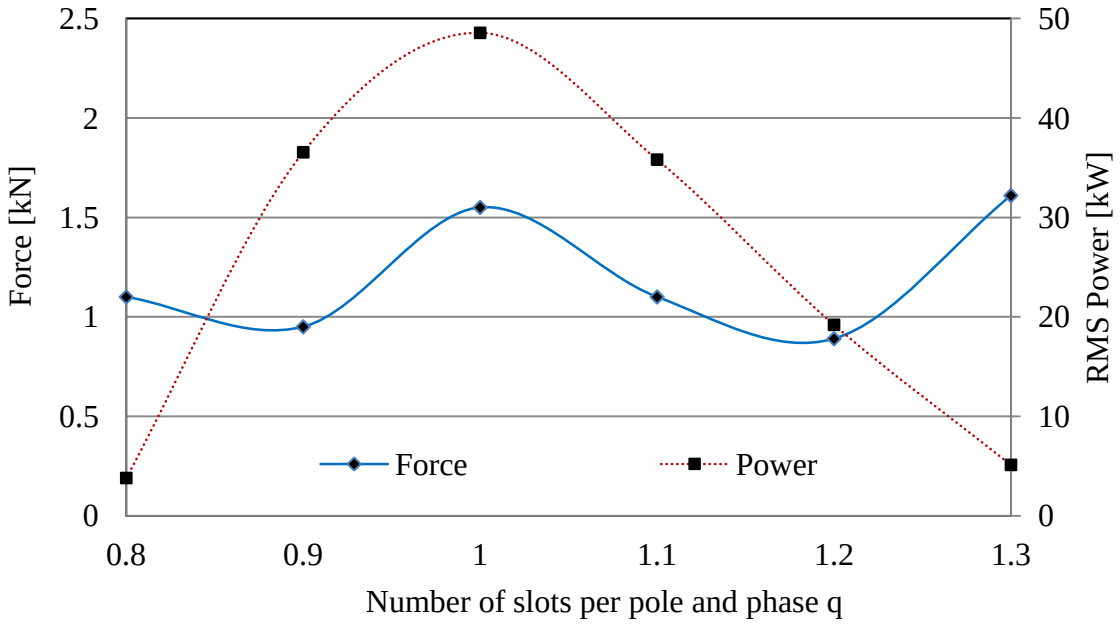

(c) RMS power output and Y-axis forces against different $\boldsymbol{q}$ as single values

Figure 57 Y-axis forces and RMS power for double-sided PMLG

To perform the simulations in the Y-axis, 3D models with high mesh resolution are used to increase the accuracy for the force calculation. A representation for the simulated forces in the time domain is given in Figure 57a and Figure 57b. The results reveal that the highest forces and the highest RMS power output occur when q = 1.

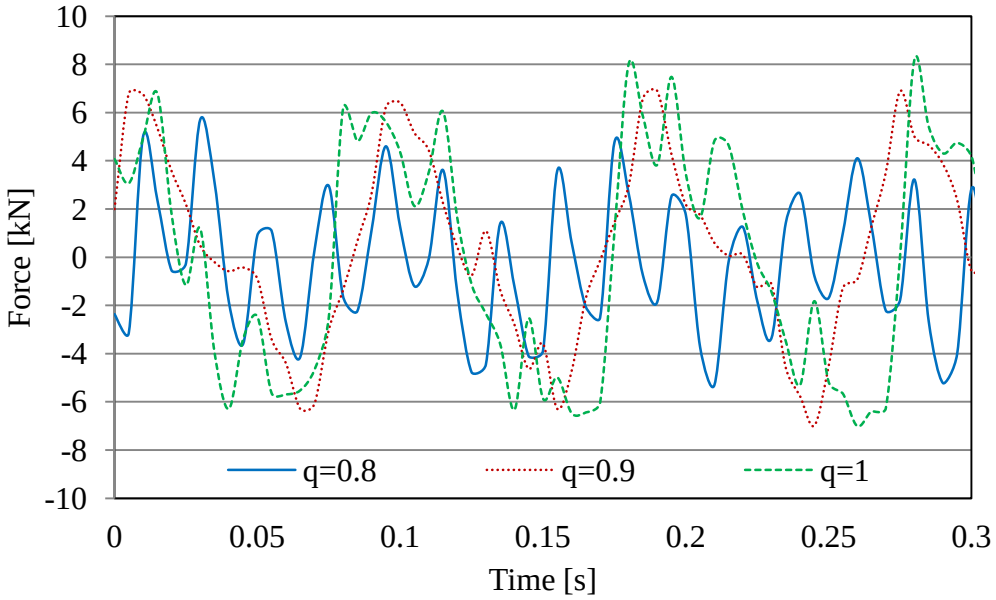

(a) X-axis magnetic forces for q = 0.8, 0.9 and 1.0

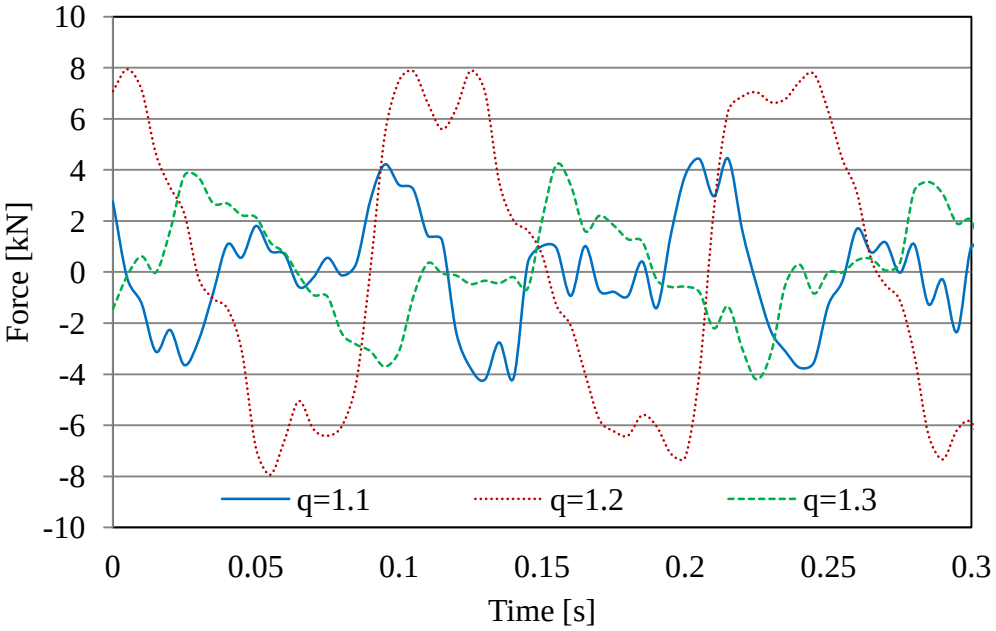

(b) X-axis magnetic forces for q = 1.1, 1.2 and 1.3

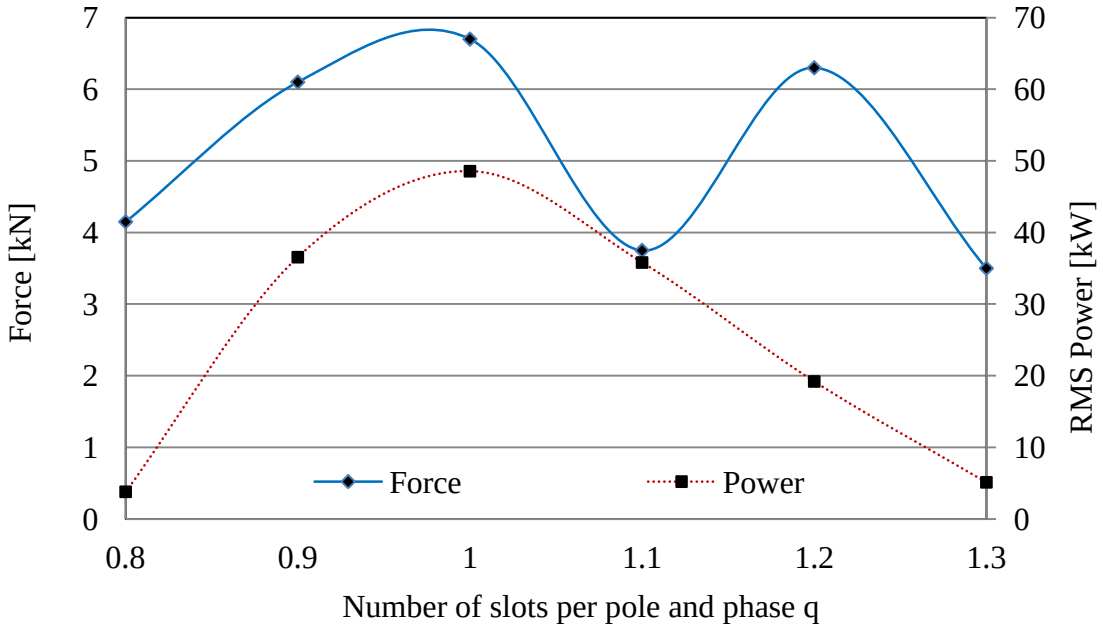

(c) RMS power output and X-axis forces against different $\boldsymbol{q}$

Figure 58 X-axis forces and RMS power for double-sided PMLG

In Figure 58a and Figure 58b, the X-axis forces are shown in the time domain. In Figure 58c, a presentation of all the forces as single number is shown. Moreover, in the same figure, the RMS powers for each q are calculated over the complete time series shown in

Figure **53**. The current density for the models with a 50 kW output power (q = 1) is 0.8 A/mm^2. It can be seen that the cogging forces follow a very similar pattern to those of the single-sided PMLG. However, their magnitude is approximately twice as great. The reason for this is the double sided structure of the generator doubles the number of teeth attracting the PMs. Moreover, the harvested electrical energy is also higher.

In Table 3, the Force-to-Power ratio for the X- and Y-axes is presented for all values of q. As the aim of the optimisation is to minimise forces and maximise electrical power, the lowest numbers in Table 3 define the optimal value for q.

Table 3 Force-to-Power ratio for X- and Y-axes

q	X-axis [N/W]	Y-axis [N/W]
0.8	1.09268	0.28963
0.9	0.16689	**0.02599**
1	0.13797	0.03192
1.1	**0.10472**	0.03072
1.2	0.32813	0.04635
1.3	0.68359	0.31445

The results for the X-axis reveal q = 1.1 as optimal and the results for the Y-axis reveal that q = 0.9 is optimal. This ratio is important because the maximum output power can be determined by knowing the level of the acceptable forces for the bearings (Y-axis) and the level of the acceptable vibrations (X-axis). Therefore, for different bearing systems and different WEC supporting structures the numbers could vary. For the purpose of this optimisation, the optimal number of q is suggested based on the lowest Force-to-Power ratio.

3.3.2.2. Effect of Different Numbers of Winding Sections

In this section, translators with different number of winding sections are simulated. Results obtained from models with windings distributed from two to nine sections are shown. All parameters except the number of the sections (and consequently the translator length) are the same as the parameters in Table 1. As the generators simulated in this section have a different number of winding sections, the total winding resistance differs and it can be calculated by:

$$R_{winding} = 2 * 0.15 * p \quad (3.17)$$

where: p is the number of winding sections connected in series.

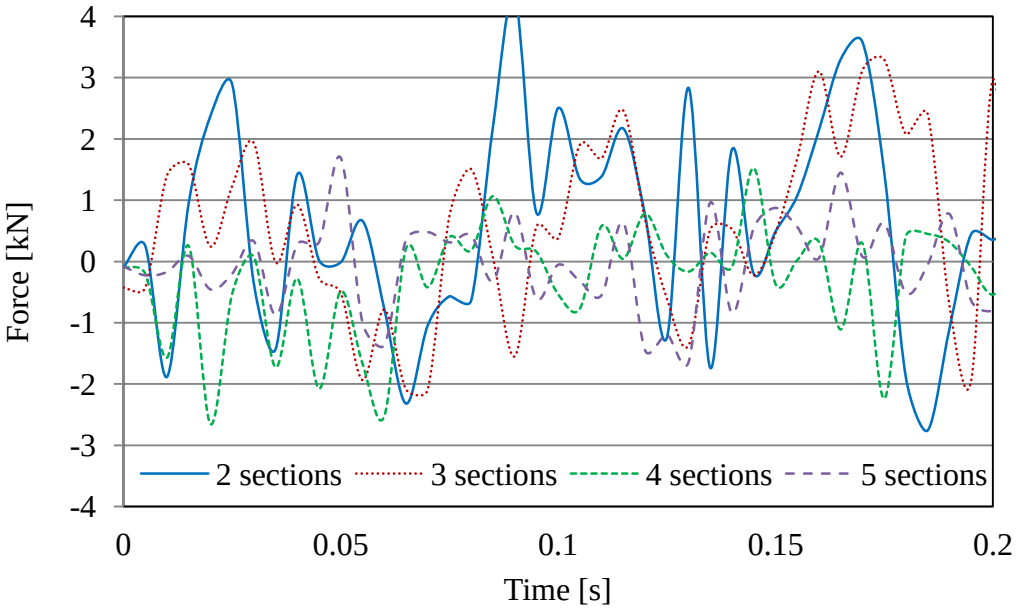

(a) Y-axis magnetic forces for 2, 3, 4 and 5 winding sections

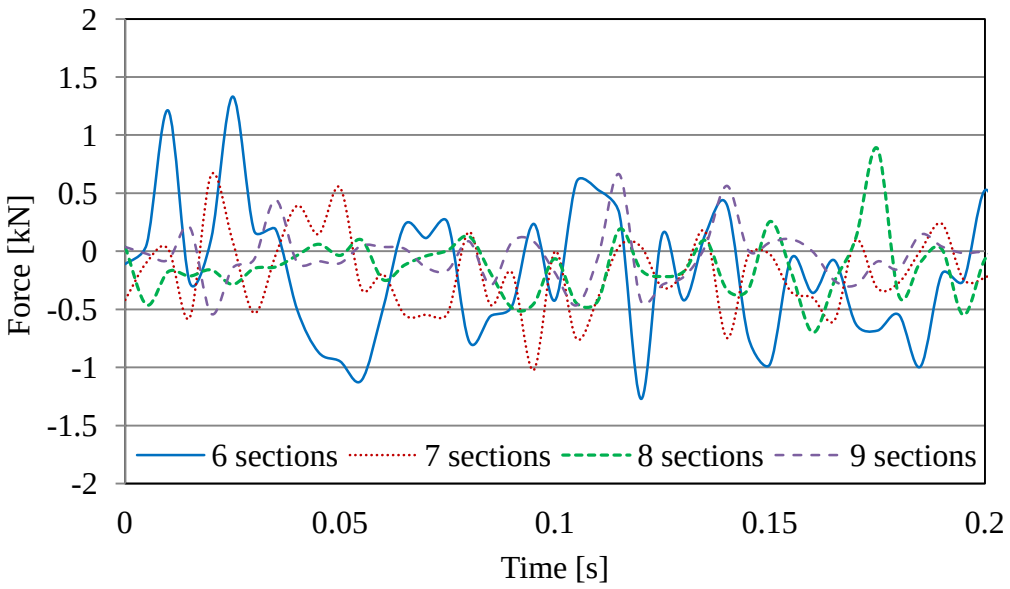

(b) Y-axis magnetic forces for 6, 7, 8 and 9 winding sections

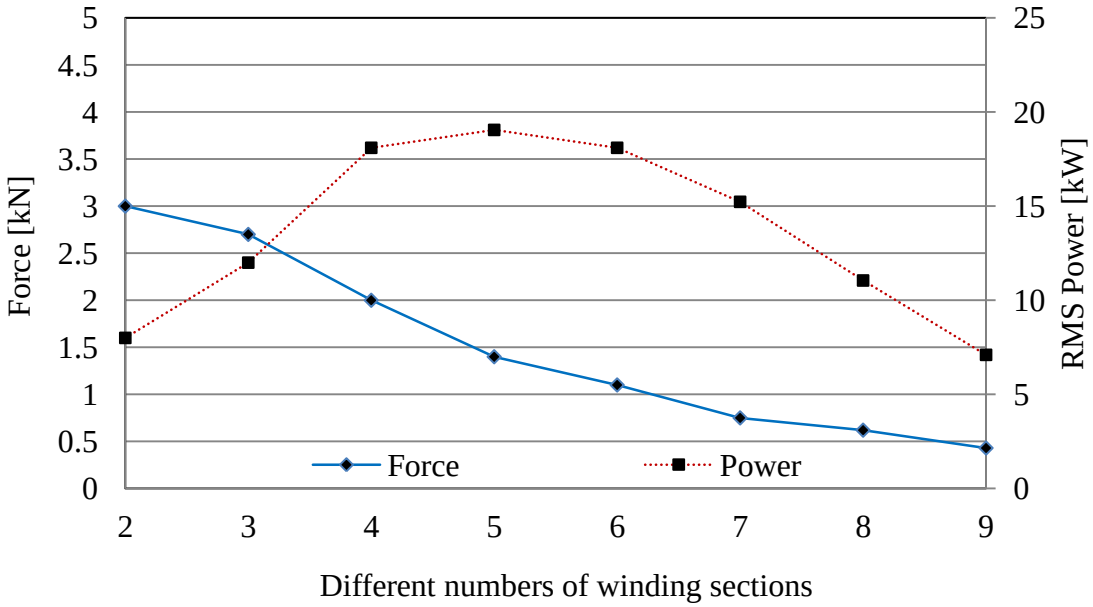

(c) Y-axis single values of forces for different numbers of winding sections

Figure 59 Y-axis forces and RMS power for double-sided PMLG

In Figure 59a and Figure 59b, the forces parallel to the Y-axis are shown in the time domain and also in Figure 59c, the force levels representative for all numbers of winding sections are calculated by the approach shown in Section 3.3.5.2.

To perform the simulations in the Y-axis, 3D models with high mesh resolution are used to increase accuracy for the force calculation. The simulation results show that the highest force appears for those generators with the lower number of winding sections. The effect from the misalignment between the stator poles and translator teeth (q =1.2) is the main reason for this result. In short translators this misalignment has less effect; however, for longer translators the misalignment becomes higher than the length of the pole. Therefore, the peaks of the cogging forces for every tooth do not occur at the same point in time. Additionally, the result for the RMS power output is also

shown in Figure 59c. It can be seen that the highest power output can be achieved with five winding sections.

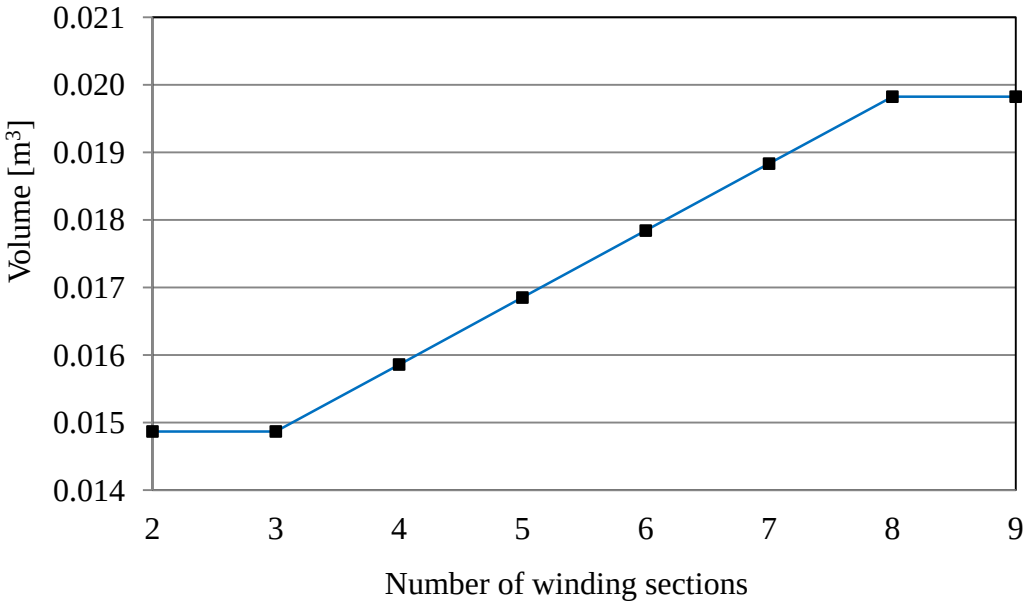

Figure 60 Volume of PM material versus different number of sections

To compare the generator models on the same basis regarding the PM volume, the simulated models should have the same length of maximum translation of the translator. Therefore, the total length of the stator is assumed to be the length of the translator plus an additional 1.5 metres, where free maximum translation is allowed. In Figure 60, the volume of permanent magnet material is calculated for generators with different numbers of sections. The results are averaged to the nearest magnetic pole.

In Figure 61a and Figure 61b the forces parallel to the X-axis are shown in the time domain. The single numbers representing the forces are shown in Figure 61c.

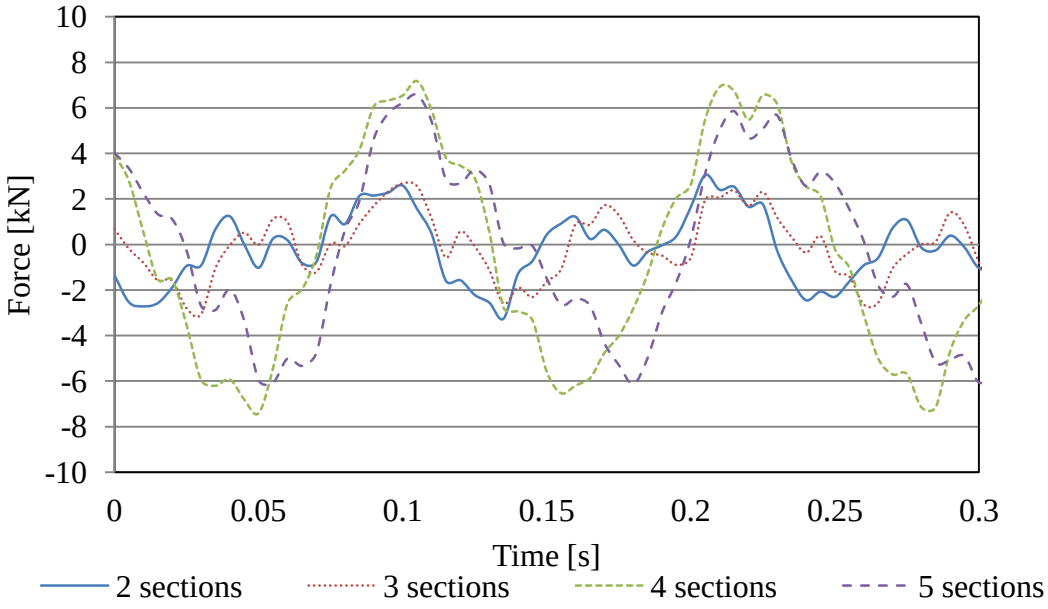

(a) X-axis (cogging forces) for 2, 3, 4 and 5 winding sections

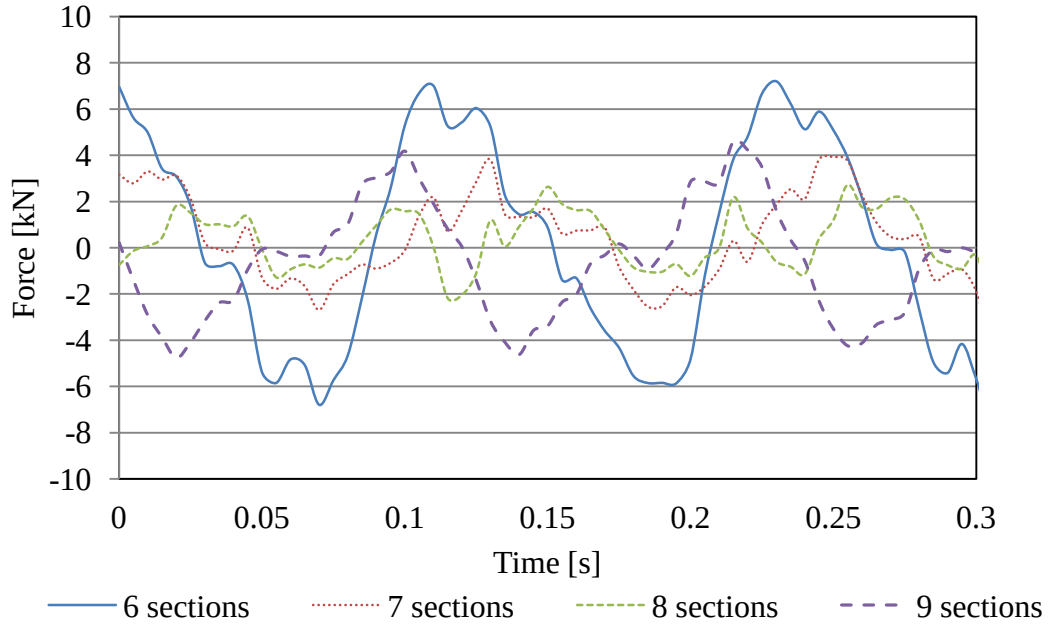

(b) X-axis (cogging forces) for 6, 7, 8 and 9 winding sections

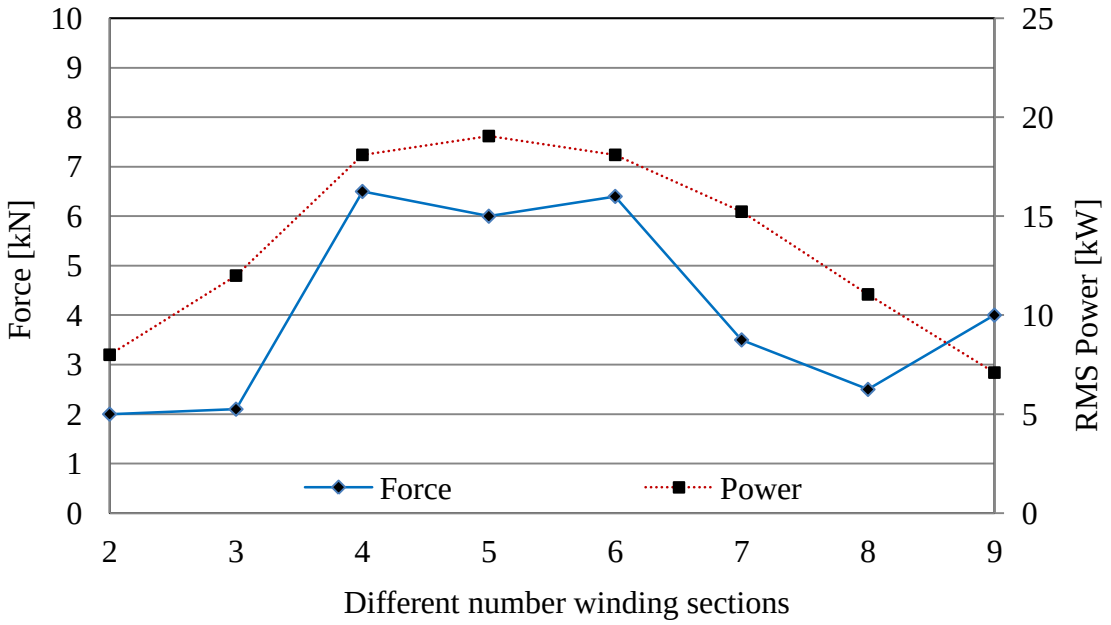

(c) X-axis single values of forces for different number winding sections

Figure 61 X-axis forces and RMS power for double sided PMLG

Table 4 shows the Force-to-Power ratio in the X- and Y-axes for generators with different number of winding sections and Power-to-PM volume ratio. The results reveal an optimal number of three winding sections for the X-axis force and seven sections for the Y-axis force.

Table 4 Force-to-Power [N/W] and Power-to-PM volume ratio [W/m3] ratios for X- and Y-axes

Number of sections	X-axis [N/W]	Y-axis [N/W]	Power-to-PM volume ratio [W/m^3]
2	0.250	0.375	579
3	**0.175**	0.225	862
4	0.359	0.110	**1156**
5	0.299	0.070	1125
6	0.354	0.061	1019
7	0.230	**0.049**	776
8	0.226	0.056	542
9	0.563	0.061	329

Another coefficient representing the efficiency of the generator is the Power-to-PM volume ratio (Table 4). This coefficient is not discussed in the previous section because of the small difference in the volumes of the PM material for different q. The aim here is to maximise the ratio; therefore, the generator with four sections can be considered optimal for this criterion.

The importance of such a comparison is triggered by the price of the permanent magnets. Recent price changes of permanent magnets by almost 800% (for the period 04/2010 to 07/2011) (Humphries 2011) makes the permanent magnet material the most expensive component of the PMLGs.

3.3.3. Optimisation of the Permanent Magnet Linear Generator

From the results shown in Figure 57, it can be observed that the highest electrical power is harvested at q =1. At this value of the slots per pole and phase, a perfect alignment among the coils and permanent magnets is established. Consequently, the generated coil voltages will be in phase and therefore, the highest total generated voltage can be achieved. However, the iron pole shoes become aligned with the permanent magnets and hence, strong cogging force is generated. On the other hand, the results shown in Figure 59, suggest that generally high numbers of winding sections reduces the cogging force due to the misalignment among the peaks of the magnetic forces between the PMs and the steel shoes. Based on the above results, it is observed that a

long stator, which consists of a number of short stators, can deliver high output power, where the power is combined from the individual short stators. Furthermore, low cogging force can be achieved by increasing the total length of the stator, where the length is the combined lengths of the small stators.

In this section, an optimised generator is suggested taking into account the results presented in Section 3.3.2. The aims of the optimisation in decreasing order of their importance are:

1. Low force parallel to the X-axis
2. Low force parallel to the Y-axis
3. High electrical output power
4. Low volumes of permanent magnet material used in the generator assembly.

Higher importance is given to those aims related to maintenance costs, which could be considerably high, due to the offshore and/or underwater operating conditions.

With regard to the above order of aims, it can be considered that the optimal solution is when q = 1.1 rather than q = 0.9. The reason for this decision is the small difference between the Force-to-Power ratio in the Y-axis (between q = 0.9 and q = 1.1) and the big difference in the Force-to-Power ratio in the X-axis (between q = 0.9 and q = 1.1).

To increase the power output and to reduce the cogging forces, a magnetically split translator is suggested. In this way the generator will be assembled from two separated translator cores translating together. The main idea is to take two short magnetic cores with low X-axis force and combine them in a long one delivering low Y-axis force. The new translator is assembled from two yokes containing three winding sections (Figure 63). The choice for

the number of winding sections is based on delivering low force in the X-direction. Furthermore, the total length of the translator of the optimised model has a very similar length to a generator with six winding sections in the Y-axis. The simulated results for the X- and Y-axes forces for the optimised generator are shown in Figure 62.

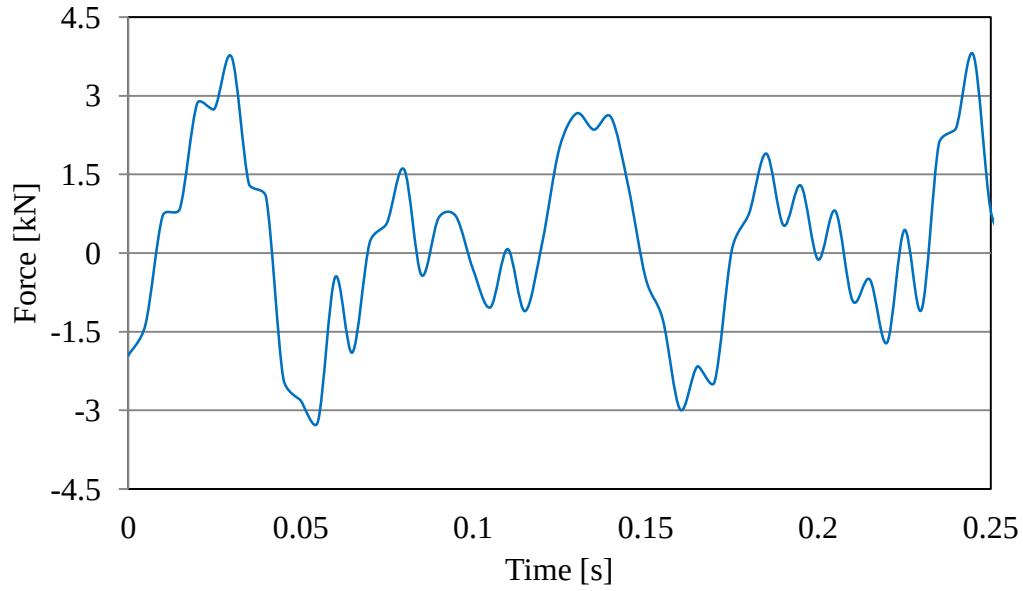

(a) X-axis (cogging force)

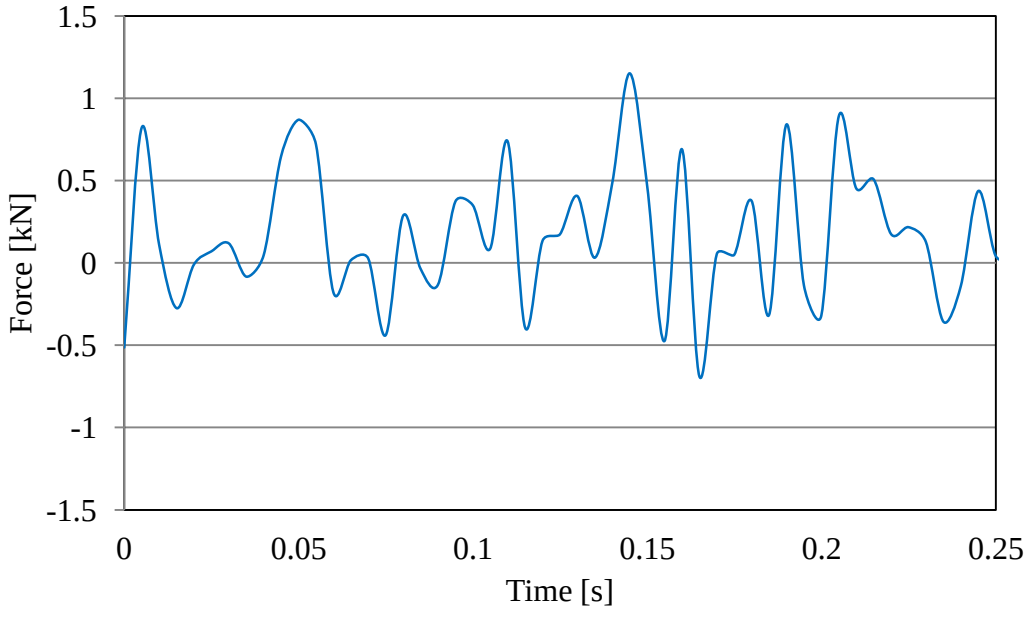

(b) Y-axis forces

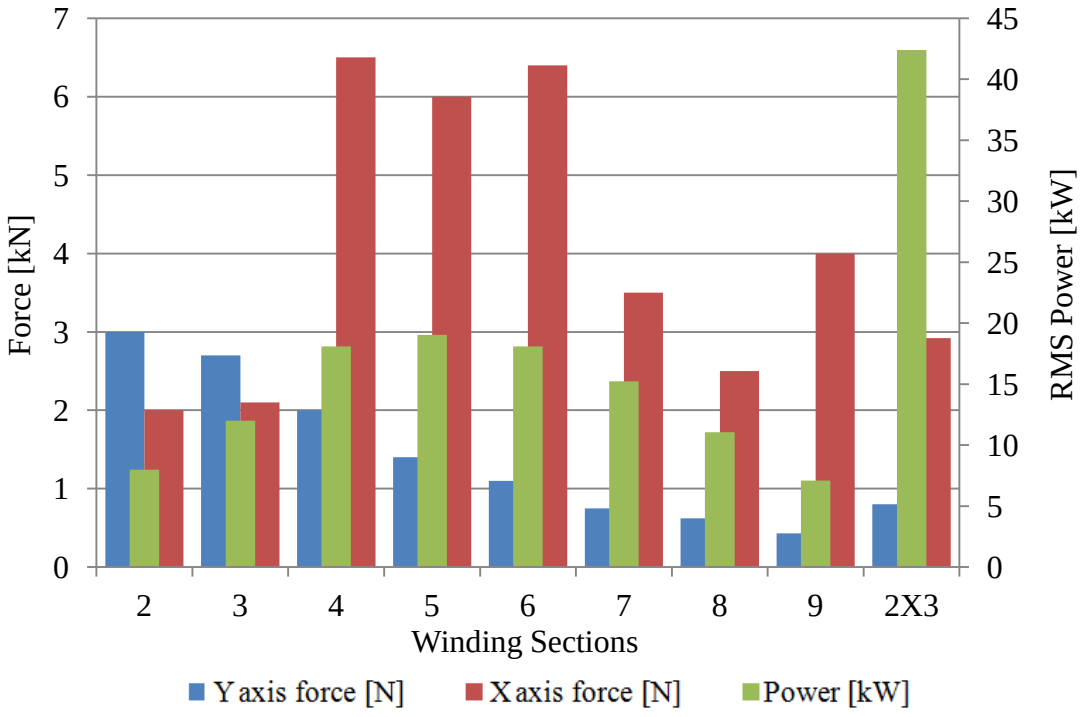

(c) Power and force comparison between PMLGs with different winding sections and the optimized model (2x3)

Figure 62 X- and Y-axes magnetic forces in the optimised model

The simulation results reveal that the RMS output power is 42.4kW and that the single force numbers for the X- and Y-axes are 2.92 kN and 0.8 kN respectively. Furthermore, the Power-to-Magnet volume ratio is 2377 W/m3 and the volume of the permanent magnet material in the PMLG is 0.018 m^3.

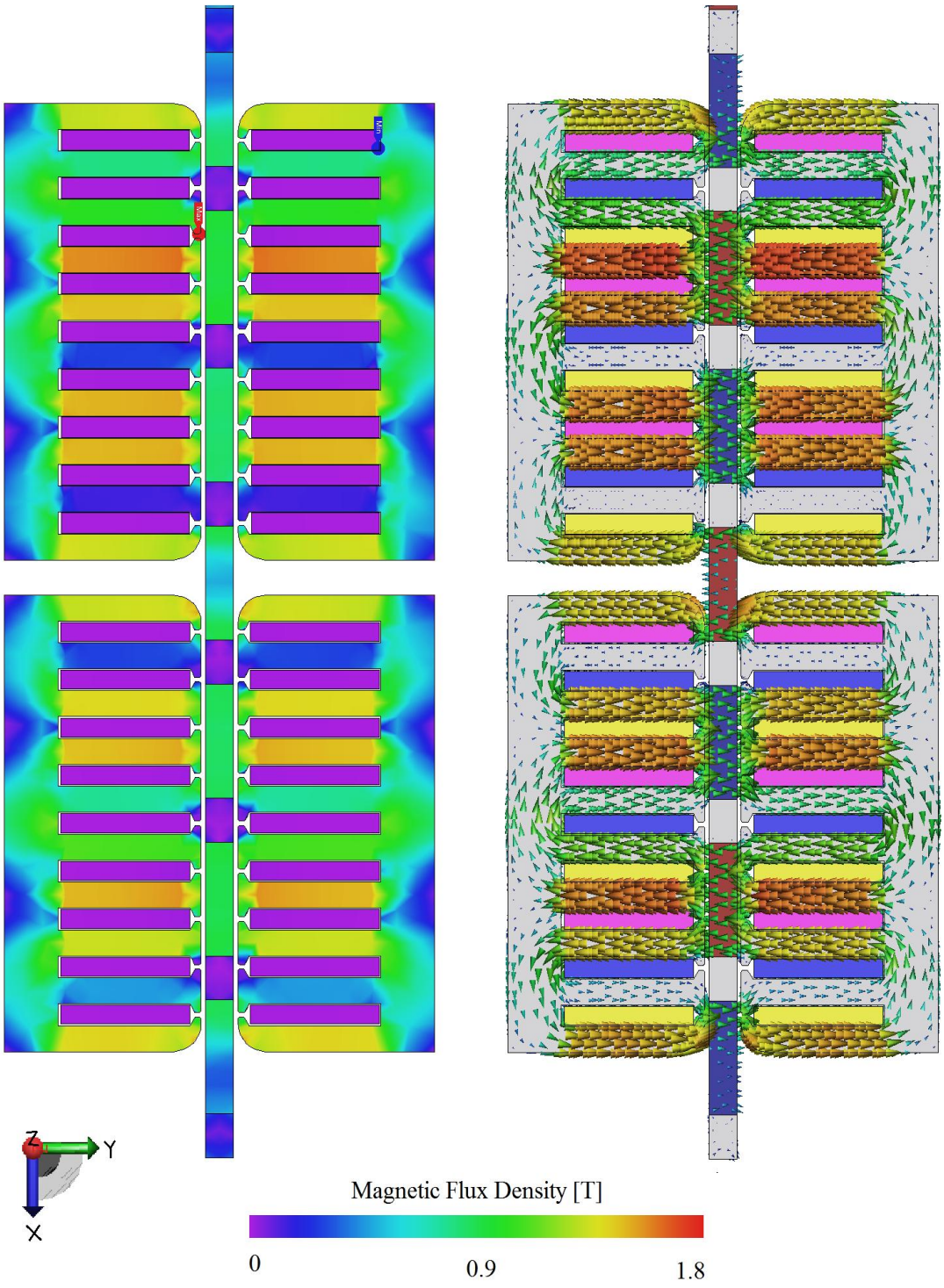

Figure 63 Magnetic flux density in the optimised generator model

High output power with regard to the amount of permanent magnet material used in the generator is achieved. The optimised model contains a very similar amount of permanent magnet material compared with the generator with six winding sections. However, the Power-to-PM volume ratio for a generator with

six winding sections is 1019 and for the optimised model it is 2377 [W/m^3], resulting in a 233% increase of the Power-to-PM volume.

Another advantage of the optimised model is the reduction of the X-axis forces by 55% and of the Y-axis forces by 28%, compared with the PMLG with six winding sections. Moreover, the magnetically separated sub-yokes of the translator are smaller physically and therefore, it is easier to maintain, transport and handle them.

3.3.4. Conclusion

The research in this chapter began with an investigation of the factors affecting the cogging force and power output in a single- and double-sided PMLGs, where the influence of the different design solutions has been presented. Furthermore, a method for calculating a single number, representing the cogging force level of a generator has been suggested.

Additionally, a double-sided PMLG is investigated with regard to the same parameters. The main analyses in this chapter are focused on suggesting an optimised design for a double-sided PMLG. As a result, a design with a magnetically separated yoke delivering better performance is proposed. The simulated results disclose that the optimised model delivers a reduction in the X- and the Y-axes forces by 55% and 28%, respectively and an increase of the output power by 233% in comparison with a model with a non-separated translator with the same volume of PM material.

4. Investigation into Iron-cored Long Stator Tubular Linear Generator

4.1. Introduction

In this chapter, an investigation into different magnetisation topologies for a Long Stator Tubular Permanent Magnet Linear Generator (LS-PMLG) is performed through a comparison based on the cogging force disturbance, the power output and the cost of the raw materials of the machines. The results obtained from the FEA simulation are compared with an existing linear generator described in (Prudell, Stoddard et al. 2010). To ensure accurate results, the generator developed in (Prudell, Stoddard et al. 2010) is built with 3D CAD and simulated using FEA and the obtained results are verified with the source.

4.2. Generators Description

Long stator generators share the same stator, where the stator consists of copper coils placed in a magnetic yoke. The coils are grouped in 15 phase windings and each winding consists of four series-connected coils. The coils are identical to the coils of the generator proposed in (Prudell, Stoddard et al. 2010) (77 turns and 1.145-ohms resistance per coil).

The translator consists of NdFeB-35 magnets attached to a magnetic core. To decrease losses in the magnetic circuit, all magnetic cores are assembled by laminated silicon steel, where the laminations are radial to the Y-axis.

Additionally, in order to increase the accuracy of the simulation results, three dimensional generator models are used in the simulations.

In this chapter, long stator generators with axial and radial magnetisation are investigated. A slice on the X-axis showing the profile for the three generators is presented in Figure 64. The main advantage of the long stator generator design is the reduction of the volume of the permanent magnet material used in its assembly. Considering the recent price rise of the neodymium metals (Humphries 2011), the potential savings of using the long stator design can be significant.

The main idea of the design adopted in the long stator designs is “swapping the configuration” of more traditional SS-PMLGs (Figure 64c), where the translator comprises coils that are exposed constantly to the PM’s flux. Reversing this structure allows a long stator to be assembled from copper coils and a short translator that consists of PMs (Figure 64a and Figure 64b).

An advantage of the topology in Figure 64c is that it allows a standard three-phase rectifier to be connected directly to the winding terminals but a significant part of the PMs’ flux does not cross the coils and therefore, this flux does not contribute to the power generation. On the other hand, the long stator design utilises the PMs in a way that the entire flux crosses the coils at any time of operation. Therefore, the main advantage from such a design is the full usability of the excitation flux established by the permanent magnets. Conversely, the long stator design has a coil configuration that is more complex and requires a system excluding the unenergised coils (coils unexposed to the PM’s flux) from the electrical circuit. If the unenergised coils remain connected in series with the energised ones, they become an inductive load.

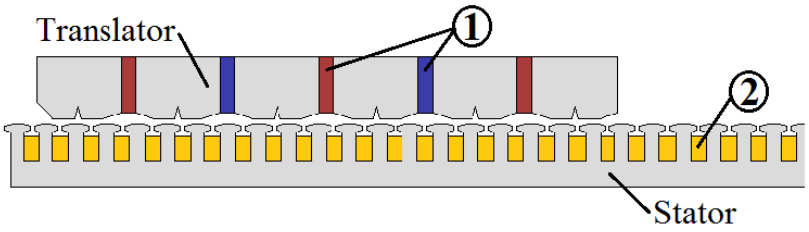

(a) LS-PMLG with axial magnetisation

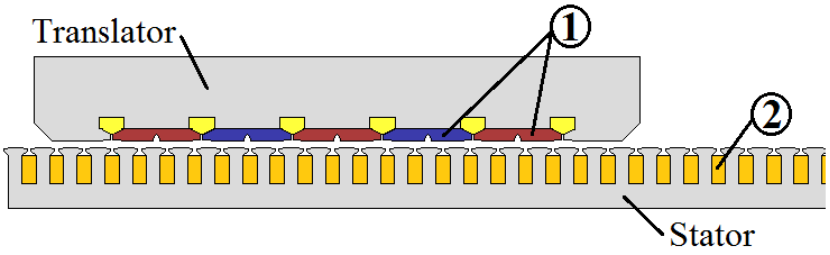

(b) LS -PMLG with radial magnetisation

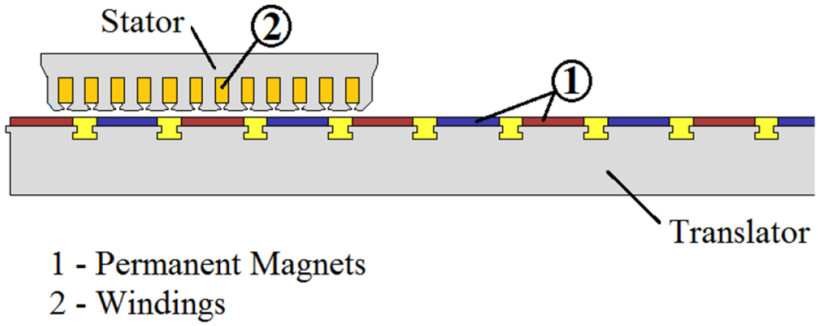

(c) SS-PMLG presented in (Prudell, Stoddard et al. 2010)

Figure 64 Overall view of the investigated generators

Two dimensional views of the different topologies investigated in this chapter are presented in Figure 65. The left-hand side of the pictures shows the magnetic flux density with the corresponding scale from 0 to 2 Tesla. The right-hand side of the pictures show the flux direction with vector arrows.

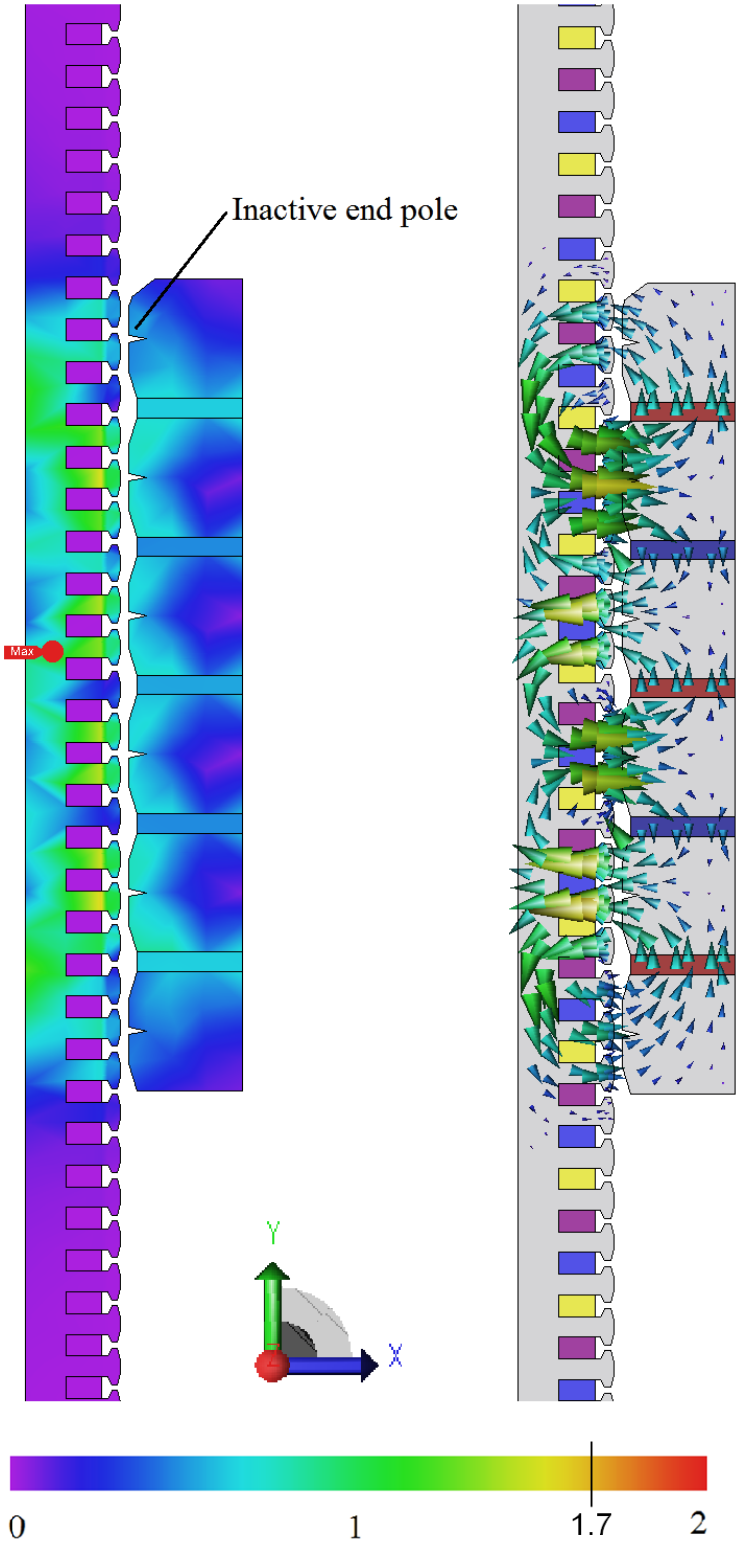

(a) Flux density [T] in the LS -PMLG with axial magnetisation

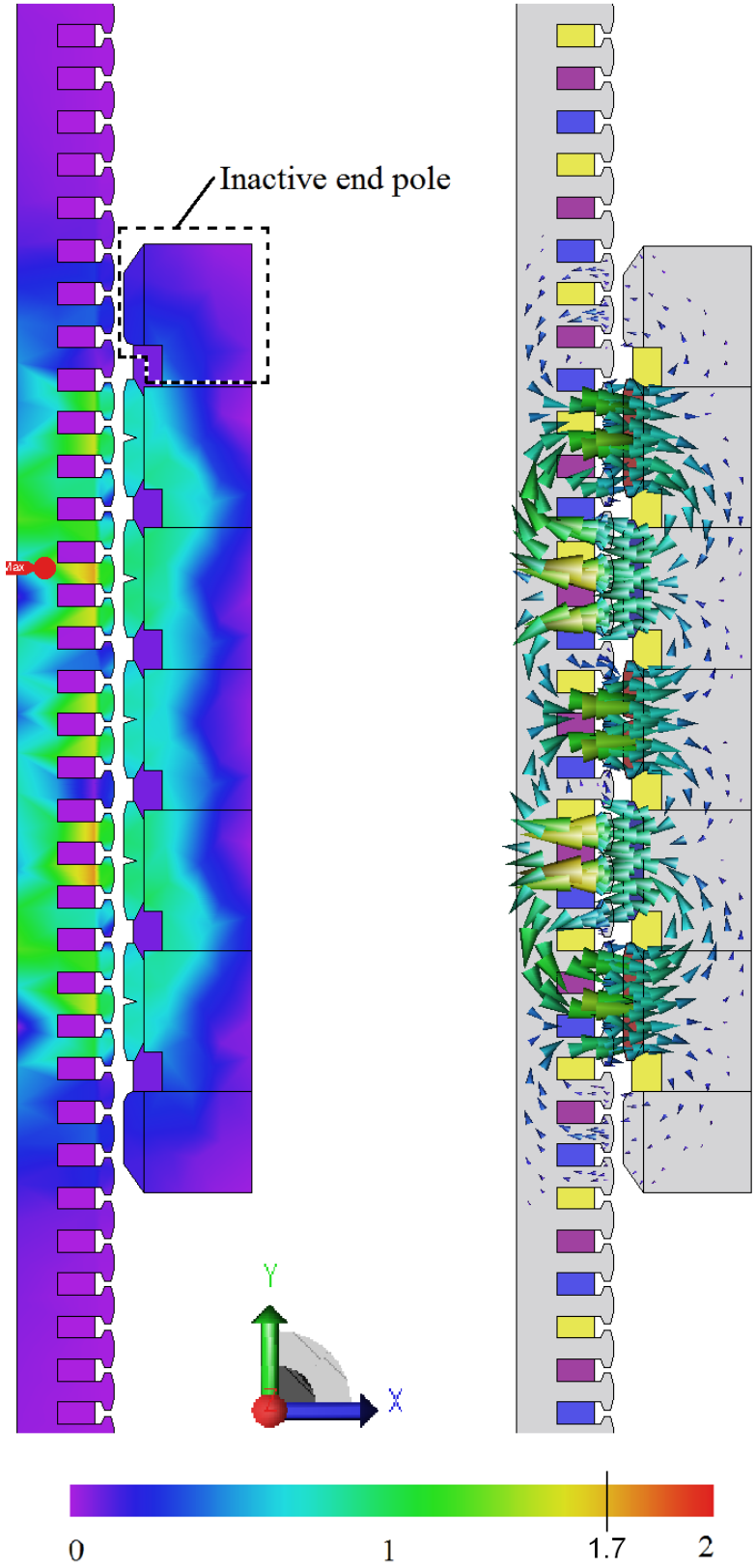

(b) Flux density [T] in the LS -PMLG with radial magnetisation

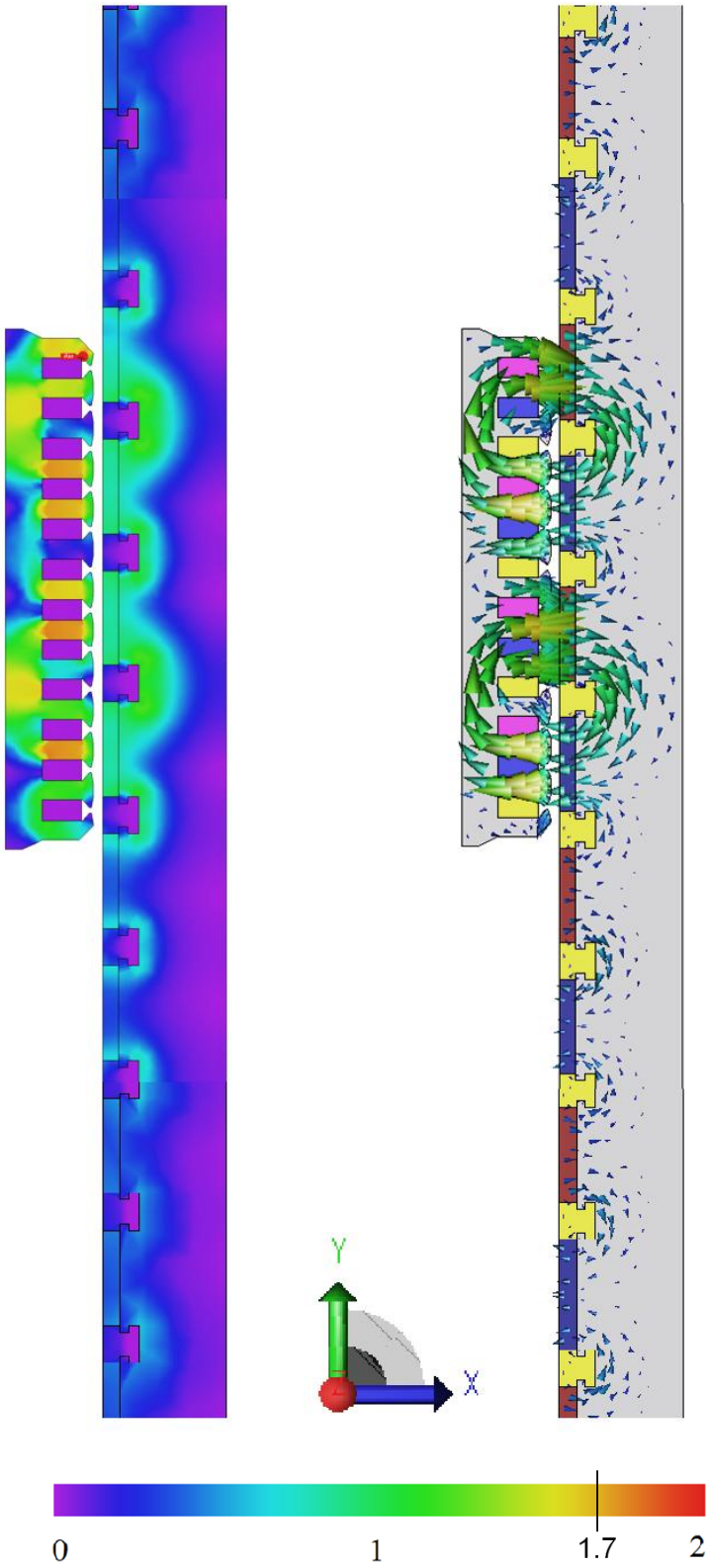

(c) Flux density [T] in the SS-PMLG shown in (Prudell, Stoddard et al. 2010)

Figure 65 Flux density [T] in the investigated generator topologies

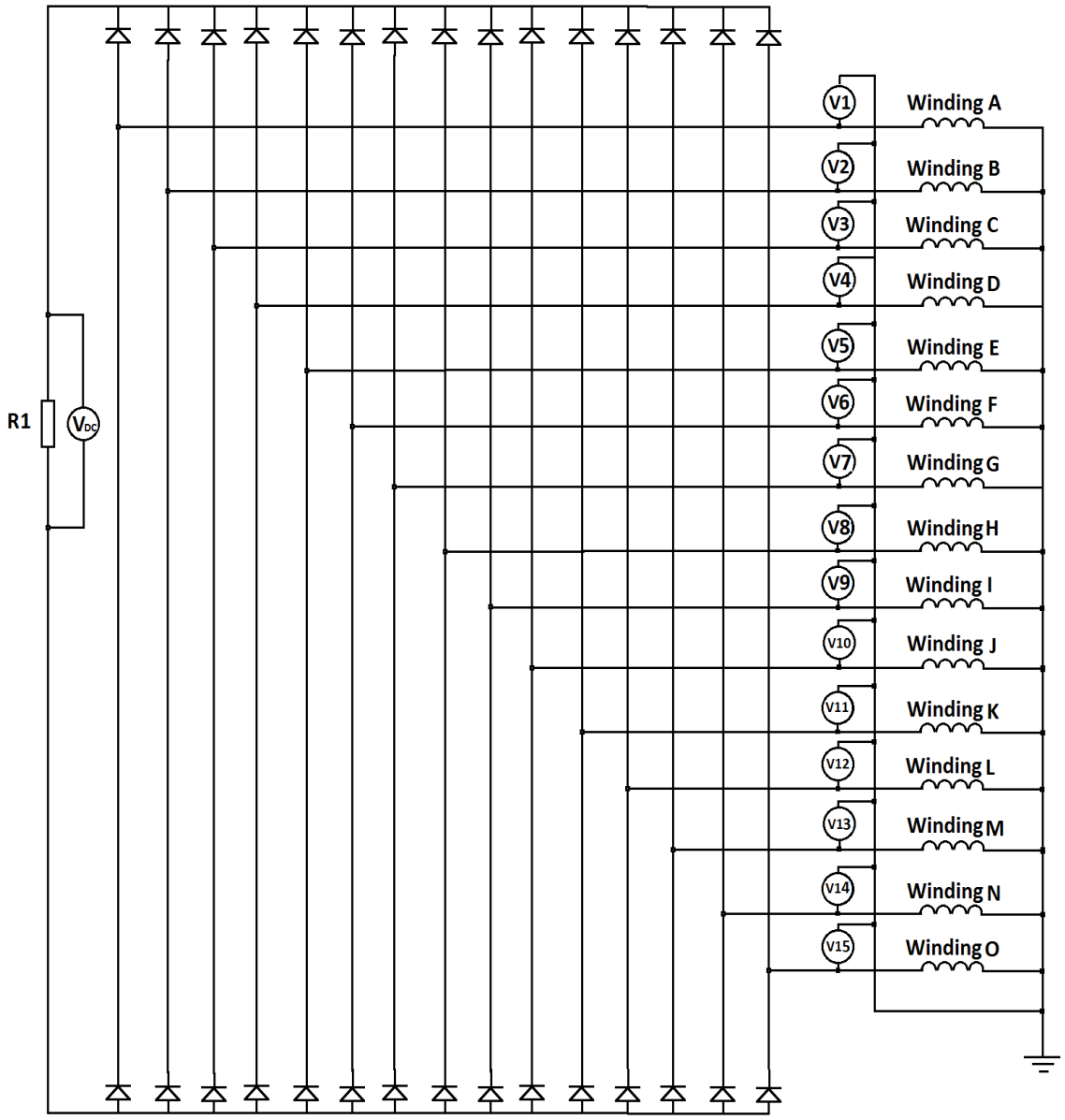

Figure 66 Passive rectification system for LS-PMLG

The electric circuit of the long stator generator is shown in Figure 66, where the output power is measured on the 5-ohm resistor (R1) after rectification. Each phase winding is assembled by four coils connected in series and the number of windings can be altered. The Voltmeters (V1 to V15) measure the voltage on every winding. The flux distribution in the SS-PMLG shown in Figure 65c can be verified with the simulated flux distribution in (Prudell, Stoddard et al. 2010), as in Figure 67.

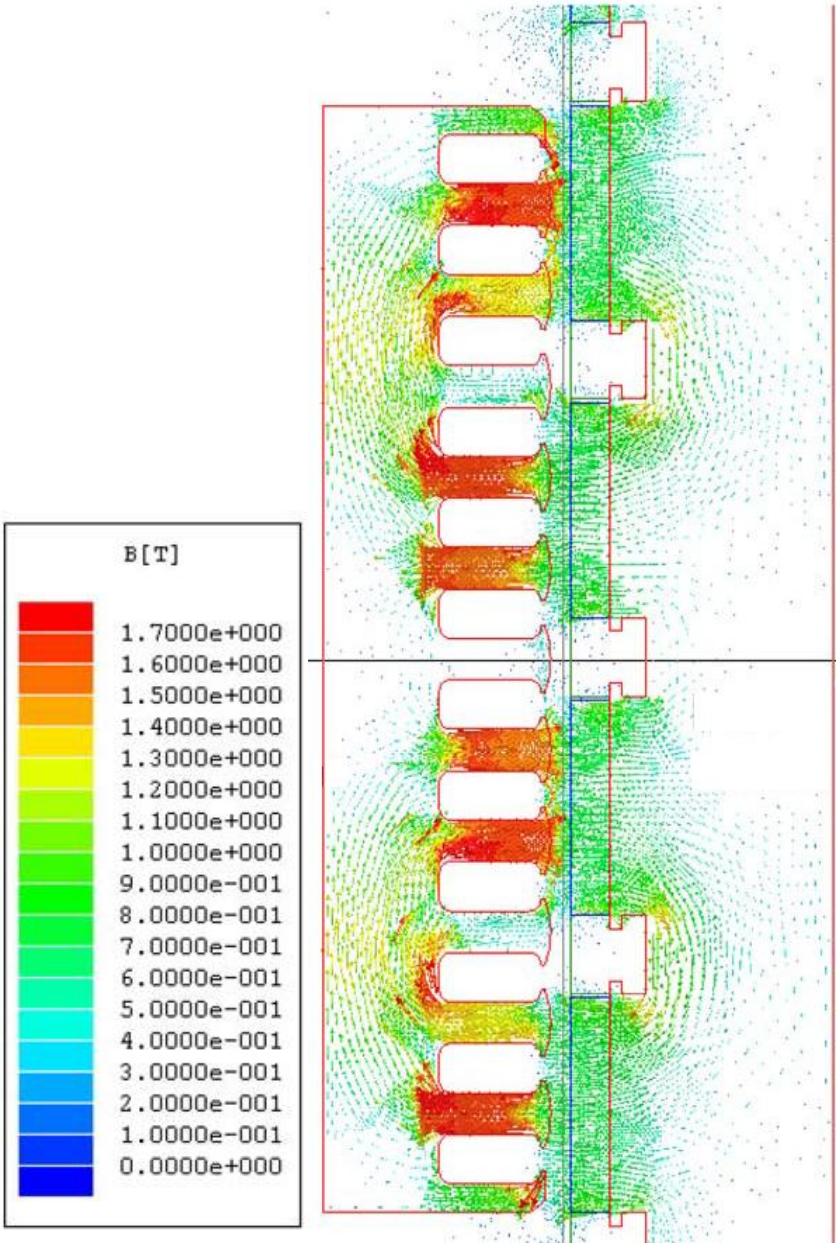

Figure 67 FEA flux distribution of the PMLG, courtesy of (Prudell, Stoddard et al. 2010)

Table 5 Main Dimensions

	Axis	SS PMLG	LS PMLG radial magnetisation	LS PMLG axial magnetisation
Stator height [mm]	Y	1152	1342	1342
Translator height [mm]	Y	284	484	422
Permanent Magnet Length [mm]	Y	52	70	10
Magnet pole pitch [mm]	Y	72	72	72
Coil pitch [mm]	Y	68	68	68
Magnets height [mm]	X	10.5	10.5	54.7
Air gap length [mm]	X	5	5	5
Turns per coil		77	77	77
Coils resistance [ohm]		1.145	1.145	1.145
Resistive load (on DC side) [ohm]		5	5	5
Coil connection within a winding		series	series	series
Windings connection		star	star	star

The main dimensions for the generators are shown in Table 5. The dimensions for all generators are given with the corresponding axis shown in Figure 65. In all simulations, the load on the generator is supplied on the DC side after passive (diode rectifier) rectification.

The magnetic circuits of the LS-PMLGs with axial and radial magnetisation are shown in Figure 68a and Figure 68b. S_{EP} are the magnetic reluctances of the inactive poles at the ends of the translator. The magnetic cores between two permanent magnets of the LS-PMLG with axial magnetisation are shown as T-shaped circuits, where the two S_{C1} and single S_{C2} reluctances are the sides. This is because of the split of the magnetic flux in the core. The magnetic reluctances can be shown as:

$$S_{T_{RAD\ in}} = 2 * S_E + 2 * S_{PM} + S_{C1} + S_C \tag{4.1}$$

$$S_{T_{RAD\ end}} = 2 * S_E + S_{PM} + S_C + S_{C1} + S_{EP} \tag{4.2}$$

where $S_{T_{RAD\ in}}$ is the total inner magnetic reluctance (pink area in Figure 68a) and $S_{T_{RAD\ end}}$ is the outer magnetic reluctance (yellow area in Figure 68a) for the radial magnetised LS-PMLG. The equivalent reluctances for the axial magnetised LS-PMLG can be shown as:

$$S_{T_{AXI\ in}} = 2 * S_E + 2 * S_{C2} + 2 * S_{C1} + S_C + S_{PM} \tag{4.3}$$

$$S_{T_{AXI\ end}} = 2 * S_E + S_C + S_{PM} + 2 * S_{C2} \tag{4.4}$$

$S_{T_{AXI\ in}}$ is the total inner magnetic reluctance (pink area in Figure 68b) and $S_{T_{AXI\ end}}$ is the outer magnetic reluctance (yellow area in Figure 68b) for the axially magnetised LS-PMLG. Furthermore, where S_E is half of the reluctance of the stator, it can be presented as:

$$S_{E1} = \frac{{S_{Tt}}^4 + {S_C}^3 * S_T + 6 * {S_{Tt}}^3 * S_C + 5 * {S_C}^2 * {S_{Tt}}^2}{4 * {S_{Tt}}^3 + {S_C}^3 + 10 * {S_{Tt}}^2 * S_C + 6 * {S_C}^2 * S_{Tt}} \tag{4.5}$$

$$S_{Tt} = S_{T1} + S_{a\,nn} \tag{4.6}$$

where nn is the number of the reluctances shown on the right-hand side (with colour code) in Figure 68a and Figure 68b.

Calculating the magnetic circuit has been done in same way as explained in section 3.2.3. The flux density result for the inner section with length of eight teeth derived from the analytical model reveals a 5% difference, compared with the static FEA results.

In this thesis, the magnetic circuit models are used to perform static calculation of the flux density in the air gap, and the results are compared with the results from the FEA.

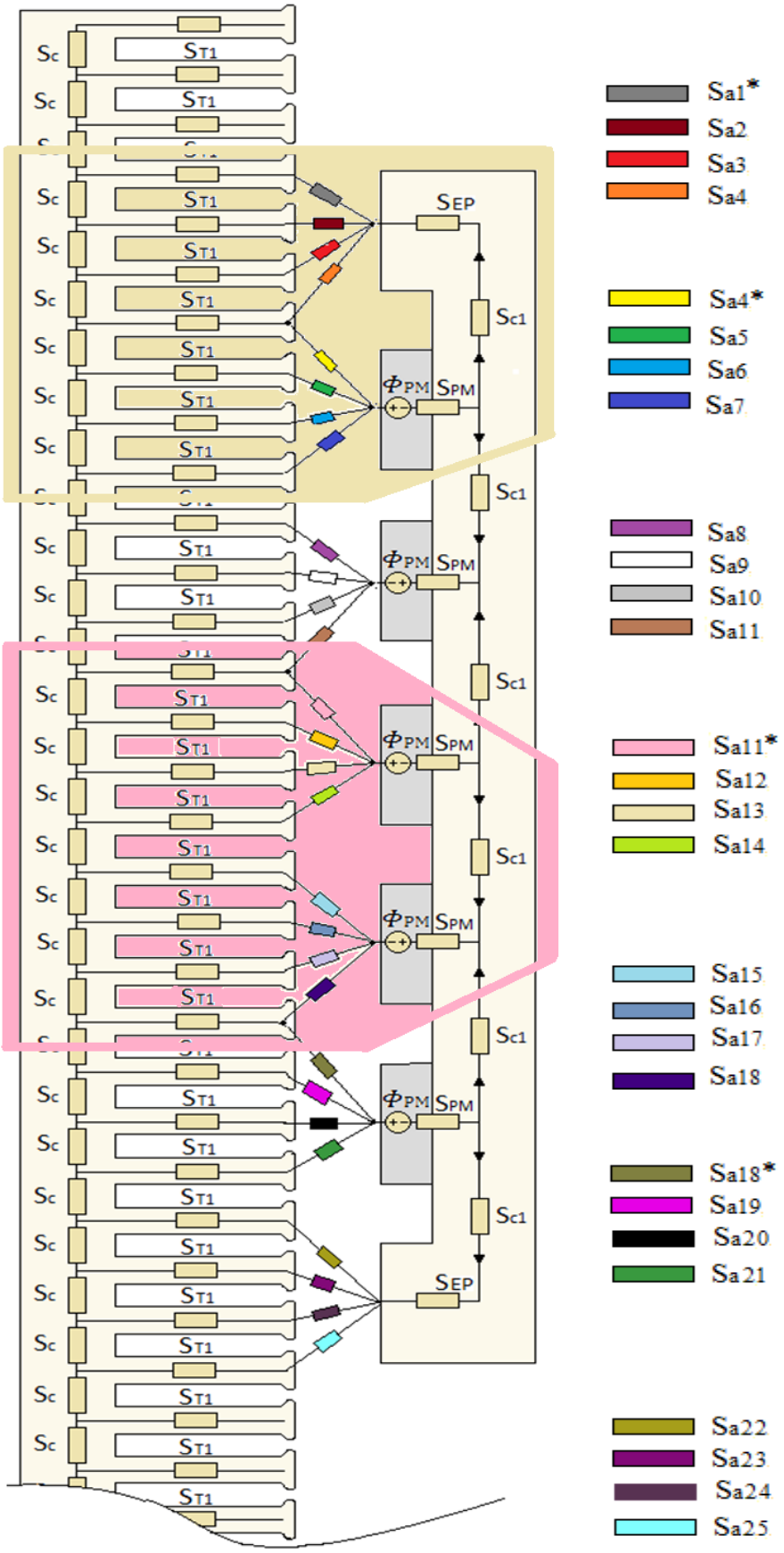

(a) Magnetic circuit of LS-PMLG with radial magnetisation

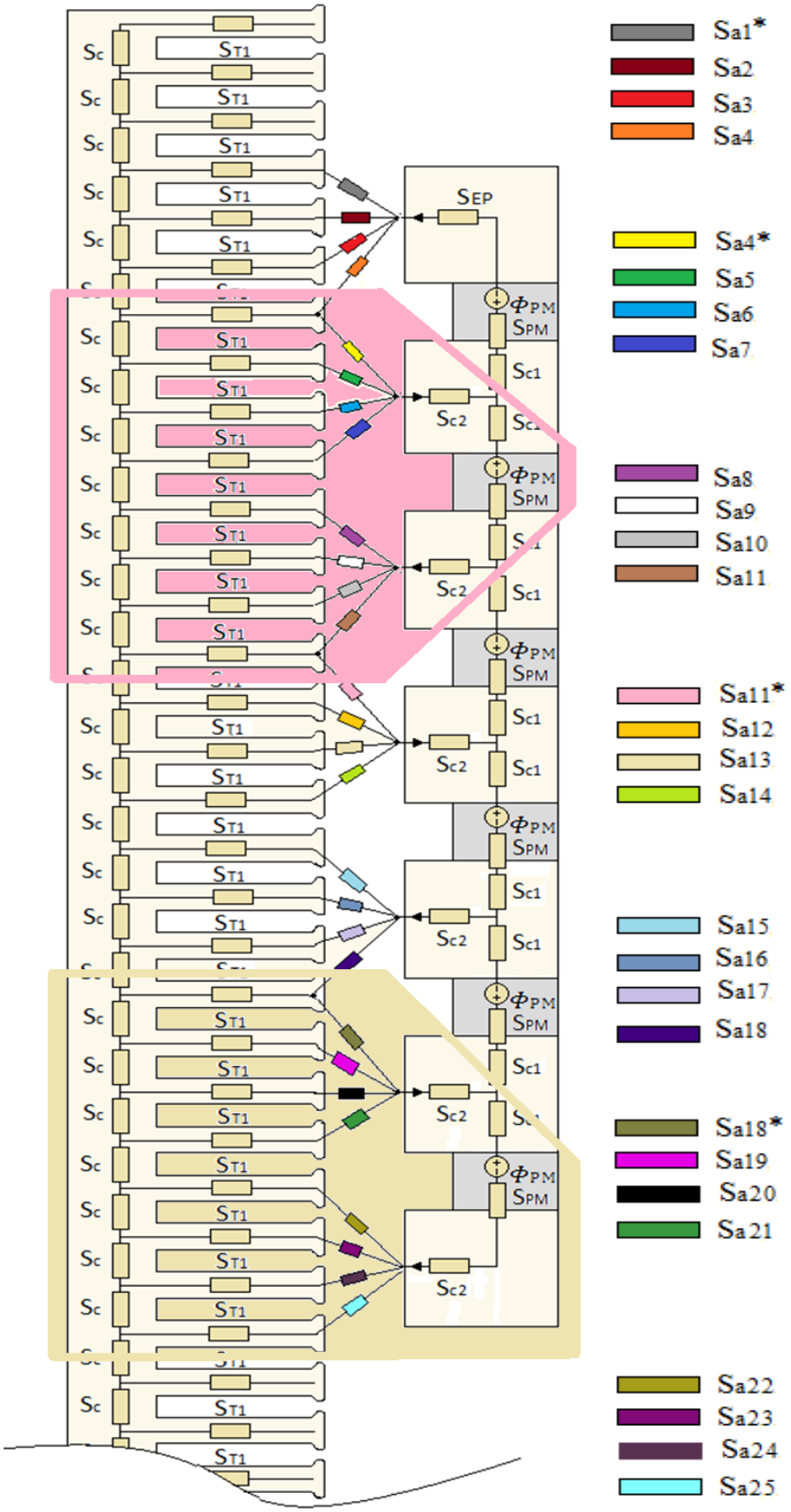

(b) Magnetic circuit of LS-PMLG with axial magnetisation

Figure 68 Magnetic circuit of the LS-PMLG

4.3. FEA Simulation Results

In the simulations performed, the following parameters are kept the same for the three generators: winding slot dimensions, shoe dimensions, number of slots per pole and phase, number of turns per coil, coil resistance and all structural material properties used in the models. This is conducted to reveal only the differences caused by the generator design and to eliminate the influence of the material properties and of the coil configuration on the performance. In this section three major sets of simulations are performed:

- The first set compares the cogging force for the SS-PMLG shown in (Prudell, Stoddard et al. 2010) with the cogging force for the LS-PMLGs having axial and radial magnetised magnets.
- The second set presents the electrical power output of the generators connected to 5-ohms resistive loads after rectification.
- The third set shows the volumes and the prices of the raw structural materials for the three machines.

4.3.1. Cogging Forces

In this chapter, the cogging forces for the three machines are compared. Initially, the SS-PMLG (Prudell, Stoddard et al. 2010) is modelled in 3D CAD and simulated in FEA. In Figure 69, a comparison between the cogging forces simulated in this chapter (Figure 69a) and the results shown in (Prudell, Stoddard et al. 2010) (Figure 69b) are given. A difference of 16% in the peak force is present between the two graphs.

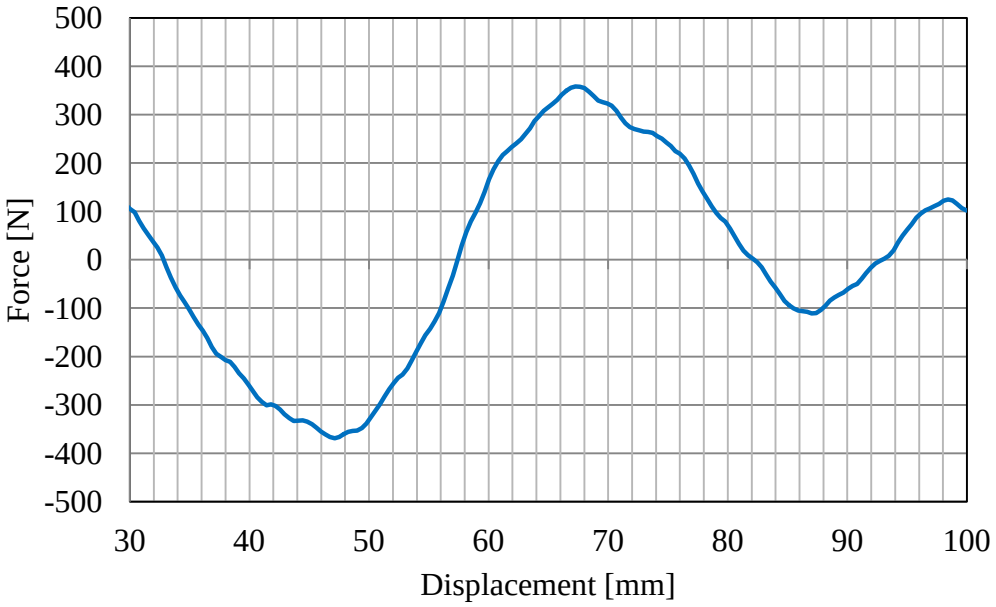

(a) FEA (JMAG) simulated cogging force verses displacement for the SS-PMLG

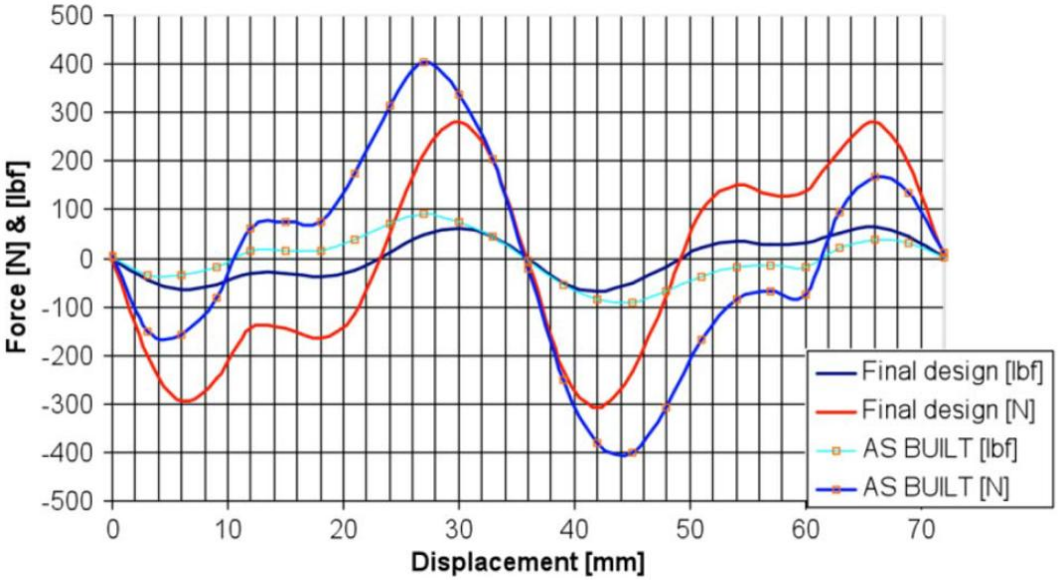

(b) Simulated and tested cogging force for the SS-PMLG, picture by courtesy of (Prudell, Stoddard et al. 2010)

Figure 69 Cogging forces comparison (Prudell, Stoddard et al. 2010) and simulations in JMAG

Several techniques, such as shaping and slotting have been applied for cogging force reduction in the LS-PMLG. The shaped profile of the magnets used in the radially magnetised LS-PMLG is shown in Figure 70a. The cogging

forces comparison is shown in Figure 70b, where the shaped profile and the square profile are analysed. In order to compare the PM rings on an equal basis, the two magnet ring volumes are set to be the same. As a result (Figure 70b), a total reduction of 30% in the peak is achieved when pole slotting and shaping is applied on the PMs.

Initially, the long stator generators have been simulated with square profiles (Figure 70a). As one of main objectives is to reduce cogging, modifications have been applied to the magnet profile. Influenced by (Kimoulakis, Kladas et al. 2009), the square profile has been modified to include to bevelled bottom profile with a 30º angle, which has been chosen based on the findings in (Kimoulakis, Kladas et al. 2009).

Furthermore, in order to reduce the cogging force even further but to keep the power output approximately the same as for the SS-PMLG, modifications of shaping and slotting the magnets have been also done. The shaping and slotting modifications were influenced by (Shabani, Milimonfared et al. 2007). Initially, an angle of 35º has been applied and the shaping (with an angle of 10.5º) has been adjusted to maintain the output power of the long stator machines close to that of the short stator PMLG.

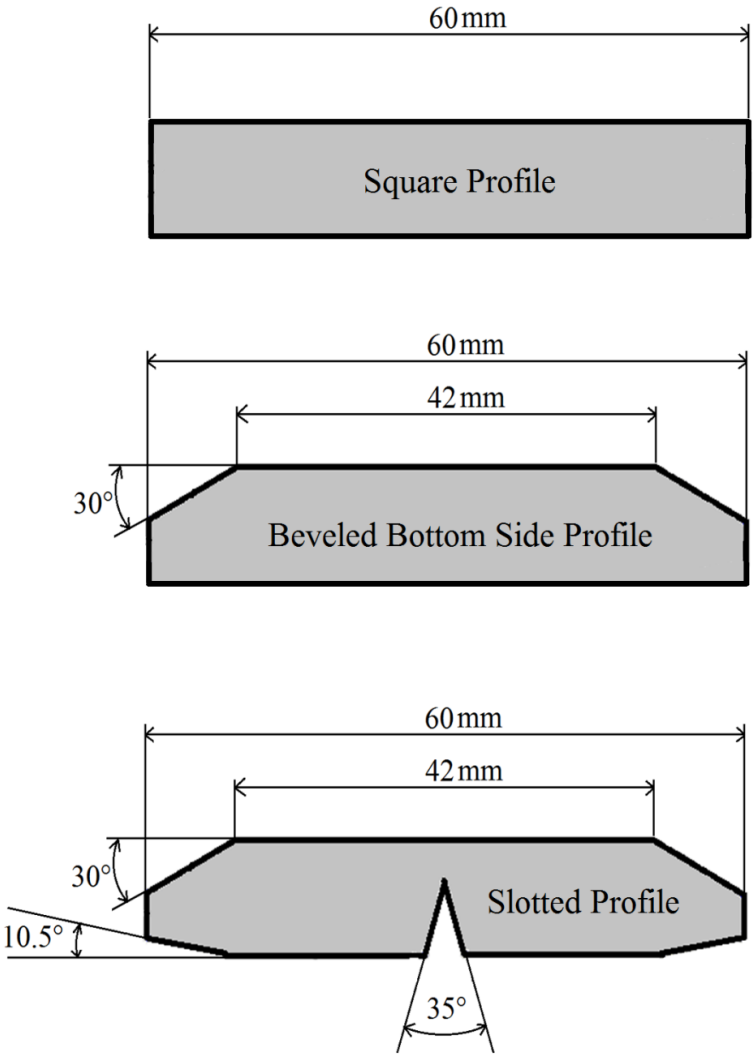

(a) Magnet shaped profile for radial magnetised LS-PMLG

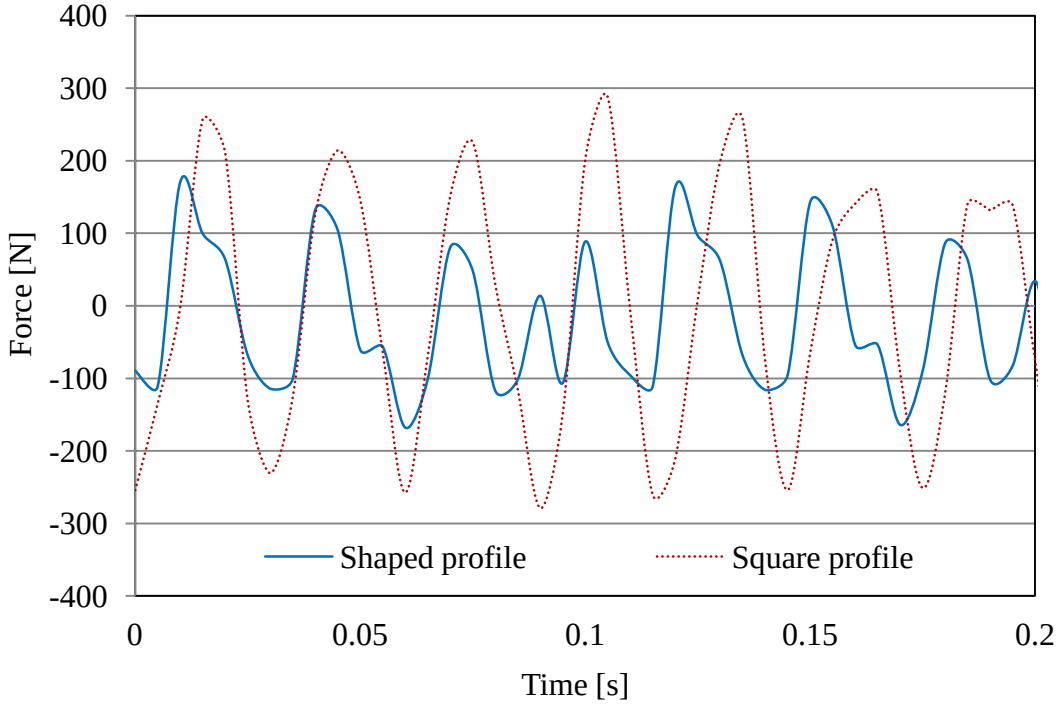

(b) Cogging forces for shaped and square profile of the PM

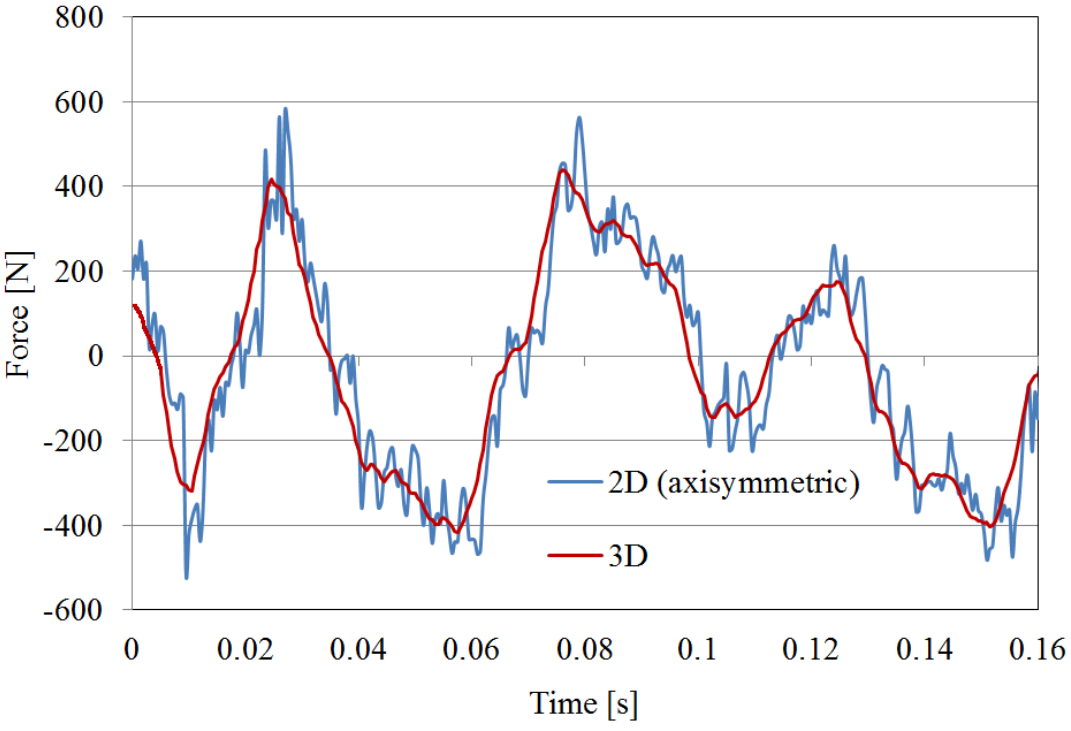

(c) Comparison between 2d axisymmetric and 3D cogging force calculation

Figure 70 Effect on the cogging force caused by shaping the PMs

A comparison of the FEA results between the cogging force calculation with a 2D-axisymmetric and a 16-degree section of the 3D model is shown in Figure 70c. The simulations reveal that the 3D results have higher accuracy; however, the 3D simulations require around seven to ten times longer computational time compared with the 2D simulations. In this section, to improve accuracy, the generators are simulated in 3D (16-degree section with applied repetitive symmetry condition).

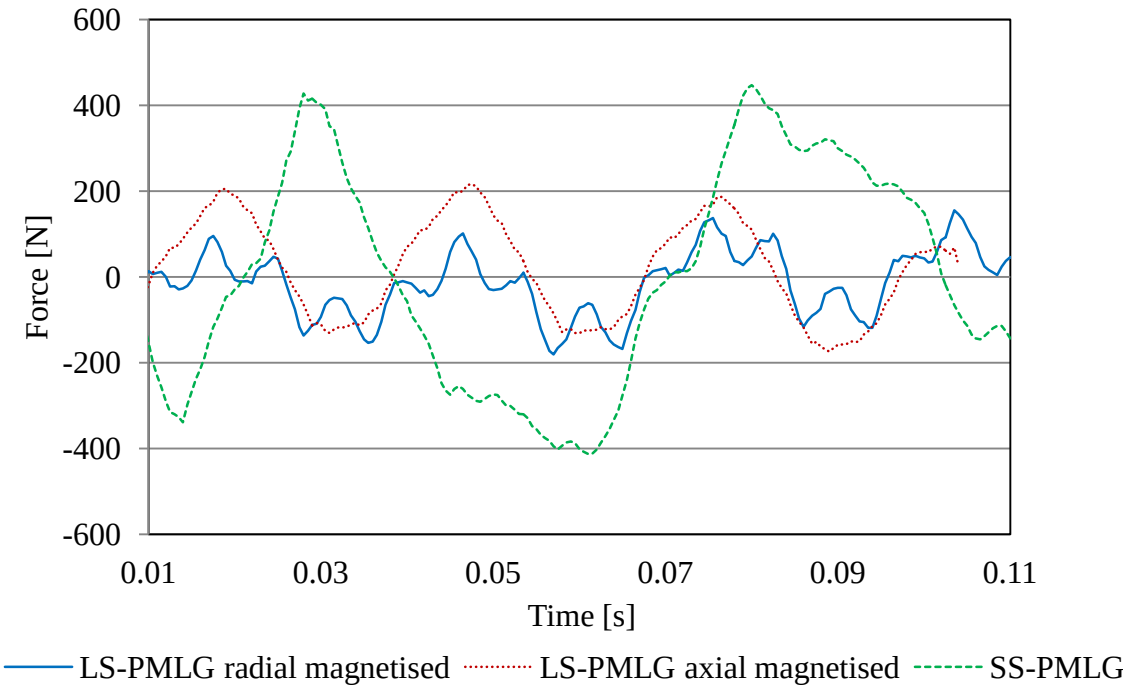

Figure 71 Cogging forces for the investigated topologies

The cogging force results for the three generators are shown in Figure 71, where it can be observed that the long stator designs have significantly lower cogging force amplitude. Compared with the cogging forces for the PMLG shown in (Prudell, Stoddard et al. 2010), the LS-PMLGs achieve a reduction of 60%.

4.3.2. Electrical Power Output

The voltage output of the SS-PMLG (Prudell, Stoddard et al. 2010) has been verified with the model of the simulated generator in this chapter. The no-load voltage (line to neutral) obtained in (Prudell, Stoddard et al. 2010) is 346 V and the no-load voltage obtained by FEA in this chapter is 330 V at a constant velocity of 0.76m/s. The difference of 4.6% is considered as acceptable in verifying the FEA model used in this chapter.

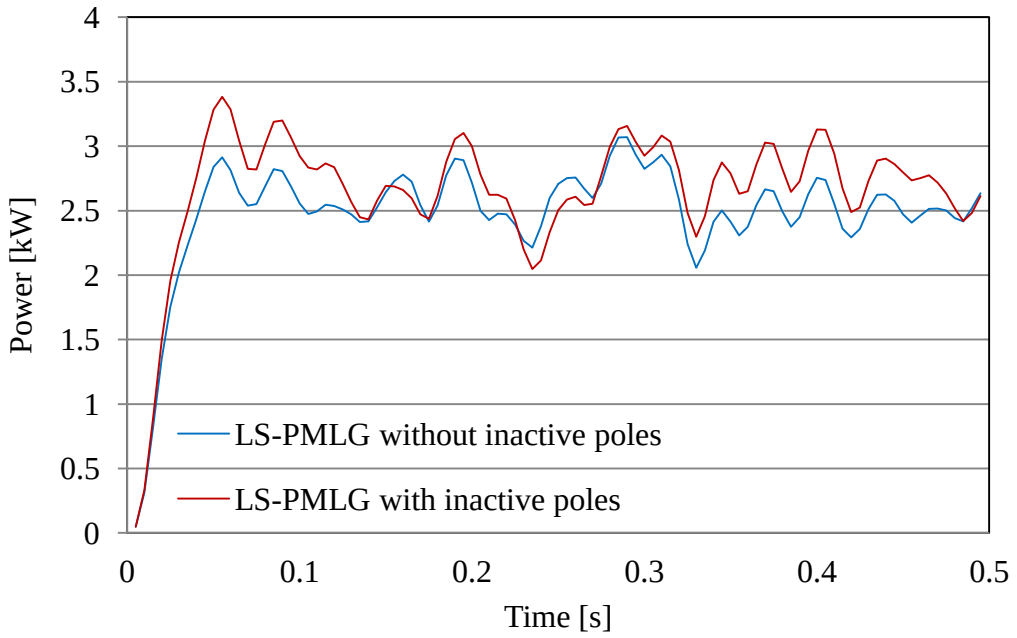

Figure 72 Power output from LS-PMLG with and without inactive poles

Another advantage of the LS-PMLG is the possibility of adding inactive poles at both ends of the translator. By installing the inactive poles, the additional flux distributed over the stator length generates a voltage in the additional coils at the ends of the translator and hence, electrical power. The RMS power outputs for the LS-PMLG both with and without the inactive poles are 2705W and 2521W respectively. The instantaneous output power can be seen in Figure 72.

As a result, the output power is boosted by an extra 7% (RMS) without the use of extra permanent magnet material.

The simulated results for the power output are shown in Figure 73, where the three generator models are simulated with a monochromatic wave set for the translator's displacement with a period of T = 2.1 seconds and height of 0.375 meters. This displacement is equal to the scaled statistical data for the sea state located north of Spain (Manana, Arroyo et al. 2011).

The following RMS output powers area achieved for the wave period of 2.1 seconds: SS-PMLG - 2.66 kW, LS-PMLG with axial magnetised magnets - 2.66 kW and LS-PMLG with radial magnetised magnets - 2.72 kW. From the result, it can be concluded that the electrical power output is very similar for the three machines.

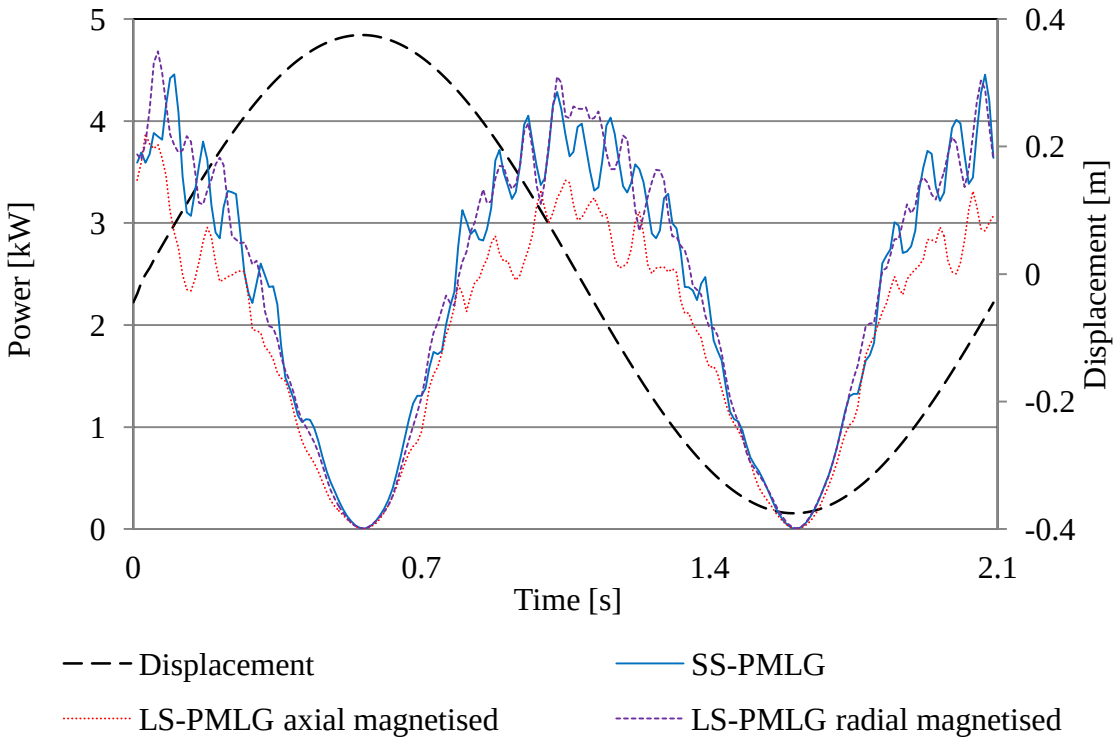

Figure 73 Power output of the SS-PMLG (Prudell, Stoddard et al. 2010) and LS-PMLGs

Owing to the design consideration for the long stator generators, not all coils generate voltage at the same time. Only the coils covered by the translator magnetic field generate voltage during displacement of the translator (Figure 74). It can be seen that the coil voltages have the same frequency but different amplitude and phase. Such a complex output requires a modified rectification system. The voltages from the long stator generators in this chapter are rectified by a passive rectification system (Figure 66).

Another benefit of the long stator design is the possibility of excluding a coil in case of failure, by using power electronics. Owing to the high number of coils, such an operation does not reduce the output of the generator significantly. Therefore, maintenance of the WEC can be postponed.

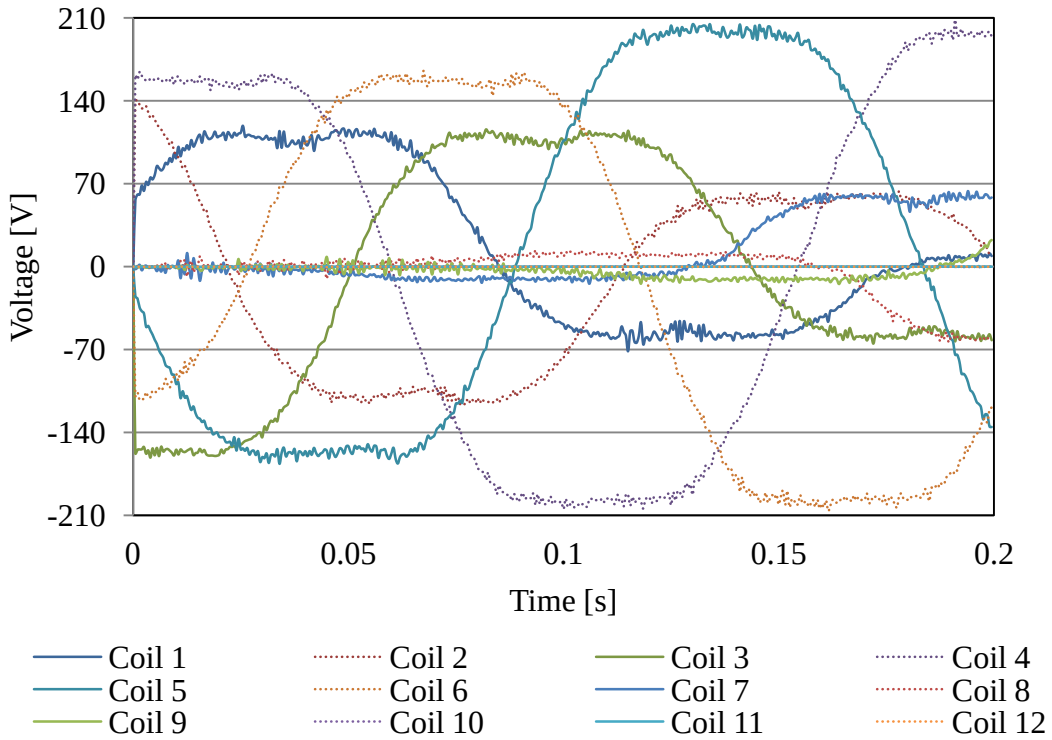

Figure 74 Voltage output for LS-PMLG

Moreover, a benefit of using the long stator design is the heat dissipation in the copper coils. In the long stator design, output electrical power is harvested from a high number of coils. Unlike the SS-PMLG in (Prudell, Stoddard et al. 2010), the coils in the LS-PMLG are not energised at all times. Hence, for the same amount of total harvested energy from the generators, the power delivered by a single coil in the LS-PMLG will be much lower than in the SS-PMLG. Consequently, the coils in the long stator generator have much lower duty cycle and therefore they are allowed a longer cooling time. Consequently, overheating of the LS-PMLG`s coils is less likely to occur compared with those of the SS-PMLG.

The DC voltage after rectification for the three generators is shown in Figure 75.

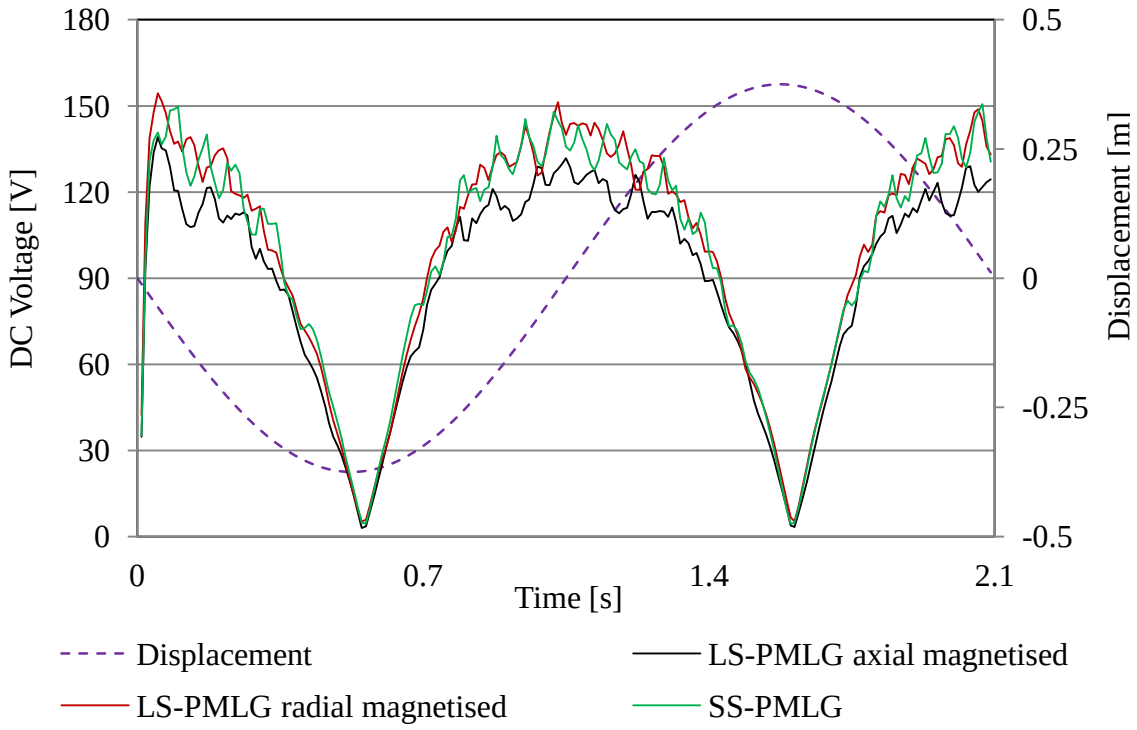

Figure 75 Rectified voltage simulated on 5ohm resistor

The long stator design involves the use of a large number of diodes (in the case of passive rectification). However, not all the diodes in the LS-PMLG rectifier are working at the same time. Only the windings (and the diodes connected to them) under the translator will be generating voltage. Therefore, a failure in a single diode will exclude one coil from operation, which does not have a significant effect on the overall output of the WEC. On the other hand, failure in a single diode in the rectifier of the SS-PMLG will reduce the WEC's output significantly.

4.3.3. Magnetic Forces under Load

When the generators are under normal operation, e.g. supplying power to the electrical grid, another source of force disturbance appears. These forces are caused by the armature reaction.

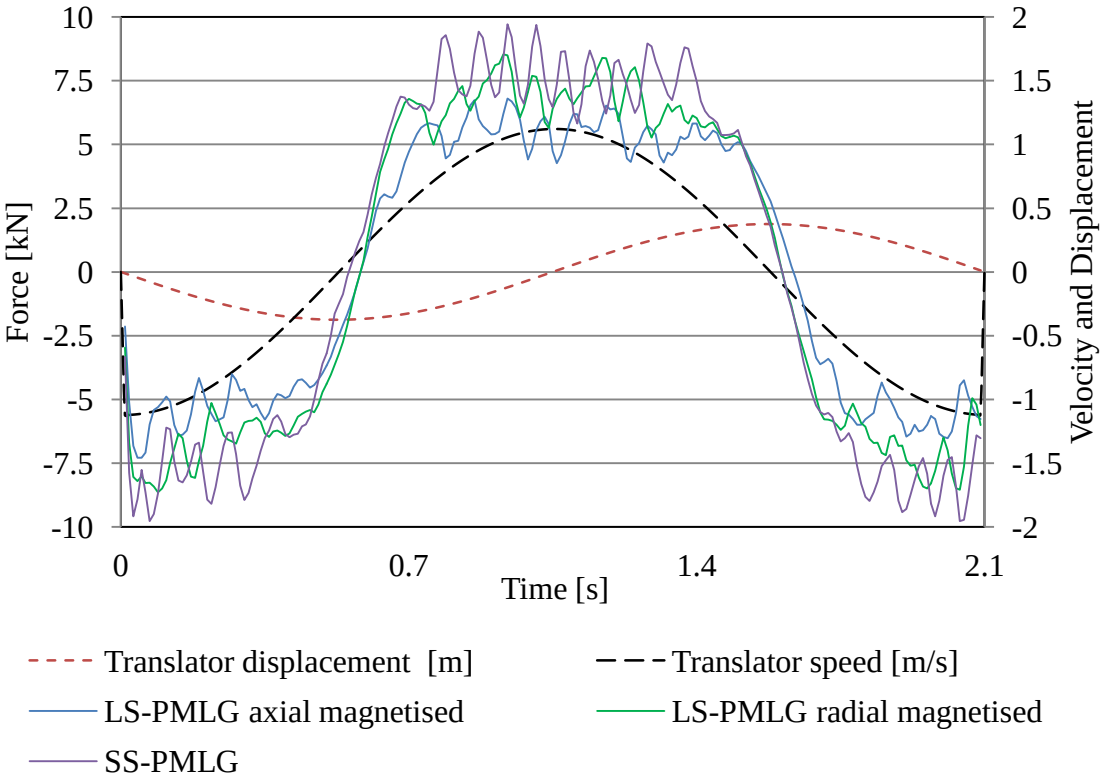

Figure 76 Total forces under load

The armature reaction generates a force opposing the linear torque of the prime mover of the WEC, which offsets the cogging force. Furthermore, the armature reaction force is proportional to the linear velocity of the generator. As seen in Figure 76, the total magnetic force is the sum of the cogging force and the armature reaction.

In the results shown in Figure 76, it can be seen that the highest total force is delivered by the SS-PMLG (Prudell, Stoddard et al. 2010) and that the lowest force is delivered by the LS-PMLG with axial magnetisation.

4.3.4. Volumes and Prices of the Active Materials

The volumes of the structural materials for both generators are shown in Table 6. As seen in the table, the total price of the long stator design is much

lower than that of the SS-PMLG (Prudell, Stoddard et al. 2010); the main difference is in the price of the permanent magnets. The price of the materials is assumed as follows: non-magnetic and non-electrical conducting material - 1.43 £/kg, copper – 5.29 £/kg (London Metal Exchange June, 2012), laminated steel – 2 £/kg (London Metal Exchange June, 2012) and PMs, NdFeB, N35 – 216 £/kg (Quotation June, 2012).

Table 6 Volumes and Price of Structural Materials

	SS PMLG	LS PMLG radial magnetisation	LS PMLG axial magnetisation
PM [m^3]	0.034	0.011	0.011
Laminated steel [m^3]	0.303	0.264	0.270
Copper [m^3]	0.0111	0.0555	0.0555
Non-magnetic and non-electrical conducting material [m^3]	0.022	0.0052	0
	SS PMLG	LS PMLG radial magnetisation	LS PMLG axial magnetisation
PM [k£]	55.5	18	18
Laminated steel [k£]	4.64	4.04	4.13
Copper [k£]	0.52	2.6	2.62
Non-magnetic and non-electrical conducting material [k£]	0.08	0.018	0
Total cost [k£]	60.74	24.66	24.75

Considering the recent price rise of the neodymium metals reported in (Humphries 2011), the payback period of the long stator design is likely to be shorter than that for the existing generator. The assembly cost is not included in the calculations but it is expected to be similar among the three generators. Generally, fewer difficulties are expected for the assembly and handling of the

PMs in the long stator generators, because of, the lower volumes of PMs used in their design.

4.4. Conclusion

The aim of this chapter is to highlight the merits of the long stator design over the existing short stator three-phase design for SS-PMLG. The areas of focus are the price of the raw assembly materials, the cogging force and electrical power output. An increase in the electrical output and a reduction in the raw materials can lead to a lower initial investment and lower RoI of the WEC. Furthermore, the reduction of the cogging force reduces vibrations and hence, can increase the life of the bearings.

In this chapter, an investigation of long stator generators has been performed by means of FEA. Long stator generators with axial and radial magnetisation have been analysed and optimised and the results reveal a cogging force reduction of up to 60% in comparison with an existing design having a short stator and similar size. Furthermore, the long stator generators simulated use three times less permanent magnet material in their assembly, which reduces the price of the raw assembly materials by 60% in comparison with existing SS-PMLG (Prudell, Stoddard et al. 2010). The results delivered in this chapter suggest that use of LS-PMLGs can reduce the production and maintenance costs of the WEC in comparison with the SS-PMLG.

5. Double-sided Air-cored Tubular Generator for Wave Energy Converters

5.1. Introduction

In this chapter a new air-cored tubular PMLG for WECs is proposed and simulated. The proposed generator design “sandwiches” the copper windings between two sets of permanent magnet rings in a tubular structure. Owing to the absence of steel in the translator, the bearings are not exposed to high magnetic forces and the cogging force can be eliminated.

5.2. Generator Description

The generator proposed in this chapter is a longitudinal flux Air-Cored (A-C) permanent magnet machine and it has a stator assembled by 48 coils, forming three phases (16 coils in each phase). The coils are supported by a separation cage made from non-magnetic and non-electrical conducting material. Due to the complexity of the assembly of the permanent magnets, it is assumed that the permanent magnets and the iron core remain static and that the windings and separation cage are translating (Figure 77).

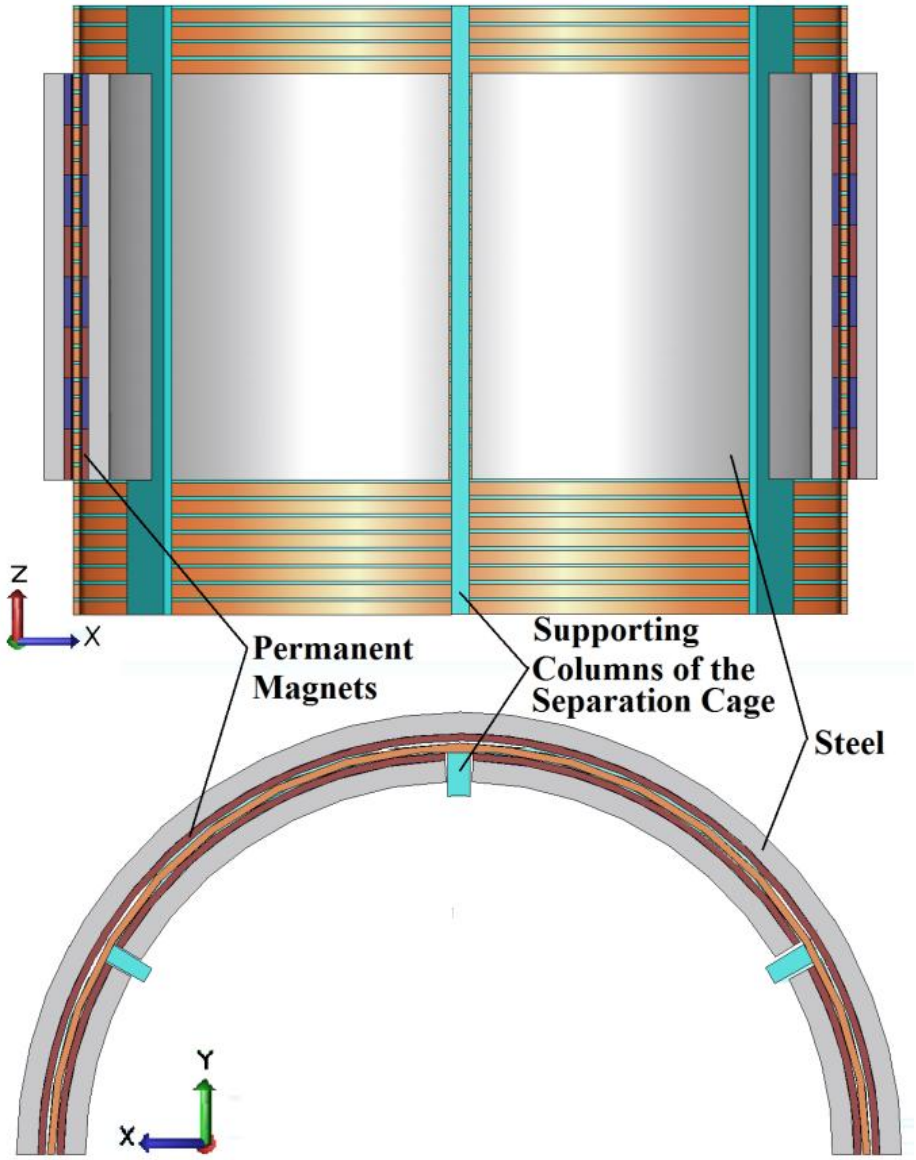

Figure 77 Overview of the proposed generator structure

Initially, air-cored generators with single-side magnet excitation were simulated but the large air gap limits the generated voltage in the coils, which results in low power output. Hence, it was decided that the coils have to be “sandwiched” between two rings of PMs. The excitation flux provided by the radially magnetised magnets (to the Z-axis), exposes the windings in a magnetic field normal to the axis of the motion. In such a field orientation, the

Lorentz forces will be directed in the same direction as the axis of translation of the generator (Z-axis).

Table 7 Main Dimensions and Electrical Characteristics

DIMENSIONS		
Parameters	Axis	
Stator length [mm]	Z	608
Stator inner radius [mm]	X	520
Iron width [mm]	X	30
Coil width [mm]	X	10
Coil length [mm]	Z	20
Separator length [mm]	Z	5
Permanent magnet width [mm]	X	10
Air gap width (including the coils) [mm]	X	16
Translator length [mm]	Z	900
Pole length [mm]	Z	76
ELECTRICAL CHARACTERISTICS		
Number of turns per coil		55
Coil resistance [ohm]		0.8
Coil connection		series
Number of supporting columns		6
Winding connection		star

The main dimensions of the generator are presented in Table 7. The inner magnets and the iron core are divided into six equal sectors (Figure 77). A space among them is left to allow the supporting columns of the separation cage to access the linear bearings. The proposed model has a separation cage with six supporting columns located at the inner circle of the machine.

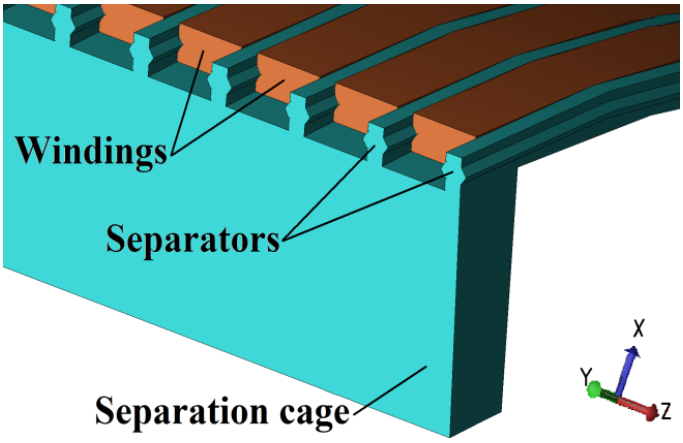

Figure 78 Section cut of the separation cage

In order to enhance the robustness of the translator, the separation cage can be manufactured from a single piece of moulded non-magnetic and non-electrical conducting material. Furthermore, when the coils are positioned among the separators, a solid casting can be applied to secure their position. The casted coils and the keys of the separators secure the coils position over the entire circle of the separation cage (Figure 79).

The dimensions for the proposed machine have been selected to be similar to the existing PMLG in order to conduct a fair comparison between them. Furthermore, the winding slots are designed to be same as in the existing PMLG; however, the keys introduce a reduction of the cross-sectional area (Figure 79) which results in a reduction of the number of turns per coil. Moreover, to reduce the air gap, the height of the coils is reduced in the X-direction and increased in the Y-direction, which results in an increase of the length of the pole in comparison with the existing PMLG.

Furthermore, to compensate for the large air gap, the length of the permanent magnets is the same as the pole length.

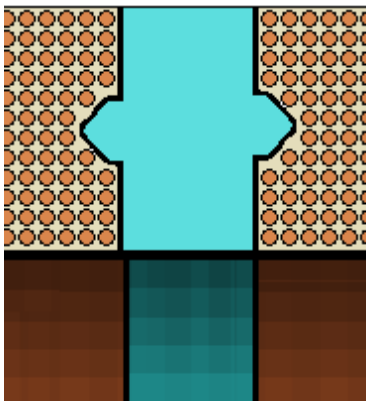

Figure 79 Coil cross-section

Similarly, the robustness of the cage is highly dependent on the number of supporting columns and the thickness of the separators. The generator is expected to be robust mainly because of the reduction of the magnetic attraction forces between the stator and the translator. Moreover, the absence of joins (such as bolt connections) in the separation cage reduces the translator's sensitivity to vibrations and increases the overall robustness of the cage.

The cost of the assembly of the proposed machine is expected to be similar to the existing SS-PMLG proposed in (Prudell, Stoddard et al. 2010). Additionally, the slot openings for the coils are larger and therefore, coil winding and maintenance is expected to be cheaper in comparison with the semi-open slots used in the machine in (Prudell, Stoddard et al. 2010). However, epoxy resin or material with similar properties is required to secure the coils in the slots.

An analytical model of the machine is created based on the magnetic circuit shown in Figure 80. Owing to the design of the machine, the magnetic reluctances remain constant during translation of the translator. S_g is the

magnetic reluctance of the air between the two pairs of magnets and S_m is the magnetic reluctance of the air between neighbouring magnets from the same side (inner or outer side). The total magnetic reluctance seen by MMF sources in a section containing two permanent magnets can be written as:

$$S_{TT} = \frac{S_g * S_{PM} + S_g * S_{C1} + S_g * S_m + 2 * S_{PM} + 2 * S_{C1}}{2 * S_{PM} + 2 * S_{C1} + S_m + 0.5 * S_g} \quad (5.1)$$

S_{TT} is the total equivalent reactance of the circuit shown in Appendix C. The results for the magnetic flux density in the gap from the analytical model and from the static FEM calculation reveal a difference of 8% in the air gap flux density.

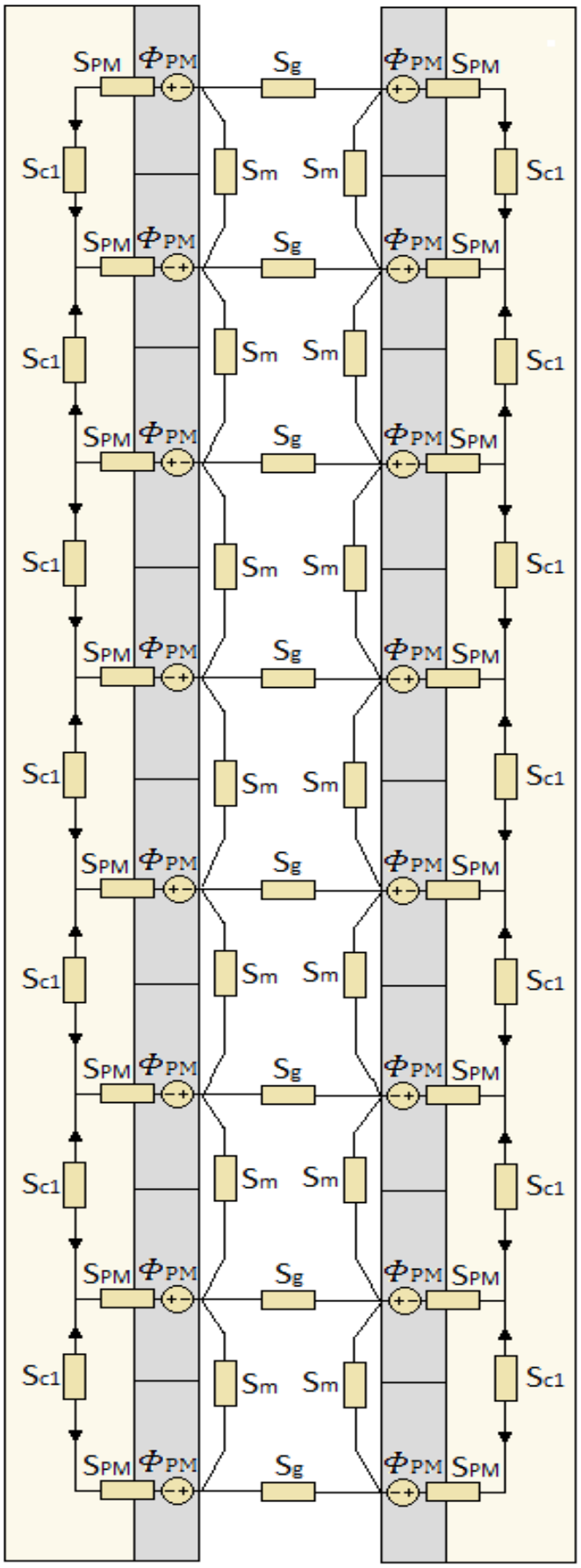

Figure 80 Magnetic circuit of the air-cored LS-PMLG

5.3. Inactive Coil Bypass System

In this chapter a new system is proposed that bypasses inactive coils. The proposed system uses the switches arranged in order to bypass the inactive coils (coils that do not generate voltage). In the proposed system, two switches per phase are connected in series with the coils generating voltage at any time of the operation. Owing to the small number of elements, the power losses in the bypassing system can be reduced significantly in comparison with the system using individual bypassing for every coil (Ran, Tavner et al. 2006).

Owing to the relatively low linear velocities and hence, the low switching frequencies of the switches, anti-parallel thyristor couples can be used.

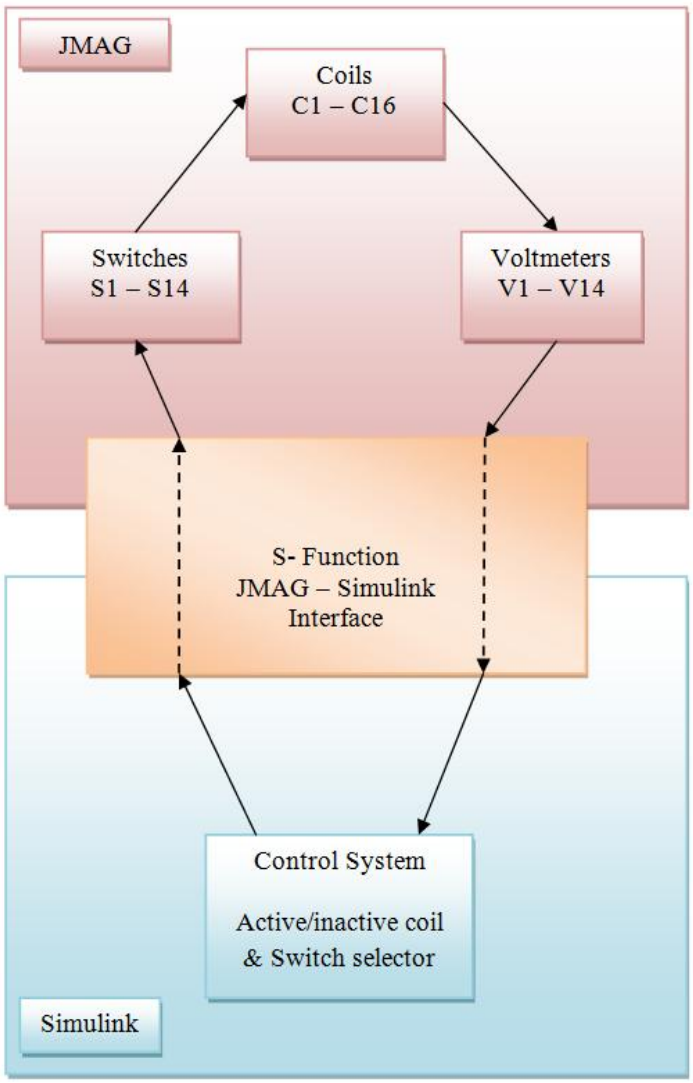

Figure 81 JMAG – Matlab/Simulink interface

In this chapter, all simulations are performed by means of FEA. Additionally, Matlab-Simulink is used for control purposes. The FEA simulations and the control circuit simulations are performed simultaneously using an external link connecting the two software packages. The high-level software configuration is shown in Figure 81.

The coils of the generator are connected in series forming three phases. The coils and the switches controlling the current flow for a single phase are shown in Figure 82. The voltmeters measuring the generated voltage are set on the coil ends (except the two middle coils, C8 and C9).

The system shown in Figure 82 has been designed specifically for the proposed generator in this chapter, in which the ratio of PM-length/translator-length is within the interval of 0.5 to 1. The active control system shown in Figure 82 will not operate if the PMs/translator ratio is lower than 0.5. The main reason for the limitation is that the system has been designed initially for the particular air-cored LS-PMLG discussed in this chapter (with a PM length longer than one-half of the coils length).

To overcome such a limitation, the circuit in Figure 83 can be used. This configuration is independent of the ratio mentioned above and therefore, it can be used for any LS-PMLG based on the principles described both in this chapter and in Chapter 4. Furthermore, the same control technique is used to control the triggering signals to the switches and the same number of two switches per phase is connected in series with the active coils for both circuits (Figure 82 and Figure 83).

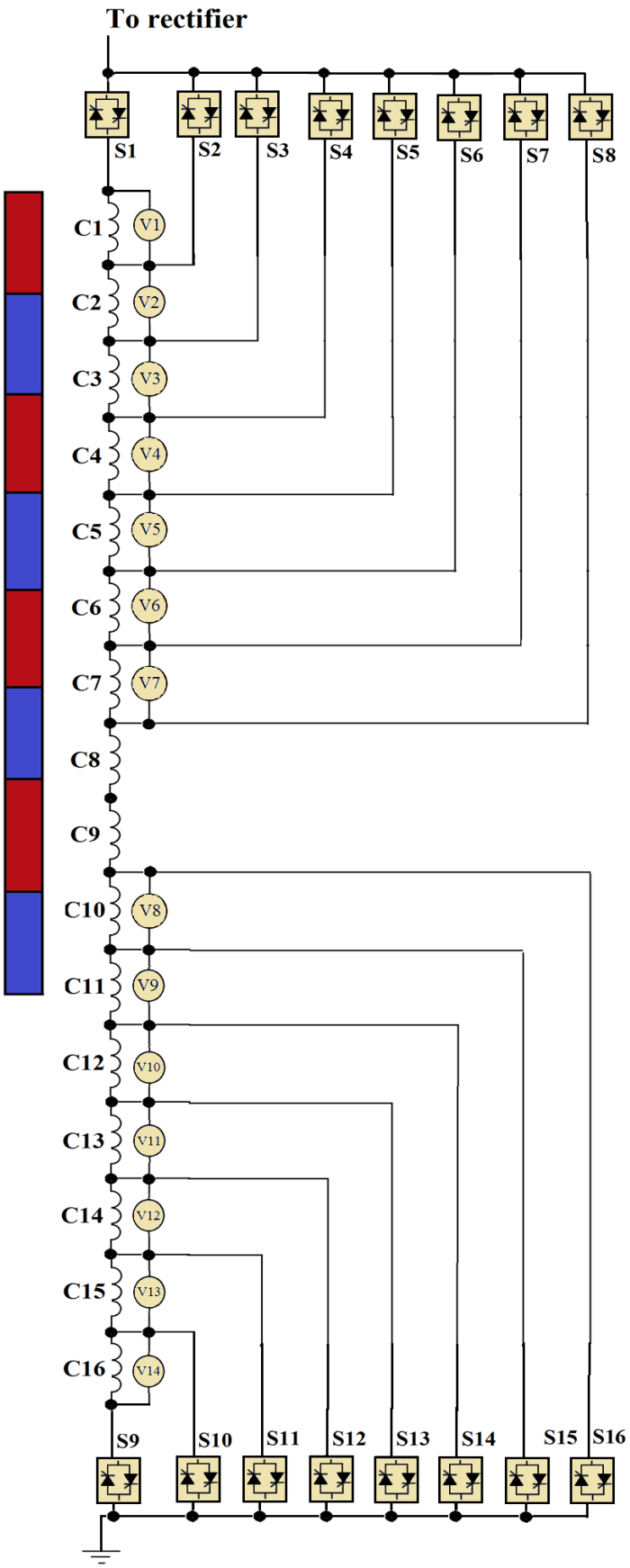

Figure 82 Single-phase coils and switches circuit 1

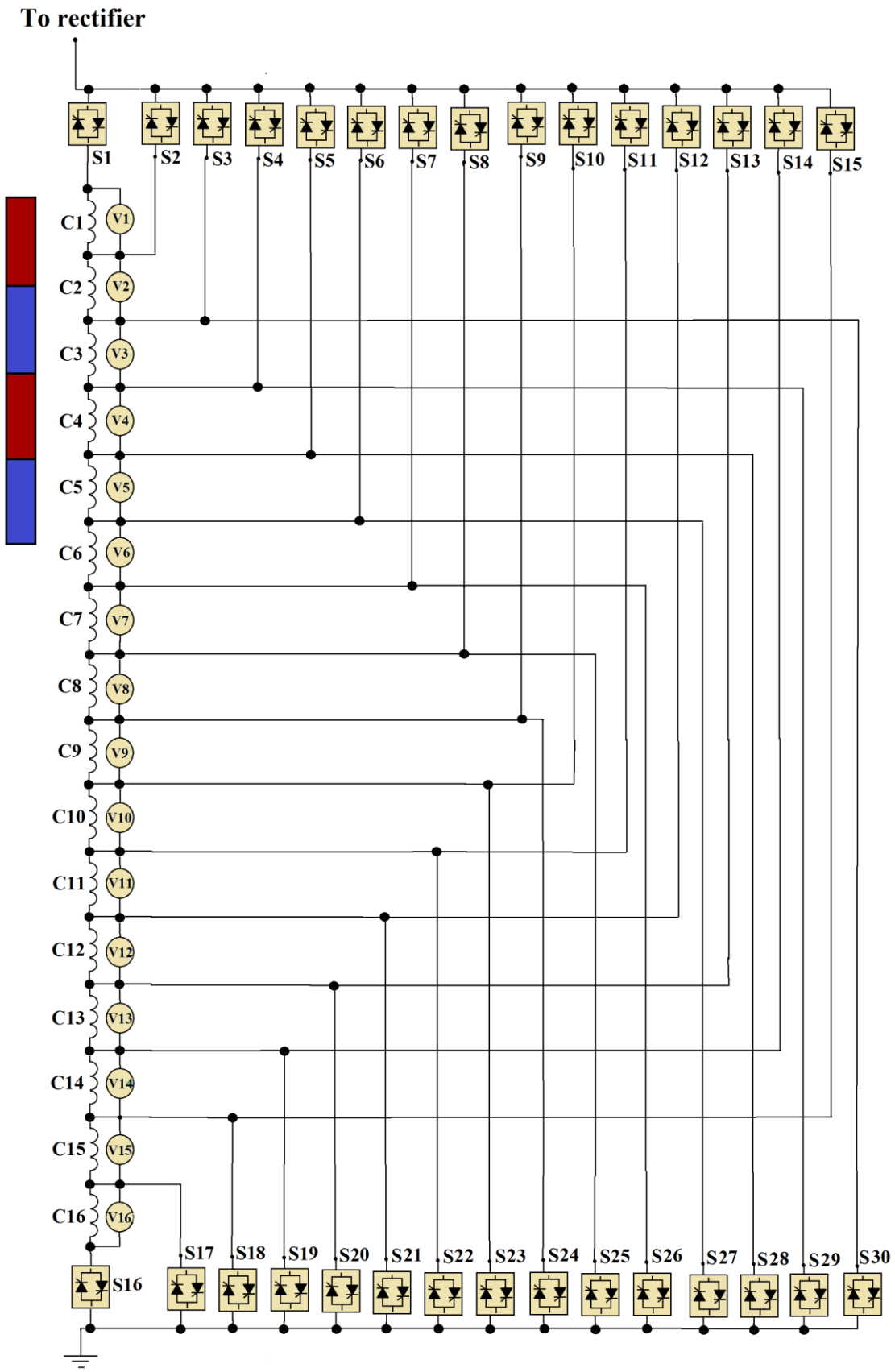

Figure 83 Single-phase coils and switches circuit 2

The principle of operation of the power circuit shown in Figure 82, is described in Figure 84, where it is assumed that the permanent magnets are located between coils C3 and C12 at a certain point of time. At this moment of time, only the above coils (C3 - C12) are generating voltage. In order to disconnect the remaining coils from the circuit, a switch “ON” is applied on switches S3 and S13 (the remaining switches are set to “OFF”). Therefore, an electrical path can be provided bypassing the remaining coils (red line). Moreover, the power circuit includes only two switches connected in series with the coils per phase. The operating principle of the circuit in Figure 83 remains the same as that in Figure 82. The difference between them comes from the increased number of switches and lines, which provides a greater number of available options for directing the phase current (Figure 85).

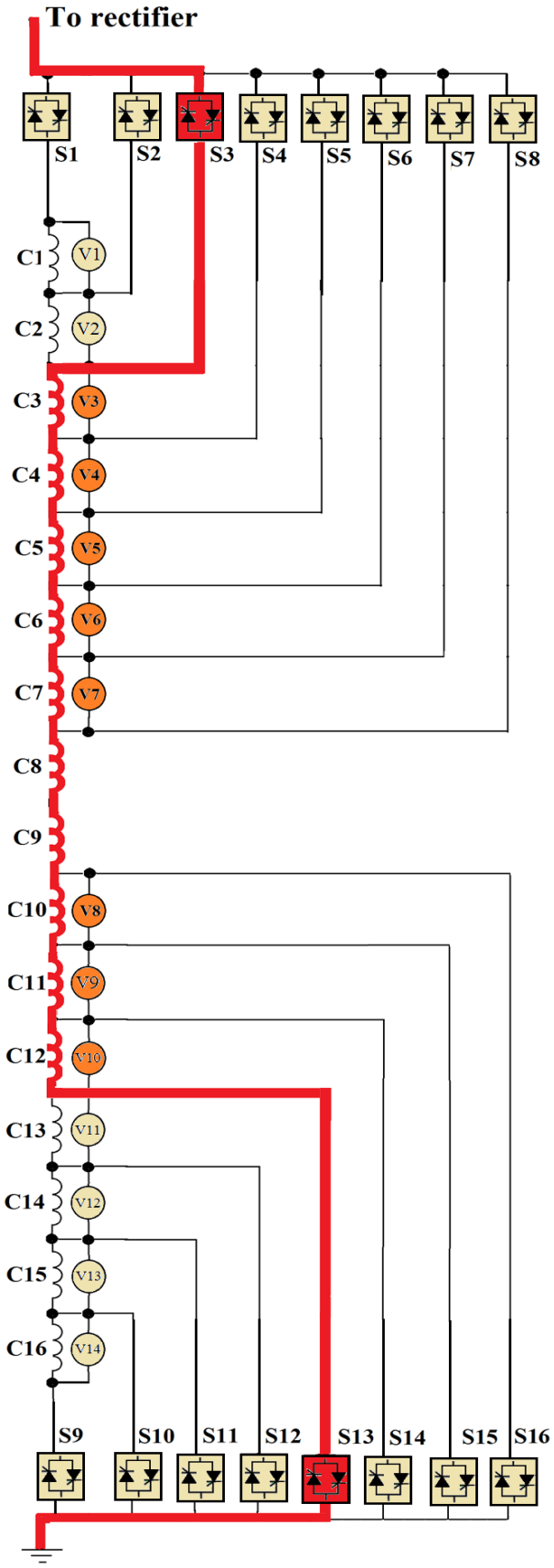

Figure 84 Operation principle of circuit 1

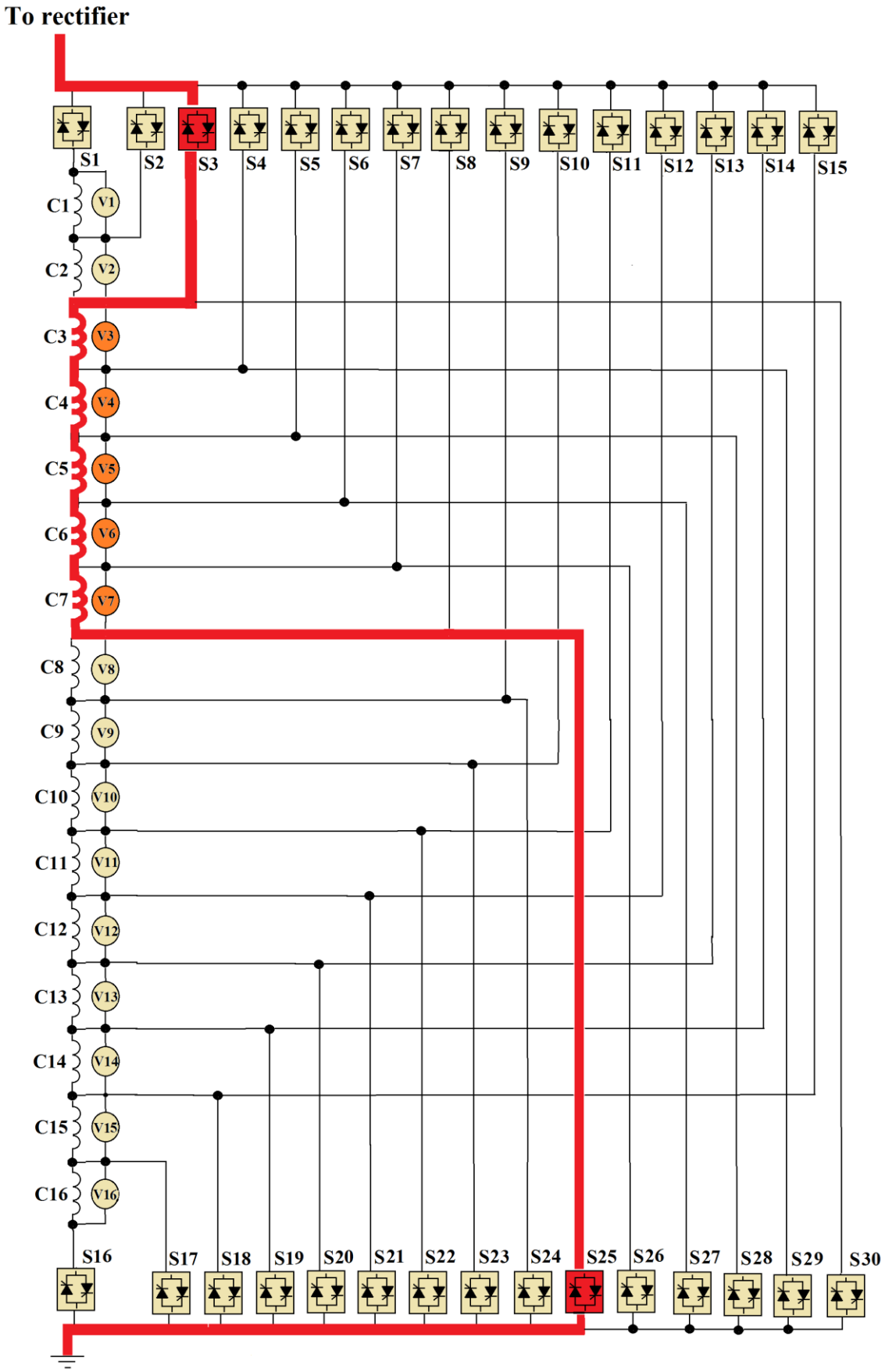

Figure 85 Operation principle of circuit 2

The operating principle of the control circuit triggering the “ON” and “OFF” signals to the switches (from S1 to S16/S30) can be explained as follows.

Based on the voltage obtained by the voltmeters V1 to V14/V16, a control system determines the active and inactive coils in the translator. In order to take only positive signals, an absolute value from the signal gained by the voltmeters is used.

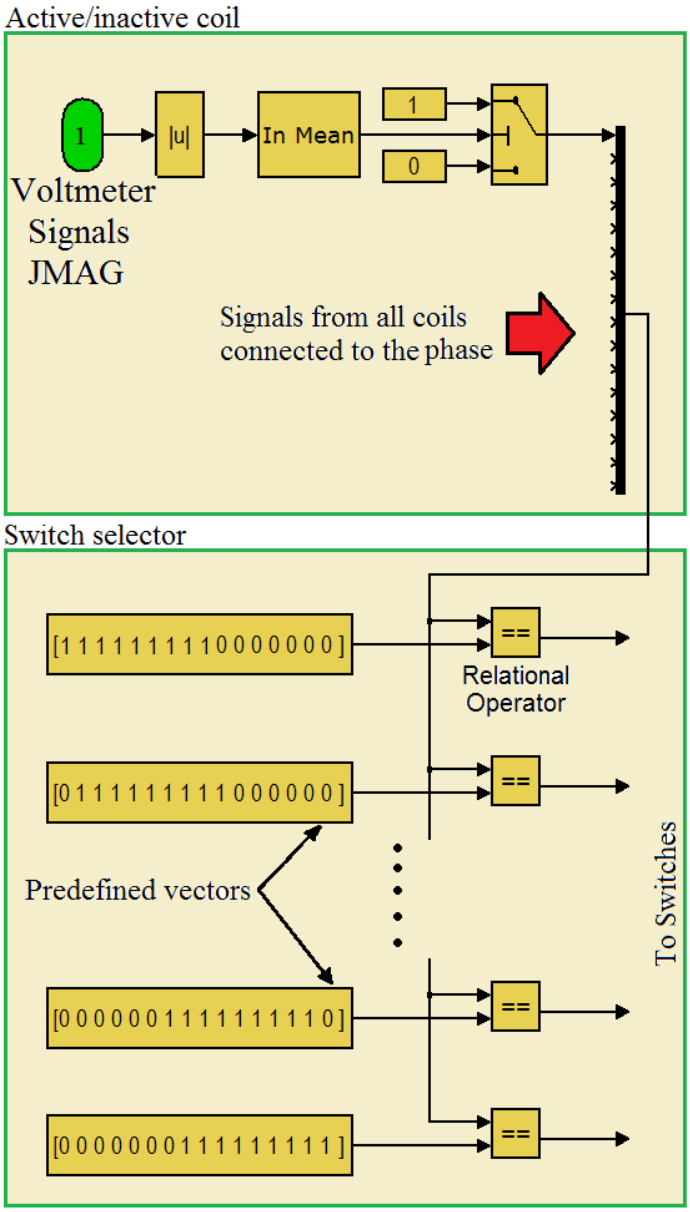

Figure 86 Switch selector and active/inactive coils in Simulink

The mean value (“In Mean”) of the voltage is used to avoid switching “OFF” the switches at zero crossing. After the consideration of activity/inactivity is made for all coils, the signals are collected on a common bus and arranged in a vector. The vector is sent to the “Switch selector” (Figure 86), where a decision for the “ON” and “OFF” signals sent to the anti-parallel thyristor switches is made (S1 to S16 in Figure 84 and S1 to S30 in Figure 85). The vector sent from the “Active/inactive” section is compared against the “Predefined vectors” by a “Relational Operator” (Figure 86). The “Predefined vectors” in the “Switch selector” are all the existing possible combinations of active and inactive coils.

The “Relational Operator” compares the vector received from the “Active/inactive coil” and generates a signal when the vector matches one of the “Predefined vectors”. This signal switches “ON” two of the switches responsible for the combination based on the “Predefined vector”. For example, if the translator is located between C3 and C12 (Figure 84), only voltmeters from V3 to V9 will generate a signal equal to 1 and the vector sent to the “Switch selector” will be: 0011111111000. The vector will match one of the “Predefined vectors” and the “Relational Operator” will switch “ON” switches S3 and S13. In such a way, an electrical path will be provided for coils C3 to C12.

Further discussion regarding the control circuit, including the S-function connecting JMAG with Simulink, as well as a graphical presentation of the Simulink model can be found in Appendix B.

5.4. Simulation Results

A monochromatic wave with period of 8.4 seconds is used as a time-velocity sequence applied to the generator translator in the simulations. Such a period is

equivalent to the energy period (T_e) of a region located north of Spain (Manana, Arroyo et al. 2011).

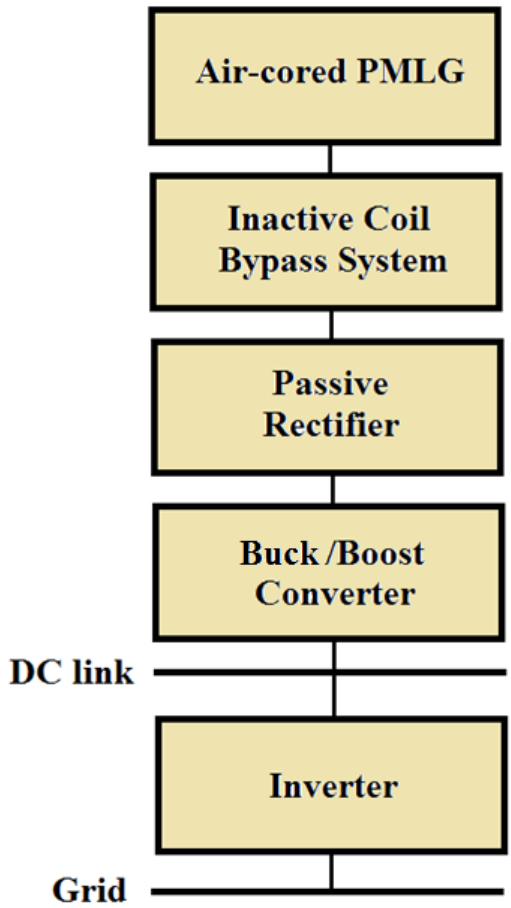

Figure 87 WEC structure - one line diagram

As seen in Table 8, the total price of the raw materials of the air-cored generator is higher than that of the existing SS-PMLG (Prudell, Stoddard et al. 2010). The volume of the permanent magnets in the air-cored generator is 26.5% greater in comparison with the iron-cored generator, which accounts for higher total price of the air-cored machine. However, the output power of the air-cored machine is approximately twice that of the iron-cored generator at the same translational velocity.

The prices of the structural materials are assumed as follows: non-magnetic and non-electrical conducting material - 1.43 £/kg, copper – 5.29 £/kg (London Metal Exchange June, 2012), laminated steel – 2 £/kg (London Metal Exchange June, 2012), magnets, NdFeB, N35 – 216£/kg (Quotation June, 2012).

Table 8 Performance Comparison

Volumes and Prices of the Assembly Materials	A-C PMLG	SS PMLG
Price of Copper [k£]	1.61	0.52
Price of Non-magnetic and non-electrical conducting material [k£]	0.11	0.08
Price of Laminated steel [k£]	1.98	4.64
Price of Permanent Magnet [k£]	70.96	55.5
Price of Total price [k£]	74.67	60.74
Volume of Copper [m^3]	0.034	0.011
Volume of Non-magnetic and non-electrical conducting material [m^3]	0.031	0.022
Volume of Laminated steel [m^3]	0.13	0.303
Volume of Permanent Magnet [m^3]	0.043	0.034
	A-C PMLG	SS PMLG
RMS Power [kW]	5.3	2.5
RMS Phase Voltage [V]	102	70
RMS Phase Current [A]	21	14
Half Peak Power [kW]	3.75	1.75
Half Peak Phase Voltage [V]	73	50
Half Peak Phase Current [A]	10	10

In Figure 88a and Figure 88b, the magnetic flux distributions in the air-cored and the iron-cored PMLGs are shown, respectively. In this figure, it can be observed that the flux density of the air-cored generator is generally lower when compared with the density of the SS-PMLG. The main reason for this is the much higher reluctance in the air gap of the air-cored generator, where the

copper coils and the separator cage are seen as air, with regard to their magnetic reluctance.

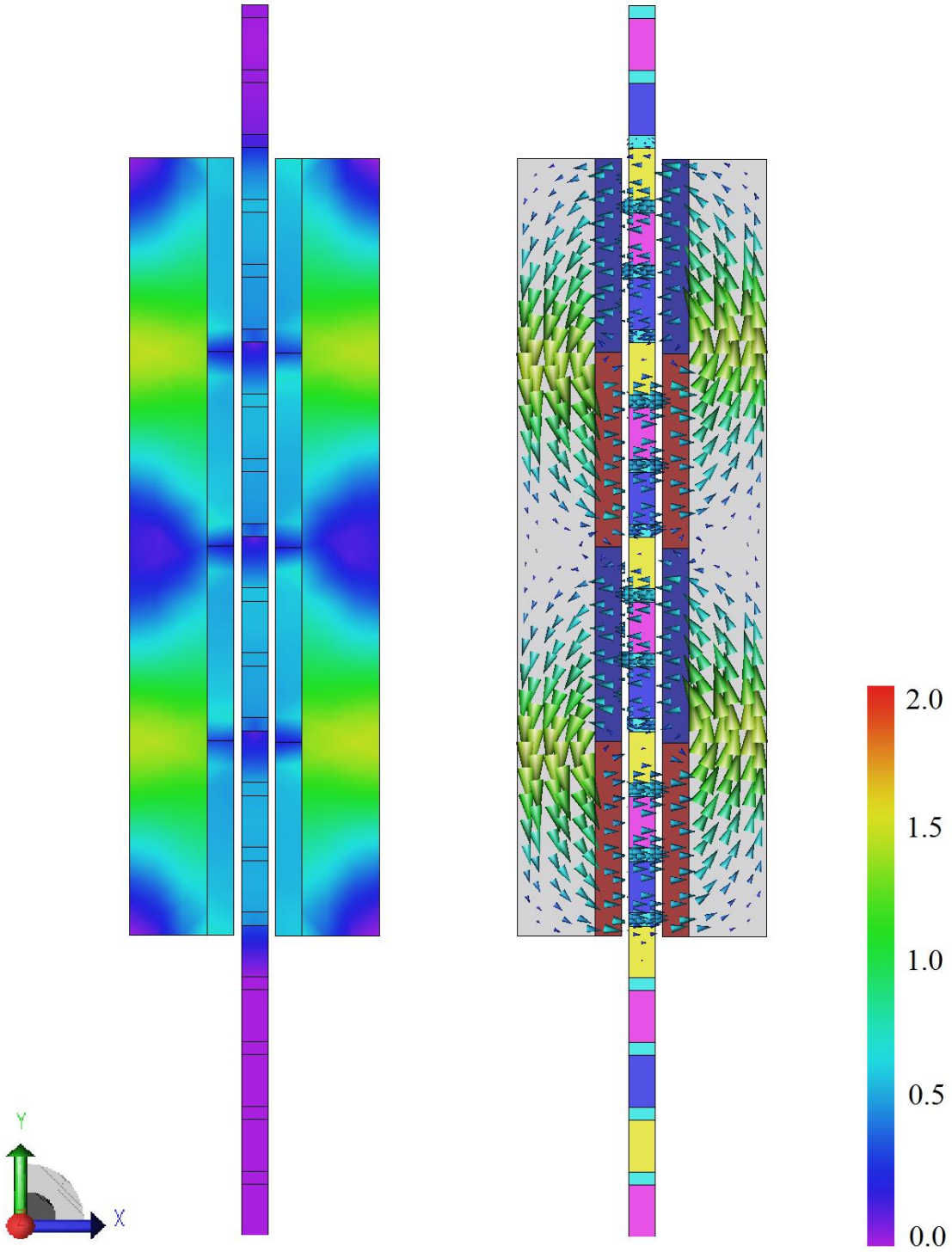

(a) Magnetic flux density in Tesla for the Air-cored LS-PMLG

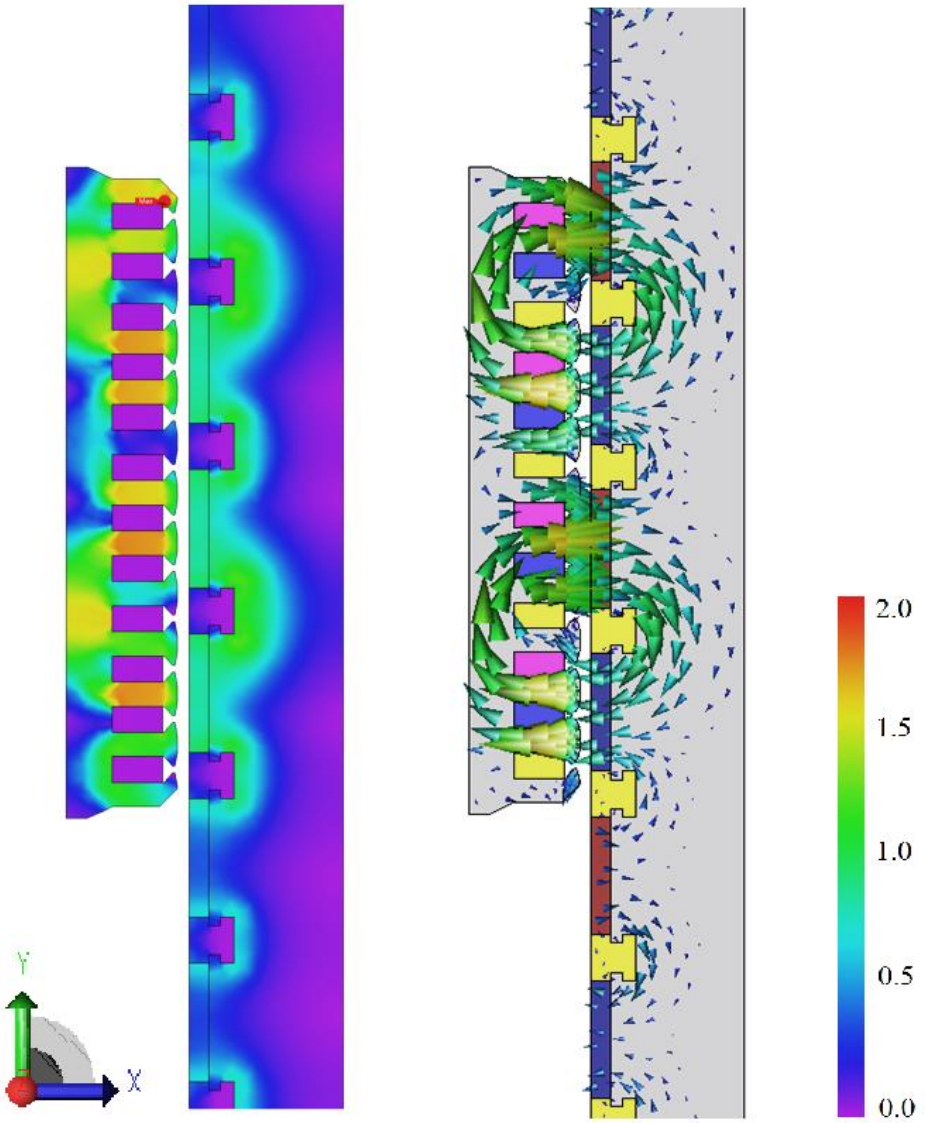

(b) Magnetic flux density in Tesla for the SS-PMLG proposed in (Prudell, Stoddard et al. 2010)

Figure 88 Magnetic flux distribution in Tesla

The simulation results for the forces under load are shown in Figure 89a and Figure 89b. The radial magnetised field directs a significant part of the forces parallel to the Z-axis. This way of directing the forces extends the life of the bearings because of their free motion on the Z-axis. If the field were established

from a single side of the PMs, high magnitudes of armature forces with radial direction would be expected (Baker, Mueller 2005).

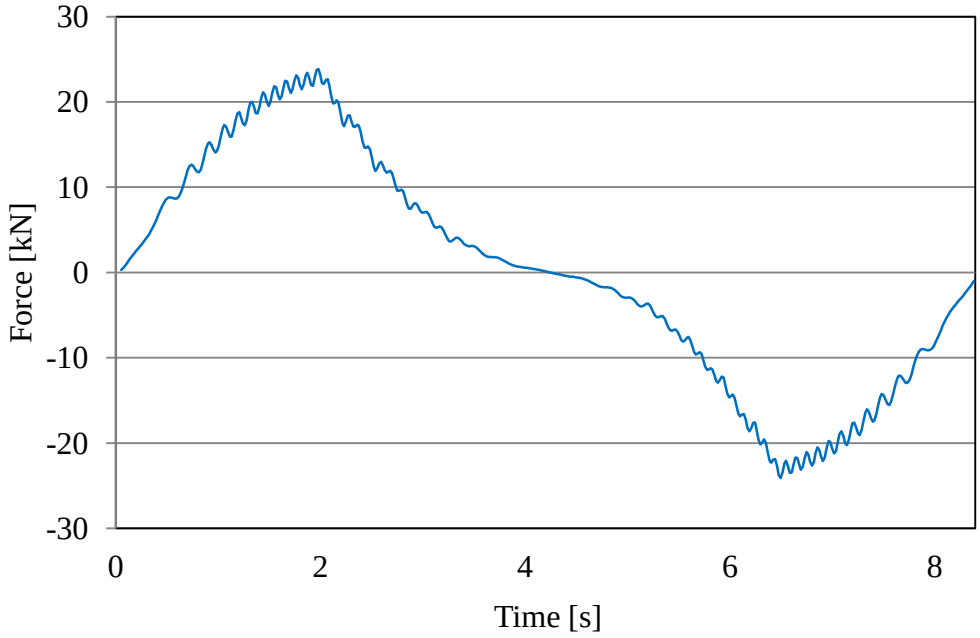

(a) Magnetic force on Z axis

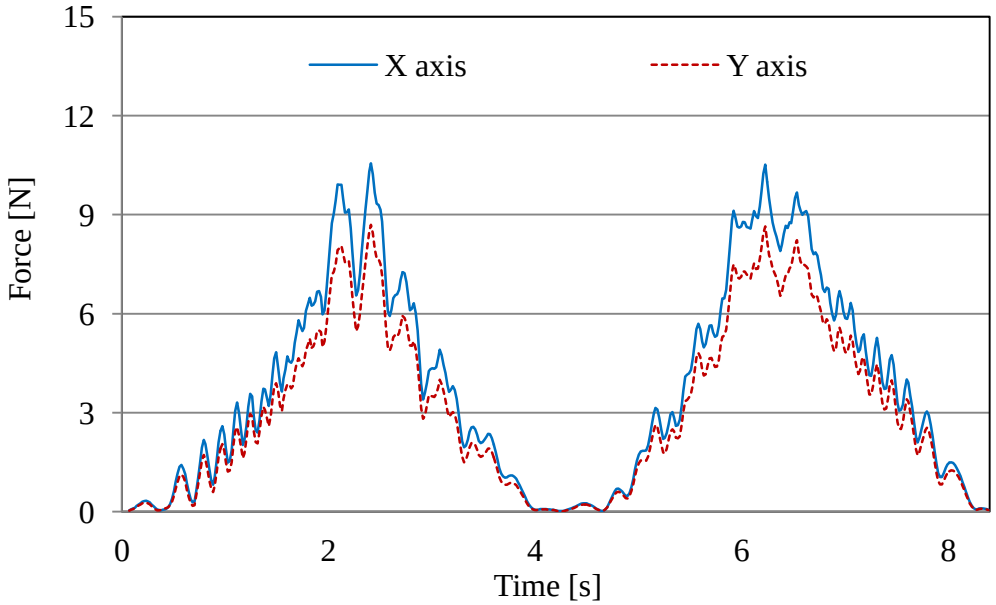

(b) Magnetic forces parallel with the X and Y axis

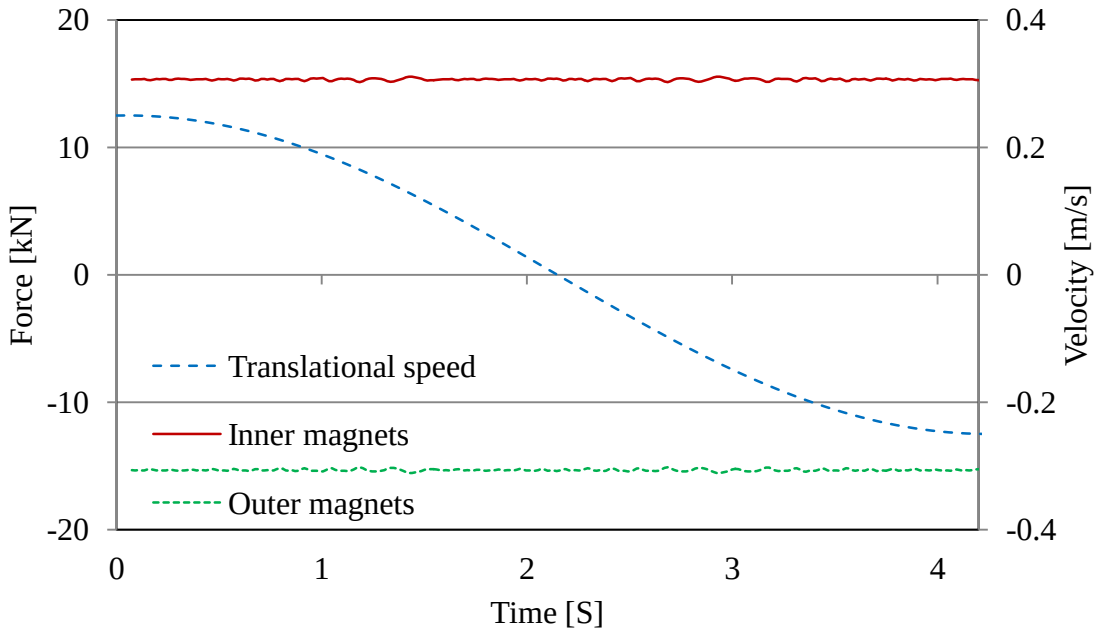

(c) Forces simulated on the inner and outer sets of magnets at constant velocity

Figure 89 Forces in the air-cored generator

In Figure 89c, the magnetic forces between the permanent magnets for a section of the generator are shown. The results present the magnitude of the attracting forces acting between the inner and outer sets of magnets for one-sixth part (arc with 60-degree angle).

As the outer magnets have full circular shape (full 360 degrees), the total radial force will remain zero due to the opposing directions of the forces and the integrity of the solid structure. If the inner magnets are fixed in a single structure, the total force can also be eliminated but the fixations between the sectors have to be strong enough to withstand the forces shown in Figure 89c and the sections have to be aligned.

In Figure 89c, it is also seen that the attracting forces between the magnets remain relatively similar regardless of the velocity of the translator.

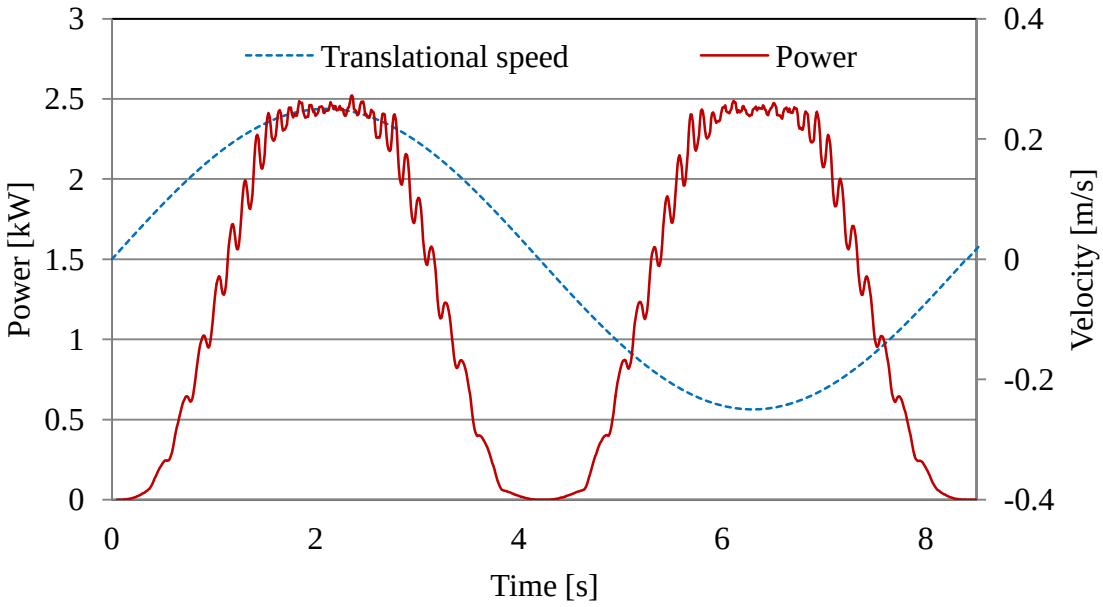

Figure 90 Power output and linear velocity

Figure 90 depicts the power output simulated on a 5-ohm resistor connected after rectification, where the RMS power is 1.61 kW.

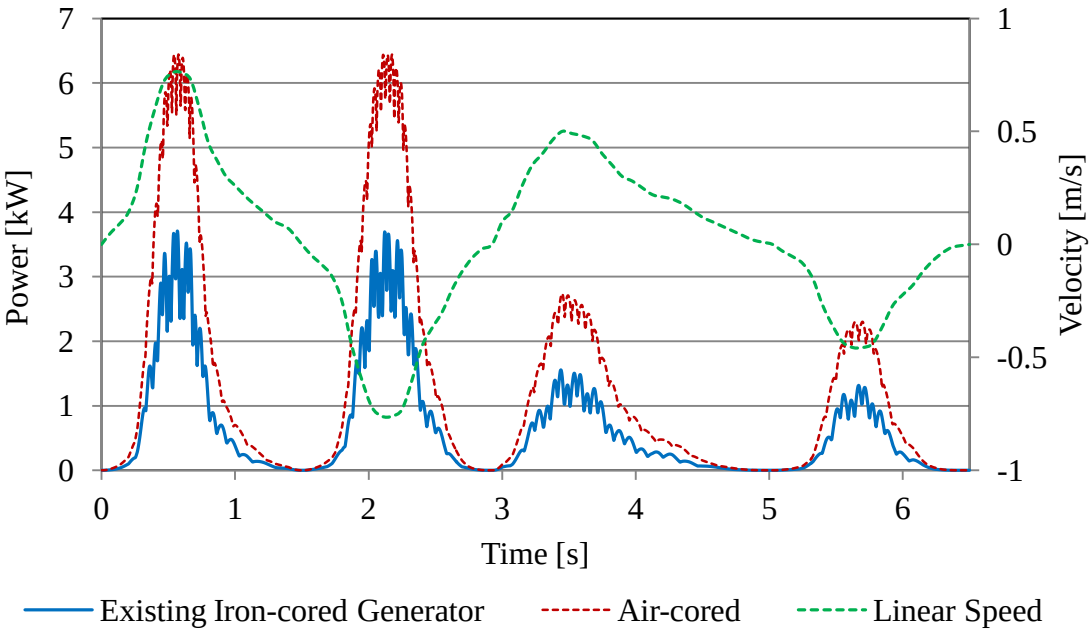

Figure 91 Power output for the proposed and existing generators

The output powers from the proposed air-cored and the existing iron-cored generators are given in Figure 91. In the simulations, the air-cored generator

achieves around double the peak power at different velocities. The velocity shown in Figure 91 is an experimentally recorded vertical displacement of marine wave and it is assumed that the generator follows strictly the waves displacement.

Furthermore, in the proposed air-cored PMLG, the number of constantly energised coils is 24, compared with 12 coils in the iron-cored machine, which increase the generated phase-voltage. Similarly, owing to the absence of iron in the translator, the cogging forces can be eliminated and hence, a q = 1 can be set to boost the generated power (Chapter 3).

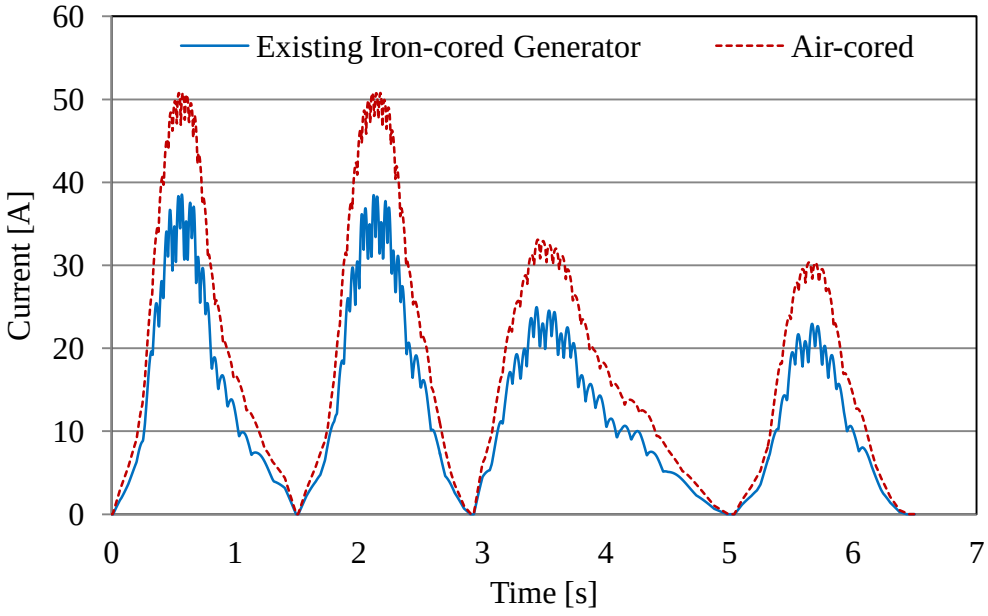

(a) DC current output

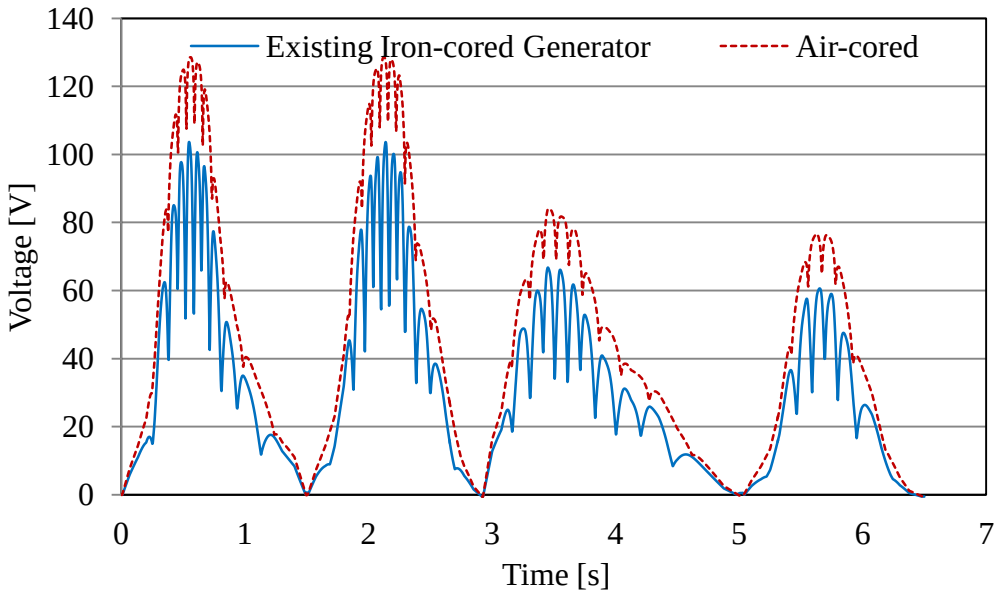

(b) DC voltage output

Figure 92 DC current and voltage after rectification

The current and the voltage simulated after rectification on the 5-ohm active resistive load are shown in Figure 92. The displacement of the translator is the same as that shown in Figure 91.

The voltage generated by several coils is shown in Figure 93 and Figure 94. Similarly, the “ON” and “OFF” triggering signals (1 and 0 volts, respectively) sent to the switch selector are plotted as well. If the signal has a value equal to 0, it means that the switch is open and if the signal has a value equal to 1, it means that the switch is closed.

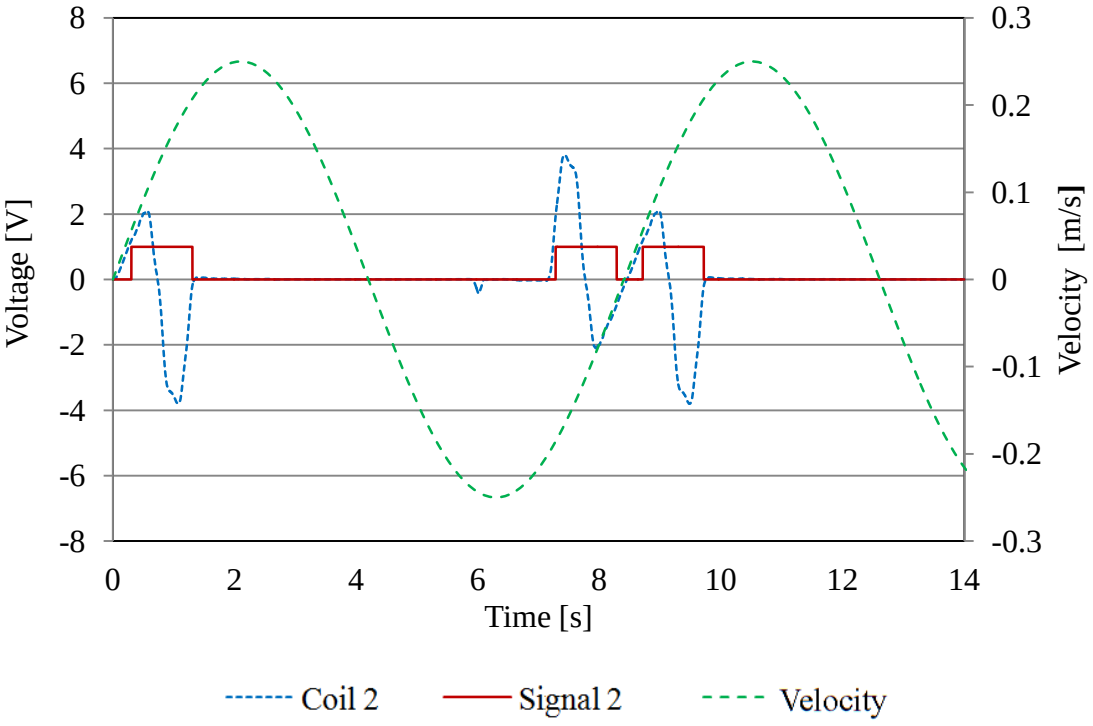

(a) Coil 2 voltage output

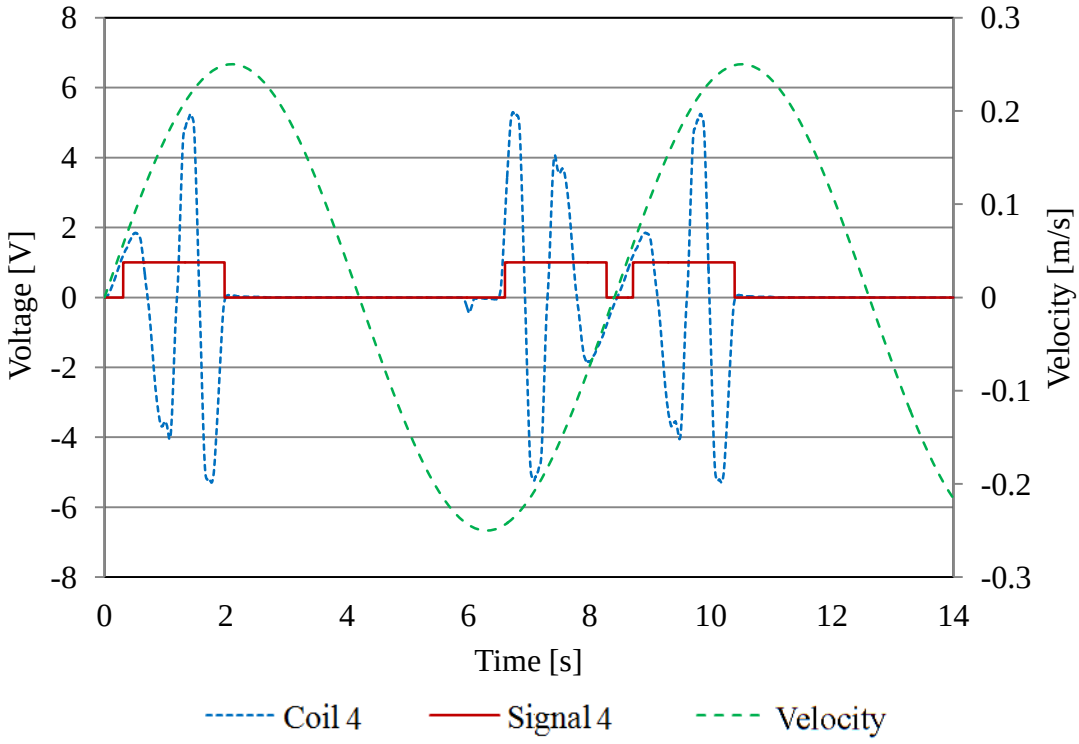

(b) Coil 4 voltage output

Figure 93 Single coil voltage and switch signal for Coils 2 and 4

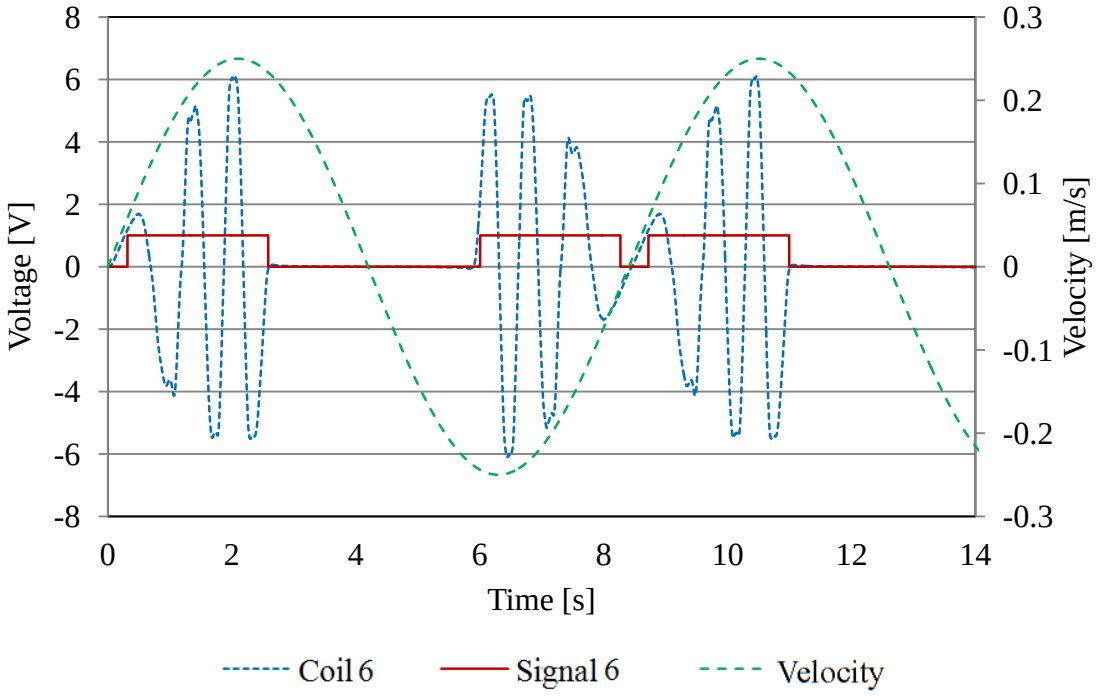

(a) Coil 6 voltage output

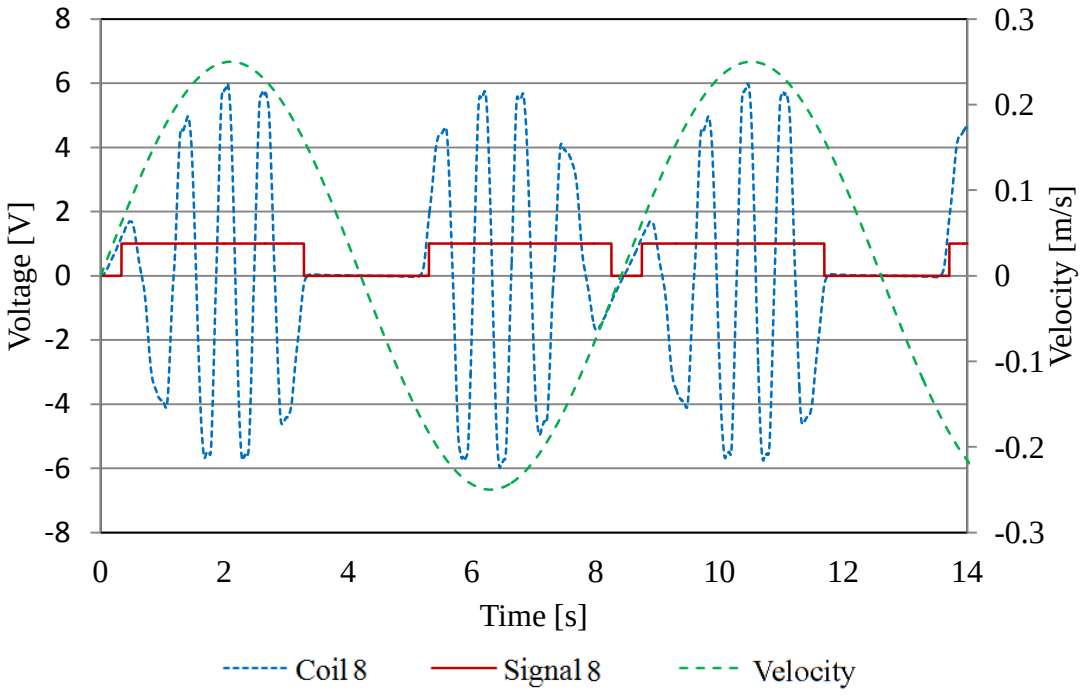

(b) Coil 8 voltage output

Figure 94 Single coil voltage and switch signal for Coils 6 and 8

The thermal losses in the previously proposed bypass systems are dependent of the number of magnet pairs and the total number of coils (Ran, 202

Tavner et al. 2006, Ran, Mueller et al. 2011). In the bypass system proposed in this thesis, the thermal losses are independent of the number of coils or of the number of magnetic poles. Therefore, by using the proposed bypass system, a reduction of the thermal losses by up to seven times is achieved in comparison with the system proposed in (Ran, Tavner et al. 2006).

The thermal loss reduction is because of the number of series-connected switches with the coils. For example, if the grid integration system, proposed in (Ran, Tavner et al. 2006), is integrated with the proposed air-cored machine and the length of the permanent magnets is same as the length of two coils, 16 switches will be needed to bypass every coil (per phase) and 14 of them will be connected in series with active coils. The proposed system is independent of the active length of the translator and has two switches per phase connected in series with the windings at any time. Therefore, the total thermal loss in the switches could be reduced by up to seven times.

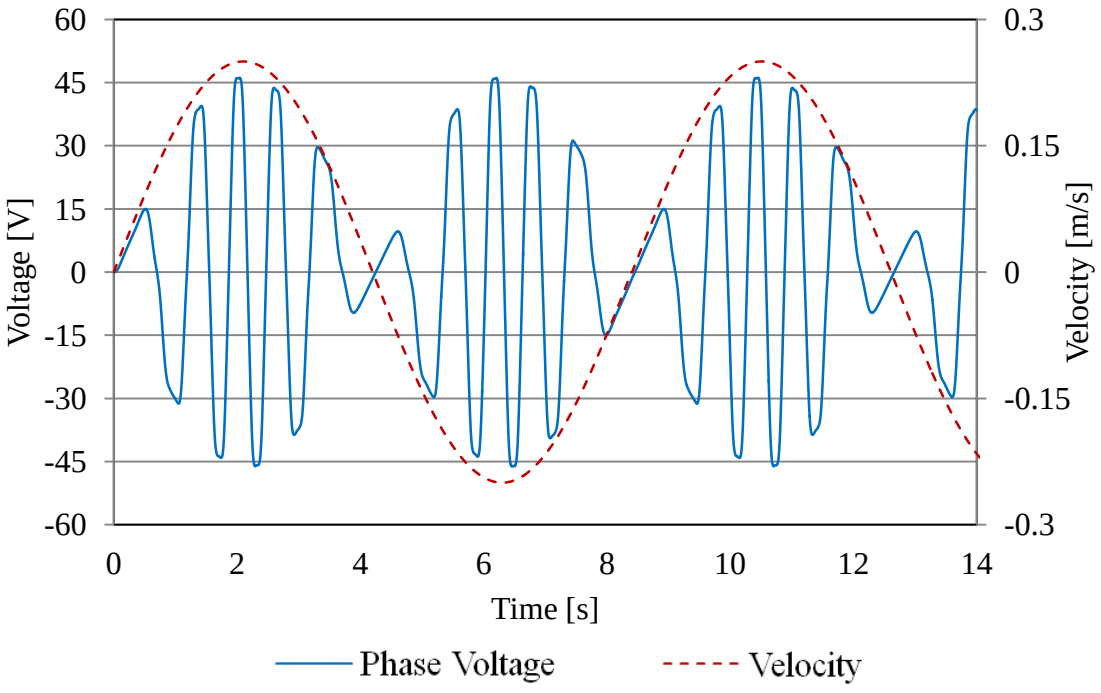

(a) Single phase voltage with sinusoidal translator motion

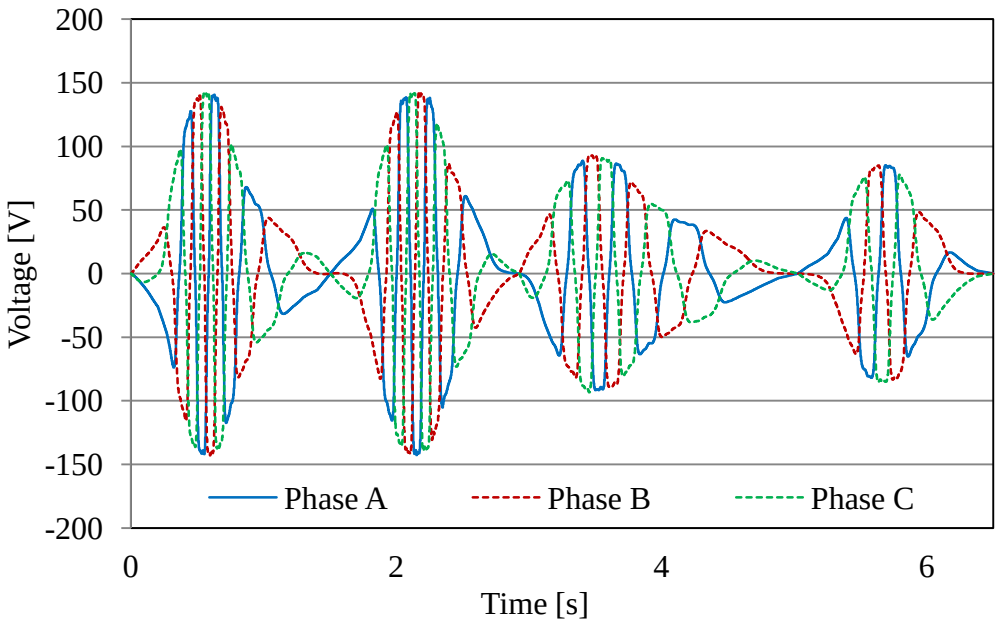

(b) Three-phase voltage

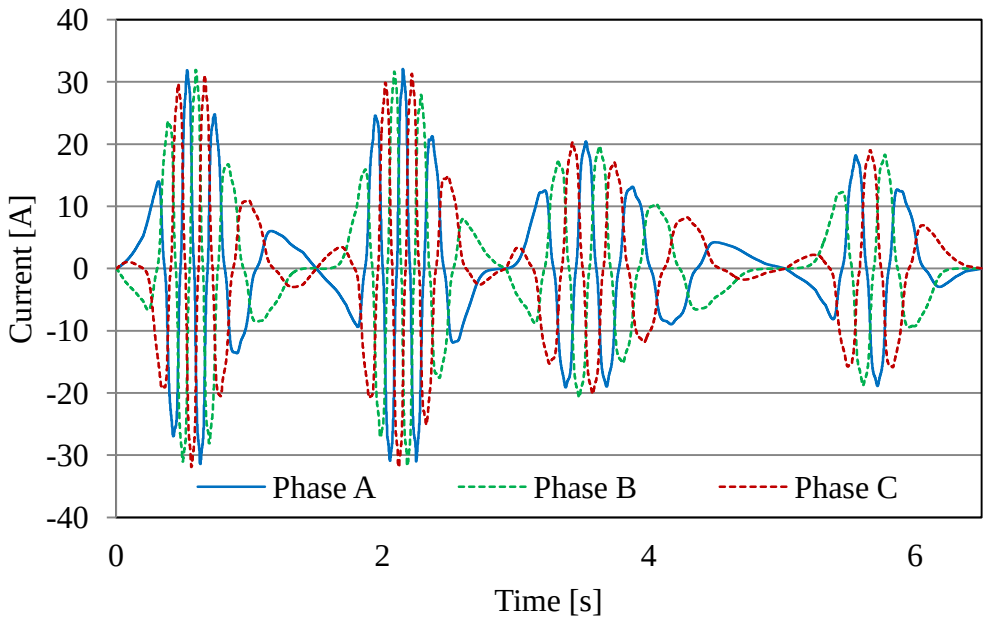

(c) Three-phase current

Figure 95 Three-phase voltage and current

In Figure 95a, the single-phase voltage is presented. The translational velocity is the sine wave with a period of 8.4s, discussed in the beginning of the

section. The three-phase voltage and current before rectification are shown in Figure 95b and Figure 95c and the linear velocity of the translator is shown in Figure 91.

5.5. Conclusion

The proposed air-cored machine has benefits over the existing iron-cored SS-PMLG in terms of total reduced volume of active material and the elimination of unwanted cogging force. Even though the results imply improved electrical power output it is acknowledged the iron-cored PMLG may not be an optimum design and hence a more detailed design study of both topologies is required to compare the proposed air-cored machine with the iron-cored SS-PMLG.

In this chapter, simulation results of a novel design of air-cored tubular generator have been presented. The 3D FEA results suggest that the proposed generator has higher power output in comparison with the existing iron-cored generator using similar volumes of structural materials and with having similar dimensions. Similarly, the results reveal that the proposed design addresses the majority of the forces occurring under-load to a direction parallel to the axis of translation.

A novel system for bypassing inactive elements has been presented and simulated. The bypassing system uses two switches working in series with the coils per phase. As a result, the thermal loss in the proposed bypass system can be reduced by up to seven times compared with previously proposed systems. Moreover, the thermal losses in the proposed bypass system are independent of the number of coils in the generator assembly.

6. Conclusions and Future Work

The research undertaken and explained in this thesis is focused on reducing the magnetic forces and on increasing the electrical power output of direct drive PMLGs. The main investigation is concentrated on developing two new designs (air- and iron-cored) for a long stator linear generator. The long stator design allows higher utilisation of the permanent magnets, where the entire flux established by the magnets is crossing the coils and therefore, generating voltage (if translation occurs).

In the case of the iron-cored generator, it is established that the use of a long stator design could decrease both the cogging force and the price of the structural materials significantly in comparison with existing SS-PMLG.

Details on the main wave energy harvesting technologies and the existing direct drive linear generators are presented systematically in the literature review.

Analytical and numerical studies of flat air-cored permanent magnet linear generators have been modelled and investigated in two machine topologies (single and double sided PMLGs). The research on the single-sided PMLG concentrates on the effect of different design solutions on the generator output power and on the cogging forces. The examination of the design variations centres on a number of factors: the number of slots per pole and phase, the number of winding sections and the number of magnet poles covering the length of the translator. The investigation into the double-sided PMLG is focused on the same parameters as for the single one. Additionally, an optimal PMLG model with a separated magnetic yoke is suggested for the double-sided PMLG. The results for the optimised model reveal a reduction in the X- and the

Y-axes forces by 55% and 28%, respectively and an increase of the output power by 233% in comparison with a model with a non-separated translator having the same volume of PM material.

A long stator tubular LS-PMLG is proposed and compared against an existing tubular SS-PMLG design. The comparison is based on the cogging force and the electrical power output. The results of the FEA simulation show a decrease of the cogging force by up to 60%. Moreover, because of the lower amount of PMs in the LS-PMLG, a 60% reduction of the raw material cost is calculated. Based on the comparison made in this chapter, it can be suggested that the use of long stator topology for PMLGs is more beneficial than the existing design.

A novel air-cored double-sided tubular PMLG has also been proposed. The suggested generator is compared with existing iron-cored tubular SS-PMLG and the FEA reveals a 47% increase in the power output. However, owing the large air gap of the air-cored generator, the volume of permanent magnet material is around 25% higher, which leads to higher total cost of the raw materials. Despite this higher price, the use of an air-cored PMLG is considered more beneficial than using an iron-cored SS-PMLG, because of the elimination of the cogging force and hence, the potential reduction of the level of vibrations. Furthermore, a novel system for bypassing unenergised coils in the air-cored generator is proposed. The systems suggest that the thermal losses in the switching devices can be reduced by up to seven times in comparison with previously proposed bypassing systems.

In the thesis, all the work has been carried out using FEA simulation tools. Even though the results for generators are highly promising, they have to be verified by experimental testing. The author recommends building a full or

scaled prototype for the verification of the FEA results. The author also believes that the use of air-cored permanent magnet generators will bring several advantages in comparison with the currently proposed iron-cored generators. The main benefit of the air-cored generators is the elimination of the cogging force within the machine. However, significantly more permanent magnet material is needed to overcome the large air gap.

The author has also considered that the double-sided air-cored generator is a promising alternative solution as a direct-drive linear generator. However, more research is required in the following areas:

1. Investigation into the manufacture and the assembly of the generator.
2. Survey of options for fixations (permanent connections) between the inner sets of magnets.
3. Research into appropriate bearing systems including thermal analysis.
4. Thermal analysis of the copper coils and the magnetic cores.
5. Fixations between the magnets and the magnetic core. Moreover, an investigation into whether the magnet rings can be assembled from a single ring or sectors forming a ring.
6. Structural integrity of the separation cage. Whether the cage is capable of handling the armature forces opposing the prime mover. In the current model, the separation cage is open from both ends. If the cage is closed from one end with 2- to 3-mm thick wall, the cage will be much stronger for handling axial forces.

Furthermore, additional work on the inactive coil bypass system is needed. In the thesis, the effects from possible inrush currents (switching inductors) and switching losses in the back-to-back thyristors have not been considered.

Moreover, limitations of the coil bypass system, such as the maximum translational velocity limiting the normal operation of the system should be outlined.

Appendix A

Magnetic Flux Distribution in the SS-PMLG proposed in (Prudell, Stoddard et al. 2010), simulated in JMAG.

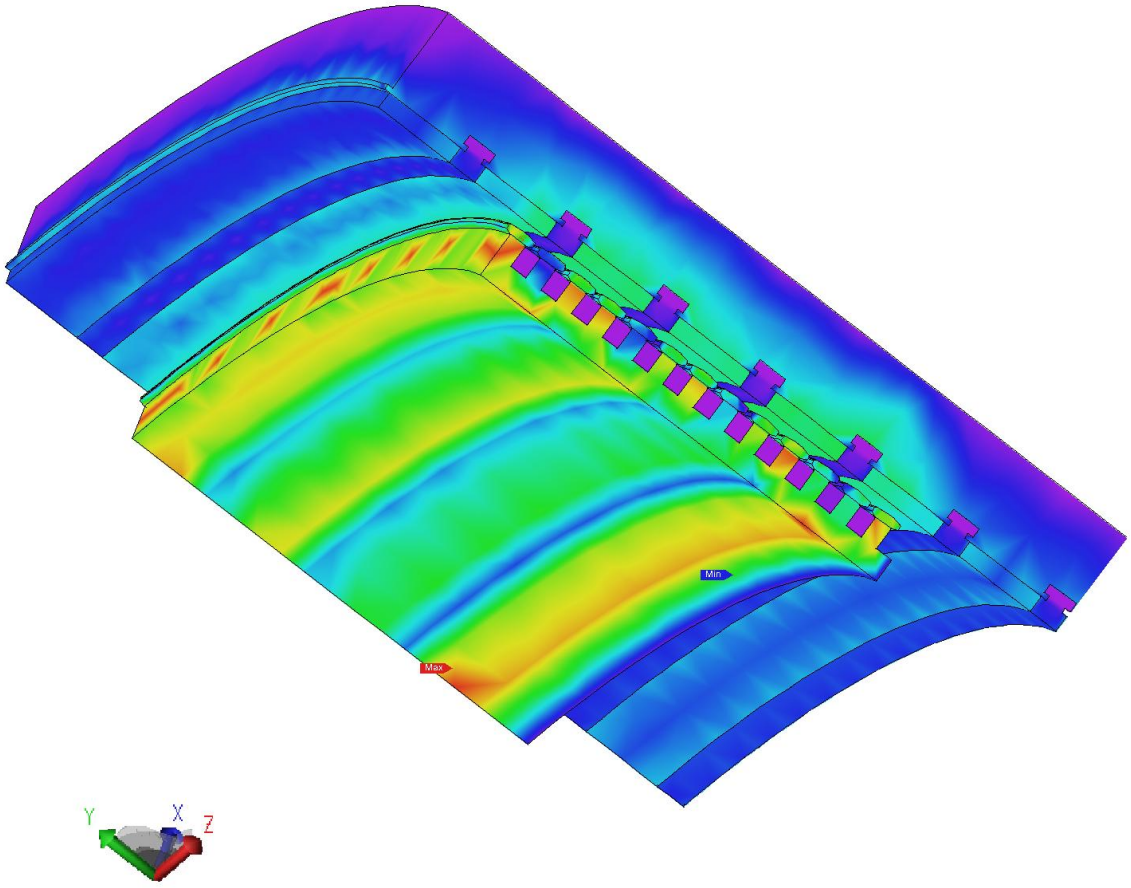

(a) 3D Flux density in Tesla in the SS-PMLG proposed in (Prudell, Stoddard et al. 2010)

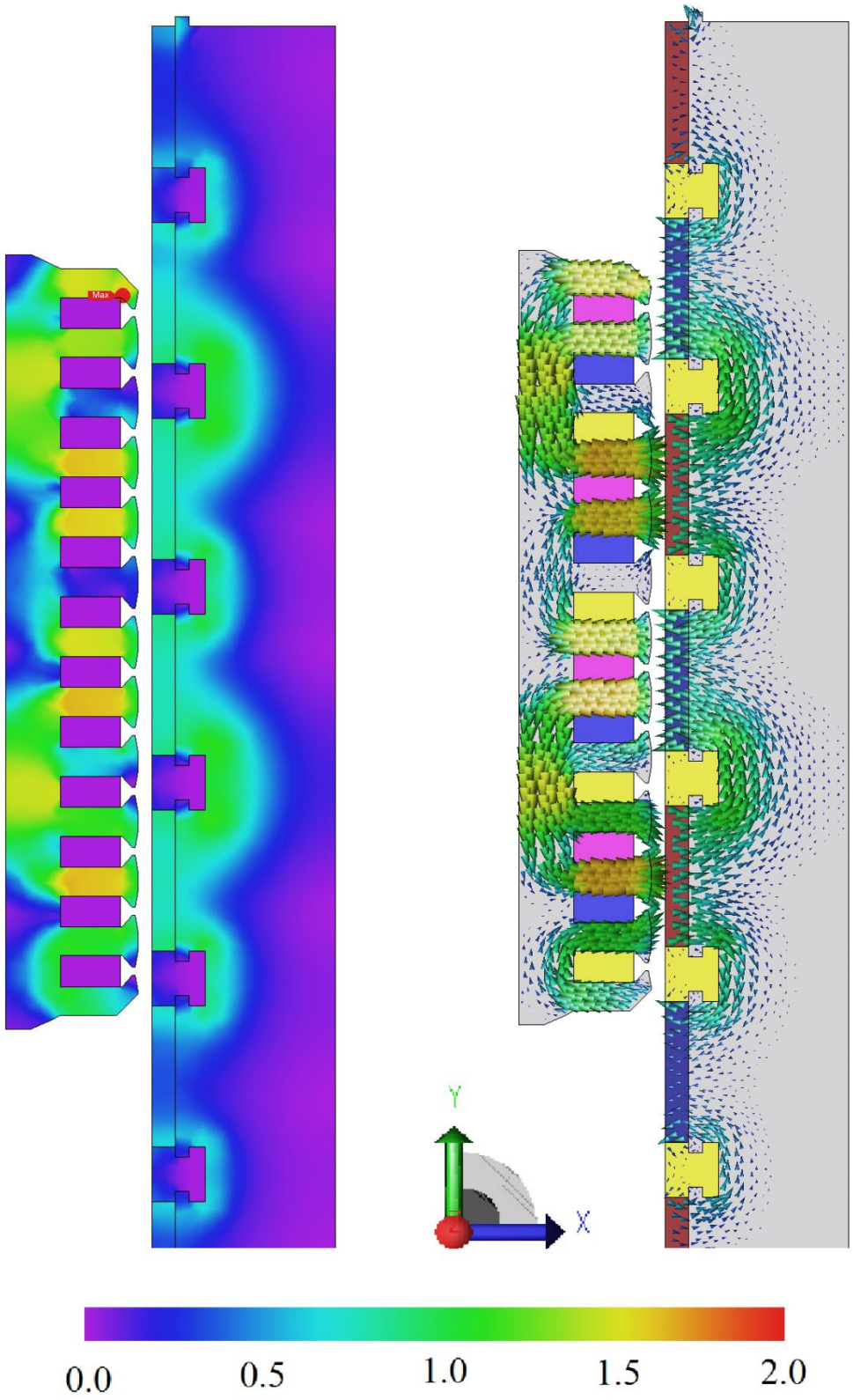

(b) 2D Flux distribution

Figure A1 Flux density in Tesla in the SS-PMLG proposed in (Prudell, Stoddard et al. 2010)

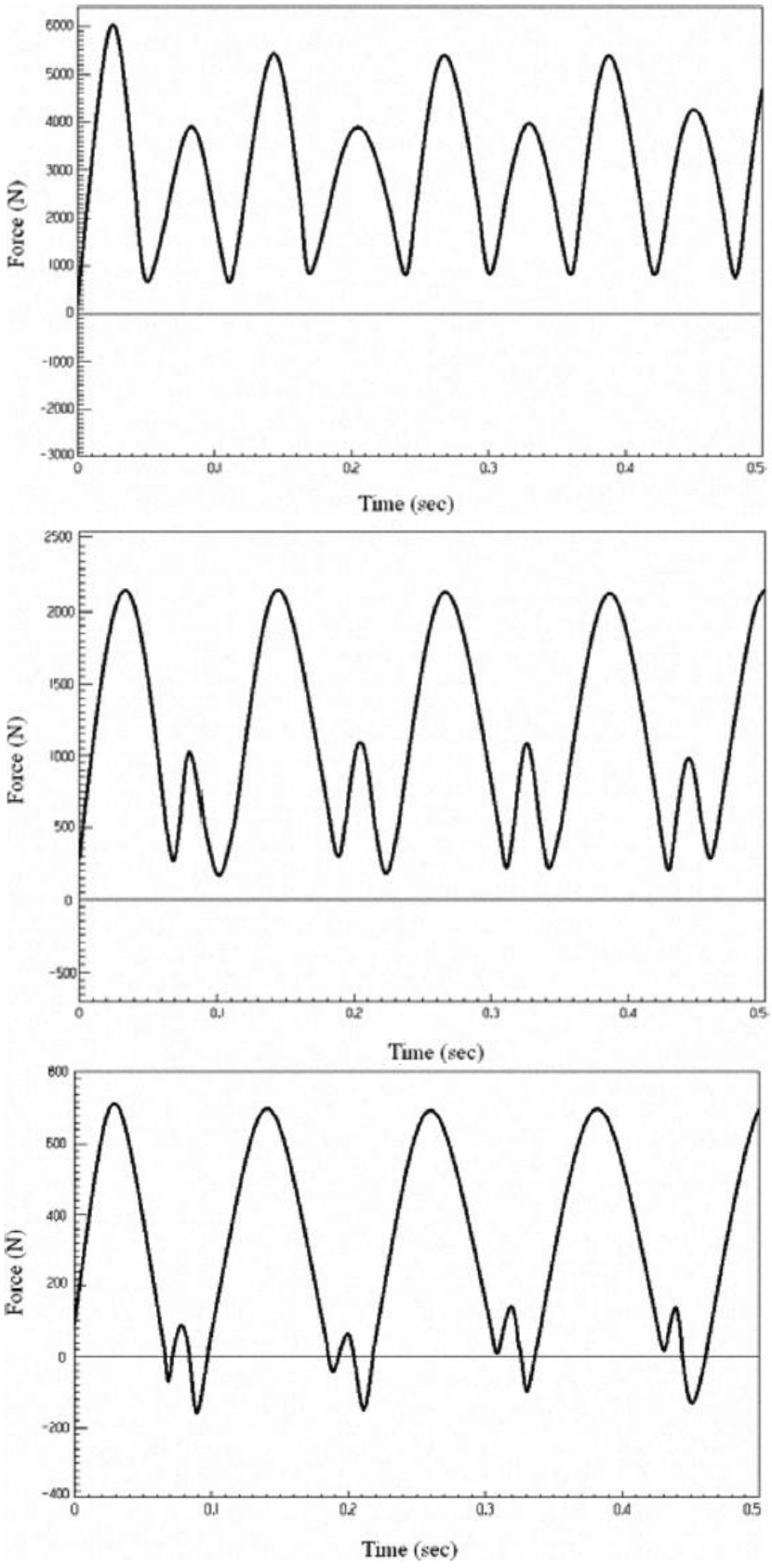

Figure A2 Difference between cogging forces for different skewing angle

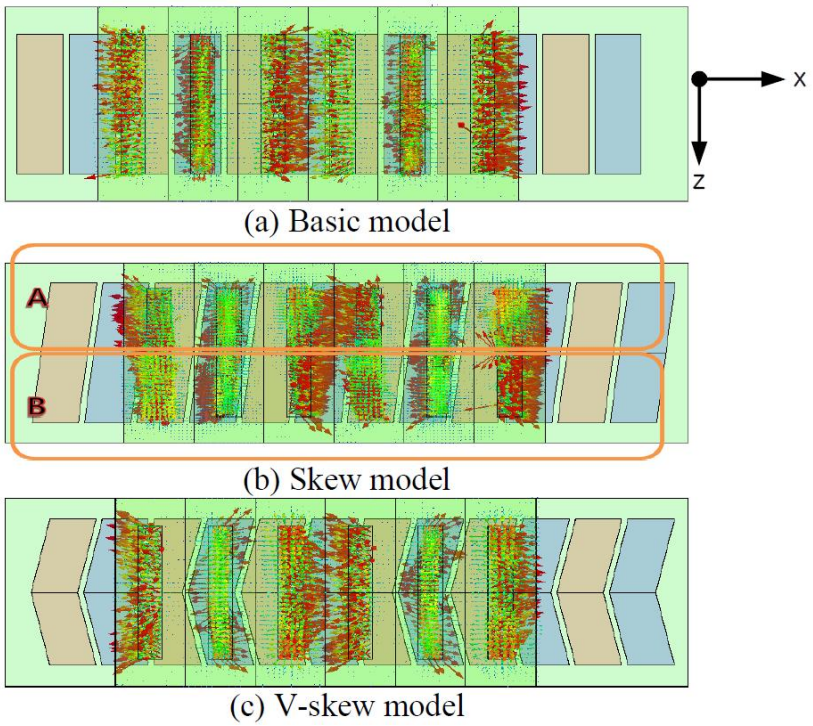

(a) Basic model

(b) Skew model

(c) V-skew model

Figure A3 Flux vector diagrams for different skew patterns (Ahn, Lee et al. 2008)

Appendix B

Further information about air-cored Long Stator Tubular PMLG and inactive coils bypass system proposed in Chapter 5

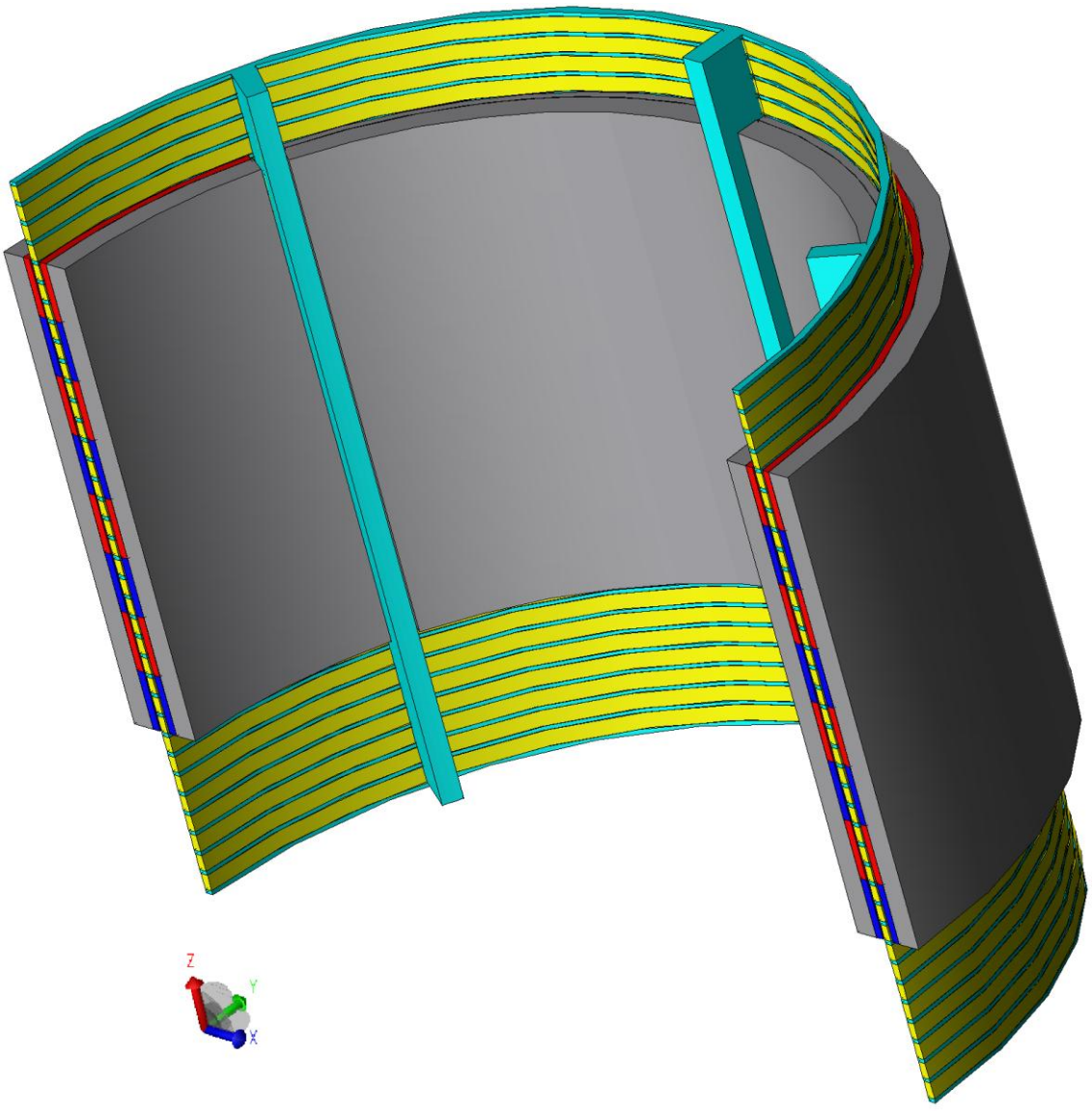

Figure B1 Three dimensional view of the air-cored generator in Chapter 5

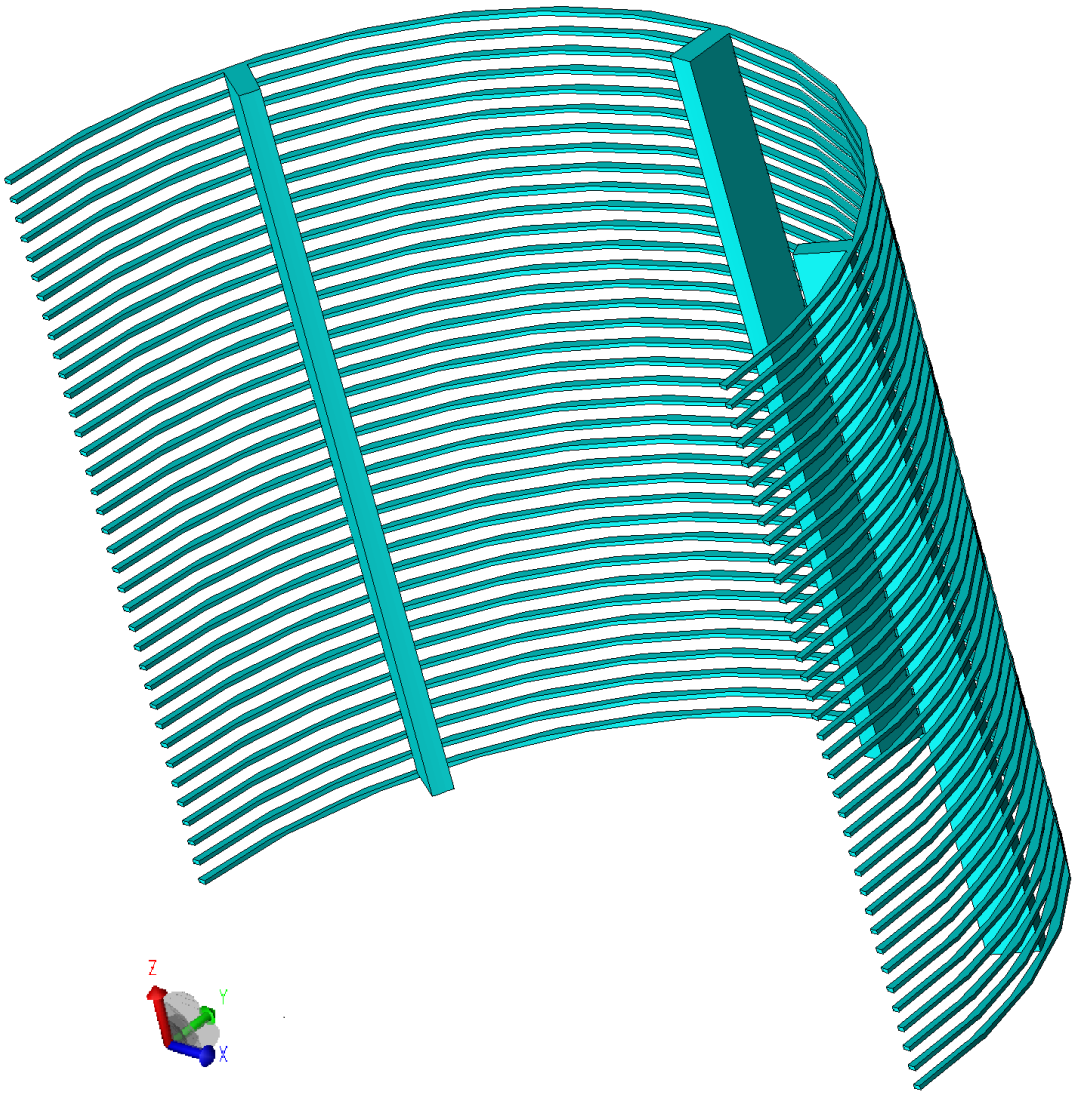

Figure B2 Three dimensional view of the separation cage of the air-cored generator in Chapter 5

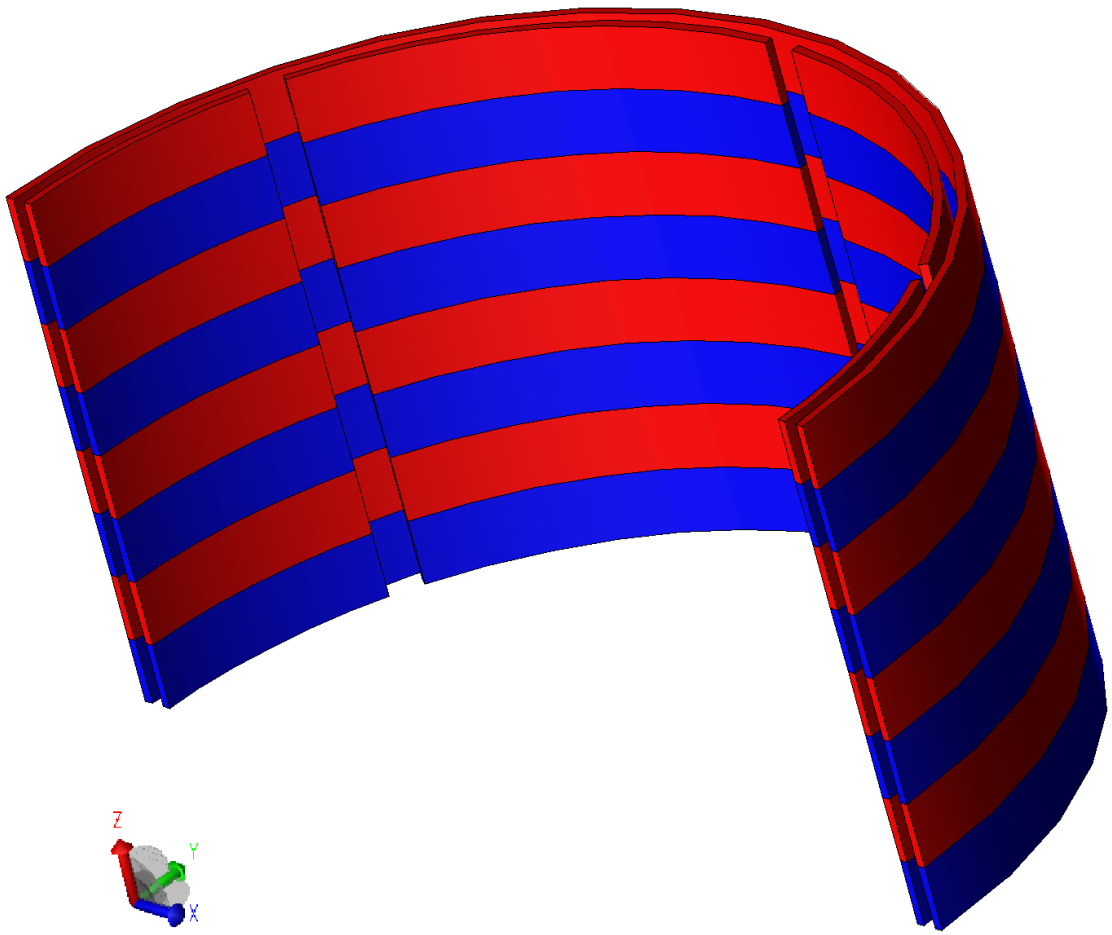

Figure B3 Three dimensional view of the permanent magnets of the air-cored generator in Chapter 5

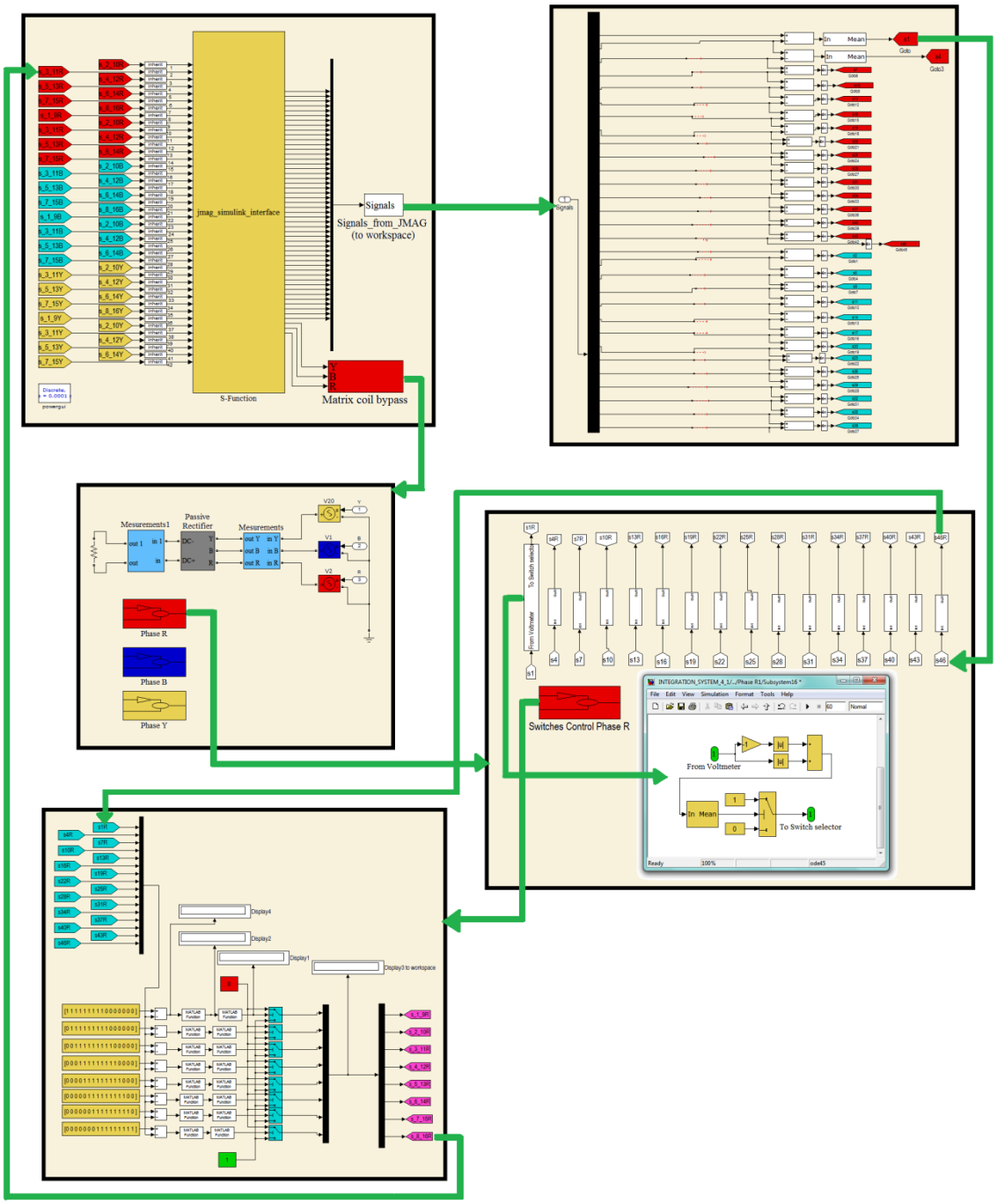

Figure B4 Overall single-phase graphical presentation of the control scheme

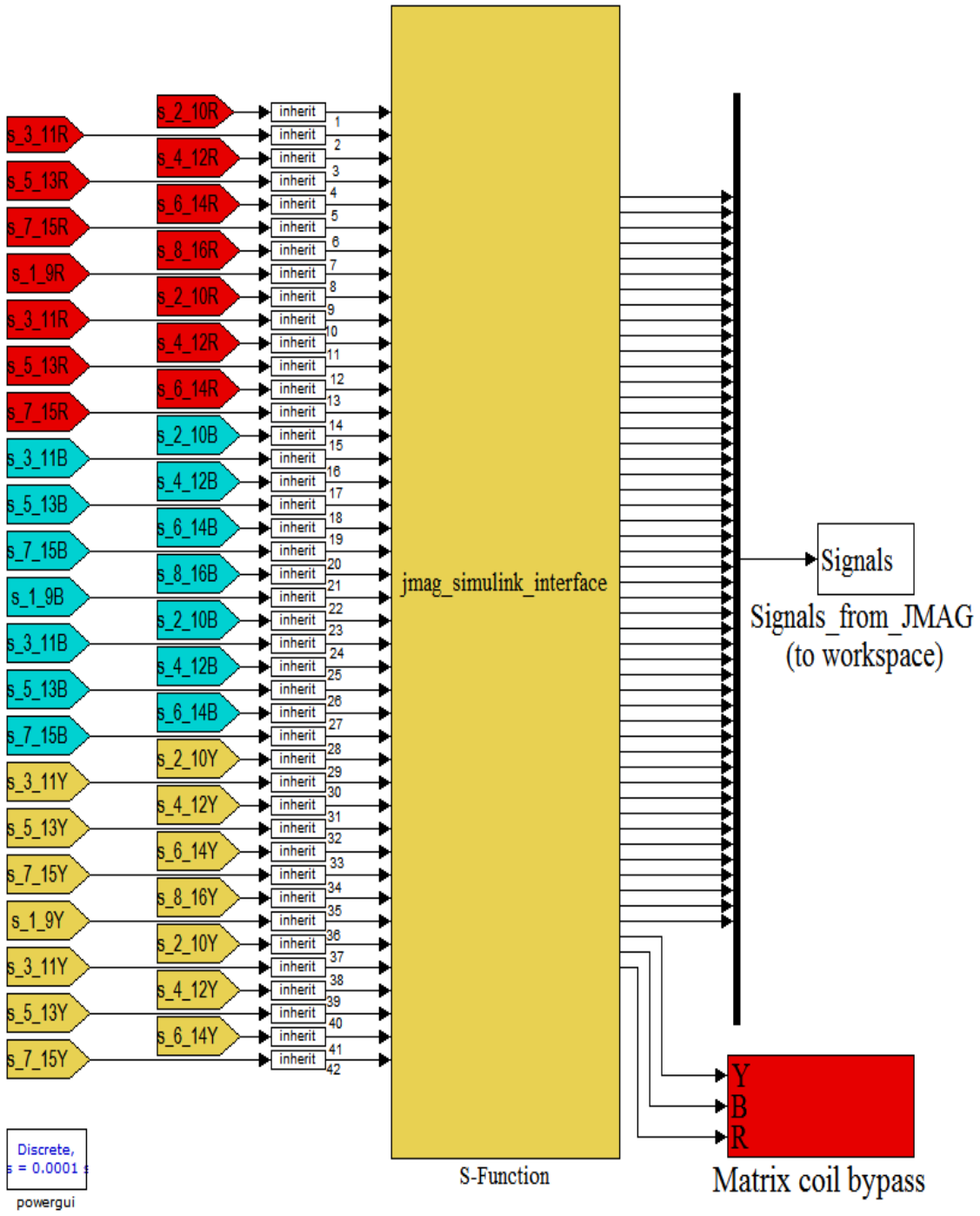

Figure B5 JMAG – Simulink Interface in Simulink

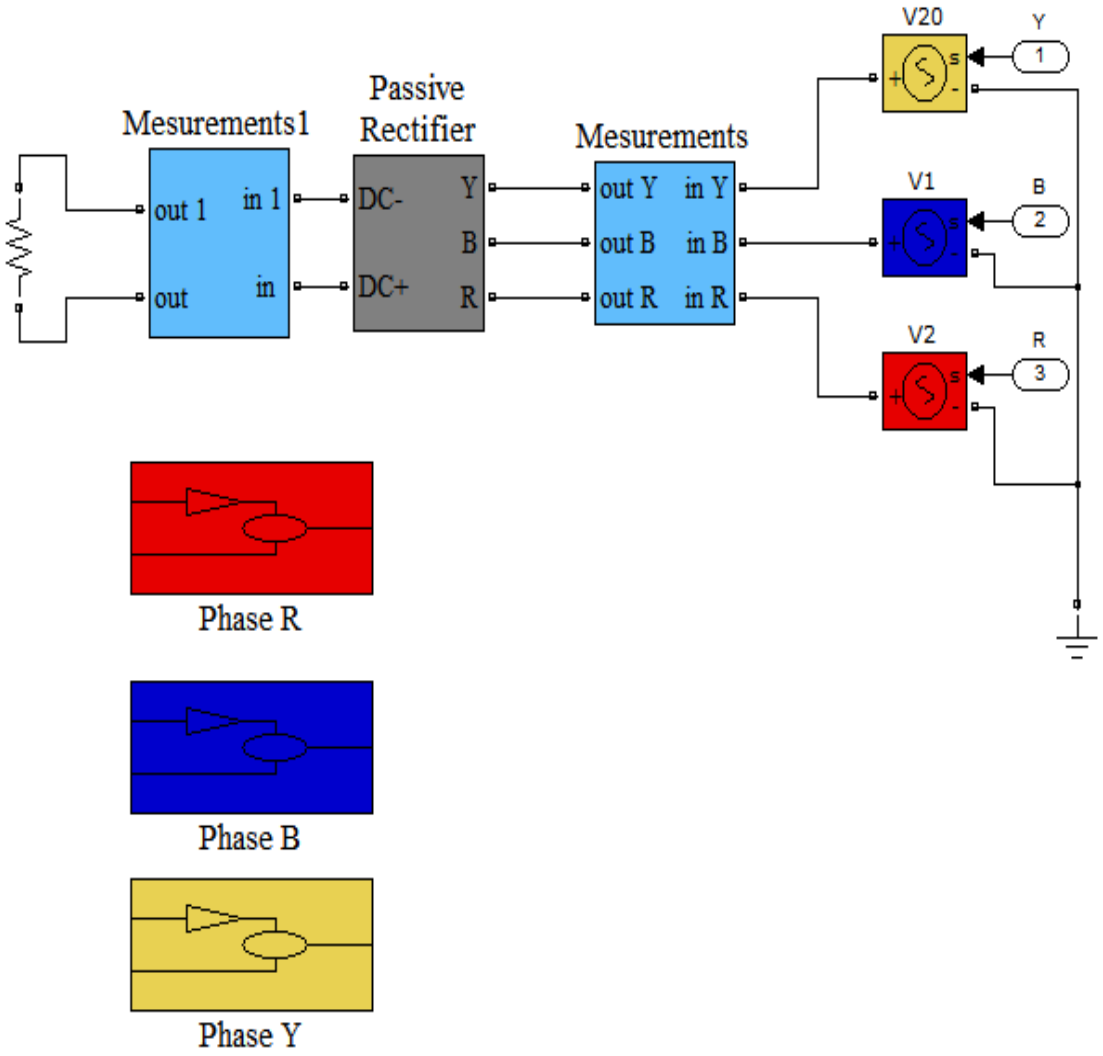

Figure B6 Power circuit under “Matrix coil bypass”, 5 ohm resistor is used and load after passive rectification

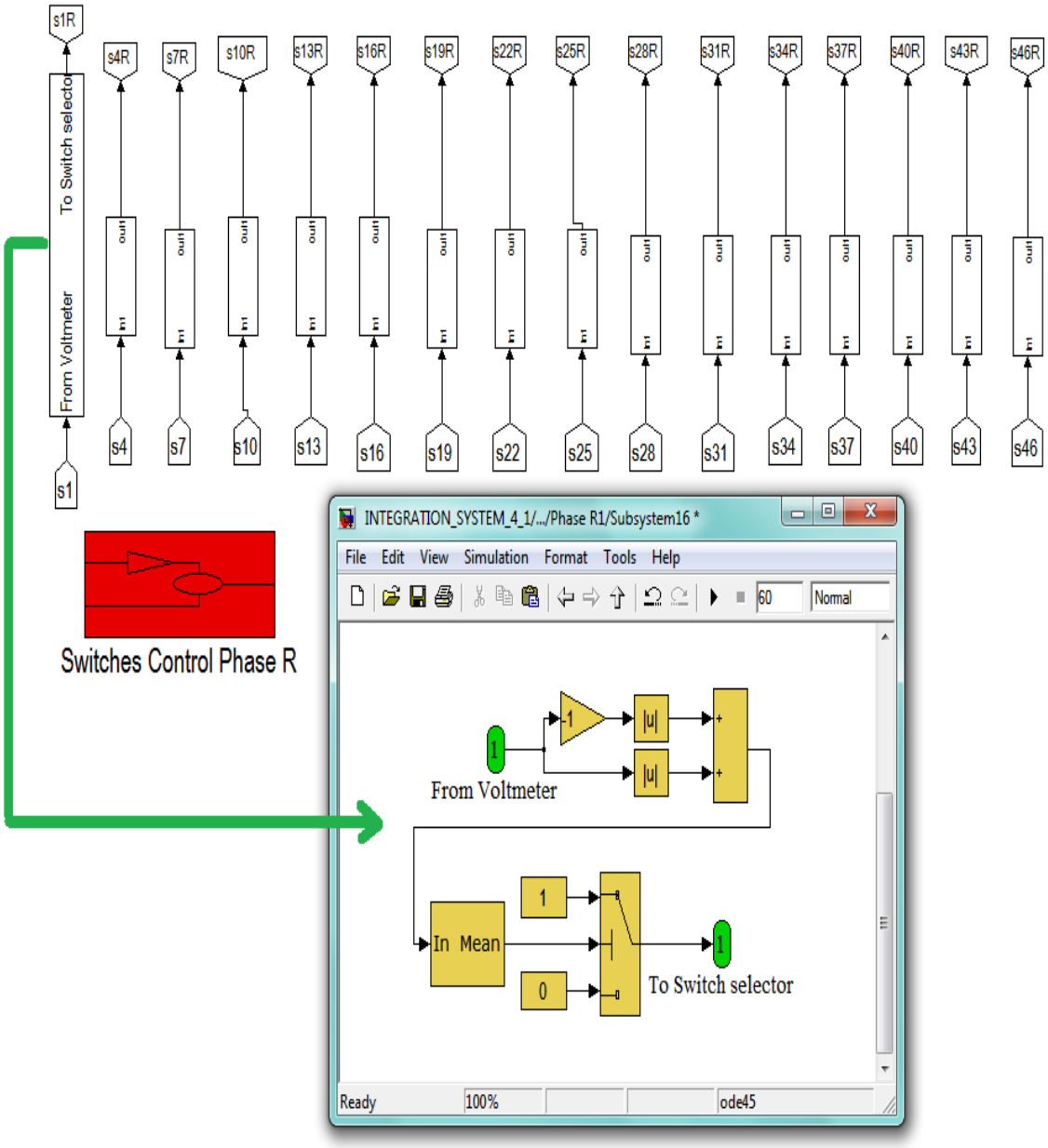

Figure B7 Control circuit under “Phase R”

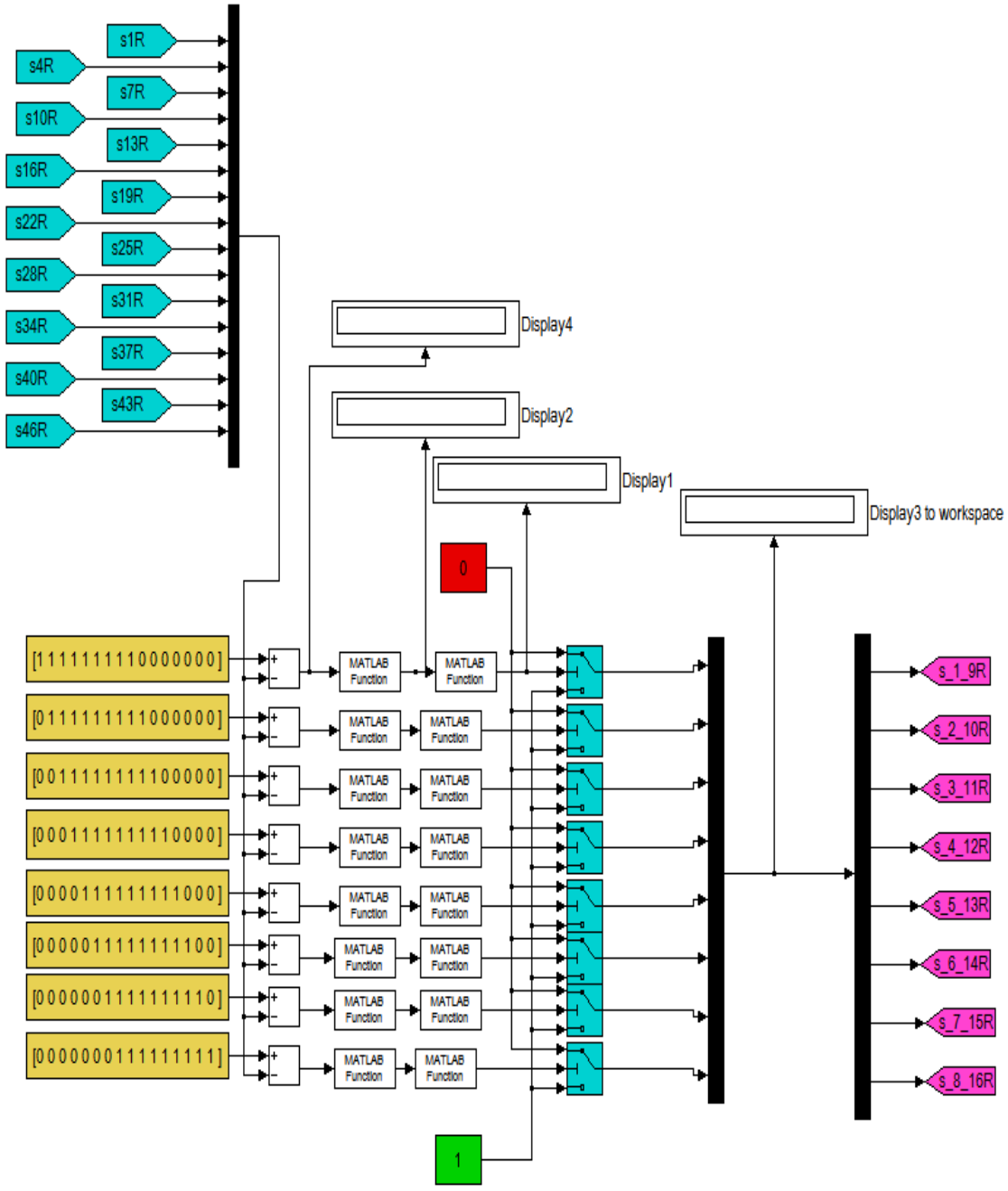

Figure B8 Control circuit under “Switches Control Phase R”

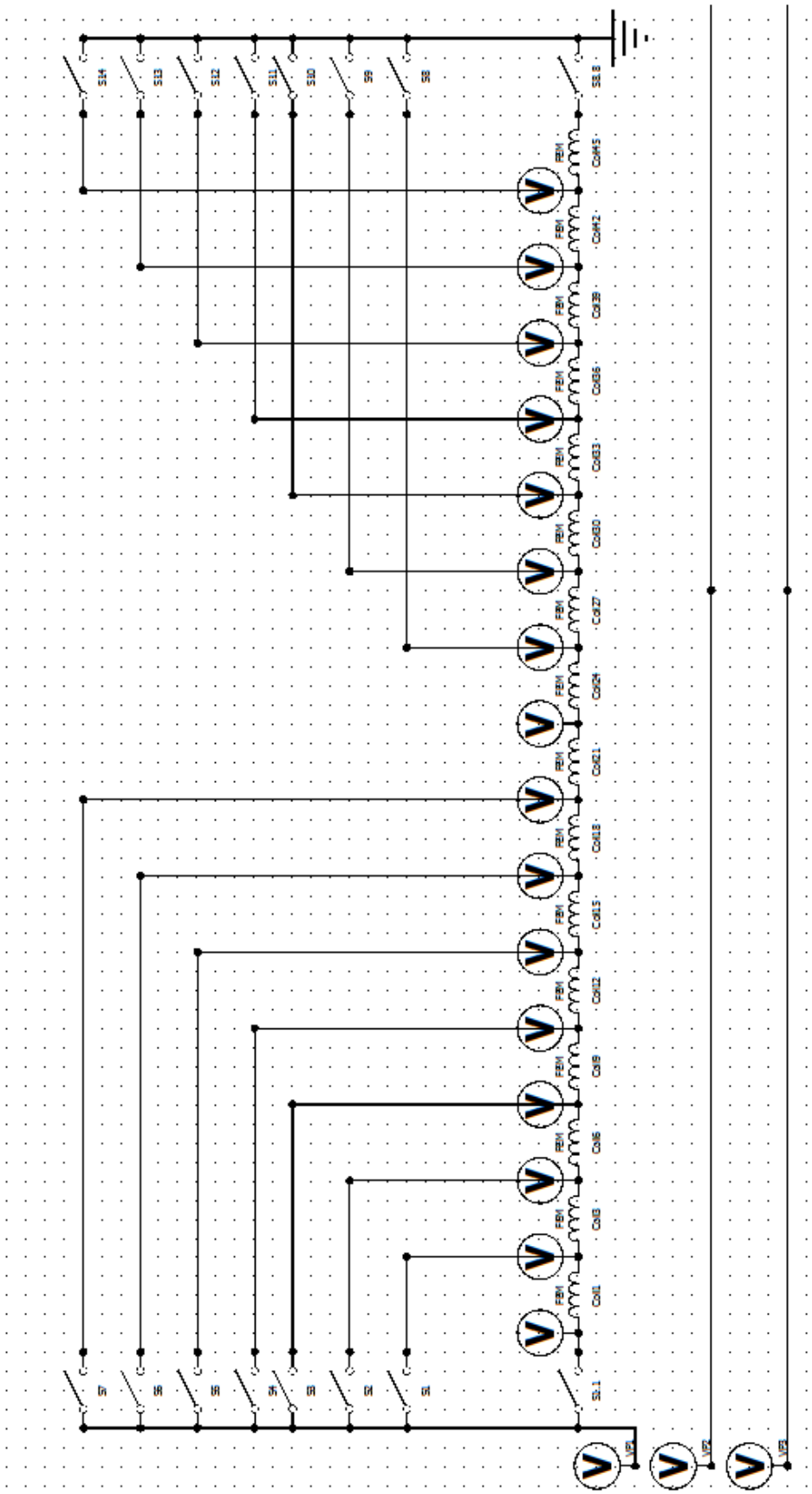

Figure B9 Coils and Switches arrangement in JMAG (for single phase)

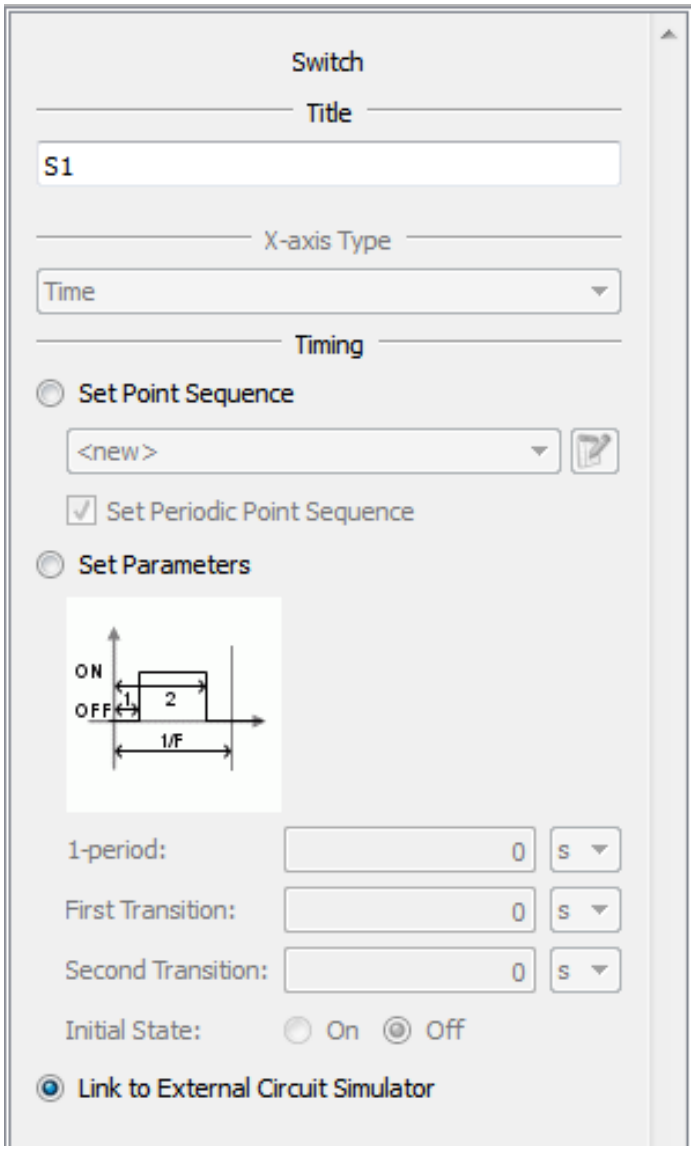

Figure B10 Switches in JMAG are controlled by External Circuit Simulator (Matlab/Simulink)

Appendix C

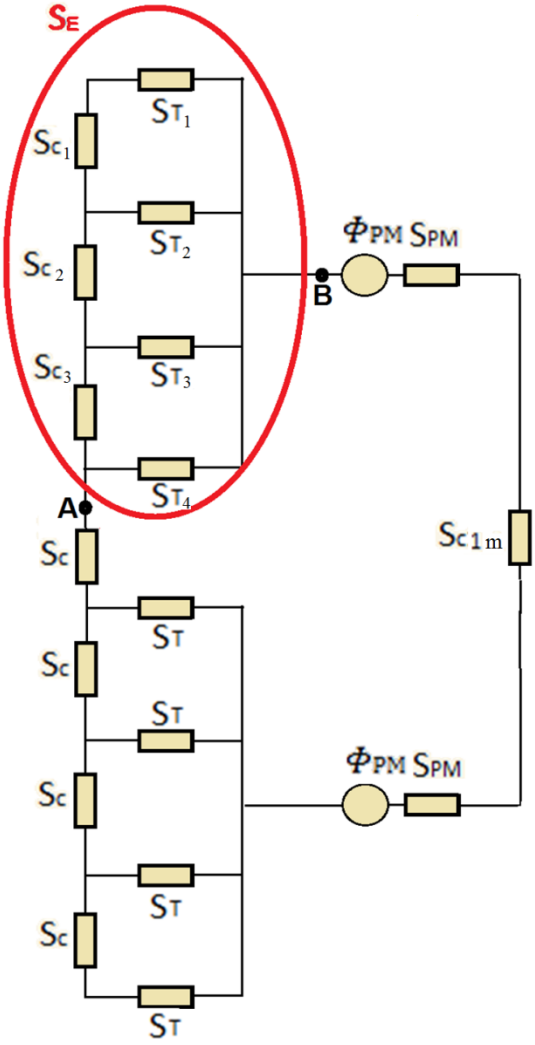

Figure C1 Magnetic circuit for single-sided PMLG. S_E is the equivalent magnetic reluctance between points A and B and S_{Total} is the total magnetic reluctance of the circuit

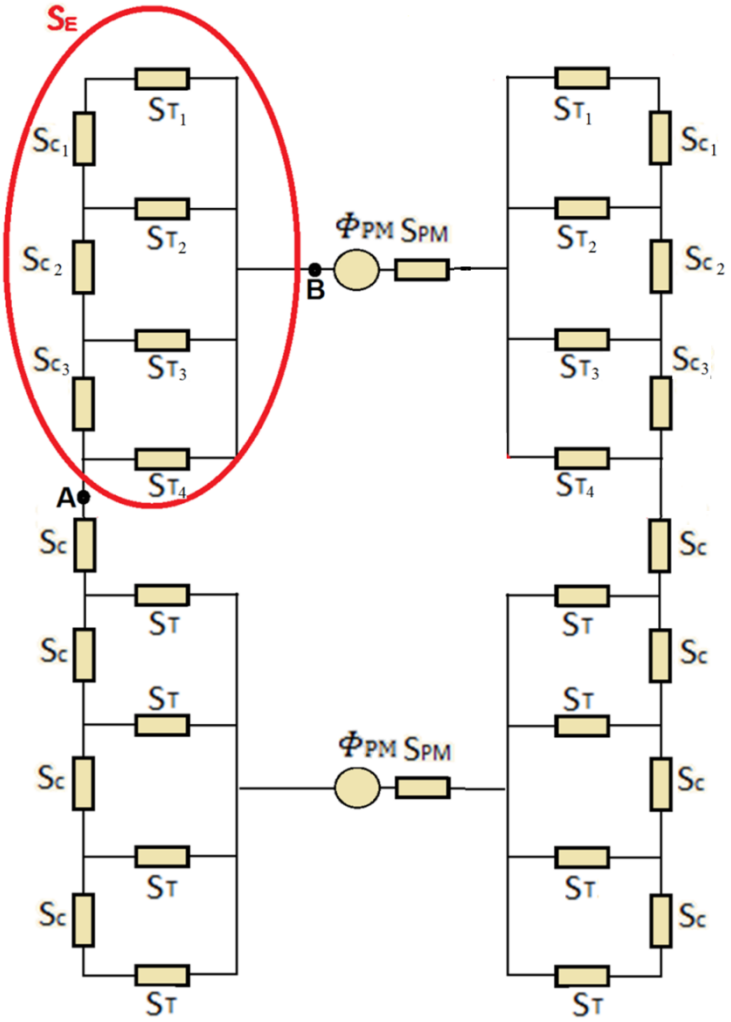

Figure C2 Magnetic circuit for double-sided PMLG. S_E is the equvalent magnetic reluctance between points A and B and S_{Total} is the total magnetic reluctance of the circuit

Single-/Double-sided PMLG:

S_{Total} can be evaluated by the following formulation where initally S_E is evaluated. In the formulation, the symbol “A‖B” means a parallel equivalent of reluctances A and B. Furthermore, “A--B” is the series

equivalent of the two reluctances. Calculating the equivalent of S_E starts from the top two reluctances in Figure C1 (Formulas C.1 to C.8).

$$S_{T1C1} = S_{T1} -\!- S_{C1} = S_T + S_C \tag{C.1}$$

$$S_{(T1C1)\|T2} = S_{T1C1} \| S_{T2} = \frac{(S_{T1} + S_{C1}) + S_T}{2S_T + S_C} \tag{C.2}$$

$$S_{((T1C1)\|T2)C2} = S_{(T1C1)\|T2} -\!- S_{C2} =$$

$$= \frac{(S_T)^2 + S_C S_T}{2S_T + S_C} + S_C \tag{C.3}$$

$$S_{(((T1C1)\|T2)C2)\|T3} = S_{((T1C1)\|T2)C2} \| S_{T3} =$$

$$= \frac{\frac{(S_T)^2 + S_C S_T + (S_C)^2 + 2S_C S_T}{2S_T + S_C} S_T}{{S_T}^2} = \tag{C.4}$$

$$= \frac{{S_T}^3 + {S_T}^2 S_C + {S_C}^2 S_T + 2{S_T}^2 S_C}{3{S_T}^2 + {S_C}^2 + 4S_T S_C} \tag{C.5}$$

$$S_{((((T1C1)\|T2)C2)\|T3)C3} = S_{(((T1C1)\|T2)C2)\|T3} -\!- S_{C3} =$$

$$= \frac{{S_T}^3 + {S_T}^2 S_C + {S_C}^2 S_T + 2{S_T}^2 S_C}{3{S_T}^2 + {S_C}^2 + 4S_T S_C} + S_C =$$

$$= \frac{{S_T}^3 + {S_C}^3 + 6{S_T}^2 S_C + 5{S_C}^2 S_T}{3{S_T}^2 + {S_C}^2 + 4S_T S_C} \tag{C.6}$$

$$S_{((((((T1C1)\|T2)C2)\|T3)C3)T4} = S_{(((((T1C1)\|T2)C2)\|T3)C3} \| S_{T4} =$$

$$= \frac{\frac{({S_T}^3 + {S_C}^3 + 6{S_T}^2 S_C + 5{S_C}^2 S_T) S_T}{3{S_T}^2 + {S_C}^2 + 4S_T S_C}}{\frac{{S_T}^3 + {S_C}^3 + 6{S_T}^2 S_C + 5{S_C}^2 S_T + 3{S_T}^3 + {S_C}^2 S_T + 4{S_T}^2 S_C}{3{S_T}^2 + {S_C}^2 + 4S_T S_C}} =$$

$$= \frac{\frac{{S_T}^4 + {S_C}^3 S_T + 6{S_T}^3 S_C + 5{S_C}^2 {S_T}^2}{3{S_T}^2 + {S_C}^2 + 4S_T S_C}}{\frac{4{S_T}^3 + {S_C}^3 + 10{S_T}^2 S_C + 6{S_C}^2 S_T}{3{S_T}^2 + {S_C}^2 + 4S_T S_C}} =$$

$$= \frac{{S_T}^4 + {S_C}^3 S_T + 6{S_T}^3 S_C + 5{S_C}^2 {S_T}^2}{4{S_T}^2 + {S_C}^3 + 10{S_T}^2 S_C + 6{S_C}^2 S_T} = S_E \quad \text{(C.7)}$$

$$S_{Total} = 2S_E + 2S_{PM} + S_{C1m} + S_C \quad \text{(C.8)}$$

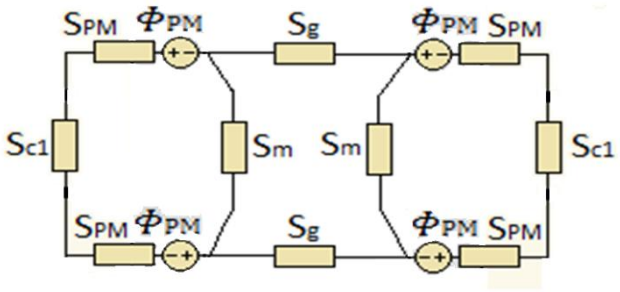

Figure C3 S_{TT} is the equivalent magnetic circuit reluctance with length equal to the length of two permanent magnets for the air-cored LS-PMLG

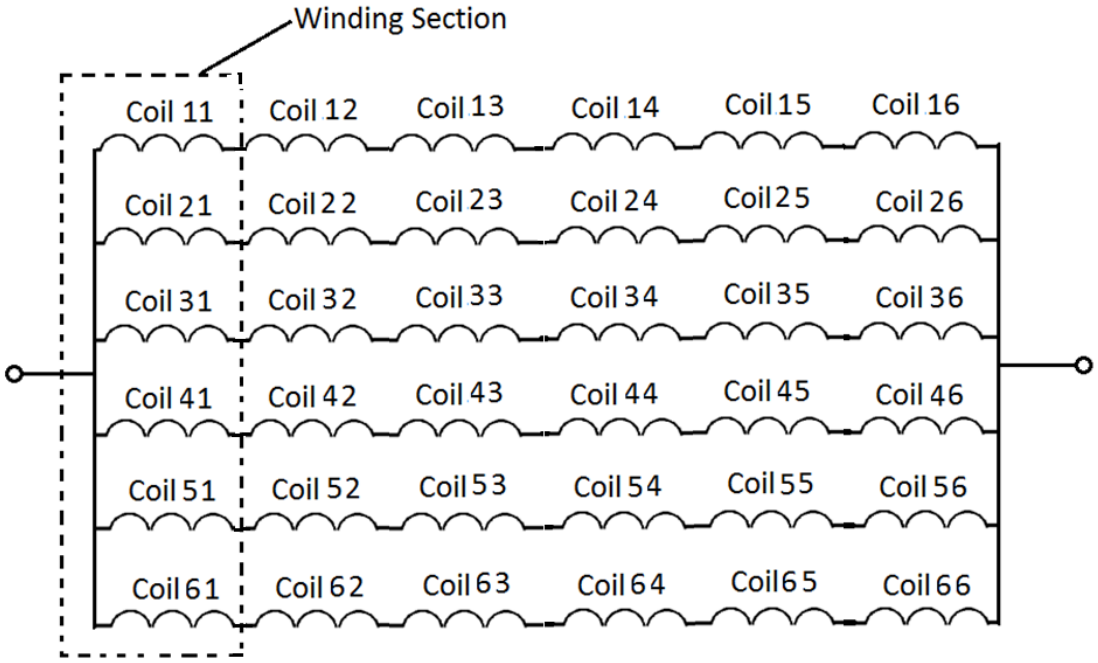

Figure C4 Single winding connection of the PMLG

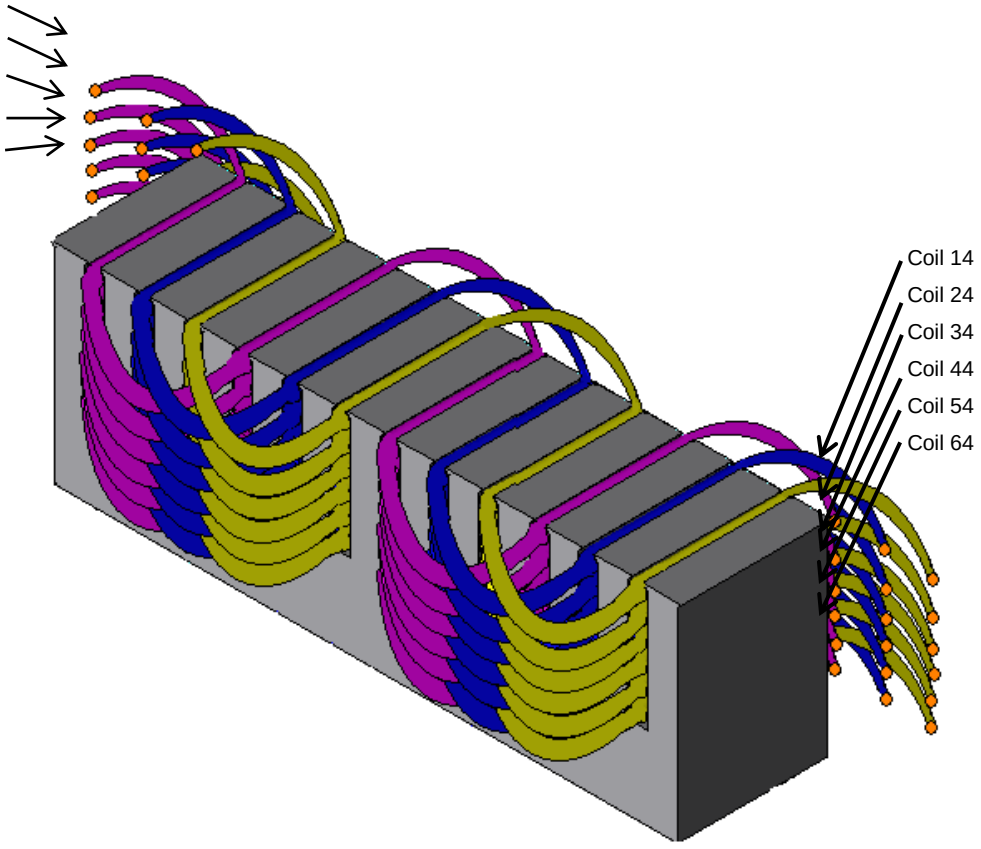

Figure C5 Winding configuration for model having 4 winding sections

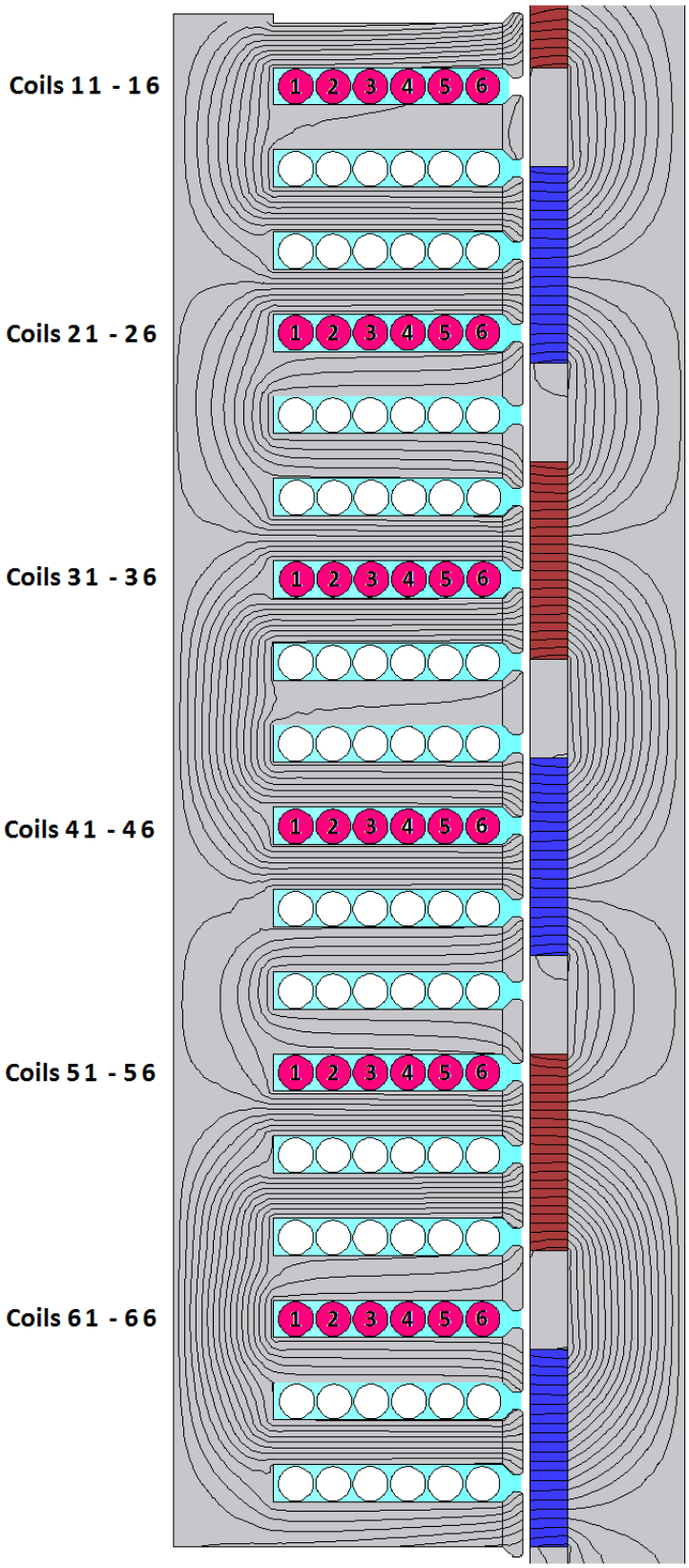

Figure C6 Winding arrangement of the PMLG

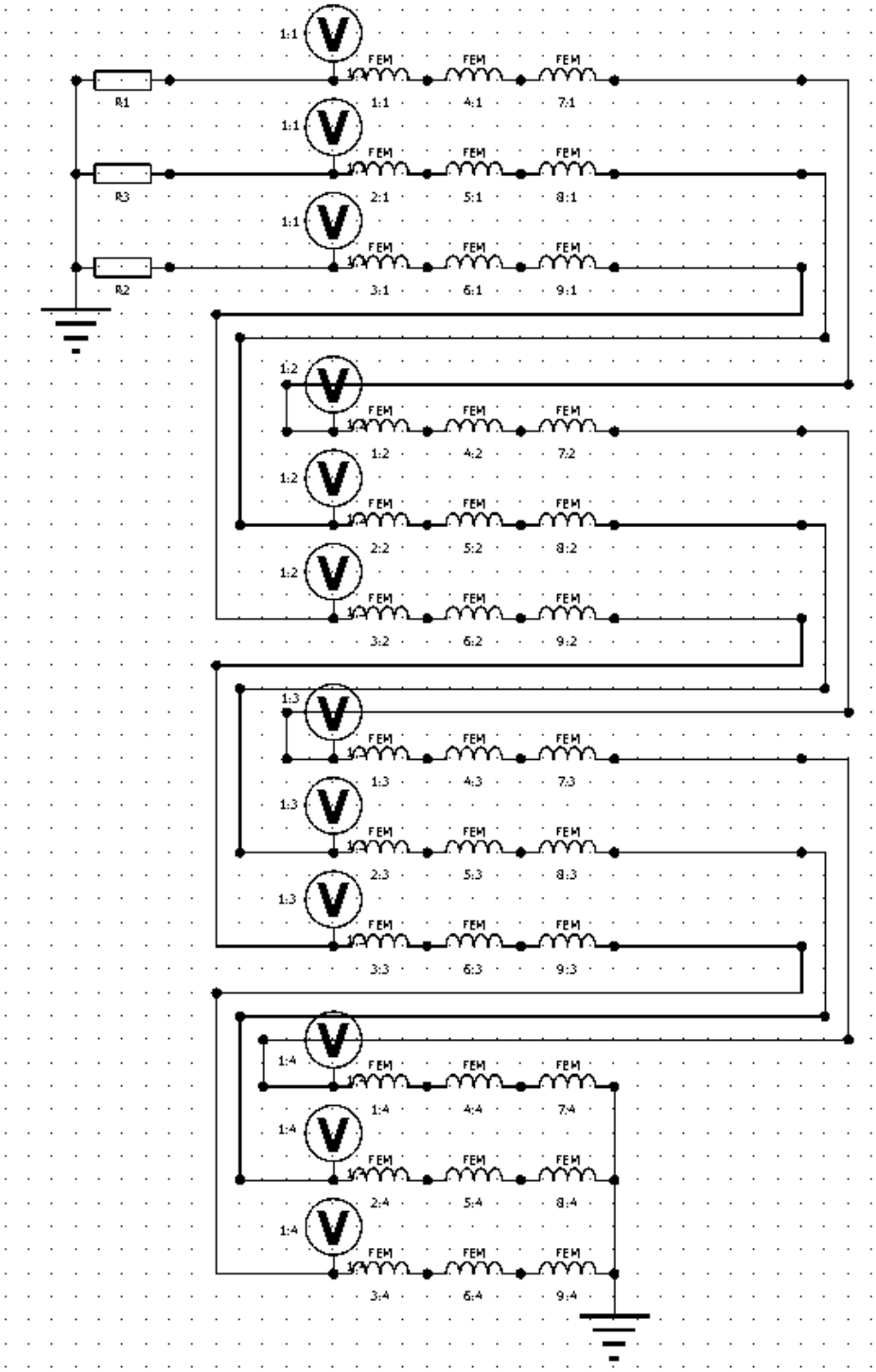

Figure C7 Winding and load circuit for the optimised double sided (2x3)

PMLG

Appendix D

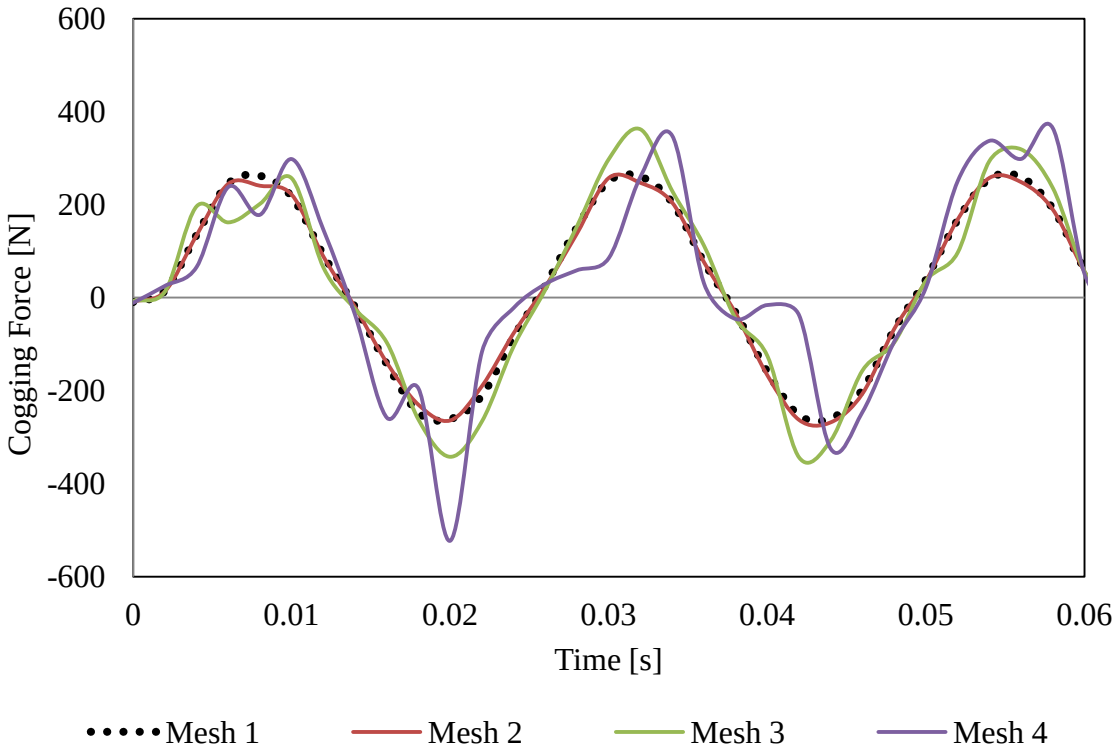

Figure D1 Effect on generated voltage caused by different size of the mesh at maximum velocity of the translator

Table D1

	Mesh 1	Mesh 2	Mesh 3	Mesh 4
Number of elements	1 000 000	500 000	140 000	70 000

In this thesis, the mesh size is different for every PMLG model and it has been selected based on the accuracy of the results of the cogging force. Figure D1 and Table D1 give the difference in the cogging force caused by different mesh sizes. The reason for comparing the cogging force is that it has high frequency (higher than the voltage and the current). In Figure D1, it can be seen that meshes with a low number of elements deliver distorted force. By increasing the number of elements, the deviations in the force results decrease.

Furthermore, it can be seen that the difference between the number of elements in Mesh 1 and Mesh 2 is double, but that the difference in the force curve is very small.

Throughout this thesis, the method for choosing the correct mesh is based on the above results for every model. Initially, meshes with a low number of elements are simulated and the number of elements has been increased until the error (for the cogging forces) caused by the mesh size reduces below 5% in comparison with a model with a mesh that has 50% fewer elements.

Appendix E

Contribution Made by Papers

Journal Papers:

N. P. Gargov, A. F. Zobaa; "Multi-phase air-cored tubular permanent magnet linear generator for wave energy converters," *Renewable Power Generation, IET* , vol.6, no.3, pp.171-176, May 2012

N. P. Gargov, A. F. Zobaa, I. Pisica, “Investigation in Multiphase Tubular Permanent Magnet Linear Generator for Wave Energy Converters”, Electric Power Components & Systems, Vol. 42, Iss. 2, Jan. 2014.

N. P. Gargov, A. F. Zobaa, I. Pisica, “Separated Magnet Yoke Design of Permanent Magnet Linear Generator for Wave Energy Converters”, Electric Power Systems Research, Elsevier, Volume 109, Pages 63-70, April 2014

Conference Papers:

N. Gargov, A. F. Zobaa, "Multiphase Tubular Permanent Magnet Linear Generator for Wave Energy Converters", IET Conference on Renewable Power Generation, RPG 2011, pp.1-5, 6-8 Sept. 2011

N. Gargov, A. F. Zobaa, G. Taylor “Structures and Forces in Direct Driven Linear Generators for Marine Wave Power Generation” *Proceedings of 2012 47th International Universities' Power Engineering Conference (UPEC),* Sept. 2012

N. Gargov, A. F. Zobaa, G. Taylor “Technologies for Direct Drive Linear Machines for Marine Wave Power Generation” *Proceedings of 2012 47th International Universities' Power Engineering Conference (UPEC),* Sept. 2012

Appendix F

Statement of the Candidate`s Contribution to Co-author Papers

The PhD candidate has the main contribution to all the papers listed in Appendix E

Appendix G

Electric Power Systems Research 109 (2014) 63–70

Contents lists available at ScienceDirect

Electric Power Systems Research

journal homepage: www.elsevier.com/locate/epsr

Separated magnet yoke for permanent magnet linear generator for marine wave energy converters

N.P. Gargov[a,*], A.F. Zobaa[b], I. Pisica[b]

[a] University of Exeter, Exeter, UK
[b] Brunel University, London, UK

ARTICLE INFO

Article history:
Received 2 January 2013
Received in revised form
22 September 2013
Accepted 24 November 2013

Keywords:
Cogging forces
Finite element method
Permanent magnet linear generator
Wave energy
Converter

ABSTRACT

In this paper the performance of a longitudinal flux permanent magnet linear generator (PMLG) for wave energy converters (WEC) is investigated. The influence of the number of slots per pole, phase q and the number of stator's winding sections are analysed. The power output and the cogging forces in the PMLG are calculated and reviewed with respect to the above design parameters. In addition, an optimised PMLG model is designed and simulated. Three-dimensional Finite Element Method (FEM) is used for solving the combined field and circuit equations of the generator.

1. Introduction

UE to the nature of marine waves, the take-off device for WECs usually operates between 0 and 2 m/s. Currently, some of the deployed WECs are designed to work with fast-speed rotational generators. In such systems, the relatively low-speed linear translation of the take-off device has to be converted to a high-speed rotational motion via an interface system. By integrating such system, the overall complexity of the WEC is increasing, whereas the efficiency and the robustness are reduced. A possible solution for overcoming such problems is a wave energy converter with a direct drive linear generator [1–4]. The linear generators are proposed for WECs to simplify the overall structure. The main problems with the linear generators are the high magnetic forces appearing between stator and translator during normal operation. These forces could reduce the lifetime of the bearings and therefore, increase the maintenance costs of the WEC. Hence, reduction of the magnetic forces in the linear generator may have significant effect on the maintenance cost.

Direct drive PMLGs have been proposed for WECs and several design solutions have been outlined in [4–12]. In [4] flat air-cored design has been suggested. The design has the advantage of eliminating the cogging force due to absence of stainless steel in the stator however, in order to generate sufficient magnetic field in the large air gap, an extra Permanent Magnets (PMs) are needed which on the other hand could increase the price of the machine.

A switched reluctance PMLG has been presented in [9]. The machine has iron-cored magnetic yokes and therefore, low magnetic reluctance path is provided however, high level of latching (cogging) forces can be expected due to the alignment of the stator and the translator. Another PMLG with excitation provided by a super conducting DC coil has been proposed in [13]. This kind of generator generally advantages from the possibility of control excitation applied on the excitation winding. On the other hand, heavy saturation in the magnetic core has been reported.

Furthermore, observations on the cogging forces [14,15] and the generated voltage harmonics [16] have also been performed on similar structure as structure presented in this paper. Additionally, constant speeds or speeds having sinusoidal shapes are common approximations for simulating PMLGs [14,16–19].

In this paper, a design for a flat longitudinal PMLG for marine wave energy is analysed. The influence of parameters, such as: the number of slots per pole, phase q, and the number of stator's winding sections are analysed with respect to the cogging forces and the output power of the PMLG. Based on the obtain results, an optimal model is proposed. The aims of the optimisation are reduction of the magnetic attraction forces between stator and translator and also increase of the electrical power output of the PMLG. By reducing the magnetic attraction force, the maintenance cost of the WEC can be reduced. Likewise, increasing the power output of the generator will reduce the pay-back time of the WEC.

FEM is used as a simulation tool because of its high accuracy. Moreover, the simulations are performed using three-dimensional

* Corresponding author.
E-mail address: ng258@exeter.ac.uk (N.P. Gargov).

0378-7796/$ – see front matter © 2013 Elsevier B.V. All rights reserved.
http://dx.doi.org/10.1016/j.epsr.2013.11.021

FEM with a time-varying electromagnetic field taking into consideration the non-linearity of the magnetic cores and the longitudinal ends of the machine. Furthermore, in the simulations full size generator models taking into account the magnetic flux distribution in the air gap and the regions at the longitudinal ends are simulated. Additionally, in order to simulate real sea conditions, an experimentally recorded vertical wave displacement is applied to the generator's translator for a period of 20 s.

The paper is organised as follows: after the introduction, a description of WEC is outlined. Then a theoretical explanation of the nodal force method used in the FEM is given. After that, a description of the investigated PMLG is given. In the next section, the results from the investigation are displayed and an optimal model is designed, before conclusions are presented.

2. Wave energy converter and forces calculations

Wave energy converter is a general title for devices that convert the kinetic energy of marine waves to electricity. The investigated PMLG in this paper is designed to be driven by a floater on the water surface, or installed in an Archimedes wave swing [20].

Generally, two types of construction employing either a non-flexible shaft [21] or a rope [22,23] have been proposed for WECs having direct drive electrical generators. The design using a non-flexible shaft is simpler, but it has only one degree of freedom and the energy absorption is limited up to 50% [24]. Furthermore, the forces normal to the motion axis are likely to be higher when using the non-flexible shaft design due to the restriction of the motion of the translator.

Conversely, an advantage of the design using a rope is that the flexibility of the rope provides additional degrees of freedom and hence, the energy absorption can be increased. Another difference in design is given by the springs, which have to be installed in order to pull the translator back to its lowest point.

Owing to the direct coupling of the take-off device and the generator, the generated voltage and the electrical frequency are in direct ratio with the translator's speed [25]. As a result, big fluctuations in the output voltage and the electrical frequency are observed during normal operation of the PMLG. In order to stabilise the fluctuation, a power-electronics converter and energy storage can be installed between the generator and the grid [26].

The calculation of the cogging forces is interesting from many perspectives. It is an important parameter for studying: the generator bearing system, the mechanical stress, and fatigue in the supporting structure. Additionally, the cogging forces are source of sound emission.

In this paper, the forces are calculated by FEA using 3D models with high mesh resolution. To increase the result accuracy the resolutions of the models have been set to around 1 million mesh nodes. The FEA software uses the nodal force method [27] as a tool for magnetic forces calculation. The nodal force method is derived from the Maxwell stress tensor and the method is proven to be as accurate as the virtual work method [27,28].The surface forces and the magnetic volume can be derived from the Maxwell stress tensor as follows:

$$f_i^{\Omega} = \partial_k T_{ik} \tag{1}$$

$$f_i^{\Gamma} = (T_{ik}|_2 - T_{ik}|_1) n_k \tag{2}$$

- n_k is the outward unit normal vector in region one and Maxwell stress tensor
- T_{ik} is given as:

$$T_{ik} = H_i B_k - \delta_{ik} w_m \tag{3}$$

- $\delta_{ik} = \begin{cases} 1 & i = k \\ 0 & i \neq k \end{cases}$ is the Kronecker's delta
- w_m is the magnetic co-energy density of the element:

$$w_m = \int_0^H B \cdot dH. \tag{4}$$

For virtual displacement δl_i the virtual work done by magnetic volume and surface force is:

$$\begin{aligned} \delta W &= \int f_i^{\Omega} \delta l_i \; d\nu + \int f_i^{\Gamma} \delta l_i \; d\Gamma \\ &= \int (\partial_i T_{ik}) \delta l_i \; d\nu + \int (T_{ik}|_2 - T_{ik}|_1) n_k \delta l_i \; d\Gamma \, . \\ &= - \int T_{ik} \partial_k \left(\delta l_i \right) \; d\nu \end{aligned} \tag{5}$$

The displacement is interpolated via the nodal shape function:

$$\delta l_i = \sum_n N_n \delta_{ni} \tag{6}$$

- N_n is the nodal shape function of the nth node. Using (5) and (6) the virtual work can be also expressed as:

$$\begin{aligned} \delta W &= - \int T_{ik} \partial_k \left(\sum_n N_n \delta l_{ni} \right) \; d\nu \\ &= - \sum_n \left(\int T_{ik} \partial_k N_n d\nu \right) \delta l_{ni} \end{aligned} \tag{7}$$

So the force acting on the nth node is given as:

$$f_{ni} = - \int_{\Omega} T_{ik} \partial_k N_n \; d\nu \tag{8}$$

Using summation for all the nodes in the part, the total force can be written as:

$$[f_n] = \begin{bmatrix} f_{nx} \\ f_{ny} \\ f_{nz} \end{bmatrix} = - \int_{\Omega} \begin{bmatrix} T_{xx} & T_{xy} & T_{xz} \\ T_{yx} & T_{yy} & T_{yz} \\ T_{zx} & T_{zy} & T_{zz} \end{bmatrix} \begin{bmatrix} \frac{\partial}{\partial x} \\ \frac{\partial}{\partial y} \\ \frac{\partial}{\partial z} \end{bmatrix} N_n \; d\nu \tag{9}$$

3. Description of the PMLG and the simulations

In this paper, it is assumed that the generator's translator is assembled from the permanent magnets and the separators. Likewise, the stator is assembled from two aligned magnetic cores on both sides of the translator with copper coils placed in slots (Fig. 1).

It is assumed that the PMLG's stator is assembled from the permanent magnets, the separators, and the upper magnetic core. The separators are made from non-magnetic and non-electrical conducting material and they are required in order to maintain the position of the permanent magnets against axial displacement. In addition, the PMLG's translator is assembled from the lower magnetic core and the windings.

The magnetic cores of the machine are formed by laminated silicon steel with a 95% stacking factor and they are treated as magnetically nonlinear material with single value magnetisation characteristics.

The translator teeth are finished with shoes to optimise the flux distribution. Generally, the implementation of shoes decreases both the power ripple and the magnetic reluctance of the air gap. In addition, reduction of the cogging forces in linear machines can

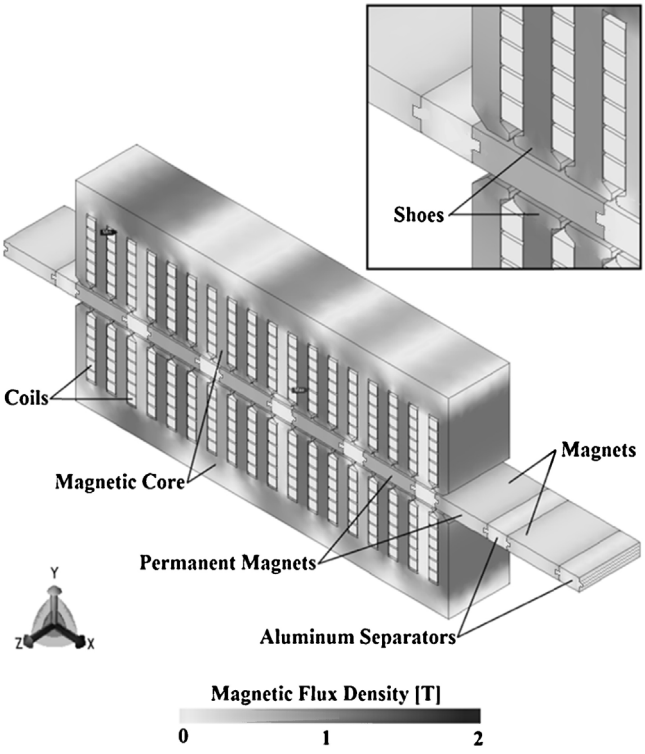

(a) Overview of the base model of the PMLG

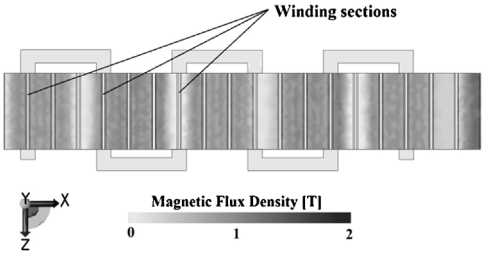

(b) Single phase distribution in the lower magnetic core, the translator and upper magnetic core are not displayed

Fig. 1. PMLG with six winding sections.

be also achieved [16]. The windings' excitation flux is provided by neodymium–iron–boron magnets with magnetisation direction parallel to the *Y*-axis. Furthermore, in order to increase the accuracy of the simulation results, the PMLG has full translator models and therefore, the influence of the longitudinal ends can be taken into account. Moreover, a repetitive boundary condition is applied to the translator, which is a common approach for linear generator simulations [17].

The main dimensions of the generator are shown in Table 1. The generator has three-phase windings, where each winding consists of six winding sections connected in series. Furthermore, each winding section consists of six coils connected in parallel. Each winding is shifted by ±120° from the other two. Additionally, every winding has a total resistance of 0.9 Ω (base model). The single- and the double-sided generator designs are inspired by [29], although the parameters have been scaled down (where appropriate) to the sizes shown in Table 1.

Additionally, the motion applied on the translator is an experimentally recorded vertical speed/time sequence of stochastic sea

Table 1
Main dimensions of the double sided PMLG.

Dimensions		
Parameter	Axis	
Translator length [mm]	*X*	612
Translator width [mm]	*Z*	600
Winding length [mm]	*Y*	88
Translator height [mm]	*Y*	318
Permanent magnet length [mm]	*X*	85
Pole pitch length [mm]	*X*	118.8
Coil slot length [mm]	*X*	15
Translator teeth length [mm]	*Y*	18
Air gap length [mm]	*Y*	2 × 3
Electrical characteristics		
Number of turns per winding section		24
Number of turns per coil		4
Number of slot per pole and phase, *q*		1.2 (6/5)
Total Winding resistance [Ω]		1.8
Resistive three-phase star connected load [Ω]		5

conditions. The sequence was recorded by a wave probe over a period of 20 s near the coast of the UK. The main focus of this paper is an optimisation of PMLG. So, it is assumed that the translator strictly follows the motion of the water surface.

The number of slots per pole and phase *q* for the generator is 1.2 (6/5). This means that five poles have the same length as six three-phase translator slots (or eighteen single-phase slots). For convenience, the value of $q = 6/5$ can be also presented as 1.2. Thus, one pole covers 1.2 translator slots. By using such a presentation for q, it is possible to analyse values that differ from the standard ones shown in [16].

4. Analytical model of the PMLG

The magnetic circuit of the double-side PMLG is shown in Fig. 2, in which Φ_{PM} is the Magneto Motive Force (MMF) source of the permanent magnets and S_C and S_{C1m} are the reluctances in the magnetic core. Similarly, S_1 to S_{19} are the magnetic reluctances of the teeth of the translator, S_{a1} to S_{a19} are the magnetic reluctances in the air gap between the permanent magnet and every single tooth. They are identified by colour codes on the right-hand side of the figure. In this magnetic circuit, it is assumed that every magnetic pole (covered by the length of the translator teeth) is connected with the closest four translator teeth. At certain positions of the translator where the teeth (end shoes) are located between two magnetic poles, they are linked with both poles and linkage is given as two reluctances: S_{ai} and S_{ai^*} (i – tooth number). Furthermore, the values of S_{PM} are the magnetic reluctances of the permanent magnets and S_{air} represents the reluctance of the air between the magnets outside the translator. These reluctances (S_{air}) are constant and they do not affect the main magnetic circuit. The purpose of showing them is to present the magnetic circuit outside the length of the translator.

The magnetic poles located outside of the translator are connected with the final one or two translator teeth. If the permanent magnet (at the longitudinal end) is outside of the translator length, it is considered that the magnet is connected to the final tooth (S_{a1}). Alternatively, if the magnet covers the last tooth it is considered that the magnet is connected to the final two translator teeth (S_{18^*} and S_{19}).

The analytical modelling technique does not take into account the effects of the saturation of iron in the magnetic cores of the generator.

The voltages generated in the coils are dependent on the magnetic flux passing the teeth surrounding them (flux over S_T). The flux path in the translator, contributing to voltage generation

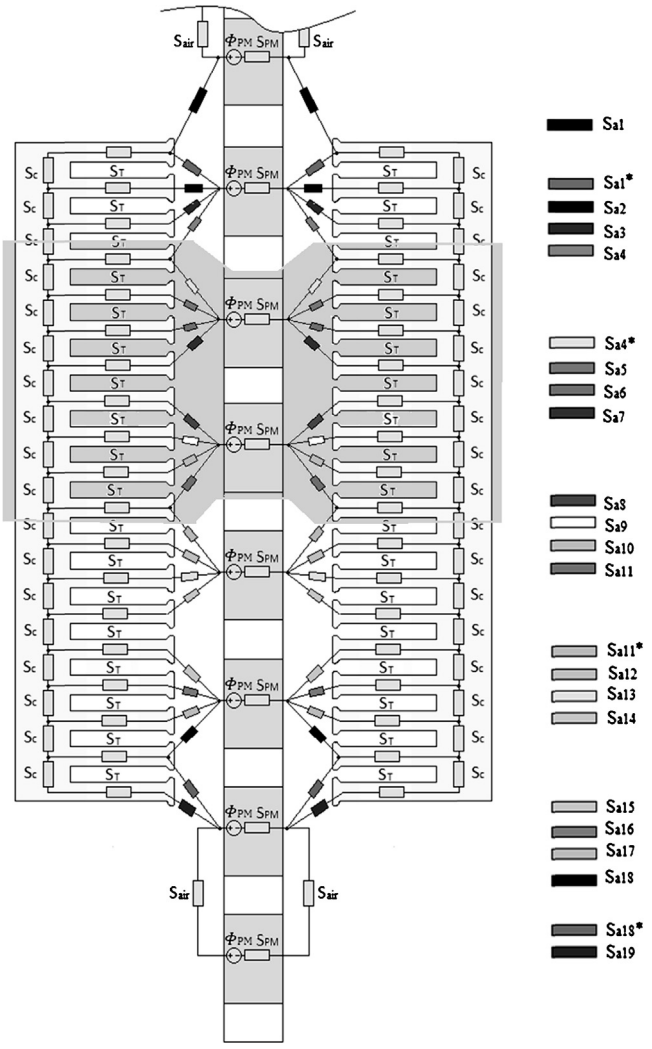

Fig. 2. Magnetic circuit of double sided PMLG.

(therefore, to energy harvesting) is through reluctances S_C–S_T–$S_{a(1-19)}$–Φ_{PM}–S_{PM}–S_{C1}–S_{PM}–Φ_{PM}–$S_{a(1-19)}$–S_T–S_C.

However, when a tooth is located between two poles such as the 4th, 11th and 18th teeth in Fig. 2, part of the flux goes through the tooth shoe, bypassing the tooth. For instance, in the case of the 4th tooth, part of the magnetic flux will follow the contour of S_{a4}–S_{a4^*}–Φ_{PM}–S_{PM}– S_{C1}–S_{PM}–Φ_{PM}–S_{a4}. Such leakage of flux is not beneficial to energy harvesting and can be considered a loss. A reduction of the flux can be achieved by altering the width of the shoes along the *X*-axis.

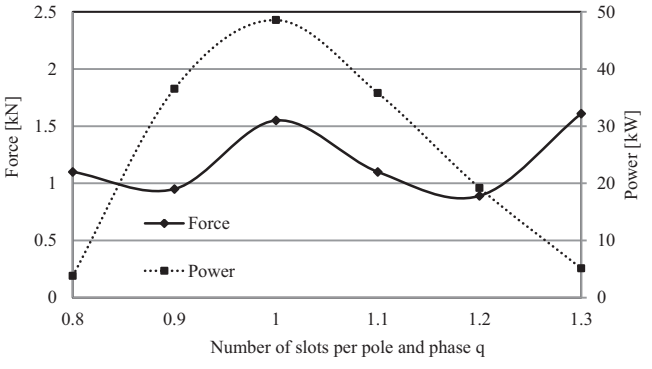

Fig. 3. *Y*-axis forces and RMS power for double-sided PMLG.

The total magnetic reluctance of a single-sided PMLG's section with a length of 8 teeth can be presented as:

$$S_{\text{Total}} = 4 \times S_E + 2 \times S_{\text{PM}} + 2 \times S_C \tag{10}$$

where S_{Total} is the total magnetic reluctance of the area indicated by shading in Fig. 2. Furthermore, where S_E is one-half of the reluctance of the translator, it can be calculated as follows:

$$S_E = \frac{{S_{Tt}}^4 + {S_C}^3 \times S_T + 6 \times {S_{Tt}}^3 \times S_C + 5 \times {S_C}^2 \times {S_{Tt}}^2}{4 \times {S_{Tt}}^3 + {S_C}^3 + 10 \times {S_{Tt}}^2 \times S_C + 6 \times {S_C}^2 \times S_{Tt}} \tag{11}$$

$$S_{Tt} = S_T + S_{a\,nn} \tag{12}$$

where *nn* is the number of the reluctances shown on the right-hand side (with code) in Fig. 2 and can be presented as:

$$S_{a\,nn} = \frac{l_{\text{gap}}}{\mu_0 \times A_r} \tag{13}$$

$$S_T = \frac{l_{\text{tooth}}}{\mu_c \times A_r} \tag{14}$$

$$S_c = \frac{l_{\text{core}}}{\mu_c \times A_r} \tag{15}$$

where l_{gap} is the length of the air gap between the centre of the permanent magnet and the centre of the shoes and l_{tooth} is the length of the coil's slots in the magnetic core. The permeability's of the air and the magnetic core are given by μ_0 and μ_c [H/m] respectively and A_r is the area of the pole face.

Using the equivalent reluctance the magnetic circuit can be presented as simple circuit with an MMF source connected to a single magnetic reluctance. Hopkinson's law is a counterpart to Ohm's law and can be used in magnetic circuits:

$$\Phi_{\text{PM}} = \psi_m \times S_E \tag{16}$$

$$\psi_m = \frac{\Phi_{PM}}{S_E} \tag{17}$$

where ψ_m is the total magnetic flux of the magnetic circuit (i.e., the flux passing S_{C1m}). Similarly, the magnetic flux density in the air gap can be presented as:

$$B = \frac{\psi_m}{A_r}. \tag{18}$$

The analytical calculations are performed using Matlab and the results for the flux density in the air gap show a difference of 5.5% in comparison with the FEA results for a static simulation.

5. Simulated FEA results

5.1. The effect of number of slots per pole and phase q on the PMLG performance

The forces affect the bearings and the supporting structure in different ways and therefore, minimising them is important with regard to maintenance costs and the structural integrity of the WEC.

The number of slots per pole and phase represents the distribution of the magnets with respect to the stator slots. It can be calculated by:

$$q = \frac{P_p}{3S_p} \tag{19}$$

- 3 is the number of phases,
- S_p is the single phase stator slots pitch,
- P_p is the pole pitch.

In the paper, the value of q is changed by varying of the pole pitch at constant stator slot pitch.

In this paper, the magnetic force levels for different values of q are presented as single numbers, where the number is evaluated from the simulated force in the time domain. The intention is to present an optimal number for q. The method for calculating the single numbers by using the time domain graphs for the cogging forces is explained below:

1. The cogging force data in time domain is converted to absolute values.
2. The value of the peak force and 60% of the peak are established.
3. The upper part of the graph (from 60% to 100%) is analysed.
4. The values from 60% to 100% where the tangent to the graph is parallel to the time axis are obtained (i.e. the force peaks).
5. Finally, an average of the values obtained and this average number is taken as representative of the force level in the sample graph.

The main objective of the above technique is to calculate two factors. The first is to show the average amplitude of the peak forces (60–100%) and the other is to take into account how often the generator reach forces higher than 60%. For example, if the majority of the peaks lie between 60% and 70%, a lower average will be established in comparison with the case where the majority of forces lie between 70% and 80%. Therefore, by using this method, not only can the peak force can be taken into account but also, it can be assessed how often that peak force is reached.

The purpose of this approach is to evaluate a single number, which is representative of the peak forces of the entire simulation period in the time domain. The minimum level (in this case 60%) can be altered. The decision that only forces higher than 60% are to be included is made in order to include a greater number of peaks. The high number of peaks is important in reducing the error in the peak forces from the FEA simulations.

In this section, the magnetic forces between the stator and translator are shown in the X- and Y-axes. The forces parallel to the X-axis do not affect the bearings directly due to the free bearing motion on the X-axis but they do cause latching of the translator, unwanted noise and vibrations [3]. The forces parallel to the Y-axis are directly destructive to the bearings and the supporting structure due to the translator's locked freedom on the Y-axis.

The forces affect the bearings and the supporting structure in different ways and therefore, minimising them is important with regard to maintenance costs and the structural integrity of the WEC.

To perform the simulations in the Y-axis, 3D models with high mesh resolution are used to increase the accuracy for the force calculation. The results reveal that the highest forces and the highest RMS power output occur when $q = 1$.

In Fig. 4, a presentation of all the forces as single number is shown. Moreover, in the same figure, the RMS powers for each q are calculated over the complete time series of the translator displacement. The current density for the models with a 50 kW output power ($q = 1$) is 0.8 A/mm^2. It can be seen that the cogging forces follow a very similar pattern to those of the single-sided PMLG. However, their magnitude is approximately twice as great. The reason for this is the double sided structure of the generator doubles the number of teeth attracting the PMs. Moreover, the harvested electrical energy is also higher.

In Table 2, the Force-to-Power ratio for the X- and Y-axes is presented for all values of q. As the aim of the optimisation is to minimise forces and maximise electrical power, the lowest numbers in Table 2 define the optimal value for q.

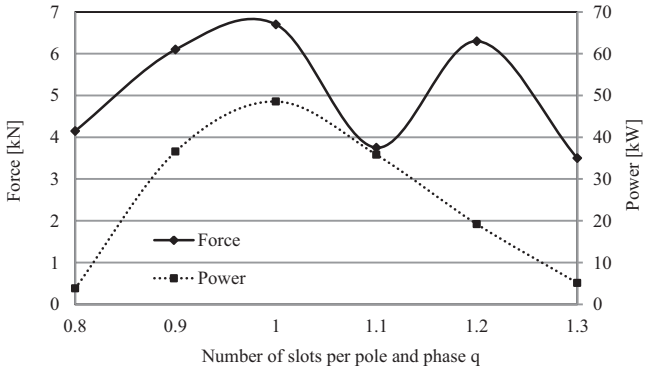

Fig. 4. X-axis forces and RMS power for double-sided PMLG.

The results for the X-axis reveal $q = 1.1$ as optimal and the results for the Y-axis reveal that $q = 0.9$ is optimal. This ratio is important because the maximum output power can be determined by knowing the level of the acceptable forces for the bearings (Y-axis) and the level of the acceptable vibrations (X-axis). Therefore, for different bearing systems and different WEC supporting structures the numbers could vary. For the purpose of this optimisation, the optimal number of q is suggested based on the lowest Force-to-Power ratio.

5.2. The effect of different numbers of winding sections on the PMLG performance

In this section, translators with different number of winding sections are simulated. Results obtained from models with windings distributed from two to nine sections are shown. As the generators simulated in this section have a different number of winding sections, the total winding resistance differs and it can be calculated by:

$$R_{\text{winding}} = 2 \times 0.15 \times p \tag{20}$$

where p is the number of winding sections connected in series.

To perform the simulations in the Y-axis, 3D models with high mesh resolution are used to increase accuracy for the force calculation. The simulation results show that the highest force appears for those generators with the lower number of winding sections. The effect from the misalignment between the stator poles and translator teeth ($q = 1.2$) is the main reason for this result. In short translators this misalignment has less effect; however, for longer translators the misalignment becomes higher than the length of the pole. Therefore, the peaks of the cogging forces for every tooth do not occur at the same point in time. Additionally, the result for the RMS power output is also shown in Fig. 5. It can be seen that the highest power output can be achieved with five winding sections.

To compare the generator models on the same basis regarding the PM volume, the simulated models should have the same length of maximum translation of the translator. Therefore, the total

Table 2
Force-to-Power ratio for X- and Y-axes.

q	X-axis [N/W]	Y-axis [N/W]
0.8	1.09268	0.28963
0.9	0.16689	**0.02599**
1	0.13797	0.03192
1.1	**0.10472**	0.03072
1.2	0.32813	0.04635
1.3	0.68359	0.31445

The values are bold to outline the lowest numbers in the table.

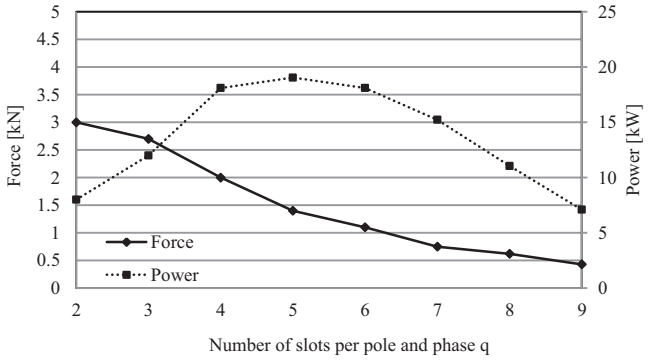

Fig. 5. *Y*-axis forces and RMS power for double-sided PMLG.

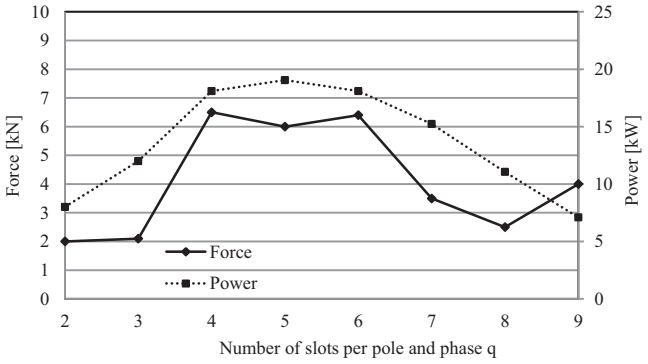

Fig. 7. *X*-axis forces and RMS power for double sided PMLG.

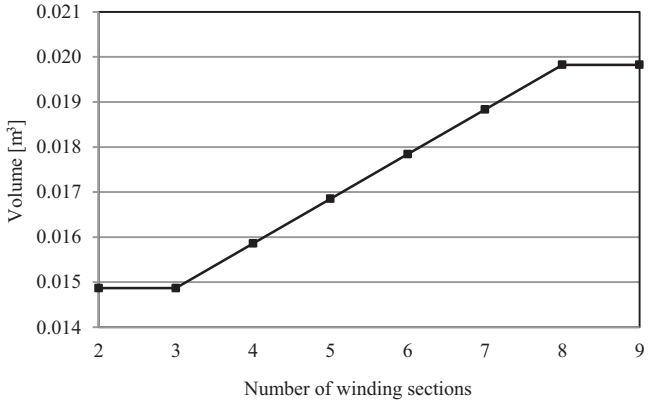

Fig. 6. Volume of PM material versus different number of sections.

length of the stator is assumed to be the length of the translator plus an additional 1.5 m, where free maximum translation is allowed. In Fig. 6, the volume of permanent magnet material is calculated for generators with different numbers of sections. The results are averaged to the nearest magnetic pole.

Table 3 shows the Force-to-Power ratio in the *X*- and *Y*-axes for generators with different number of winding sections and Power-to-PM volume ratio. The results reveal an optimal number of three winding sections for the *X*-axis force and seven sections for the *Y*-axis force.

Another coefficient representing the efficiency of the generator is the Power-to-PM volume ratio (Table 3). This coefficient is not discussed in the previous section because of the small difference in the volumes of the PM material for different q. The aim here is to maximise the ratio; therefore, the generator with four sections can be considered optimal for this criterion.

The importance of such a comparison is triggered by the price of the permanent magnets. Recent price changes of permanent magnets by almost 800% (for the period 04/2010 to 07/2011) [30] makes the permanent magnet material the most expensive component of the PMLGs.

Table 3
Force-to-Power [N/W] and Power-to-PM volume [W/m³] ratios for *X*- and *Y*-axes.

Number of sections	*X*-axis [N/W]	*Y*-axis [N/W]	Power-to-PM volume ratio [W/m³]
2	0.250	0.375	579
3	**0.175**	0.225	862
4	0.359	0.110	**1156**
5	0.299	0.070	1125
6	0.354	0.061	1019
7	0.230	**0.049**	776
8	0.226	0.056	542
9	0.563	0.061	329

The values are bold to outline the lowest numbers in the table.

5.3. Optimisation of the PMLG

From the results shown in Fig. 3, it can be observed that the highest electrical power is harvested at $q = 1$. At this value of the slots per pole and phase, a perfect alignment among the coils and permanent magnets is established. Consequently, the generated coil voltages will be in phase and therefore, the highest total generated voltage can be achieved. However, the iron pole shoes become aligned with the permanent magnets and hence, strong cogging force is generated. On the other hand, the results shown in Fig. 5, suggest that generally high numbers of winding sections reduces the cogging force due to the misalignment among the peaks of the magnetic forces between the PMs and the steel shoes. Based on the above results, it is observed that a long stator, which consists of a number of short stators, can deliver high output power, where the power is combined from the individual short stators. Furthermore, low cogging force can be achieved by increasing the total length of the stator, where the length is the combined lengths of the small stators.

In this section, an optimised generator is suggested taking into account the results presented in Section 3.3.2. The aims of the optimisation in decreasing order of their importance are:

1. Low force parallel to the *X*-axis.
2. Low force parallel to the *Y*-axis.
3. High electrical output power.
4. Low volumes of permanent magnet material used in the generator assembly.

Higher importance is given to those aims related to maintenance costs, which could be considerably high, due to the offshore and/or underwater operating conditions.

With regard to the above order of aims, it can be considered that the optimal solution is when $q = 1.1$ rather than $q = 0.9$. The reason for this decision is the small difference between the Force-to-Power ratio in the *Y*-axis (between $q = 0.9$ and $q = 1.1$) and the big difference in the Force-to-Power ratio in the *X*-axis (between $q = 0.9$ and $q = 1.1$) (Fig. 7).

To increase the power output and to reduce the cogging forces, a magnetically split translator is suggested. In this way the generator will be assembled from two separated translator cores translating together. The main idea is to take two short magnetic cores with low *X*-axis force and combine them in a long one delivering low *Y*-axis force. The new translator is assembled from two yokes containing three winding sections. The choice for the number of winding sections is based on delivering low force in the X-direction. Furthermore, the total length of the translator of the optimised

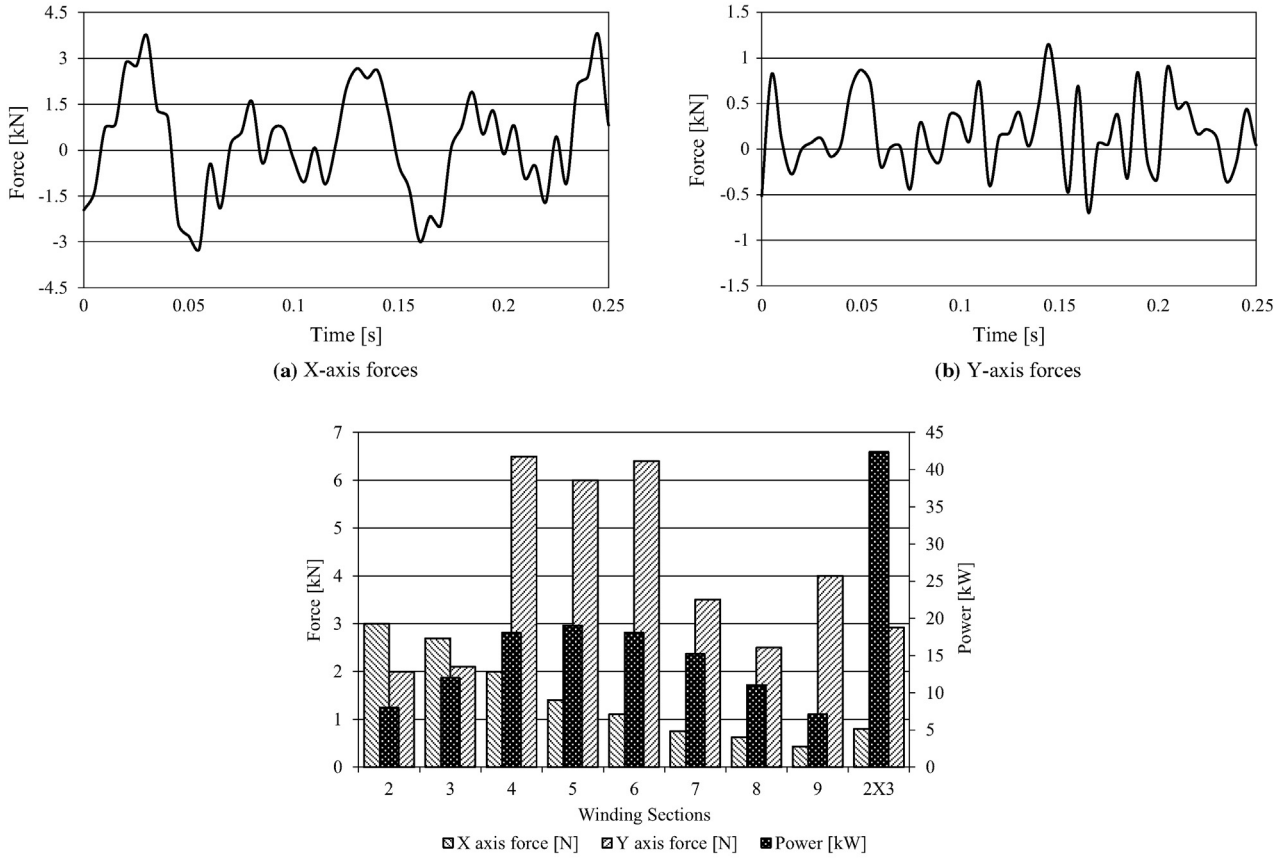

(a) X-axis forces

(b) Y-axis forces

(c) Power and force comparison between PMLGs with different winding sections and the optimized model (2x3)

Fig. 8. *X*- and *Y*-axes magnetic forces in the optimised model.

model has a very similar length to a generator with six winding sections in the *Y*-axis. The simulated results for the *X*- and *Y*-axes forces for the optimised generator are shown in Fig. 8c.

The simulation results reveal that the RMS output power is 42.4 kW and that the single force numbers for the *X*- and *Y*-axes are 2.92 kN and 0.8 kN respectively. Furthermore, the Power-to-Magnet volume ratio is 2377 W/m^3 and the volume of the permanent magnet material in the PMLG is 0.018 m^3.

High output power with regard to the amount of permanent magnet material used in the generator is achieved. The optimised model contains a very similar amount of permanent magnet material compared with the generator with six winding sections. However, the Power-to-PM volume ratio for a generator with six winding sections is 1019 and for the optimised model it is 2377 [W/m^3], resulting in a 233% increase of the Power-to-PM volume (Fig. 8c).

Another advantage of the optimised model is the reduction of the *X*-axis forces by 55% and of the *Y*-axis forces by 28%, compared with the PMLG with six winding sections. Moreover, the magnetically separated sub-yokes (Fig. 9) of the translator are smaller physically and therefore, it is easier to maintain, transport and handle them.

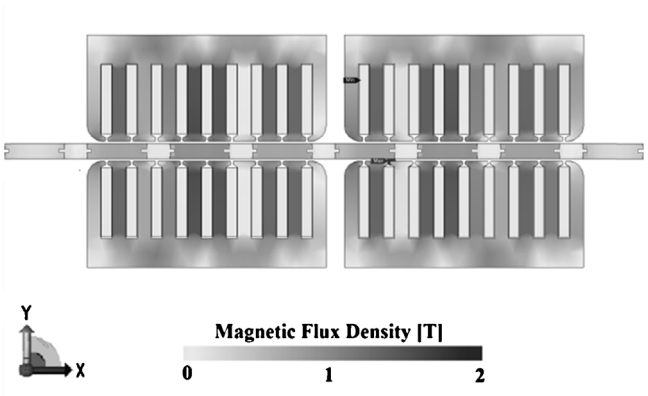

Fig. 9. Magnetic flux density in the optimised generator model.

6. Conclusions

The research in this paper began with an investigation of the factors affecting the cogging force and power output in a single- and double-sided PMLGs, where the influence of the different design solutions has been presented. Furthermore, a method for calculating a single number, representing the cogging force level of a generator has been suggested.

Additionally, a double-sided PMLG is investigated with regard to the same parameters. The main analyses in this paper are focused on suggesting an optimised design for a double-sided PMLG. As a result, a design with a magnetically separated yoke delivering better performance is proposed. The simulated results disclose that the optimised model delivers a reduction in the *X*- and the *Y*-axes forces by 55% and 28%, respectively and an increase of the output power by 233% in comparison with a model with a non-separated translator with the same volume of PM material.

Acknowledgement

The authors would like to thank the PRIMaRE project for the sponsorship and the support for this work.

References

[1] K. Rhinefrank, E.B. Agamloh, A. von Jouanne, A.K. Wallace, J. Prudell, K. Kimble, J. Aills, E. Schmidt, P. Chan, B. Sweeny, A. Schacher, Novel ocean energy permanent magnet linear generator buoy, Renewable Energy 31 (7) (2006) 1279–1298.
[2] J.K.H. Shek, D.E. Macpherson, M.A. Mueller, J. Xiang, Reaction force control of a linear electrical generator for direct drive wave energy conversion, IET Renewable Power Generation 1 (2007) 17–24.
[3] J. Prudell, M. Stoddard, E. Amon, T.K.A. Brekken, A. von Jouanne, A permanent-magnet tubular linear generator for ocean wave energy conversion, IEEE Transactions on Industry Applications 46 (2010) 2392–2400.
[4] N. Hodgins, O. Keysan, A.S. McDonald, M.A. Mueller, Design and testing of a linear generator for wave-energy applications, IEEE Transactions on Industrial Electronics 59 (2012) 2094–2103.
[5] D. Li, B. Bai, Q. Yu, D. Chen, Cogging force minimization in a permanent magnet linear generator for sea wave energy extraction applications, in: ICEET'09. International Conference on Energy and Environment Technology, 2009, 2009, pp. 552–554.
[6] M. Ashabani, J. Milimonfared, J. Shokrollahi-Moghani, S. Taghipour, M. Aghashabani, Mitigation of cogging force in axially magnetized tubular permanent-magnet machines using iron pole-piece slotting, IEEE Transactions on Magnetics 44 (2008) 2158–2162.
[7] J.K.H. Shek, D.E. Macpherson, M.A. Mueller, Experimental verification of linear generator control for direct drive wave energy conversion, IET Renewable Power Generation 4 (2010) 395–403.
[8] C. Boström, M. Leijon, Operation analysis of a wave energy converter under different load conditions, IET Renewable Power Generation 5 (2011) 245–250.
[9] Yi Pu, Shijie Zhou, J. Gu, Hao Chen, Chenjin Zhang, A novel linear switch reluctance generator system, in: 2012 IEEE International Conference on Automation and Logistics (ICAL), 2012, pp. 421–427.
[10] Zanxiang Nie, R. Xi Xiao, P. McMahon, Clifton, Yunxiang Wu, Shiyi Shao, Emulation and control methods for direct drive linear wave energy converters, IEEE Transactions on Industrial Informatics 9 (2013) 790–798.
[11] N.P. Gargov, A.F. Zobaa, Multi-phase air-cored tubular permanent magnet linear generator for wave energy converters, IET Renewable Power Generation 6 (2012) 171–176.
[12] N. Gargov, A.F. Zobaa, Multiphase tubular permanent magnet linear generator for wave energy converters, in: IET Conference on Renewable Power Generation (RPG 2011), 2011, pp. 1–5.
[13] O. Keysan, M.A. Mueller, A linear superconducting generator for wave energy converters, in: 6th IET International Conference on Power Electronics, Machines and Drives (PEMD 2012), 2012, pp. 1–6.
[14] N.M. Kimoulakis, A.G. Kladas, J.A. Tegopoulos, Cogging force minimization in a coupled permanent magnet linear generator for sea wave energy extraction applications, IEEE Transactions on Magnetics 45 (2009) 1246–1249.
[15] N.P. Gargov, A.F. Zobaa, G.A. Taylor, Structural designs and forces in direct drive linear generators for marine wave power generation, in: 47th International Universities Power Engineering Conference (UPEC), 2012, 2012, pp. 1–6.
[16] I.A. Ivanova, O. Agren, H. Bernhoff, M. Leijon, Simulation of wave-energy converter with octagonal linear generator, IEEE Journal of Oceanic Engineering 30 (2005) 619–629.
[17] O. Danielsson, M. Eriksson, M. Leijon, Study of a longitudinal flux permanent magnet linear generator for wave energy converters, International Journal of Energy Research 30 (2006) 1130–1145.
[18] O. Danielsson, M. Leijon, Flux distribution in linear permanent-magnet synchronous machines including longitudinal end effects, IEEE Transactions on Magnetics 43 (2007) 3197–3201.
[19] V.D. Colli, P. Cancelliere, F. Marignetti, R. Di Stefano, M. Scarano, A tubular-generator drive for wave energy conversion, IEEE Transactions on Industrial Electronics 53 (2006) 1152–1159.
[20] M. Prado, H. Polinder, Direct drive in wave energy conversion – AWS full scale prototype case study, in: 2011 IEEE Power and Energy Society General Meeting, 2011, pp. 1–7.
[21] N.M. Kimoulakis, P.E. Kakosimos, A.G. Kladas, Power generation by using point absorber wave energy converter coupled with linear permanent magnet generator, in: 7th Mediterranean Conference and Exhibition on Power Generation, Transmission, Distribution and Energy Conversion (MedPower 2010), 2010, pp. 1–5.
[22] J. Falnes, Principles for capture of energy from ocean waves, in: Tech. Rep. N-7034, Department of Physics, NTNU, Trondheim, Norway, 1997.
[23] K. Thorburn, M. Leijon, Farm size comparison with analytical model of linear generator wave energy converters, Ocean Engineering 34 (4) (2007) 908–916.
[24] D. Evans, A theory for wave-power absorption by oscillating bodies, Journal of Fluid Mechanics 77 (1976).
[25] H. Polinder, J.G. Slootweg, M.J. Hoeijmakers, J.C. Compter, Modeling of a linear PM Machine including magnetic saturation and end effects: maximum force-to-current ratio, IEEE Transactions on Industry Applications 39 (2003) 1681–1688.
[26] G. Yang, D. Chun-yang, Y. Lu, L. Sun, Model of permanent magnet inductor type synchronous motor, in: APEC'03. Eighteenth Annual IEEE Applied Power Electronics Conference and Exposition, vol. 1, 2003, 2003, pp. 69–74.
[27] Yan Xiuke, Xie Dexin, Zhang Yihuang, Yu Cunzhan, Application of nodal force method to switched reluctance motor, in: ICEMS 2003. Sixth International Conference on Electrical Machines and Systems, vol. 1, 2003, 2003, pp. 174–176.
[28] Jae Seop Ryu, Yan Xiuke, Chang Seop Koh, Xie Dexin, Song-Yop Hahn, 3D adaptive finite element method with edge elements [for machine calculations], in: ICEMS 2001. Proceedings of the Fifth International Conference on Electrical Machines and Systems, vol. 2, 2001, 2001, pp. 1174–1177.
[29] O. Danielsson, K. Thorburn, M. Eriksson, M. Leijon, Permanent magnet fixation concepts for linear generator, in: Proceedings of the 5th European Wave Energy Conference, Cork, Ireland, 2003, pp. 117–124.
[30] H. Humphries, Rare Earth Elements: The Global Supply Chain, Congressional Research Service, 2011.

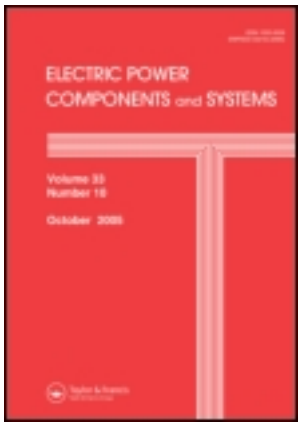

Electric Power Components and Systems
Publication details, including instructions for authors and subscription information:
http://www.tandfonline.com/loi/uemp20

Investigation of Multi-phase Tubular Permanent Magnet Linear Generator for Wave Energy Converters

N. P. Gargov [a] , A. F. Zobaa [b] & I. Pisica [b]
[a] College of Engineering Mathematics and Physical Sciences , University of Exeter , Cornwall , UK
[b] School of Engineering and Design , Brunel University , Uxbridge , UK
Published online: 06 Jan 2014.

To cite this article: N. P. Gargov , A. F. Zobaa & I. Pisica (2014) Investigation of Multi-phase Tubular Permanent Magnet Linear Generator for Wave Energy Converters, Electric Power Components and Systems, 42:2, 124-131, DOI: 10.1080/15325008.2013.848496

To link to this article: http://dx.doi.org/10.1080/15325008.2013.848496

Electric Power Components and Systems, 42(2):124–131, 2014

ISSN: 1532-5008 print / 1532-5016 online
DOI: 10.1080/15325008.2013.848496

Taylor & Francis
Taylor & Francis Group

Investigation of Multi-phase Tubular Permanent Magnet Linear Generator for Wave Energy Converters

N. P. Gargov,[1] A. F. Zobaa,[2] and I. Pisica[2]
[1]College of Engineering Mathematics and Physical Sciences, University of Exeter, Cornwall, UK
[2]School of Engineering and Design, Brunel University, Uxbridge, UK

Electric Power Components and Systems 2014.42:124-131.

CONTENTS

Abstract—In this article, an investigation into different magnetization topologies for a long stator tubular permanent magnet linear generator is performed through a comparison based on the cogging force disturbance, the power output, and the cost of the raw materials of the machines. The results obtained from finite element analysis simulation are compared with an existing linear generator described in [1]. To ensure accurate results, the generator developed in [1] is built with 3D CAD and simulated using the finite-element method, and the obtained results are verified with the source.

1. INTRODUCTION

Generally, direct-drive technologies for wave energy converters (WEC) reduce the complexity and increase the reliability of the WEC due to their design simplicity. The avoidance of mechanical or hydraulic systems in direct-drive WECs can reduce the installation and maintenance costs. However, problems with the generator, such as high magnetic forces, have been reported. Searching for alternative power generation methods has become an important topic in the last couple of decades owing to global warming, lack of fossil fuel resources, and the increasing environmental pollution. Currently, renewable energy provides a sustainable solution with its zero carbon emission release during operation. Marine wave energy generation is relevantly underdeveloped, unlike other renewable sources, such as wind and photovoltaic, but it has vast potential [2]. The direct-drive WEC's simplicity could lead to higher reliability; however, such problems as large generator sizes and, hence, high magnetic forces have been reported [3].

A number of concepts for direct-drive WECs has been presented [4–15]. Caused by the relatively low vertical speeds of the marine waves and the desire for high output power, the generators share large sizes and, hence, high magnetic forces, such as cogging forces. In linear permanent magnet (PM) iron-cored machines, the cogging forces can cause vibrations, noise,

Keywords: linear generator, wave energy, cogging forces
Received 17 January 2013; accepted 22 September 2013
Address correspondence to Mr. Nikola Gargov, College of Engineering Mathematics and Physical Sciences, University of Exeter, Cornwall, TR10 9EZ, UK. E-mail: ng258@exeter.ac.uk

Electric Power Components and Systems 2014.42:124-131.

and unattended latching [9]. Therefore analyzing the cogging forces is necessary when the bearings and supporting structure of the WEC are designed.

Another challenge related to direct-driven generators is the electrical output. As the voltage and frequency are proportional to the translational speed, the electrical output varies over the length of each wave. Due to the electrical grid connection requirements, an integration system stabilizing the output voltage and electrical frequency is required. Such integration systems are usually designed with a back-to-back converter using energy storage connected to the DC link [16, 17].

In this article, an investigation for different magnetization topologies for the long stator PM linear generator (LS-PMLG) is conducted. The investigation does a comparison based on the cogging forces, power output, and cost of raw materials of the machines. The results obtained from the simulations are compared with an existing technology for the short stator PM linear generator (SS-PMLG) in [9]. To ensure accurate results, the generator developed in [9] is simulated using the finite-element method (FEM), and the results are verified with the source.

Additionally, slotting of PMs is an effective way of reducing the cogging forces. A reduction is achieved by displacing the peaks of the cogging forces where the total cogging force (all cogging forces added together) is much lower that the individual forces [18]. The study done in [18] presented a cogging forces reduction, where, by applying the technique, a reduction of around 30%–40% can be achieved. However, the study does not show the additional magnetic reluctance added to the magnetic circuit due to the increased air gap lengths in the slots. Likewise, the effects on the output power or the induced voltage have not been mentioned.

A different approach for cogging force reduction [19] is manipulating the profile shape of the PMs. The results are obtained by means of the FEM and reveal that a bevelled bottom profile could reduce the cogging forces compared with a square profile.

Likewise, another very effective way to decrease the cogging forces is reducing the air regions among the teeth. The use of semi-opened coil slots rather than open slots can decrease the cogging by 34% [20].

To conduct a complete investigation, the effects of the proposed techniques on the electrical power output must be addressed.

2. COGGING FORCE CALCULATION

The normal operation of every electromagnetic machine is dependent on the forces causing vibrations and has a latching effect on the translator/rotor. Knowledge on the forces is very important for evaluation of mechanical vibrations and noise emissions. Furthermore, the forces are essential when the bearings, foundations, and supporting structures are designed. In the FEM used herein, magnetic forces are calculated by means of the nodal force method [21–23]. The surface forces and the magnetic volume can be derived from the Maxwell stress tensor as follows:

$$f_i^{\Omega} = \partial_k T_{ik}, \tag{1}$$

$$f_i^{\Gamma} = (T_{ik}|_2 - T_{ik}|_2) n_k, \tag{2}$$

where $\hat{n}$ is the outward unit normal vector in region one, and Maxwell stress tensor T_{ik} is given as:

$$T_{ik} = H_i B_k - \delta_{ik} w_m, \tag{3}$$

where $\delta_{ik} = \begin{cases} 1 & i = k \\ 0 & i \neq k \end{cases}$ is Kronecker's delta. Likewise, w_m is the magnetic co-energy density of the element:

$$w_m = \int_0^H B.dH. \tag{4}$$

For virtual displacement δ_l, the virtual work done by the magnetic volume and surface force is

$$\begin{aligned} \delta W &= \int f_i^{\Omega} \delta l_i dv + \int f_i^{\Gamma} \delta l_i d\Gamma \\ &= \int (\partial_i T_{ik}) \delta l_i dv + \int (T_{ik}|_2 - T_{ik}|_1) n_k \delta l_i d\Gamma \\ &= -\int T_{ik} \partial_k (\delta l_i) dv. \end{aligned} \tag{5}$$

The displacement δ_l is interpolated via the nodal shape function:

$$\delta l_i = \sum_n N_n \delta_{ni}, \tag{6}$$

where N_n is the nodal shape function of the nth node. Using Eqs. (5) and (6), the visual work can be also expressed as

$$\begin{aligned} \delta W &= -\int T_{ik} \partial_k \left(\sum_n N_n \delta l_{ni} \right) dv \\ &= -\sum_n \left(\int T_{ik} \partial_k N_n dv \right) \delta l_{ni}. \end{aligned} \tag{7}$$

The force acting on the nth node is thus given as

$$f_{ni} = -\int_{\Omega} T_{ik} \partial_k N_n dv. \tag{8}$$

Using a summation for all nodes, the total force can be written as

$$[fn] = \begin{bmatrix} f_{nx} \\ f_{ny} \\ f_{nz} \end{bmatrix} = -\int_{\Omega} \begin{bmatrix} T_{xx} & T_{xy} & T_{xz} \\ T_{yx} & T_{yy} & T_{yz} \\ T_{zx} & T_{zy} & T_{zz} \end{bmatrix} \begin{bmatrix} \frac{\partial}{\partial x} \\ \frac{\partial}{\partial y} \\ \frac{\partial}{\partial z} \end{bmatrix} N_n dv. \tag{9}$$

3. MULTIPHASE GENERATOR

Long stator generators share the same stator, where the stator consists of copper coils placed in a magnetic yoke. The coils are grouped in 15 phase windings, and each winding consists of 4 series-connected coils. The coils are identical to the coils of the generator proposed in [1] (77 turns and 1.145-ohm resistance per coil).

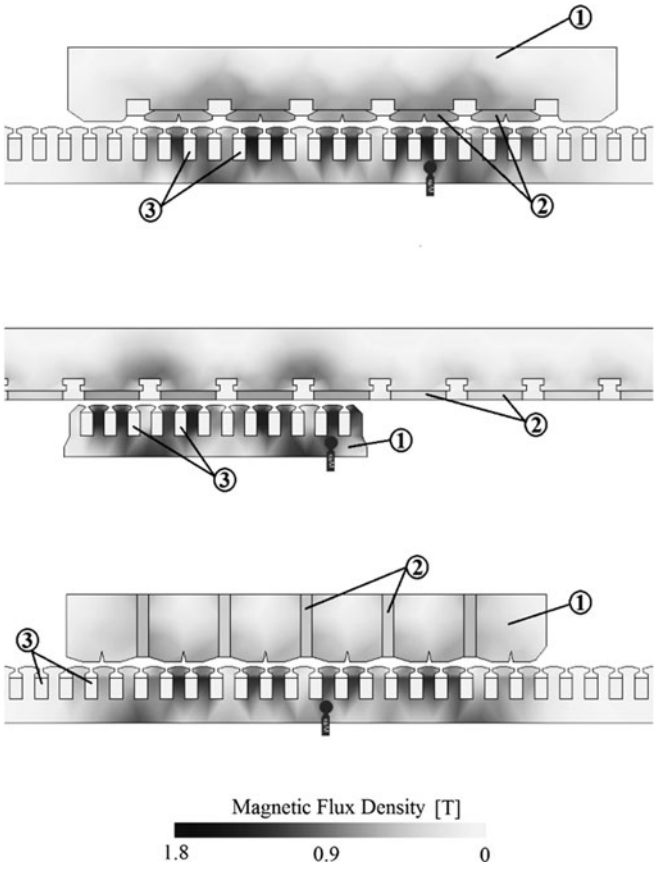

FIGURE 1. Two-dimensional view of LS-PMLG with radial magnetized magnets (top), SS-PMLG shown in [1] (middle), and LS-PMLG with axial magnetized magnets (bottom), where 1 denotes the translators, 2 denotes the PMs, and 3 denotes the coils.

The translator consists of NdFeB-35 magnets attached to a magnetic core. To decrease losses in the magnetic circuit, all magnetic cores are assembled by laminated silicon steel, where the laminations are radial to the Y-axis. Additionally, in order to increase the accuracy of the simulation results, three-dimensional generator models are used in the simulations.

In this article, long stator generators with axial and radial magnetization are investigated. A slice on the X-axis showing the profile for the three generators is presented in Figure 1. The main advantage of the long stator generator design is the reduction of the volume of the PM material used in its assembly. Considering the recent price rise of the neodymium metals [24], the potential savings of using the long stator design can be significant.

The main idea of the design adopted in the long stator designs is "swapping the configuration" of more traditional SS-PMLGs (Figure 1), where the translator comprises coils are exposed constantly to the PM's flux. Reversing this structure allows a long stator to be assembled from copper coils and a short translator that consists of PMs (Figure 1).

An advantage of the topology for the SS-PMLG is that it allows a standard three-phase rectifier to be connected directly to the winding terminals, but a significant part of the PM flux does not cross the coils; therefore, this flux does not contribute to the power generation. On the other hand, the long stator design utilizes the PMs in a way that the entire flux crosses the coils at any time of operation. Therefore, the main advantage from such a design is the full usability of the excitation flux

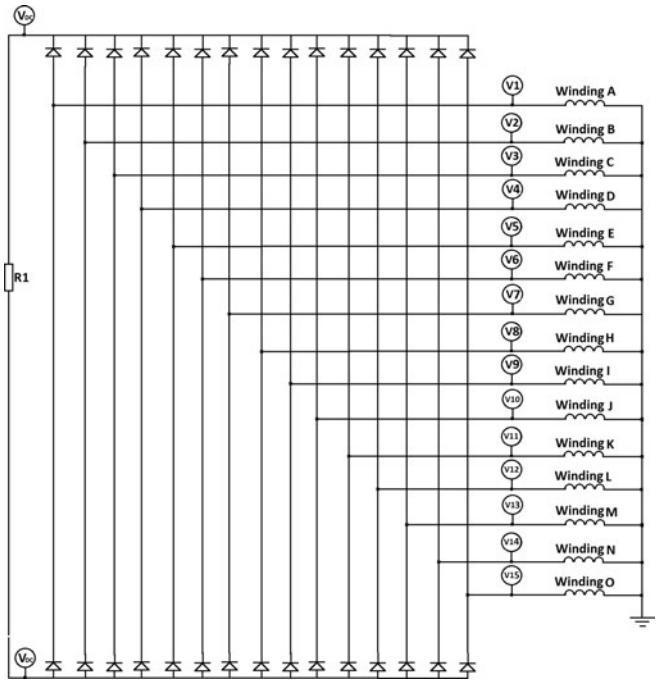

FIGURE 2. Passive rectification system for LS-PMLG.

	Axis	SS-PMLG	LS-PMLG radial magnetization	LS-PMLG axial magnetization
Stator height (mm)	*Y*	1152	1342	1342
Translator height (mm)	*Y*	284	484	422
PM length (mm)	*Y*	52	70	10
Magnet pole pitch (mm)	*Y*	72	72	72
Coil pitch (mm)	*Y*	68	68	68
Magnets height (mm)	*X*	10.5	10.5	54.7
Air gap length (mm)	*X*	5	5	5
Turns per coil		77	77	77
Coils resistance (ohm)		1.145	1.145	1.145
Resistive load (on DC side; ohm)		5	5	5
Coil connection within a winding		Series	Series	Series
Windings connection		Star	Star	Star

TABLE 1. Main dimensions

Electric Power Components and Systems 2014.42:124-131.

established by the PMs. Conversely, the long stator design has a coil configuration that is more complex and requires a system excluding the unenergized coils (coils unexposed to the PM flux) from the electrical circuit. If the unenergized coils remain connected in series with those that are energized, they become an inductive load. The main dimensions of all machines are shown in Table 1.

The electric circuit of the long stator generator is shown in Figure 2, where the output power is measured on a 5-ohm resistor (R1) after rectification. Each phase winding is assembled by four coils connected in series, and the number of windings can be altered. The voltmeters (V1 to V15) measure the voltage on every winding.

4. SIMULATION RESULTS

In the simulations performed, the following parameters are kept the same for the three generators: winding slot dimensions, shoe dimensions, number of slots per pole and phase, number of turns per coil, coil resistance, and all structural material properties used in the models. This is conducted to reveal only the differences caused by the generator design and to eliminate the influence of the material properties and of the coil configuration on the performance. In this section, three major sets of simulations are performed.

- The first set compares the cogging force for the SS-PMLG shown in [1] with the cogging force for the LS-PMLGs having axial and radial magnetized magnets.
- The second set presents the electrical power output of the generators connected to 5-ohm resistive loads after rectification.
- The third set shows the volumes and the prices of the raw structural materials for the three machines.

4.1. Cogging Forces

Cogging forces are caused by the interaction between the magnetic field of the PMs and the iron core of the PMLG. Such interaction has a latching effect on the translator. Moreover, the cogging forces are independent from the magnetic fields generated by the armature currents [25].

The cogging forces try to align the magnets with the steel core in a position that minimizes the total reluctance of the magnetic circuit. When a minimum reluctance path is established at a certain position, the magnetic forces oppose any external force trying change this position (position on the *Y*-axis). The cogging forces generate both vibrations that have to be maintained by the bearings and the supporting structure and unwanted noise and latching of the generator's translator [1, 18, 26].

Several techniques, such as shaping and slotting, have been applied for cogging force reduction in the LS-PMLG. The shaped profile of the magnets used in the radially magnetized LS-PMLG is shown in Figure 3(a). The cogging forces comparison is shown in Figure 3(b), where the shaped profile and the square profile are analyzed. To compare the PM rings on an equal basis, the two magnet ring volumes are set to be the same. As a result (Figure 3(b)), a total reduction of 30% in the peak is achieved when pole slotting and shaping is applied on the PMs.

Initially, the long stator generators were simulated with square profiles (Figure 3(a)). As one of main objectives is to reduce cogging, modifications have been applied to the magnet profile. Influenced by [19], the square profile has been modified

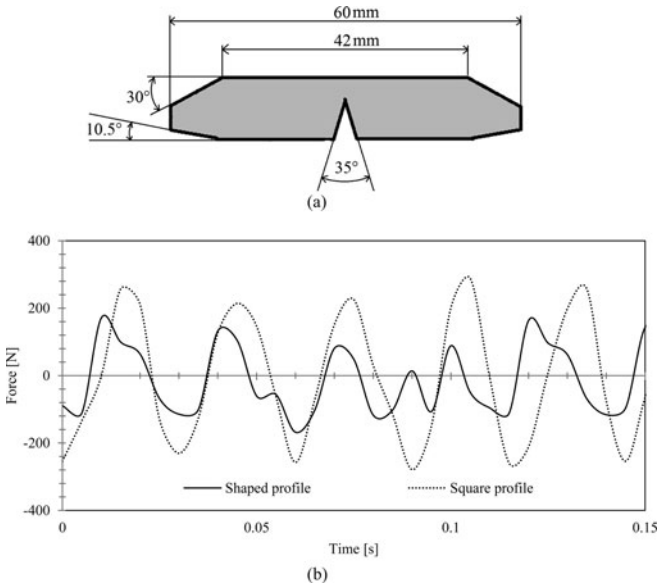

FIGURE 3. Effect on cogging force caused by shaping PMs: (a) magnet profile for radial magnetized LS-PMLG with radial magnetization and (b) cogging forces for shaped and square magnet profile.

to include to bevelled bottom profile with a 30° angle, which has been chosen based on the findings in [19].

Furthermore, to reduce the cogging force even further, but to keep the power output approximately the same as for the SS-PMLG, modifications of shaping and slotting the magnets have been also done. The shaping and slotting modifications were influenced by [18]. Initially, an angle of 35° was applied, and the shaping (with an angle of 10.5°) was adjusted to maintain the output power of the long stator machines close to that of the SS-PMLG.

The cogging force results for the three generators are shown in Figure 4, where it can be observed that the long stator designs have significantly lower cogging force amplitude. Compared with the cogging forces for the PMLG shown in [1], the LS-PMLGs achieve a reduction of 60%.

4.2. Power Output

The voltage output of the SS-PMLG [1] has been verified with the model of the simulated generator in this article. The no-load voltage (line to neutral) obtained in [1] is 346 V, and the no-load voltage obtained by finite element analysis (FEA) in this article is 330 V at a constant velocity of 0.76 m/s. The difference of 4.6% is considered as acceptable in verifying the FEA model used in this article.

Another advantage of the LS-PMLG is the possibility of adding inactive poles at both ends of the translator. By installing the inactive poles, the additional flux distributed over the stator length generates a voltage in the additional coils at

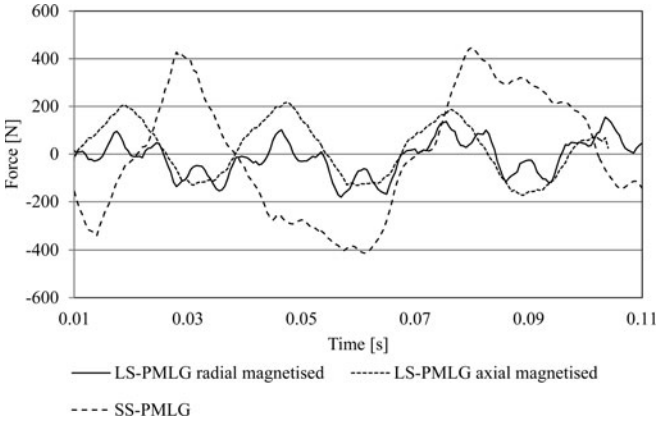

FIGURE 4. Cogging forces for investigated topologies.

the ends of the translator and, hence, electrical power. The RMS power outputs for the LS-PMLG both with and without the inactive poles are 2705 and 2521 W, respectively. The instantaneous output power can be seen in Figure 5. As a result, the output power is boosted by an extra 7% (RMS) without the use of extra PM material.

The simulated results for the power output are shown in Figure 6, where the three generator models are simulated with a monochromatic wave set for the translator's displacement with a period of $T = 2.1$ sec and height of 0.375 m. This displacement is equal to the scaled statistical data for the sea state located north of Spain [27].

The following RMS output powers are achieved for the wave period of 2.1 sec: the SS-PMLG is 2.66 kW, the LS-PMLG with axial magnetized magnets is 2.66 kW, and the LS-PMLG with radial magnetized magnets is 2.72 kW. From the result, it can be concluded that the electrical power output is very similar for the three machines.

Owing to the design consideration for the long stator generators, not all coils generate voltage at the same time. Only the

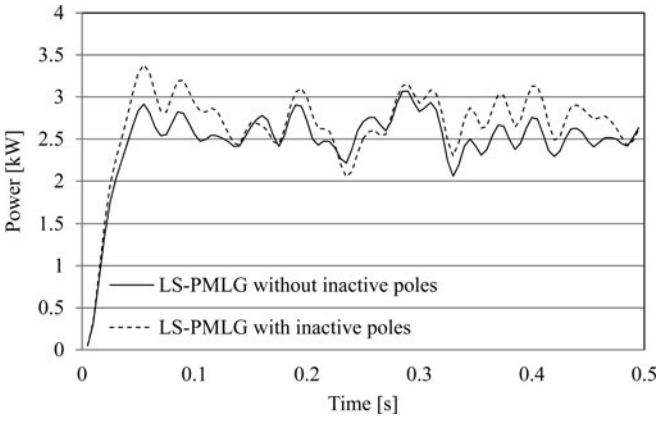

FIGURE 5. Power output from LS-PMLG with and without inactive poles.

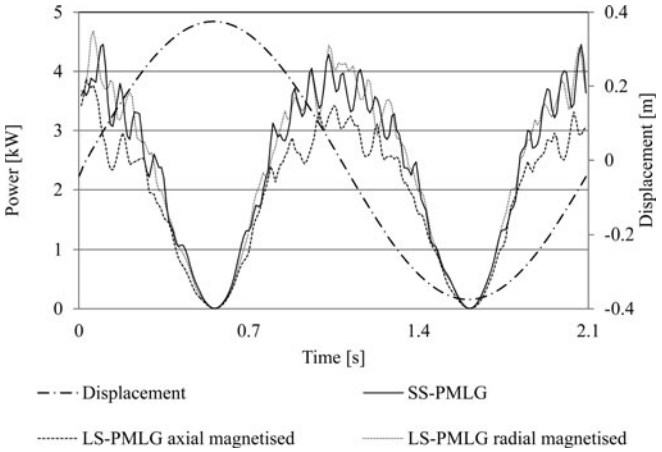

FIGURE 6. Power output of the SS-PMLG [1] and LS-PMLGs.

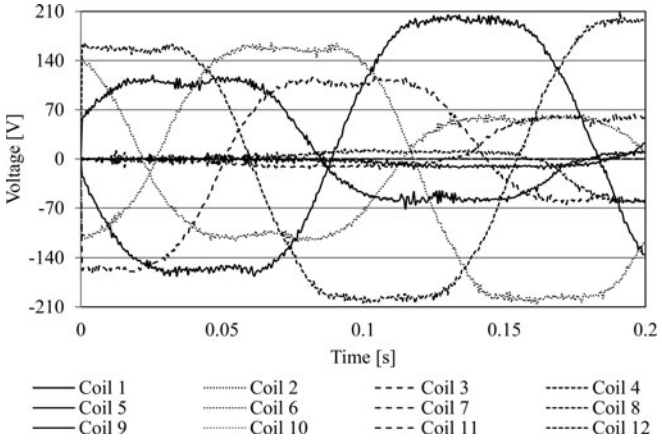

FIGURE 7. Voltage output for LS-PMLG.

coils covered by the translator magnetic field generate voltage during displacement of the translator (Figure 7). It can be seen that the coil voltages have the same frequency but different amplitude and phase. Such a complex output requires a modified rectification system. The voltages from the long stator generators in this article are rectified by a passive rectification system.

Another benefit of the long stator design is the possibility of excluding a coil in case of failure by using power electronics. Owing to the high number of coils, such an operation does not reduce the output of the generator significantly. Therefore, maintenance of the WEC can be postponed.

Moreover, a benefit of using the long stator design is the heat dissipation in the copper coils. In the long stator design, output electrical power is harvested from a high number of coils. Unlike the SS-PMLG in [1], the coils in the LS-PMLG are not energized at all times. Hence, for the same amount of total harvested energy from the generators, the power delivered by a single coil in the LS-PMLG will be much lower than in the SS-PMLG. Consequently, the coils in the long stator generator have a much lower duty cycle, and therefore, they are allowed a longer cooling time. Consequently, overheating of the LS-PMLG coils is less likely to occur compared with those of the SS-PMLG.

4.3. Volumes and Price of the Structural Materials

The volumes of the structural materials for both generators are shown in Table 2, where it is seen that the total price of the long stator design is much lower than that of the SS-PMLG [1]; the main difference is in the price of the PMs. The price of the materials is assumed as follows: non-magnetic and non-electrical conducting material is 1.43 £/kg (2.28 $/kg); copper is 5.29 £/kg (8.46 $/kg) [28]; laminated steel is 2 £/kg (3.20 $/kg) [28]; and PMs, NdFeB, and N35 is 216 £/kg (345.60 $/kg) [29].

Considering the recent price rise of the neodymium metals reported in [24], the payback period of the long stator design is likely to be shorter than that for the existing generator. The assembly cost is not included in the calculations, but it is expected to be similar among the three generators. Generally, fewer difficulties are expected for the assembly and handling

	SS-PMLG	LS-PMLG radial magnetisation	LS-PMLG axial magnetization
PM (m^3)	0.034	0.011	0.011
Laminated steel (m^3)	0.303	0.264	0.270
Copper (m^3)	0.0111	0.0555	0.0555
Non-magnetic and non-electrical conducting material (m^3)	0.022	0.0052	0
PM (k£)	55.5 ($88.80)	18 ($28.80)	18 ($28.80)
Laminated steel (k£)	4.64 ($7.42)	4.04 ($6.46)	4.13 ($6.61)
Copper (k£)	0.52 ($0.83)	2.6 ($4.16)	2.62 ($4.19)
Non-magnetic and non-electrical conducting material (k£)	0.08 ($0.13)	0.018 ($0.03)	0
Total cost (k£)	60.74 ($97.18)	24.66 ($39.46)	24.75 ($39.60)

TABLE 2. Volumes and price of structural materials

Electric Power Components and Systems 2014.42:124-131.

of the PMs in the long stator generators because of the lower volumes of PMs used in their design.

5. CONCLUSIONS

The aim of this article is to highlight the merits of the long stator design over the existing short stator three-phase design for SS-PMLGs. The areas of focus are the price of the raw assembly materials, the cogging force and electrical power output. An increase in the electrical output and a reduction in the raw materials can lead to a lower initial investment and lower return of investment (RoI) of the WEC. Furthermore, the reduction of the cogging force reduces vibrations and, hence, can increase the life of the bearings.

In this article, an investigation of long stator generators has been performed by means of FEA. Long stator generators with axial and radial magnetization have been analyzed and optimized, and the results reveal a cogging force reduction of up to 60% in comparison with an existing design having a short stator and similar size. Furthermore, the long stator generators simulated use three times less PM material in their assembly, which reduces the price of the raw assembly materials by 60% in comparison with existing SS-PMLGs [1]. The results delivered in this article suggest that use of LS-PMLGs can reduce the production and maintenance costs of the WEC in comparison with the SS-PMLG.

ACKNOWLEDGMENT

The authors would like to thank the PRIMaRE project for the support and the funding of this work.

REFERENCES

[1] Prudell, J., Stoddard, M., Amon, E., Brekken, T. K. A., and von Jouanne, A., "A permanent-magnet tubular linear generator for ocean wave energy conversion," *IEEE Trans. Industry Appl.*, Vol. 46, pp. 2392–2400, 2010.

[2] Tavana, H. M., "Study of wave energy potential in tonekabon (N iran)," *1st International Conference on Developments in Renewable Energy Technology (ICDRET)*, pp. 1–3, 2009.

[3] Faiz, J., Ebrahimi-Salari, M., and Shahgholian, G., "Reduction of cogging force in linear permanent-magnet generators," *IEEE Trans. Magnet.*, Vol. 46, pp. 135–140, 2010.

[4] Du, Y., Chau, K. T., Cheng, M., Fan, Y., Zhao, W., and Li, F., "A linear stator permanent magnet Vernier HTS machine for wave energy conversion," *IEEE Trans. Appl. Superconduct.*, Vol. 22, pp. 5202505–5202505, 2012.

[5] Du, Y., Chau, K. T., Cheng, M., Fan, Y., Wang, Y., Hua, W., and Wang, Z., "Design and analysis of linear stator permanent magnet Vernier machines," *IEEE Trans. Magnet.*, Vol. 47, pp. 4219–4222, 2011.

[6] McDonald, A. S., Crozier, R., Caraher, S., Mueller, M. A., and Chick, J. P., "Integrated design of direct-drive linear generators for wave energy converters," *International Conference on Sustainable Power Generation and Supply (SUPERGEN '09)*, pp. 1–7, 2009.

[7] Liu, C. T., Lin, C. L., Hwang, C. C., and Tu, C. H., "Compact model of a slotless tubular linear generator for renewable energy performance assessments," *IEEE Trans. Magnet.*, Vol. 46, pp. 1467–1470, 2010.

[8] Shek, J. K. H., Macpherson, D. E., and Mueller, M. A., "Experimental verification of linear generator control for direct drive wave energy conversion," *Renew. Power Generat.*, Vol. 4, pp. 395–403, 2010.

[9] Prudell, J., Stoddard, M., Amon, E., Brekken, T. K. A., and Jouanne, A. V., "A permanent-magnet tubular linear generator for ocean wave energy conversion," *IEEE Trans. Industry Appl.*, Vol. 46, pp. 2392–2400, 2010.

[10] Gargov, N., and Zobaa, A. F., "Multiphase tubular permanent magnet linear generator for wave energy converters," *IET Conference on Renewable Power Generation (RPG 2011)*, pp. 1–5, 2011.

[11] Gargov, N. P., and Zobaa, A. F., "Multi-phase air-cored tubular permanent magnet linear generator for wave energy converters," *Renew. Power Generat.*, Vol. 6, pp. 171–176, 2012.

[12] Kashani, M., Hosseina, M., and Darabi, A., "Design of synchronous motor with high-temperature superconductive field windings for marine propulsion applications," *Elect. Power Compon. Syst.*, Vol. 41, pp. 413–426, 2013.

[13] Shi, X., and Chang, S., "Commutation force ripple reduction in a novel linear brushless DC actuator based on predictive current control," *Elect. Power Compon. Syst.*, Vol. 39, pp. 1609–1620, 2013, 2011.

[14] Garcia-Amorós, J., Andrada, P., and Blanqué, B., "Design procedure for a longitudinal flux flat linear switched reluctance motor," *Elect. Power Compon. Syst.*, Vol. 40, pp. 161–178, 2013, 2011.

[15] Tosifian, M. H., Nazarzadeh, J., and Abedi, M., "A new dynamical model of linear induction machines," *Elect. Power Compon. Syst.*, Vol. 40, pp. 1319–1338, 2013, 2012.

[16] Ran, L., Tavner, P. J., Mueller, M. A., Baker, N. J., and McDonald, S., "Power conversion and control for a low speed, permanent magnet, direct-drive, wave energy converter," *3rd IET International Conference on Power Electronics, Machines and Drives*, pp. 17–21, 2006.

[17] Goel, P. K., Singh, B., Murthy, S. S., and Tiwari, S. K., "Three-phase four-wire autonomous wind energy conversion system using permanent magnet synchronous generator," *Elect. Power Compon. Syst.*, Vol. 38, pp. 367–386, 2013, 2010.

[18] Shabani, M. A., Milimonfared, J., and Taghipour, S., "Cogging force mitigation of tubular permanent magnet machines with magnet dividing," *International Conference on Electrical Machines and Systems (ICEMS)*, pp. 810–814, 2007.

[19] Kimoulakis, N. M., Kladas, A. G., and Tegopoulos, J. A., "Cogging force minimization in a coupled permanent magnet linear generator for sea wave energy extraction applications," *IEEE Trans. Magnet.*, Vol. 45, pp. 1246–1249, 2009.

[20] Faiz, J., Ebrahimi-Salary, M., and Shahghplian, G., "Cogging force alleviation in linear permanent magnet generators," *AFRICON '09*, pp. 1–6, 2009.

[21] Xiuke, Y., Dexin, X., Yihuang, Z., and Cunzhan, Y., "Application of nodal force method to switched reluctance motor," *Sixth*

Electric Power Components and Systems 2014.42:124-131.

International Conference on Electrical Machines and Systems (ICEMS 2003), pp. 174–176, 2003.

[22] Azari, M. N., and Mirsalim, M., "Performance analysis of a line-start permanent magnet motor with slots on solid rotor using finite-element method," *Elect. Power Compon. Syst.*, Vol. 41, pp. 1159–1172, 2013.

[23] Ranlöf, M., and Lundin, U., "Finite element analysis of a permanent magnet machine with two contra-rotating rotors," *Elect. Power Compon. Syst.*, Vol. 37, pp. 1334–1347, 2013, 2009.

[24] Humphries, H., "Rare earth elements: The global supply chain," Congressional Research Service, 2011.

[25] Bascetta, L., Magnani, G., and Rocco, P., "Force ripple compensation in linear motors with application to a parallel kinematic machine," *IEEE/ASME International Conference on Advanced Intelligent Mechatronics*, pp. 1–6, 2007.

[26] Ashabani, M., Milimonfared, J., Shokrollahi-Moghani, J., Taghipour, S., and Aghashabani, M., "Mitigation of cogging force in axially magnetized tubular permanent-magnet machines using iron pole-piece slotting," *IEEE Trans. Magnet.*, Vol. 44, pp. 2158–2162, 2008.

[27] Manana, M., Arroyo, A., Silio, D., Delgado, F., Perez, S., Fernandez, I., Moreno, V., Pigazo, A., Zobaa, A., Roa, P., and Cardenal, J., "WET: A wave energy toolbox for oscillating-body converters," *IEEE OCEANS*, pp. 1–3, Spain, 2011.

[28] Available at: http://www.metalprices.com.

[29] Available at: http://www.ukmag.net.

BIOGRAPHIES

N. P. Gargov received his BSc from Technical University of Sofia, Bulgaria and his MSc from Brunel University, UK. He is currently working towards his PhD with University of Exeter, UK. His area of interest is renewable energy. He is also currently working with National Grid, UK on projects related to identifying future challanges in the performance and the operability of GB transmission network.

A. F. Zobaa received the B.Sc.(Hons.), M.Sc., and Ph.D. degrees in electrical power and machines from Cairo University, Giza, Egypt, in 1992, 1997, and 2002, respectively. Since 1992, he has been with the Department of Electrical Power and Machines and the Faculty of Engineering, Cairo University, where he has been Associate Professor since April 2008. From 2007 to 2010, he was a Senior Lecturer in renewable energy with the University of Exeter, Cornwall, U.K. Currently, he is also a Senior Lecturer in power systems with Brunel University, Uxbridge, U.K. Dr. Zobaa is the Editor-in-Chief for the *International Journal of Renewable Energy Technology*, and also an Editorial Board member, Editor, Associate Editor, and Editorial Advisory Board member for many international journals, including Electric Power Components and Systems. He is a Fellow of the Institution of Engineering and Technology (IET), the Energy Institute of U.K., the Chartered Institution of Building Services Engineers, the Royal Society of Arts, and the Higher Education Academy of U.K. His main areas of expertise are lighting applications, power quality, (marine) renewable energy systems, grid integration, smart grids and energy management.

I. Pisica is Research Fellow at Brunel University – School of Engineering and Design. She received her MsC from the Academy of Economic Studies of Bucharest and her PhD from University Politehnica of Bucharest. She is member of IEEE and IET since 2011. Currently, she is working on the EPSRC funded project ADEPT (Advanced Dynamic Energy Pricing and Tariffs) and her research interests include artificial intelligence techniques, communications and SCADA systems in electrical power engineering, renewable energy sources, smart consumers and smart grids.

Electric Power Components and Systems 2014.42:124-131.

Techset Composition Ltd, Salisbury
Doc: H:/lee/RPG/Articles/Pagination/RPG20110190.3d

www.ietdl.org

Published in IET Renewable Power Generation
Received on 12th July 2011
Revised on 30th January 2012
doi: 10.1049/iet-rpg.2011.0190

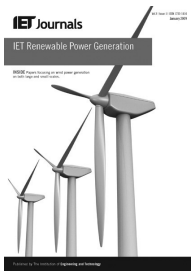

ISSN 1752-1416

Multi-phase air-cored tubular permanent magnet linear generator for wave energy converters

N.P. Gargov[1] *A.F. Zobaa*[2]

[1]*College of Engineering Mathematics and Physical Sciences, University of Exeter, Cornwall TR10 9EZ, UK*
[2]*School of Engineering and Design, Brunel University, Uxbridge, Middlesex, UB8 3PH, UK*
E-mail: ng258@exeter.ac.uk

Abstract: Direct driven permanent magnet linear generators (PMLGs) are an alternative solution for wave energy converters (WECs). Generally, problems such as high magnetic attraction forces between the permanent magnets and the magnetic core are associated with direct driven PMLG. To eliminate the attraction, air-cored generators can be used. They do not contain any stainless steel in either the stator or the rotor and therefore there is no magnetic attraction between the moving and the stationary parts. In this study, a novel design of multi-phase air-cored PMLG is proposed. The main advantage of the generator is the reduction in the Lorentz forces acting on the bearings by addressing the force in the direction parallel to the motion axis and elimination of cogging forces. Additionally, in the study a new system bypassing inactive coils is proposed and simulated as part of the grid integration system. The system achieves implementation of a small number of elements connected in series with the coils and hence the thermal losses in the grid integration system are reduced. All simulations are made by means of finite-element (FE) software working simultaneously with Matlab/Simulink.

1 Introduction

In the past couple of decades a number of different systems converting energy from ocean waves into electricity have been proposed. For instance, in Pelamis high-speed induction generators working in combination with hydraulic systems are used [1]. Moreover, turbine-driven synchronous generators are used in Wevedragon [2]. In order to simplify the wave energy converter (WEC) structure and improve reliability, direct driven permanent magnet linear generators (PMLGs) using the low-speed motion of the waves have been employed [3, 4]. Generator designs have been proposed in [3, 4], and also problems connected with high magnetic forces have been pointed out [5]. Such high forces could significantly reduce the life of the bearings and increase maintenance of the WEC. Further, the forces generate vibrations which can affect the foundations and the supporting structure of the WEC. In order to eliminate the magnetic forces between the stator and the translator, air-cored PMLGs have been proposed [6, 7]. Owing to the absence of stainless steel in the translator, the attraction forces between the stator and the translator have been eliminated. However, the Lorentz forces do exist. In the recently proposed air-cored generator design, the Lorentz forces are radial to the motion direction [8].

In this paper, a new air-cored tubular PMLG designed for WECs is proposed and simulated. The proposed generator design 'sandwiches' the windings between two sets of permanent magnets (PMs) in a tubular structure. Owing to the absence of steel in the translator, the bearings are not exposed to high attrition magnetic forces. However, a higher volume of PM material has to be used because of the high magnetic reluctance in the air gap. In order to reduce the volume of the PM material used in the generator's assembly, generators with a high number of coils have been proposed [9]. The number of coils vary with regard to the desired length of the generator. Since the PMs partially cover the winding coils, a number of coils remain outside the PM's flux, at any time of operation. To avoid current passing inactive coils (thermal losses) and additional inductance, several techniques have been proposed [10, 11]. In [10] a technique using anti-parallel thyristor pairs bypassing the inactive coils has been proposed. However, owing to the high thermal loss in the thyristor switches connected in series with the coils, another system adopting individual rectification for every coil has been presented in [11].

In this paper, a new system that bypasses inactive coils is proposed. The proposed system also uses the anti-parallel thyristor pairs arranged in order to bypass the inactive coils. However, a maximum number of two thyristor switches per phase, working in series with the coils, is achieved at any time of operation. Owing to the small number of elements the power losses in the bypassing system can be significantly reduced.

In this paper, all simulations are made by means of finite-element (FE). Moreover, Matlab–Simulink is used for control purposes. The FE simulations and the circuit simulations (Matlab–Simulink) are done simultaneously using an external link connecting the two software packages.

2 Generator under study

The proposed generator has a stator assembled by 48 coils forming three phases (16 coils in each phase). The coils are supported by an aluminium separation cage. Owing to the complexity of the assembly of the PMs, it is assumed that the PMs and the iron core remain static and the windings and aluminium cage are translating.

The flux is provided by radial magnetised magnets (to the *z*-axis). The main idea of this assembly is the windings to be placed in a magnetic field normal to the axis of the motion. In such a way, the Lorentz forces will be directed in the same direction as the axis of motion of the generator (Fig. 1).

The main dimensions of the generator are presented in Table 1. The inner magnets and the iron core are divided into six equal sectors (Fig. 1). A space among them is left to allow the supporting columns of the separation cage to access the linear bearings. The proposed model has aluminium cage with six supporting columns. The number of supporting columns varies with the magnitude of the Lorentz force.

In order to enhance the robustness of the translator, the separation cage can be manufactured from a single piece of moulded aluminium. Further, when the coils are positioned among the separators, a solid casting can be applied to secure their position. The casted coils and the keys of the separators secure the coils position over the entire circle of the separation cage (Fig. 2).

Likewise, the robustness of the cage is highly dependent on the number of supporting columns and the thickness of the separators. The generator is expected to be robust mainly owing to reduction of the magnetic attraction forces between the stator and the translator. Moreover, the absence of joins (such as bolt connections) in the separation cage reduces the translator̀s sensitivity from vibrations and increases the overall robustness of the cage.

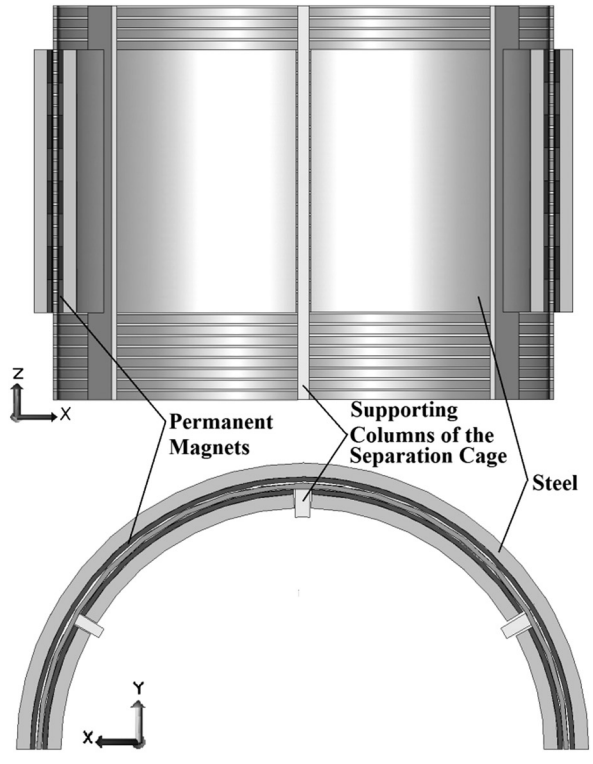

Fig. 1 *Overview of the generator structure*

Table 1 Main dimensions and parameters Q1

stator length, mm	608
stator inner radius, mm	520
iron width, mm	30
coil width, mm	10
coil length, mm	20
aluminium separation length, mm	5
PM width, mm	10
air gap, mm (including the coils)	16
translator length, mm	900
pole length, mm	76
number of turns per coil	55
coil resistance, Ω	0.8
coil connection	series
number of supporting columns	6

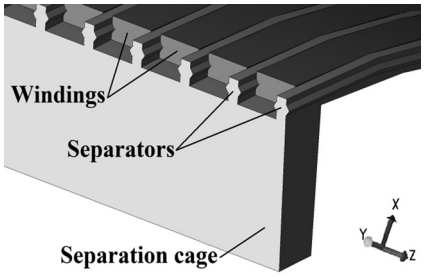

Fig. 2 *Section cut of the separation cage*

The cost of the assembly of the proposed machine is expected to be similar to the existing PMLG proposed in [4]. This is because no stainless steel sheets are used in the translator. In addition, the slot openings for the coils are larger, and so the coil̀s winding and maintenance are expected to be cheaper in comparison with the semi-open slots used in the machine in [4]. However, epoxy resin or material with similar properties is required to secure the coils into the slots.

3 Inactive coil bypass system

The coils of the generator are grouped in three phases, connected in series. The coils and the switches controlling the current flow for a single phase are shown in Fig. 3. The voltmeters measuring the generated voltage are installed on the coil̀s ends (except the two middle coils, C8 and C9). Nine consecutive coils will be exposed to the flux established by the magnets at any time of normal operation.

Based on the voltage obtained by the voltmeters (V1–V14), a control system determines the active/inactive coils (Fig. 4). In order to take only positive voltage, an absolute value from the signal gained by the voltmeters is used. The mean value of the voltage is used in order to avoid switching ‘off’ the switches at zero-crossing. After the consideration of active/inactive is made for all coils, the signals are arranged in a vector and passed to the switch selector (Fig. 4).

The switch selector determines the ‘on’ and ‘off’ signals sent to the anti-parallel thyristor switches (S1–S14). The vector formed by the signals from the voltmeters is compared with predefined vectors by a relational operator (Fig. 4). The predefined vectors are all the possible combinations formed by nine consecutive coils. They also

doi: 10.1049/iet-rpg.2011.0190

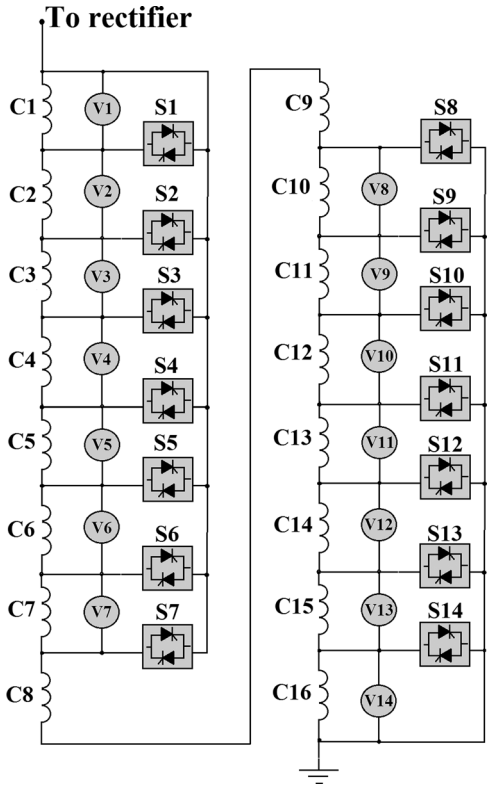

Fig. 3 *Single-phase coil and switches arrangement*

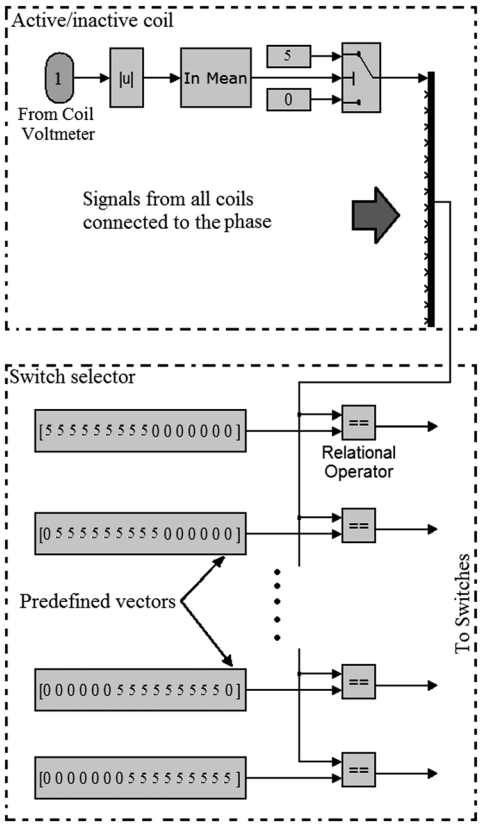

Fig. 4 *Switch selector (lower) and active/inactive coils (upper) for a single phase*

represent the location of the translator. When the variable vector formed by the voltmeters matches a predefined vector, a switching 'on' signal triggers a set of switches. For example, if the coils from C3 to C11 are active (the absolute voltage value is higher than 3 V), switches S2 and S10 are turned 'on' and the rest stay 'off' (Fig. 3). In such a way a maximum of two switches are working in series with coils at any time of operation. This system eliminates the flow of current through a large number of elements (switches and inactive coils) and hence the overall thermal losses. In addition, by using the proposed system a three-phase output with $\pm 120^{\circ}$ phase shift is achieved.

4 Simulation results

A monochromatic wave with a period of 8.4 s was used as a time-speed sequence in the simulations. Such a period is equal to the energy period (T_e) of the region located north of Spain [12].

As seen in Table 2, the total price of the raw materials of the air-cored generator is lower. This is mainly because of the reduced amount of steel used in the generator. Likewise, Table 2 shows that the PM volume in the air-cored generator is about 25% more in comparison with the iron-cored generator. Moreover, the output power of the air-cored machine is around twice more compared with the iron-cored at the same translational speed. On the other hand, the multi-phase coils require a more complicated integration system. The prices per kilogram for the assembly materials have been taken from [7] and also the price of aluminium is assumed to be the same as the price of stainless steel.

The objective of the inactive coil bypass system is to reduce the impedance of the series-connected elements. Owing to the relatively low linear speeds and hence low switching frequencies of the switches (Fig. 8), anti-parallel thyristors are used because of their high-power rating.

If the field is established from a single side of the PMs, high magnitudes of the Lorentz forces radial direction are expected [8]. The simulation results for the Lorentz forces are shown in Figs. 7*a* and *b*. The advantage of the radial magnetised (to the *z*-axis) field is because a significant part of the forces is directed in parallel to the *z*-axis. This way of directing the Lorentz forces extends the life of the bearings owing to their free motion on the *z*-axis.

In Fig. 7*c* the magnetic forces between the PMs for a one-sixth section of the generator (Fig. 1) are shown. The results present the magnitude of the attracting forces acting between the inner and outer set magnets. Since the outer magnets have full circular shape, the total radial force (*z*-axis) will remain zero owing to the opposing directions of the forces.

Table 2 Total price of the raw materials of the air-cored generator Q1

	Tubular air-cored PMLG	Existing PMLG [4]
Volumes/prices of the assembly materials		
copper, m^3/k£	0.034/1.53	0.011/0.49
aluminium, m^3/k£	0.031/0.25	0.022/0.18
stainless steel, m^3/k£	0.13/2.29	0.3/6.95
PM, m^3/k£	0.043/6.83	0.034/5.35
total price, k£	10.9	12.97
RMS/half peak performance at constant translational speed of 0.76 m/s		
three-phase power, kW	5.3/3.75	2.5/1.75
phase voltage, V	102/73	70/50
phase current, A	21/10	14/10

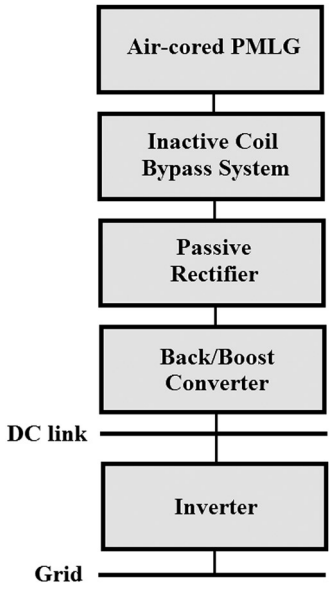

Q2 **Fig. 5** *WEC structure – one line diagram*

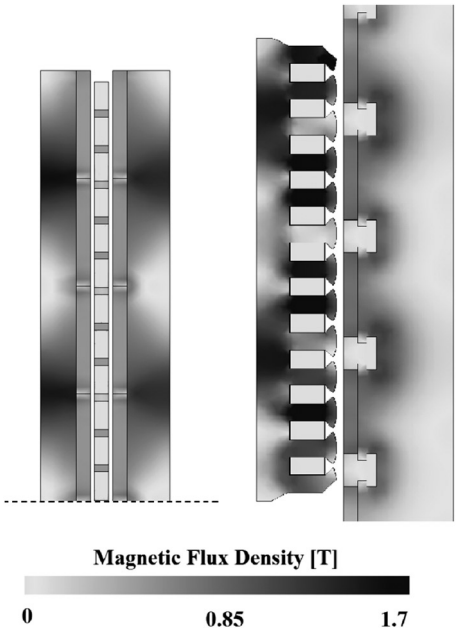

Fig. 6 *Magnetic flux distribution for half stator of the multi-phase air-cored generator (left) and PMLG [4] (right)*

If the inner magnets sections are fixed in a single structure, the total force will also be eliminated but, the fixations have to be strong enough to withstand the forces and also the forcès magnitudes have to be taken into account in the fixations design. Since all the magnets are static, the forces shown in Fig. 7*c* do not affect the bearings. In Fig. 7*c*, it has also been seen that the attracting forces between the magnets remain relatively the same regardless of the speed of the translator.

The thermal losses in previously proposed bypass systems are dependent on the number of translator magnet pairs and the total number of coils [10, 11]. In the proposed bypass system the thermal losses are not dependent on the number of coils or the number of magnetic poles. Using the proposed design parameters, reduction of the thermal losses up to seven times is achieved in comparison with the system proposed in [10].

A voltage generated by a single coil is shown in Fig. 8. Likewise, the 'on' and 'off' triggering signals (1 and 0 V, respectively,) sent to the switch selector can be seen in the figure. It is seen that the coils do not generate voltage at all times, and therefore during the period from 2 to 6 s, the coil (Fig. 8) has to be disconnected from the series winding configuration, otherwise it becomes an inductive load.

In Fig. 9 the power output simulated on a 5 Ω resistor connected after rectification and boosting the DC voltage is shown. The half-peak and the RMS power are 4.92 and

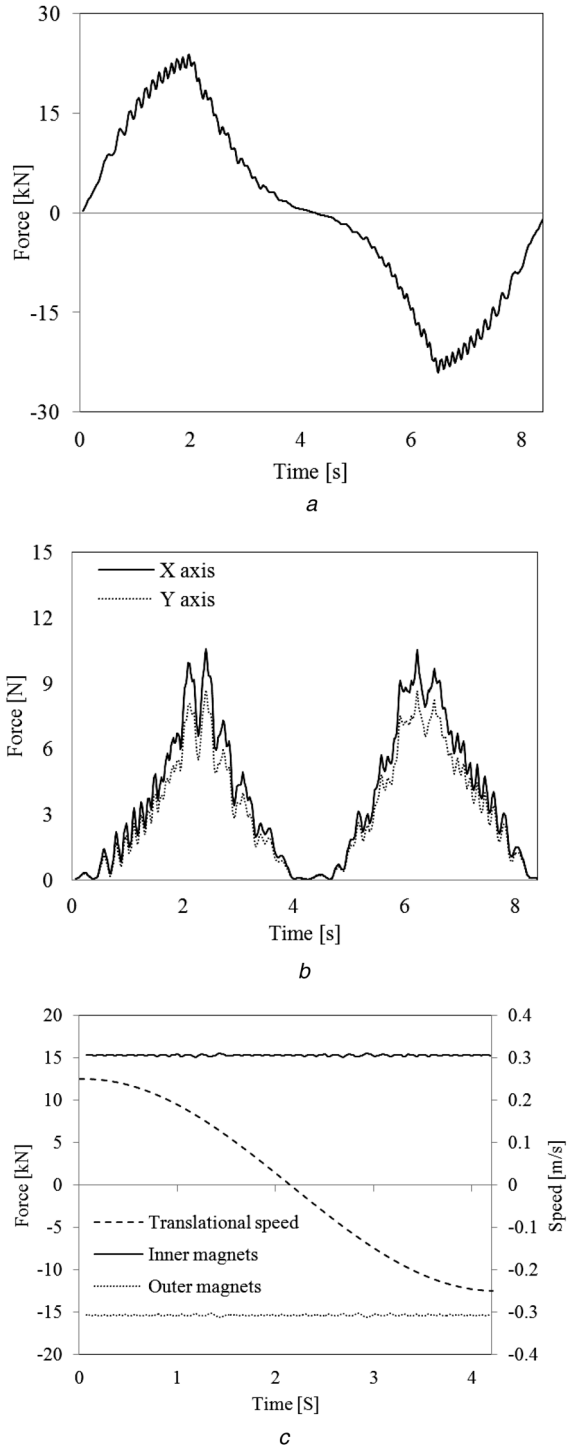

Fig. 7 *Lorentz forces*

a Lorentz force on the *z*-axis
b Lorentz forces parallel with the *X* and *Y* axes
c Forces simulated on the inner and outer sets of magnets at constant speed

doi: 10.1049/iet-rpg.2011.0190

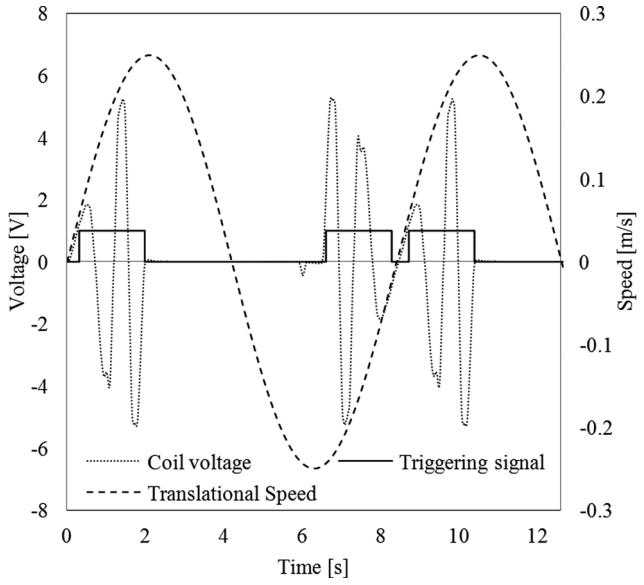

Fig. 8 *Single-coil voltage and switch signal*

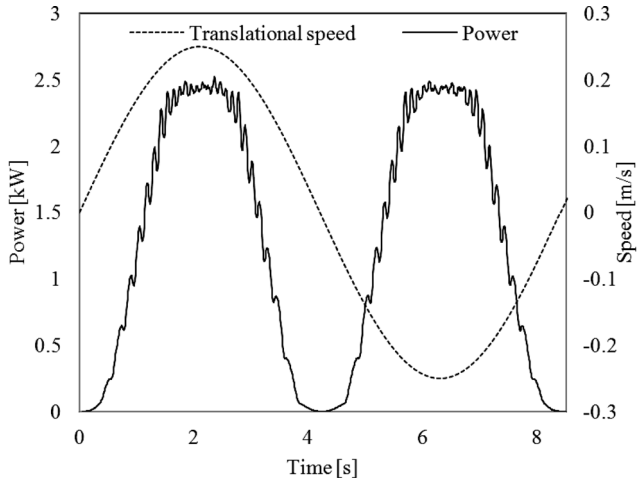

Fig. 9 *Power output*

1.61 kW, respectively. In order to increase the performance of the WEC array a power electronics control (back/boost) can be applied to the generator output. Additionally, control on the DC voltage allows a control strategy for both stiffness and dumping forces [13].

Energy storage has not been used in the simulations shown in Figs. 7–9. However, smoothing of the output power can be achieved by adding energy storage in the DC link and increasing the number of the WECs connected in the array.

5 Discussion

The proposed air-cored PMLG is designed to be used in a wave point absorber or Archimedes wave swing. Owing to the significant force reduction, in comparison with iron-cored machines, the bearings can support the columns of the separation cage by either single or double sides.

Generally, problems with coil overheating are not expected. As seen in Fig. 8 the coils do not generate voltage at all times, which increases the cooling time. In comparison, the coils in the generator proposed in [4] are constantly generating power during the motion of the translator.

Likewise, the winding arrangement allows the insulation of a coil in case of a failure. Such insulation is not going to affect the power output significantly owing to the high number of coils. As a result the maintenance activities in such a case can be postponed, which can reduce the maintenance cost.

6 Conclusion

In this paper, the simulation results of a novel design of air-cored tubular generator have been presented. The results are obtained using FE externally linked with Matlab/Simulink. The results confirm that the proposed generator has higher-power output in comparison with the existing iron-cored using similar volumes of structural materials and size. Likewise, the results reveal that the proposed design addresses the majority of the Lorentz forces in parallel to the motion axis. As a result the ratio between the radial and the axial Lorentz forces is significantly reduced. In addition, a new system bypassing the inactive elements has been presented and simulated. The bypassing system achieves a maximum of two switches working in series with the coils per phase. Therefore a thermal loss (in the bypass system) up to seven times lower than the previously proposed systems has been achieved. Likewise, the thermal loss in the proposed bypass system is not dependent on the number of coils in the generator assembly.

7 Acknowledgment

The authors acknowledge the technical support of Dr Helen Smith, College of Engineering Mathematics and Physical Sciences, University of Exeter, UK, during the preparation of this work.

8 References

1 Yemm, R.W., Henderson, R.M., Taylor, C.A.E.: 'The OPD Palamis WEC: current status and onward programme'. Fourth European Wave Energy Conf., Aalborg, Denmark, 2000

2 Jasinski, M., Malinowski, M., Kazmierkowski, M.P., Sorensen, H.C., Friis-Madsen, E., Swierczynski, D.: 'Control of AC/DC/AC converter for multi MW wave dragon offshore energy conversion system'. IEEE Int. Symp. on Industrial Electronics, ISIE 2007, 4–7 June 2007, pp. 2685–2690

3 Nor, K.M., Arof, H., Wijono, : 'Design of a 5 kW tubular permanent magnet linear generator'. 39th Int. Universities Power Engineering Conf., UPEC 2004, 6–8 September 2004, vols 1 and 2, pp. 528–532 Q3

4 Prudell, J., Stoddard, M., Amon, E., Brekken, T.K.A., von Jouanne, A.: 'Permanent-magnet tubular linear generator for ocean wave energy conversion', *IEEE Trans. Ind. Appl.*, 2010, **46**, (6), pp. 2392–2400

5 Ashabani, M., Milimonfared, J., Shokrollahi-Moghani, J., Taghipour, S., Aghashabani, M.: 'Mitigation of cogging force in axially magnetized tubular permanent-magnet machines using iron pole-piece slotting', *IEEE Proc. Trans. Magn.*, 2008, **44**, (9), pp. 2158–2162

6 Chayopitak, N., Taylor, D.G.: 'Performance assessment of air-core linear permanent-magnet synchronous motors', *IEEE Proc. Trans. Magn.*, 2008, **44**, (10), pp. 2310–2316

7 Crozier, R., Mueller, M.: 'Modelling and first order optimisation of the air-cored tubular PM machine using polynomial approximation'. 18th Int. Conf. on Electrical Machines, ICEM 2008, 6–9 September 2008, pp. 1–6

8 Mueller, M.A., Baker, N.J.: 'Direct drive electrical power take-off for offshore marine energy converters'. Proc. IMechE, 2005, vol. 219, Part A

9 Baker, N.J., Mueller, M.A., Ran, L., Tavner, P.J., McDonald, S.: 'Development of linear test rig for electrical power take off from waves'. Proc. Institute of Marine Engineering, Science and Technology, No. A10, 2007, pp. 3–15

10 Ran, L., Tavner, P.J., Mueller, M.A., Baker, N.J., McDonald, S.: 'Power conversion and control for a low speed, permanent magnet, direct-drive,

wave energy converter'. Third IET Int. Conf. on Power Electronics, Machines and Drives, 2006, March 2006, pp. 17–21
11 Ran, L., Mueller, M.A., Ng, C., *et al.*: 'Power conversion and control for a linear direct drive permanent magnet generator for wave energy', *IET Trans. Renew. Power Gener.*, 2011, **5**, (1), pp. 1–9
12 Manana, M., Arroyo, A., Silio, D., *et al.*: 'WET: a wave energy toolbox for oscillating-body converters'. OCEANS, 2011 IEEE – Spain, 6–9 June 2011, pp. 1–3
13 Wu, F., Zhang, X.P., Ju, P., Sterling, M.J.H.: 'Optimal control for AWS-based wave energy conversion system', *IEEE Trans. Power Syst.*, 2009, **24**, (4), pp. 1747–1755
Q4 14 Mueller, M.A., Baker, N.J., Ran, L., *et al.*: 'Experimental tests of an air-cored PM tubular generator for direct drive wave energy converters'. Fourth IET Conf. on Power Electronics, Machines and Drives, PEMD 2008, 2–4 April 2008, pp. 747–751
15 Cheng-Tsung, L., Chien-Lin, L., Chang-Chou, H., Chun-Hung, T.: 'Compact model of a slotless tubular linear generator for renewable energy performance assessments', *IEEE Proc. Trans. Magn.*, 2010, **46**, (6), p. 1467
16 McDonald, A.S., Crozier, R., Caraher, S., Mueller, M.A., Chick, J.P.: 'Integrated design of direct-drive linear generators for wave energy converters'. Int. Conf. on Sustainable Power Generation and Supply, SUPERGEN '09, 6–7 April 2009, pp. 1–7
17 McDonald, A.S., Mueller, M.A., Polinder, H.: 'Structural mass in direct-drive permanent magnet electrical generators', *IET Trans. Renew. Power Gener.*, 2008, **2**, (1), pp. 3–15
18 Hodgins, N., Keysan, O., McDonald, A., Mueller, M.: 'Design and testing of a linear generator for wave energy applications', *IEEE*
Q5 *Trans. Ind. Electron.*, 2011, (99), p. 1
19 Kimoulakis, N.M., Kakosimos, P.E., Kladas, A.G.: 'Hybrid technique for dynamic modelling of the performance of linear generators with skewed mounted permanent magnets', *IEEE Proc. Trans. Magn.*, 2011, **47**, (5), pp. 906–909
20 Li, D., Bai, B., Yu, Q., Zhu, B.: 'Research on a floating type of wave power generator'. Fifth IEEE Conf. on Industrial Electronics and Applications, 15–17 June 2010, pp. 469–472
21 Baker, N.J., Mueller, M.A., Spooner, E.: 'Permanent magnet air-cored tubular linear generator for marine energy converters'. Second Int. Conf. on Power Electronics, Machines and Drives, PEMD 2004, 31 April 2004, vol. 2, pp. 862–867
22 Hyun Choi, J., Su Baek, Y.: 'Theoretical analysis and its applications of a PM synchronous motor with minimized cogging force', *IEEE Proc. Trans. Magn.*, 2009, **45**, (10), pp. 4692–4695
23 Kimoulakis, N.M., Kakosimos, P.E., Kladas, A.G.: 'Power generation by using point absorber wave energy converter coupled with linear permanent magnet generator'. Seventh Mediterranean Conf. and Exhibition on Power Generation, Transmission, Distribution and Energy Conversion, Agia Napa, Cyprus, 7–10 November 2010
24 Prudell, J., Stoddard, M., Brekken, T.K.A., von Jouanne, A.: 'A novel permanent magnet tubular linear generator for ocean wave energy'. Energy Conversion Congress and Exposition, ECCE 2009, 20–24 September 2009, pp. 3641–3646
25 Shek, J.K.H., Macpherson, D.E., Mueller, M.A.: 'Experimental verification of linear generator control for direct drive wave energy conversion', *IET Trans. Renew. Power Gener.*, 2010, **4**, (5), pp. 395–403
26 Chunhua, L., Chau, K.T., Jiang, J.Z.: 'A permanent-magnet hybrid brushless integrated starter–generator for hybrid electric vehicles', *IEEE Trans. Ind. Electron.*, 2010, **57**, (12), pp. 4055–4064
27 Zhou, Z., Knapp, W., MacEnri, J., *et al.*: 'Permanent magnet generator control and electrical system configuration for Wave Dragon MW wave energy take-off system'. IEEE Int. Symp. on Industrial Electronics, ISIE 2008, 30 June–2 July 2008, pp. 1580–1585
28 Bascetta, L., Magnani, G., Rocco, P.: 'Force ripple compensation in linear motors with application to a parallel kinematic machine'. IEEE/ASME Int. Conf. on Advanced Intelligent Mechatronics, 4–7 September 2007, pp. 1–6
29 McKeever, P., Ng, C., Taylor, M., Spooner, E., Mueller, M.A., Crozier, R.C.: 'Snapper wave energy capture – the mechanical challenge'. UK Magnetic Society – Technologies for Renewable energy, Alstom Grid UK, Stafford, One Day Seminar, 9 March 2011

doi: 10.1049/iet-rpg.2011.0190

Bibliography

ABIGAIL WACHER, N., K., 2010. Mathematical and Numerical Modeling of the AquaBuOY Wave Energy Converter. *Mathematics-in-Industry Case Studies Journal,* Volume 2, pp. pp. 16-33.

ABPMER THE MT OFFICE, 2008. *Atlas of UK Marine Renewable Energy Resources: Atlas Pages A Strategic Environmental Assessment Report.* Proudman Oceanographic Laboratory.

AHMED, T., NISHIDA, K. and NAKAOKA, M., 2010. Grid power integration technologies for offshore ocean wave energy, *Energy Conversion Congress and Exposition (ECCE), 2010 IEEE* 2010, pp. 2378-2385.

AHN, H.G., LEE, S.H., LEE, D.Y., JANG, K.B. and KIM, G.T., 2008. A Study on the Characteristics of PMLSM According to Permanent Magnet Arrangement, *Industry Applications Society Annual Meeting, 2008. IAS '08. IEEE* 2008, pp. 1-6.

ALBERDI, M., AMUNDARAIN, M., GARRIDO, A.J., GARRIDO, I. and MASEDA, F.J., 2011. Fault-Ride-Through Capability of Oscillating-Water-Column-Based Wave-Power-Generation Plants Equipped With Doubly Fed Induction Generator and Airflow Control. *Industrial Electronics, IEEE Transactions on,* 58(5), pp. 1501-1517.

ANDREAS OBERHOFER, P.M., July 2012. *Energy Storage Technologies & Their Role in Renewable Integration.* http://www.geni.org/globalenergy/research/energy-storage-technologies/Energy-Storage-Technologies.pdf: Global Energy Network Institute (GENI).

ANNUAR, A.Z., MACPHERSON, D.E., FOREHAND, D.I.M. and MUELLER, M.A., 2012. Optimum power control for arrays of direct drive wave energy converters, *Power Electronics, Machines and Drives (PEMD 2012), 6th IET International Conference on* 2012, pp. 1-6.

ASHABANI, M., MILIMONFARED, J., SHOKROLLAHI-MOGHANI, J., TAGHIPOUR, S. and AGHASHABANI, M., 2008. Mitigation of Cogging Force in Axially Magnetized Tubular Permanent-Magnet Machines Using Iron Pole-Piece Slotting. *Magnetics, IEEE Transactions on,* 44(9), pp. 2158-2162.

BABARIT, A., CUCLOS, G. and CLEMENT, A.H., 2003. Benefit of Latching Control for a Heaving Wave Energy Device in Random Sea, *Proceedings of the 2003 International Offshore and Polar Engineering Conference* 2003, pp. 341-348.

BABARIT, A. and CLÉMENT, A.H., 2006. Optimal latching control of a wave energy device in regular and irregular waves. *Applied Ocean Research,* 28(2), pp. 77-91.

BAKER, N.J. and MUELLER, M., 2005. Direct drive electrical power take-off for offshore marine energy converters. *Proceedings of the Institution of Mechanical Engineers Part A Journal of Power and Energy,* 219, pp. 223-234.

BAKER, N.J., MUELLER, M.A., RAN, L., TAVNER, P.J. and MCDONALD, S., 2007. *Development of Linear test rig for electrical Power take off from waves*. *Journal of Marine Engineering and Technology,* A10, pp. 3-15.

BAKER, N.J., 2003. *Linear generators for direct drive marine renewable energy converters*, University of Durham.

BAKER, N.J., MUELLER, M.A. and SPOONER, E., 2004. Permanent magnet air-cored tubular linear generator for marine energy converters, *Power Electronics, Machines and Drives, 2004. (PEMD 2004). Second International Conference on (Conf. Publ. No. 498)* 2004, pp. 862-867 Vol.2.

BASCETTA, L., MAGNANI, G. and ROCCO, P., 2007. Force ripple compensation in linear motors with application to a parallel kinematic machine, *Advanced intelligent mechatronics, 2007 IEEE/ASME international conference on* 2007, pp. 1-6.

BRACCO, G., GIORCELLI, E., MATTIAZZO, G., MARIGNETTI, F., CARBONE, S. and ATTAIANESE, C., 2011. Design and experiments of linear tubular

generators for the Inertial Sea Wave Energy Converter, *Energy Conversion Congress and Exposition (ECCE), 2011 IEEE* 2011, pp. 3864-3871.

BRIAN ELMEGAARD, W.B., *Efficiency of Compressed Air Energy Storage.* http://orbit.dtu.dk/fedora/objects/orbit:72193/datastreams/file_6324034/content: DTU Technical University of Denmark, Department of Mechanical Engineering,.

BULATOV, I., PERRY, S.J. and KLEMEŠ, J.J., 2009. A new emerging energy technology-Pelamis-demonstration of the assessment by EMINENT tool, *Chemical Engineering Transactions* 2009, pp. 105-110.

CHOI, J.H. and BAEK, Y.S., 2009. Theoretical Analysis and Its Applications of a PM Synchronous Motor With Minimized Cogging Force. *Magnetics, IEEE Transactions on,* 45(10), pp. 4692-4695.

CHRISTENSEN, N.P., 2005. *Report on the current state and the need for further research on CO2Capture and Storage.* Rev 6.

CLÉMENT, A., MCCULLEN, P., FALCÃO, A., FIORENTINO, A., GARDNER, F., HAMMARLUND, K., LEMONIS, G., LEWIS, T., NIELSEN, K., PETRONCINI, S., PONTES, M.-., SCHILD, P., SJÖSTRÖM, B., SØRENSEN, H.C. and THORPE, T., 2002. Wave energy in Europe: current status and perspectives. *Renewable and Sustainable Energy Reviews,* 6(5), pp. 405-431.

CZECH, B., BAUER, P., POLINDER, H. and KORONDI, P., 2009. Modeling and simulating an Archimedes Wave Swing park in steady state conditions, *Power Electronics and Applications, 2009. EPE '09. 13th European Conference on* 2009, pp. 1-10.

DANIELSSON, O., ERIKSSON, M. and LEIJON, M., 2006. Study of a longitudinal flux permanent magnet linear generator for wave energy converters. *International Journal of Energy Research,* 30(14), pp. 1130-1145.

DANIELSSON, O. and LEIJON, M., 2007. Flux Distribution in Linear Permanent-Magnet Synchronous Machines Including Longitudinal End Effects. *Magnetics, IEEE Transactions on,* 43(7), pp. 3197-3201.

DANIELSSON, O., LEIJON, M. and SJOSTEDT, E., 2005. Detailed study of the magnetic circuit in a longitudinal flux permanent-magnet synchronous linear generator. *Magnetics, IEEE Transactions on,* 41(9), pp. 2490-2495.

DOMINGUES, E.G., SILVA, L.R. and BRADL, H., 2008. Evaluation of the methane and electrical energy potential and carbon credits revenues from the Goiânia landfill, *Transmission and Distribution Conference and Exposition: Latin America, 2008 IEEE/PES* 2008, pp. 1-6.

ENTEC UK LIMITED 2010, 2010. *Marine Renewable Energy.*

EVANS D., 1976. A theory for Wave-Power absorption by oscillating bodies. *Journal of Fluid Mechanics,* 77.

FAIZ, J., EBRAHIMI-SALARI, M. and SHAHGHOLIAN, G., 2010. Reduction of Cogging Force in Linear Permanent-Magnet Generators. *Magnetics, IEEE Transactions on,* 46(1), pp. 135-140.

FAIZ, J., EBRAHIMI-SALARY, M. and SHAHGHPLIAN, G., 2009. Cogging force alleviation in linear permanent magnet generators, *AFRICON, 2009. AFRICON '09.* 2009, pp. 1-6.

FALNES, J., 1997. *Principles for capture of energy from ocean waves.* N-7034. Trondheim, Norway: Department of Physics, NTNU,.

GARCIA-ALZORRIZ, J.A., GRAU, J., CORDOBA, R. and MUELA, J., 2011. A novel double-sided flat rectangular linear permanent magnets synchronous generator for sea wave energy application, *Electrical and Electronics Engineering (ELECO), 2011 7th International Conference on* 2011, pp. I-248-I-252.

GHITA, C., CHIRILA, A.I., DEACONU, I.D., NAVRAPESCU, V. and ILINA, D.I., 2008. Numerical modeling of the electric linear generators based on the sea waves energy, *Electrotechnical Conference, 2008. MELECON 2008. The 14th IEEE Mediterranean* 2008, pp. 640-645.

GUINEVERE, J., LIPO, T. and VENKATARAMANAN, G., 2010. *A Doubly-Fed Linear Generator for Ocean Wave Energy Conversion.*

www.inore.org/download.php?dID=495: Wave Energy Presentation, WEMPEC Annual Review Meeting.

HASANIEN, H.M., ABD-RABOU, A.S. and SAKR, S.M., 2010. Design Optimization of Transverse Flux Linear Motor for Weight Reduction and Performance Improvement Using Response Surface Methodology and Genetic Algorithms. *Energy Conversion, IEEE Transactions on,* 25(3), pp. 598-605.

HODGINS, N., KEYSAN, O., MCDONALD, A. and MUELLER, M., 2010. Linear generator for direct drive wave energy applications, *Electrical Machines (ICEM), 2010 XIX International Conference on* 2010, pp. 1-6.

HODGINS, N., KEYSAN, O., MCDONALD, A.S. and MUELLER, M.A., 2012. Design and Testing of a Linear Generator for Wave-Energy Applications. *Industrial Electronics, IEEE Transactions on,* 59(5), pp. 2094-2103.

HODGINS, N., MUELLER, M.A., TEASE, W.K. and STATON, D., 2010. Thermal model of an induction generator in oscillating water column wave energy converter, *Power Electronics, Machines and Drives (PEMD 2010), 5th IET International Conference on* 2010, pp. 1-6.

HUMPHRIES, H., 2011. *Rare Earth Elements: The Global Supply Chain.* Congressional Research Service.

IVANOVA, I.A., AGREN, O., BERNHOFF, H. and LEIJON, M., 2005. Simulation of wave-energy converter with octagonal linear generator. *Oceanic Engineering, IEEE Journal of,* 30(3), pp. 619-629.

JOSEPH SIMMONS, ARDETH BARNHART, STANLEY REYNOLDS, YOUNG-JUN SON, ALEX CRONIN, AUGUST 2010. *Study of Compressed Air Energy Storage with Grid and Photovoltaic Energy Generation.* College of Engineering, the Eller College of Management and the Arizona Research Institute for Solar Energy.

JOSEPH, D.M. and CRONJE, W.A., 2007. Design and Analysis of a Double-Sided Tubular Linear Synchronous Generator with Particular Application to

Wave-Energy Conversion, *Power Engineering Society Conference and Exposition in Africa, 2007. PowerAfrica '07. IEEE* 2007, pp. 1-8.

KEYSAN, O., MCDONALD, A., MUELLER, M., DOHERTY, R. and HAMILTON, M., 2010. C-GEN, a lightweight direct drive generator for marine energy converters, *Power Electronics, Machines and Drives (PEMD 2010), 5th IET International Conference on* 2010, pp. 1-6.

KEYSAN, O. and MUELLER, M.A., 2012. A linear superconducting generator for wave energy converters, *Power Electronics, Machines and Drives (PEMD 2012), 6th IET International Conference on* 2012, pp. 1-6.

KIMOULAKIS, N.M., KAKOSIMOS, P.E. and KLADAS, A.G., 2011. Hybrid Technique for Dynamic Modeling of the Performance of Linear Generators With Skewed Mounted Permanent Magnets. *Magnetics, IEEE Transactions on,* 47(5), pp. 906-909.

KIMOULAKIS, N.M., KLADAS, A.G. and TEGOPOULOS, J.A., 2009. Cogging Force Minimization in a Coupled Permanent Magnet Linear Generator for Sea Wave Energy Extraction Applications. *Magnetics, IEEE Transactions on,* 45(3), pp. 1246-1249.

KIMOULAKIS, N.M., KAKOSIMOS, P.E. and KLADAS, A.G., 2010. Power Generation by using point absorber wave energy converter coupled with linear permanent magnet generator, *Power Generation, Transmission, Distribution and Energy Conversion (MedPower 2010), 7th Mediterranean Conference and Exhibition on* 2010, pp. 1-5.

KORDE, U.A., 2002. Latching control of deep water wave energy devices using an active reference. *Ocean Engineering,* 29(11), pp. 1343-1355.

KRISTOF SCHLEMMER, FRANZ FUCHSHUMER, NORBERT BÖHMER, RONAN COSTELLO, CARLOS VILLEGAS, 2011. Design and Control of a Hydraulic Power Take-off for an Axi-symmetric Heaving Point Absorber, *European Wave and Tidal Energy Conference 2011 (EWTEC)*, 5 - 9 September 2011.

LEIJON, M., BERNHOFF, H., AGREN, O., ISBERG, J., SUNDBERG, J., BERG, M., KARLSSON, K.E. and WOLFBRANDT, A., 2005. Multiphysics simulation of wave energy to electric energy conversion by permanent magnet linear generator. *Energy Conversion, IEEE Transactions on,* 20(1), pp. 219-224.

LI, D., BAI, B., YU, Q. and ZHU, B., 2010. Research on a floating type of wave power generator, *Industrial Electronics and Applications (ICIEA), 2010 the 5th IEEE Conference on* 2010, pp. 469-472.

LI, D., BAI, B., YU, Q. and CHEN, D., 2009. Cogging Force Minimization in a Permanent Magnet Linear Generator for Sea Wave Energy Extraction Applications, *Energy and Environment Technology, 2009. ICEET '09. International Conference on* 2009, pp. 552-554.

LIU, C.T., LIN, C.L., HWANG, C.C. and TU, C.H., 2010. Compact Model of a Slotless Tubular Linear Generator for Renewable Energy Performance Assessments. *Magnetics, IEEE Transactions on,* 46(6), pp. 1467-1470.

LONDON METAL EXCHANGE, June, 2012-last update, http://www.metalprices.com.

MANANA, M., ARROYO, A., SILIO, D., DELGADO, F., PEREZ, S., FERNANDEZ, I., MORENO, V., PIGAZO, A., ZOBAA, A., ROA, P. and CARDENAL, J., 2011. WET: A wave energy toolbox for oscillating-body converters, *OCEANS, 2011 IEEE - Spain* 2011, pp. 1-3.

MARKUS MUELLER AND ROBIN WALLACE, 2008. Enabling science and technology for marine renewable energy. *Journal of Energy Policy,* 36, pp. 4376-4382.

MCDONALD, A.S., CROZIER, R., CARAHER, S., MUELLER, M.A. and CHICK, J.P., 2009. Integrated design of direct-drive linear generators for wave energy converters, *Sustainable Power Generation and Supply, 2009. SUPERGEN '09. International Conference on* 2009, pp. 1-7.

MINCIUNESCU, P., SCORTESCU, M. and MARINESCU, S., 2010. Design considerations of permanent magnet brushless generators, *Electrical and*

Electronics Engineering (ISEEE), 2010 3rd International Symposium on 2010, pp. 327-331.

MUELLER, M.A., 2002. Electrical generators for direct drive wave energy converters. *Generation, Transmission and Distribution, IEE Proceedings-,* 149(4), pp. 446-456.

MUELLER, M.A. and BAKER, N.J., 2003. Modelling the performance of the vernier hybrid machine. *Electric Power Applications, IEE Proceedings -,* 150(6), pp. 647-654.

NOLAN, G.A., RINGWOOD, J.V., LEITHEAD, W. and BUTLER, S., 2005. *Optimal damping profiles for a heaving buoy wave-energy converter*, *Proceedings of the Fifteenth International Offshore and Polar Engineering Conference* 2005, pp. 477-485.

O. DANIELSSON, K. THORBURN, M. ERIKSSON, M. LEIJON, 2003. Permanent magnet fixation concepts for linear generator, *Proceedings of the 5th European Wave Energy Conference, Cork (Ireland)* 2003, pp. pp.117-124.

OPREA, C.A., MARTIS, C.S., BIRO, K.A. and JURCA, F.N., 2010. Design and testing of a four-sided permanent magnet linear generator prototype, *Electrical Machines (ICEM), 2010 XIX International Conference on* 2010, pp. 1-6.

ORMAZA, M.A., GOITIA, M.A., HERNANDEZ, I.G. and HERNANDEZ, A.J.G., 2009. Wells turbine control in wave power generation plants, *Electric Machines and Drives Conference, 2009. IEMDC '09. IEEE International* 2009, pp. 177-182.

O'SULLIVAN, D.L. and LEWIS, A.W., 2011. Generator Selection and Comparative Performance in Offshore Oscillating Water Column Ocean Wave Energy Converters. *Energy Conversion, IEEE Transactions on,* 26(2), pp. 603-614.

PARLIAMENTARY OFFICE OF SCIENCE AND TECHNOLOGY, June 2011. *Carbon Footprint of Electricity Generation.* Number 383. POST NOTE UPDATE: .

PARLIAMENTARY OFFICE OF SCIENCE AND TECHNOLOGY, 2006. *Postnote - Carbon footprint of electricity generation.* 268.

PERRY Y. LI, ERIC LOTH, TERRENCE W. SIMON, JAMES D. VAN DE VEN, STEPHEN E. CRANE, *Compressed Air Energy Storage for Offshore Wind Turbines.* http://www.me.umn.edu/~lixxx099/papers/CAES_IFPE_2011.pdf: University of Minnesota, University of Virginia, Worcester Polytechnic Institute, LightSail Energy, Inc.

PIRISI, A., MUSSETTA, M., GRUOSSO, G. and ZICH, R.E., 2010. An optimized three phase TPM-LiG for marine applications, *Power Electronics Electrical Drives Automation and Motion (SPEEDAM), 2010 International Symposium on* 2010, pp. 1712-1717.

POLINDER, H., DAMEN, M.E.C. and GARDNER, F., 2004. Linear PM Generator system for wave energy conversion in the AWS. *Energy Conversion, IEEE Transactions on,* 19(3), pp. 583-589.

POLINDER, H., MUELLER, M.A., SCUOTTO, M. and GODEN DE SOUSA PRADO, M, 2007. Linear generator systems for wave energy conversion, *Proceedings of the 7th European Wave and Tidal Energy Conference* 2007.

POLINDER, H. and SCUOTTO, M., 2005. Wave energy converters and their impact on power systems, *Future Power Systems, 2005 International Conference on* 2005, pp. 9 pp.-9.

POLINDER, H., SLOOTWEG, J.G., HOEIJMAKERS, M.J. and COMPTER, J.C., 2003. Modeling of a linear PM Machine including magnetic saturation and end effects: maximum force-to-current ratio. *Industry Applications, IEEE Transactions on,* 39(6), pp. 1681-1688.

PRADO, M. and POLINDER, H., 2011. Direct drive in wave energy conversion — AWS full scale prototype case study, *Power and Energy Society General Meeting, 2011 IEEE* 2011, pp. 1-7.

PRUDELL, J., STODDARD, M., AMON, E., BREKKEN, T.K.A. and VON JOUANNE, A., 2010. A Permanent-Magnet Tubular Linear Generator for Ocean

Wave Energy Conversion. *Industry Applications, IEEE Transactions on,* 46(6), pp. 2392-2400.

QUOTATION, A.A., June, 2012-last update, http://www.ukmag.net.

RAN, L., MUELLER, M.A., NG, C., TAVNER, P.J., ZHAO, H., BAKER, N.J., MCDONALD, S. and MCKEEVER, P., 2011. Power conversion and control for a linear direct drive permanent magnet generator for wave energy. *Renewable Power Generation, IET,* 5(1), pp. 1-9.

RAN, L., TAVNER, P.J., MUELLER, M.A., BAKER, N.J. and MCDONALD, S., 2006. Power Conversion and Control for a Low Speed, Permanent Magnet, Direct-Drive, Wave Energy Converter, *Power Electronics, Machines and Drives, 2006. The 3rd IET International Conference on* 2006, pp. 17-21.

ROSS, D., 1995. 'Power from the Waves'*. Oxford University Press*.

S H SALTER, J R M TAYLOR, N J CALDWELL, 2002. Power conversion mechanisms for wave energy. *Engineering for the Maritime Environment,* Vol216 Part M, pp. 1-27.

SCHOEN, M.P., HALS, J. and MOAN, T., 2008. Robust control of heaving wave energy devices in irregular waves, *Control and Automation, 2008 16th Mediterranean Conference on* 2008, pp. 779-784.

SCHUTTE, J. and STRAUSS, J.M., 2010. Optimisation of a transverse flux linear PM generator using 3D finite element analysis, *Electrical Machines (ICEM), 2010 XIX International Conference on* 2010, pp. 1-6.

SHABANI, M.A., MILIMONFARED, J. and TAGHIPOUR, S., 2007. Cogging force mitigation of tubular permanent magnet machines with magnet dividing, *Electrical Machines and Systems, 2007. ICEMS. International Conference on* 2007, pp. 810-814.

SHIBAIKE, A., SANADA, M. and MORIMOTO, S., 2007. Suitable Configuration of Permanent Magnet Linear Synchronous Generator for Wave Power Generation, *Power Conversion Conference - Nagoya, 2007. PCC '07* 2007, pp. 210-215.

SPOONER, E. and HAYDOCK, L., 2003. Vernier hybrid machines. *Electric Power Applications, IEE Proceedings -,* 150(6), pp. 655-662.

SZABO, L., OPREA, C., VIOREL, L.-. and BIRO, K.A., 2007. Novel Permanent Magnet Tubular Linear Generator for Wave Energy Converters, *Electric Machines & Drives Conference, 2007. IEMDC '07. IEEE International* 2007, pp. 983-987.

TAVANA, H.M., 2009. Study of wave energy potential in Tonekabon (N Iran), *Developments in Renewable Energy Technology (ICDRET), 2009 1st International Conference on the* 2009, pp. 1-3.

TAYLOR, J.R.M. and MACKAY, I., 2001. *The design of an eddy current dynamometer for a free-floating sloped IPS buoy*, *Proceedings of Marine Renewable Energy Conference* 2001, pp. 67-74.

TAYLOR, J.R.M. and MACKAY, I., *The Design of an eddy current dynamometer for a free-floating sloped IPS buoy.* University of Edinburgh, UK: .

THORBURN, K. and LEIJON, M., 2007. Farm size comparison with analytical model of linear generator wave energy converters. *Ocean Engineering,* 34(5–6), pp. 908-916.

THORPE, T., 1999. *A Brief Review of Wave Energy", ETSU Report R120.* www.mech.ed.ac.uk/research/wavepower/Tom%20Thorpe/Tom%20Thorpe%20report.pdf: .

VAN ZYL, A.W., JEANS, C.G., CRUISE, R.J. and LANDY, C.F., 1999. Comparison of force to weight ratios between a single-sided linear synchronous motor and a tubular linear synchronous motor, *Electric Machines and Drives, 1999. International Conference IEMD '99* 1999, pp. 571-573.

VERMAAK, R. and KAMPER, M.J., 2010. Design of a novel air-cored permanent magnet linear generator for wave energy conversion, *Electrical Machines (ICEM), 2010 XIX International Conference on* 2010, pp. 1-6.

VINING, J., LIPO, T.A. and VENKATARAMANAN, G., 2010. Self-synchronous control of doubly-fed linear generators for ocean wave energy applications,

Energy Conversion Congress and Exposition (ECCE), 2010 IEEE 2010, pp. 2386-2391.

VINING, J., LIPO, T.A. and VENKATARAMANAN, G., 2009. Design and optimization of a novel hybrid transverse / longitudinal flux, wound-field linear machine for ocean wave energy conversion, *Energy Conversion Congress and Exposition, 2009. ECCE 2009. IEEE* 2009, pp. 3726-3733.

WANG, J., JEWELL, G.W. and HOWE, D., 1999. A general framework for the analysis and design of tubular linear permanent magnet machines. *Magnetics, IEEE Transactions on,* 35(3), pp. 1986-2000.

WELLS, J.R., CHAPMAN, L., KREIN, P.T. and WALLS, T., 2001. Linear induction machine design for instructional laboratory development, *Electrical Insulation Conference and Electrical Manufacturing & Coil Winding Conference, 2001. Proceedings* 2001, pp. 319-322.

WU, F., ZHANG, X.P., JU, P. and STERLING, M.J.H., 2009. Optimal Control for AWS-Based Wave Energy Conversion System. *Power Systems, IEEE Transactions on,* 24(4), pp. 1747-1755.

YANG G., CHUN-YANG, D., LU Y. and SUN L., 2003. Model of permanent magnet inductor type synchronous motor, *Applied Power Electronics Conference and Exposition, 2003. APEC '03. Eighteenth Annual IEEE* 2003, pp. 69-74 vol.1.

ZANXIANG NIE, XI XIAO, MCMAHON, R., CLIFTON, P., YUNXIANG WU and SHIYI SHAO, 2013. Emulation and Control Methods for Direct Drive Linear Wave Energy Converters. *Industrial Informatics, IEEE Transactions on,* 9(2), pp. 790-798.

ZOU, J., WANG, Q. and XU, Y., 2011. Influence of the Permanent Magnet Magnetization Length on the Performance of a Tubular Transverse Flux Permanent Magnet Linear Machine Used for Electromagnetic Launch. *Plasma Science, IEEE Transactions on,* 39(1), pp. 241-246.